Syracuse University

SURFACE

Dissertations - ALL   SURFACE

June 2018

multimedia transmission over wireless networks: performance analysis and optimal resource allocation

Chuang Ye
Syracuse University

Follow this and additional works at: https://surface.syr.edu/etd

Part of the Engineering Commons

Recommended Citation

Abstract

In recent years, multimedia applications such as video telephony, teleconferencing, and video streaming, which are delay sensitive and bandwidth intensive, have started to account for a significant portion of the data traffic in wireless networks. Such multimedia applications require certain quality of service (QoS) guarantees in terms of delay, packet loss, buffer underflows and overflows, and received multimedia quality. It is also important to note that such requirements need to be satisfied in the presence of limited wireless resources, such as power and bandwidth. Therefore, it is critical to conduct a rigorous performance analysis of multimedia transmissions over wireless networks and identify efficient resource allocation strategies.

Motivated by these considerations, in the first part of the thesis, performance of hierarchical modulation-based multimedia transmissions is analyzed. Unequal error protection (UEP) of data transmission using hierarchical quadrature amplitude modulation (HQAM) is considered in which high priority (HP) data is protected more than low priority (LP) data. In this setting, two different types of wireless networks are considered. Specifically, multimedia transmission over cognitive radio networks and device-to-device (D2D) cellular wireless networks is addressed. Closed-form bit error rate (BER) expressions are derived and optimal power control strategies are determined.

Next, throughput and optimal resource allocation strategies are studied for multimedia transmission under delay QoS and energy efficiency (EE) constraints. A Quality-Rate (QR) distortion model is employed to measure the quality of received video in terms of peak signal-to-noise ratio (PSNR) as a function of video source rate.

Effective capacity (EC) is used as the throughput metric under delay QoS constraints. In this analysis, four different wireless networks are taken into consideration:

- First, D2D underlaid wireless networks are addressed. Efficient transmission mode selection and resource allocation strategies are analyzed with the goal of maximizing the quality of the received video at the receiver in a frequency-division duplexed (FDD) cellular network with a pair of cellular users, one base station and a pair of D2D users under delay QoS and EE constraints.

- A full-duplex communication scenario with a pair of users and multiple subchannels in which users can have different delay requirements is addressed. Since the optimization problem is not concave or convex due to the presence of interference, optimal power allocation policies that maximize the weighted sum video quality subject to total transmission power level constraint are derived by using monotonic optimization theory. The optimal scheme is compared with two suboptimal strategies.

- A full-duplex communication scenario with multiple pairs of users in which different users have different delay requirements is addressed. EC is used as the throughput metric in the presence of statistical delay constraints since deterministic delay bounds are difficult to guarantee due to the time-varying nature of wireless fading channels. Optimal resource allocation strategies are determined under bandwidth, power and minimum video quality constraints again using the monotonic optimization framework.

- A broadcast scenario in which a single transmitter sends multimedia data to multiple receivers is considered. The optimal bandwidth allocation and the optimal power allocation/power control policies that maximize the sum video quality subject to total bandwidth and minimum EE constraints are derived. Five different resource allocation strategies are investigated, and the joint opti-

2

mization of the bandwidth allocation and power control is shown to provide the best performance. Tradeoff between EE and video quality is also demonstrated.

In the final part of the thesis, power control policies are investigated for streaming variable bit rate (VBR) video over wireless links. A deterministic traffic model for stored VBR video, taking into account the frame size, frame rate, and playout buffers is considered. Power control and the transmission mode selection with the goal of maximizing the sum transmission rate while avoiding buffer underflows and overflows under transmit power constraints is exploited in a D2D wireless network. Another system model involving a transmitter (e.g., a base station (BS)) that sends VBR video data to a mobile user equipped with a playout buffer is also adopted. In this setting, both offline and online power control policies are considered in order to minimize the transmission power without playout buffer underflows and overflows. Both dynamic programming and reinforcement learning based algorithms are developed.

MULTIMEDIA TRANSMISSION OVER WIRELESS NETWORKS: PERFORMANCE ANALYSIS AND OPTIMAL RESOURCE ALLOCATION

By

Chuang Ye

M.S., Zhejiang University, Zhengjiang, China, 2012

DISSERTATION

Submitted in partial fulfillment of the requirements for the degree of

Doctor of Philosophy in Electrical and Computer Engineering

Syracuse University

June 2018

Acknowledgements

First, I would like to thank my advisors, Prof. Mustafa Cenk Gursoy and Prof. Senem Velipasalar Gursoy, for their help and guidance during my entire Ph.D. study. In this period, I have gained much experience in research, and completed many studies in the area of multimedia wireless communication.

I would like to thank all my Ph.D. defense committee members Prof. Jianshun Zhang, Prof. Biao Chen, Prof. Qinru Qiu, Prof. Pramod Varshney and Prof. Sucheta Soundarajan for carefully reading my thesis.

I would also like to thank my parents, and my girlfriend Yaqi for supporting me to pursue my Ph.D. degree.

Finally, I would like to thank all my labmates and friends for their support during these years at Syracuse. I had really wonderful time studying and working with them.

Table of Contents

List of Figures

xvi

List of Tables

Chapter 1

Introduction

1.1 Resource Constrained Multimedia Wireless Transmissions

With the significant improvements in wireless technology, multimedia applications such as video telephony, teleconferencing, and video streaming, which are delay sensitive and bandwidth intensive, have started to account for a significant portion of the data traffic over wireless networks. For instance, as revealed in [1], mobile video traffic was already 60% of the entire mobile data traffic in 2016, and it is predicted that three-fourths of the world's mobile data traffic will be video by 2021. The overwhelming growth in the volume of multimedia content, multimedia traffic and wireless multimedia applications is drastically increasing the demand for more bandwidth. With this and the fact that prime portion of the spectrum has already been allocated, bandwidth scarcity has become one of the major bottlenecks in wireless services. To satisfy the increasing demand for communication and provide better user experience, several technologies have been proposed according to different applications.

According to the report from the Spectrum-Policy Task Force of the Federal Communications Commission (FCC) [2], the spectrum scarcity is mainly caused by the

underutilization and inefficient usage in many portions of the spectrum rather than the limited range of usable frequencies. Cognitive radio has been proposed to realize dynamic spectrum access in order to overcome the spectrum underutilization problem by allowing the unlicensed users (i.e., cognitive or secondary users) to access the licensed spectrum without causing harmful interference to the licensed users (i.e., primary users) [3], [4]. In cognitive radio systems, the unlicensed (i.e., secondary) users can coexist with the licensed (i.e., primary) users by changing transmission power level according to primary user activity or transmit only when there is no primary user activity. Additionally, device-to-device (D2D) communication is another technology that efficiently reuses the occupied spectrum. In D2D communications, device users (DUs) can communicate with each other directly rather than transmitting data through a cellular base station (BS) while potentially sharing the spectral resources with cellular users. Several benefits may be provided by enabling D2D communication. First, DUs can obtain high data transmission rate and low end-to-end delay due to the short communication distance, which is critical for real time video transmission. Secondly, DUs can more efficiently use resources such as bandwidth or transmission power when communicating directly with each other over a short distance even though the existence of interferences. Additionally, by offloading traffic from the BS, sharing the spectral resources and managing the interference, D2D communication can improve the spectral efficiency of cellular networks. Moreover, in full-duplex (FD) transmission scheme, transmitter can transmit and receive data simultaneously using the same frequency band. Since the transmitter can send and receive data using the same spectral resources, the utilization of the spectrum is higher, which leads to higher transmission rates. However, operating in FD mode leads to self-interference that lowers the signal to interference plus noise ratio (SINR) inevitably. Therefore, how to balance the more efficient utilization of the spectrum with interference management in FD systems is a critical issue.

In addition to bandwidth, transmission energy/power also plays an important role in wireless communications since energy is a limited resource especially in mobile applications. Hence, a common type of resource adaptation is efficiently and optimally allocate the available transmission energy/power in order to enhance the system performance. Indeed, optimal power control policies are extensively studied in the context of wireless systems. However, most work concentrated on rate-maximizing policies without taking into account multimedia quality metrics, delay requirements, and energy efficiency constraints.

1.2 Literature Review

1.2.1 Multimedia Transmission over Cognitive Radio Channels under Sensing Uncertainty

Recently, cognitive radio (CR) has been proposed to realize dynamic spectrum access (DSA) in order to overcome the spectrum underutilization problem by allowing the unlicensed users (i.e., cognitive or secondary users) to access the licensed spectrum without causing harmful interference to the licensed users (i.e., primary users) [3], [4]. DSA strategies can be mainly categorized into three models, namely dynamic exclusive use model, open radio spectrum sharing, and hierarchical radio spectrum access model [5]. Dynamic exclusive use model provides dynamic spectrum allocation and spectrum rights, which allow license holders to sell and trade the spectrum. Therefore, spectrum auction and market based policies for resource allocation lead to a profitable way of utilizing the spectrum [6] – [7]. While users can access the spectrum on a non-priority basis in the open sharing model, there is a hierarchy between the access rights of the primary and cognitive users in the hierarchical spectrum access model. In particular, the primary users have priority in accessing the spectrum, and cognitive users can either coexist with the primary users by varying their

transmission power according to primary user activity and interference constraints, or transmit only when there is no active primary user in the channel. Therefore, spectrum sensing is an essential functionality of CR systems in order to detect the temporarily unused frequency bands [8]. Along with this, efficient design of medium access control protocol has an important role for exploiting the spectrum opportunities [9].

Existing literature mainly focuses on the performance of spectrum sensing methods and the throughput of CR systems. There have been relatively limited number of studies on multimedia transmission in CR networks. The work in [10] mainly focused on the optimization of the overall received quality of MPEG-4 fine grained scalable video multicast by considering proportional fairness and also primary user protection from harmful interference in CR networks. In [11], the optimal channel and path selection strategy for streaming multiple videos over a multi-hop CR network was proposed in the presence of imperfect sensing decisions and a constraint on the collision probability. The authors in [12] proposed an optimal packet loading strategy for multimedia transmissions of secondary users by considering each channel with different primary user activity. The authors in [13] jointly optimized the quantization step size of source coding, modulation type and channel coding parameters in order to minimize the expected video distortion over CR networks subject to a packet delay constraint. In [14], an optimal subcarrier and antenna selection scheme that maximizes the aggregate visual quality of the received video in downlink CR networks was proposed. In [15], a channel allocation scheme was introduced to meet the different quality of experience (QoE) requirements of the secondary users. The recent work in [16] proposed a cross-layer scheduling scheme for OFDM-based CR systems in which optimal subcarrier assignment, power and modulation allocation were performed for each incoming multimedia packet. The authors in [17] investigated the optimal assignment of cognitive users to idle-sensed channels to maximize the visual quality of

4

downlink multiuser video streaming. Also, the work in [18] mainly focused on improving the quality of H.264/SVC video at the secondary receiver in multi-channel CR networks. Moreover, the authors in [19] studied joint adaptation of scalable video coding (SVC) and transmission rate to minimize the average energy consumption of cognitive users subject to quality of service (QoS) requirements.

1.2.2 Multimedia Transmission over Device-to-Device Wireless Networks

To satisfy the increasing demand for local device communication and provide better user experience, device-to-device (D2D) communications have been proposed as a promising technique for LTE-Advanced systems [20, 21]. In D2D communication, device users (DUs) can communicate with each other directly rather than transmitting and receiving data through a cellular base station (BS). Several benefits may be provided by enabling D2D communication. First, DUs can obtain high data transmission rate and low end-to-end delay due to the short communication distance. Secondly, DUs can save energy and resources when communicating directly with each other over a short distance under certain quality constraints. Finally, other users in the cellular network can have access to more spectral resources since DUs communicate just occupying one direct link rather than uplink and downlink, as used in cellular mode.

In [22], a base-station aided scheme was proposed for increasing the throughput of wireless video transmissions in D2D communication systems by exploiting the redundancy of user requests and the considerable storage capacity of smartphones and tablets. The authors in [23] proposed a joint channel and power allocation scheme in underlay multicast D2D communications in order to maximize the sum throughput of active cellular users (CUs) and feasible D2D groups in a cell under a certain level of signal-to-interference-plus-noise ratio (SINR) for both the CUs and D2D groups.

A maximum weight bipartite matching based scheme was developed to assign the optimal channel for each feasible D2D group. Joint mode selection, channel assignment and power control in D2D communications were addressed in [24] with the goal of maximizing the overall system throughput while guaranteeing the SINR of both D2D and cellular links. Three communication modes were considered for D2D users. In [25], energy-efficient uplink resource sharing for mobile D2D multimedia communications underlaid with cellular networks with multiple potential D2D pairs and cellular users was studied. The problem was formulated as a nontransferable coalition formation game and a distributed coalition formation algorithm based on the merge-and-split rule and the Pareto order was developed. In [26], optimal power control for resource sharing between CUs and DUs was derived for maximizing the energy efficiency of a DU under throughput constraints for both the DU and the CU in a cellular network. A distributed algorithm for the implementation of the optimal power control was proposed and validated numerically. Traditional D2D schemes mainly focus on maximizing the system throughput without taking into account quality-of-service (QoS) provisioning. [27] developed a framework to investigate the impact of delay-QoS requirements on the performance of D2D and cellular communications over underlaying wireless networks, and proposed optimal power allocation schemes with statistical QoS provisioning for two channel modes.

1.2.3 Quality-Driven Resource Allocation for Full-Duplex Wireless Video Transmission under Delay Constraints

The authors in [28] proposed a strategy to maximize the sum quality of the received reconstructed videos subject to different delay constraints on different users and a total bandwidth constraint in a multiuser setup by allocating the optimal amount of bandwidth to each user in a downlink wireless network. A content-aware framework for spectrum- and energy-efficient mobile association and resource allocation in wire-

less heterogeneous networks was proposed in [29]. Two content-aware performance metrics, namely quality-of-experience-aware spectral efficiency (QSE) and quality-of-experience-aware energy efficiency (QEE), were used to capture spectrum usage and energy consumption from the perspective of video quality. The goal was to obtain the optimal system level QSE and QEE by determining the mobile association and allocating the resources optimally via nonlinear fractional programming approach and dual decomposition method. In this work, delay QoS constraints were not considered. Reference [30] addressed the maximization of the system throughput subject to delay QoS and average power constraints for time-division multiple access (TDMA) communication links. [31] proposed a QoS-driven power and rate adaptation scheme that aims at maximizing the throughput of multichannel systems subject to a given delay QoS constraint over wireless links. The authors in [32] developed an optimal power allocation scheme for the cognitive network with the goal of maximizing the effective capacity of the secondary user link under constraints on the primary user's outage probability and secondary user's average and peak transmission power. The scheme also satisfied the QoS requirements of both secondary users and primary users simultaneously. Statistical QoS provisioning in next generation heterogeneous mobile cellular networks is investigated in [33]. The authors in [34] proposed a QoS-driven power allocation scheme for full-duplex (FD) wireless links with the goal of maximizing the overall effective capacity (EC) under a given delay QoS constraint. Two models, namely local transmit power related self-interference (LTPRS) model and local transmit power unrelated self-interference (LTPUS), were built to analyze the full-duplex transmission, respectively. However, an approximation of the sum Shannon capacity was used under the assumption that signal-to-interference-plus-noise ratio is much larger than 1. [35] considered the problem of distributed power allocation in an FD wireless network consisting of multiple pairs of nodes with the goal of maximizing the network-wide capacity. Shannon capacity was used as the per-

7

formance metric and the optimal transmission powers for the FD transmitters were derived based on the high SINR approximation.

The problem of joint subchannel allocation and power control was discussed in many studies. For instance, resource allocation in multicell uplink orthogonal frequency division multiple access (OFDMA) systems was considered in [36], and the problem was solved via noncooperative games for subcarrier allocation and transmit power control. [37] proposed a joint power control and subchannel allocation for OFDMA femtocell networking using distributed auction game in order to minimize the total power radiated by the femtocell base station and guaranteeing the throughput. [38] considered the problem of joint subcarrier and power allocation for the downlink of a multiuser OFDM cellular network in order to minimize the power consumption subject to meeting the target rates of all users in the network. The authors in [39] considered the adaptive subcarrier assignment and fair power control strategy that minimize a cost function of average relay powers in multiuser wireless OFDM networks.

1.2.4 Quality-Driven Resource Allocation for Wireless Video Transmissions under Energy Efficiency and Delay Constraints

The authors in [28] proposed a strategy to maximize the sum quality of the received reconstructed videos subject to different delay constraints at different users and a total bandwidth constraint in a multiuser setup by allocating the optimal amount of bandwidth to each user. They also derived user admission and scheduling policies that enable selecting a maximal user subset such that all selected users can meet their statistical delay requirements. In [40], a joint power and sub-carrier assignment polity under delay aware QoS requirement was proposed to improve power efficiency

in vehiche-to-roadside infrastructure communication networks in terms of minimizing power consumption. A cross-layer transmission scheme for video streaming over the interference-infected ad hoc networks was presented and investigated in [?] to maximize the average video quality of the whole network. The quality of video was calculated by using distortion introduced by lossy video compression and packet loss.

Problem of resource allocation was discussed in many previous studies. For instance, [41] built a video rate distortion model using a distortion metric called structural similarity index to investigate the resource allocation and optimization issues for the multimedia transmission over downlink orthogonal frequency division multiple access (OFDMA) wireless networks. A cross-layer problem was formulated with the goal of achieving equal structural similarity of multi-resolution video sequences among users under a set of rate constraints. The authors in [42] developed an application-layer transmission scheme to effectively deliver mobile high-frame rate (HFR) video over multiple wireless access networks under the delay and total bandwidth constraints. First, an unequal frame scheduling approach was proposed to minimize the total distortion. Second, an error resilience scheme was introduced at the receiver side to balance the out-of-order and overdue video packets to diminish the error propagations. The proposed scheme reduced the probability of frame loss and frame drops. The authors in [43] addressed a utility-proportional optimization for multimedia applications that are relying on scalable video coding (SVC)-encoded video signals. A smooth approximation of the utility function was used to come up with a convex formulation and a dual-based distributed algorithm was proposed for rate allocation and bandwidth sharing under the link capacity constraints in the system. In [?], the authors considered the power allocation of the physical layer and the buffer delay of the upper application layer in energy harvesting green networks. The problem is to minimize the mean buffer delay under battery and buffer constraints.

The multimedia transmission problem was also studied with different types of

wireless networks. In [44], a learning-based and QoE-driven spectrum handoff scheme was proposed with the goal of maximizing the multimedia users' satisfaction in cognitive radio networks. A mixed preemptive and non-preemptive resume priority MG1 queueing model was built for modeling the spectrum usage behavior for prioritized multimedia applications. The reinforcement learning was employed to maximize the quality of video transmission in the long term. A QoE-aware power allocation for device-to-device (D2D) video transmission was proposed with the target of maximizing the video quality while minimizing the data rate variations over the time-varying wireless channels in [45]. A dual decomposition technique was used to solve the optimization problem subject to the minimum rate requirement, maximum transmit power level and maximum allowable interference level constraints. The authors in [39] considered the adaptive subcarrier assignment and fair power control strategy that minimize a cost function of average relay powers for multiuser wireless OFDM networks. In [46], an enery-video aware multipath transport protocol was proposed to enable the energy-efficient and quality-guaranteed live video streaming over heterogeneous wireless networks. To address the energy-efficient bandwidth aggregation with regard to the stringent delay and quality constraints imposed by wireless video transmission, [47] presented an energy quality aware bandwidth aggregation scheme.

Energy efficiency (EE), measured by the data rate normalized by the transmission power or equivalently the number of communicated bits per unit energy, is also considered as a key factor in wireless systems. However, improving EE may result in a decrease in the throughput, which in return leads to a degradation in the quality of the reconstructed video at the receiver. Motivated by these considerations, the authors in [48] addressed delay-QoS-driven spectrum and energy efficiency optimization in which effective capacity (EC) is maximized under transmission power and minimum energy efficiency constraints.

1.2.5 Power Control for VBR Video Streaming over Wireless Networks

Recently, scheduling algorithms to transmit multiple video streams from a base station to mobile clients were investigated in [49]. With the proposed algorithms, the vulnerability to stalling was reduced by allocating slots to videos in a way that maximizes the minimum "playout lead" across all videos with an epoch-by-epoch framework. The distribution of prefetching delay and the probability generating function of playout buffer starvation for constant bit rate (CBR) streaming was modeled in [50]. The framework to characterize the throughput variation caused by opportunistic scheduling at the BS, and the playback variation of variable bit rate (VBR) traffic were considered as an extension. The flow dynamics have dominant influence on QoE metrics compared to the variation of throughput caused by fast channel fading and that of video playback rate caused by VBR streaming. Authors in [51] proposed algorithms to find the optimal transmit powers for the base stations with the goal of maximizing the sum transmission rate while VBR video data can be delivered to mobile users without causing playout buffer underflows or overflows. A deterministic model for VBR video traffic that considers video frame sizes and playout buffers at the mobile users was adopted. [52], and reference [53] investigated effective admission control schemes for VBR videos over wireless networks in terms of bandwidth and QoS requirements.

A deterministic model for VBR video traffic that considers video frame sizes and playout buffers at the mobile users was adopted. In [54], the authors investigated an energy-efficient video downlink transmission by predicting the download rate at the receiver. An optimal packet scheduling problem in a single-user energy harvesting wireless communication system was proposed in [55]. The time by which all packets are delivered was minimized by adaptively changing the transmission rate according to the traffic load and available energy. The problem of online packet scheduling to

minimize the required conventional grid energy for transmitting a fixed number of packets given a common deadline was considered in [56]. The proposed algorithm tried to finish the transmission of each packet assuming that all future packets are going to arrive at equal time intervals within the left-over time. The authors in [57] considered online power control with the goal of maximizing the long-term average throughput in an energy harvesting system with random independent and identically distributed (i.i.d.) energy arrivals and a finite battery for data transmission. A simple online power control policy was proved to be universally near-optimal for all parameter values.

1.3   Outline and Main Contributions

In Chapter 3, we analyze the performance of multimedia transmission based on hierarchical quadrature amplitude modulation (HQAM) with power control in CR systems. The main contributions of this chapter can be summarized as follows:

- Unlike the aforementioned works in [10] – [15], we have considered an error-resilient method called unequal error protection (UEP), which provides different levels of protection to different parts of the multimedia data in order to increase the robustness of transmission against wireless channel impairments, e.g., noise, interference from other users and fading. HQAM is an efficient UEP technique in which high priority (HP) data bits are mapped to the first two most significant bits (MSBs) of each constellation point whereas low priority (LP) data bits are mapped to the rest of the bits. We identify the optimal maximum a posteriori probability (MAP) decision rule for HQAM and new expressions for computing the bit error rates (BERs) of HP data bits and LP data bits in the presence of sensing errors for any given fading distribution. We further derive closed-form expressions for BERs of HP bits and LP bits for 16-HQAM averaged over

Nakagami-m fading, which is chosen due to its ability of representing a wider range of fading severities.

- HQAM based multimedia transmission without power control in non-cognitive context has been analyzed recently [58] – [59]. Different from these works, we obtain optimal power adaptation schemes to minimize the weighted sum of average BERs of HP bits and LP bits in sensing-based spectrum sharing CR systems subject to peak/average transmit power constraints along with average interference power constraint under imperfect sensing decisions. In sensing-based spectrum sharing CR systems, cognitive users sense the channel to determine the primary user activity and then adapt their transmission power levels according to the channel sensing decisions. It is assumed that either instantaneous channel side information (CSI) or statistical CSI is available to determine optimal power levels. We note that our results are also different from the work in [60], where the authors derived optimal power control schemes by assuming that the primary user always exists in the channel, and therefore secondary users do not perform any channel sensing.

- A low-complexity optimal power control algorithm under peak/average transmit power and average interference power constraints is proposed. Also, we analyze and approximate the optimal power control schemes at high SNR levels, and obtain closed-form power expressions in terms of the Lambert-W function, which is easy to evaluate.

- We analyze the transmission of H.264/MPEG-4 coded video and JPEG200 coded image using conventional QAM and HQAM in terms of peak signal-to-noise ratio (PSNR) quality and number of retransmissions in a CR system. We further investigate the relations between sensing errors, optimal transmission powers, number of retransmissions and the received data quality.

In Chapter 4, with the motivation that prior studies in the literature have not considered the bit error rate (BER) performance metric in the context of multimedia wireless transmissions in a D2D network, we again employ an error resilient method called unequal error protection (UEP), which provides different levels of protection to different parts of the multimedia data in order to increase the robustness of transmission against wireless channel impairments. The multimedia data is divided into two parts: 1) high priority (HP) bits, which are mapped to the two most significant bits (MSBs); and 2) low priority (LP) bits, which are mapped to the two least significant bits (LSBs). Hierarchical quadrature amplitude modulation (HQAM) is employed to give the MSBs of each constellation point more protection. Maximal-ratio combining (MRC) is used in order to maximize the SINR and optimal power control is proposed in order to minimize the weighted sum of average HP BERs and LP BERs.

In Chapter 5, we investigate video transmission over D2D underlaid wireless networks under QoS and energy efficiency constraints. Three different transmission modes are considered in this chapter, and transmission mode selection and resource allocation with the goal of maximizing the quality of the received video at the receiver with a pair of cellular users, one base station and a pair of D2D users is studied. Additionally, in the cellular mode, a frequency-division duplexed based communication strategy is proposed, in which the uplink and downlink operate in two different frequency bands with different bandwidths. Moreover, throughput in the considered three different modes is derived, and the optimal mode is chosen under QoS and energy efficiency constraints.

In Chapter 6, wireless video transmission over full-duplex channels is studied. QoS requirements such as statistical delay constraints are considered in order to provide the desired performance levels to the end-users in real-time video transmissions. A communication scenario with a pair of users and multiple subchannels in which users can have different delay requirements is addressed. A logarithmic model of the quality-

rate relation is used for predicting the quality of the reconstructed video. Based on this, the optimal power allocation problem that maximizes the weighted sum video quality subject to total transmission power constraints is proposed and the policy is derived by using monotonic optimization theory. The optimal scheme is compared with two suboptimal strategies.

In Chapter 7, the literature works have not considered statistical QoS requirements, bandwidth limitations, power limitations and interference jointly in full-duplex wireless networks. In this thesis, we address the problem of maximizing the weighted sum quality of reconstructed videos at the receivers subject to total bandwidth, minimum video quality, maximum transmission power and delay QoS constraints by allocating the bandwidth and determining the optimal power level for each user when statistical channel side information (CSI) is available in the full-duplex wireless network. Since the optimization problem is neither a concave nor convex problem due to the existence of the interference, we employ the monotonic optimization (MO). Our more specific contributions include the following:

1. We reformulate the optimization problem as a monotonic optimization problem, and propose a framework to study full-duplex communication via monotonic optimization.

2. We derive several key properties of the optimal solution space.

3. We develop algorithms to efficiently determine the optimal resource allocation policies. In particular, we develop algorithms for enclosing polyblock initialization, projection onto the upper boundary, and iterative derivation of new enclosing polyblocks.

4. We analyze the impact of important system parameters (e.g., video quality parameters, QoS constraints, and weights) on the optimal resource allocation strategies and received video quality in terms of peak signal-to-noise ratio.

In Chapter 8, the literature works have not simultaneously addressed statistical delay QoS requirements, bandwidth limitations and EE constraints while also considering the quality of wireless multimedia transmissions. In this thesis, we employ a holistic approach in a broadcast scenario and study the problem of maximizing the sum quality of reconstructed videos at the receivers subject to total bandwidth, EE and delay QoS constraints by 1) allocating the bandwidth and determining the optimal power level for each user when statistical channel side information (CSI) is available, and 2) allocating the bandwidth and adapting the instantaneous power for each user when the transmitter has instantaneous CSI.

In Chapter 9, we consider the problem of streaming VBR videos in D2D wireless networks. VBR video has stable video quality across frames at the cost of large variations in the frame size or bit rate, where CBR video has a stable bit rate but the visual qualities of the frames may vary significantly. We consider a deterministic traffic model for stored VBR video, taking into account the frame size, frame rate, and playout buffers as in [61] and [62]. We exploit power control and the transmission mode selection with the goal of maximizing the sum transmission rate while avoiding underflows and overflows under transmit power constraints in a D2D wireless network.

In Chapter 10, we consider the VBR videos streaming in a point-to-point wireless network. We exploit power control with the goal of minimizing the transmission power level during the entire transmission session. The optimal offline power control strategy is proposed as a dynamic programming and two online power control strategies are presented. The initial online power control policies that minimize the transmit power consumption in the communication session is based on grouped water filling strategy. Subsequently, reinforcement learning (RL) based approach is employed for the second online power control policy.

1.4   Bibliographic Note

- The results in Chapter 3 appeared in the journal paper:

    - C. Ye, G. Ozcan, M. C. Gursoy and S. Velipasalar, "Multimedia Transmission Over Cognitive Radio Channels Under Sensing Uncertainty," in *IEEE Transactions on Signal Processing*, vol. 64, no. 3, pp. 726-741, Feb 2016.

- The results in Chapter 4 appeared in the conference paper:

    - C. Ye, M. C. Gursoy and S. Velipasalar, "Multimedia transmission over device-to-device wireless links," in *IEEE International Conference on Multimedia and Exop (ICME)*, Seattle, WA, 2016, pp. 1-6.

- The results in Chapter 6 appeared in the conference paper:

    - C. Ye, M. C. Gursoy and S. Velipasalar, "Optimal Resource Allocation for Full-Duplex Wireless Video Transmissions under Delay Constraints," in *IEEE Wireless Communications and Networking Conference (WCNC)*, San Francisco, CA, 2017, pp. 1-6.

- The results in Chapter 7 appeared in the accepted journal paper:

    - C. Ye, M. C. Gursoy and S. Velipasalar, "Quality-Driven Resource Allocation for Full-Duplex Delay-Constrained Wireless Video Transmissions," in *IEEE Transactions on Communication*, 2018.

- The results in Chapter 8 are reported in the submitted journal paper:

    - C. Ye, M. C. Gursoy and S. Velipasalar, "Quality-Driven Resource Allocation for Wireless Video Transmissions under Energy Efficiency and Delay Constraints," in *IEEE Acess*, 2018.

- The results in Chapter 9 appeared in the conference paper:

– C. Ye, M. C. Gursoy and S. Velipasalar, "Power Control and Mode Selection for VBR Video Streaming in D2D Networks," in *IEEE Wireless Communications and Networking Conference (WCNC)*, Barcelona, Spain, April 2018.

Chapter 2

Preliminaries

2.1 16-HQAM Constellation

16-HQAM, which provides two priority layers, HP and LP. In particular, HP data bits occupy the two most significant bits of each symbol point while LP data bits occupy the rest of the bits of the symbol. On the other hand, the conventional 16-QAM is non-hierarchical with each layer having the same reliability. Fig. 2.1 shows the constellation diagram of Gray-encoded 16-HQAM, in which neighboring signal points differ only by one bit and the signal points in the same quadrant have the same HP bits. In the figure, $2d_{1,i}$ and $2d_{2,i}$ represent the minimum distance between each
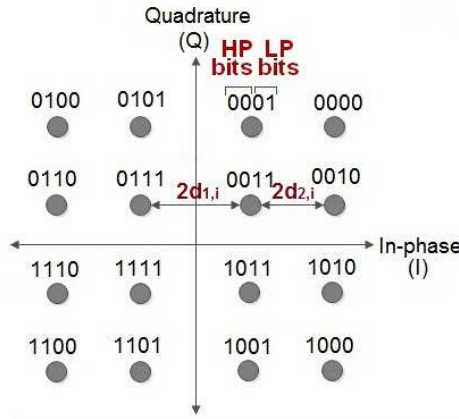
Figure 2.1: Signal constellation diagram of Gray coded 16-HQAM

19

quadrant and the minimum distance between the signal constellation points within each quadrant, respectively. Let us define the ratio $\alpha_i = d_{1,i}/d_{2,i}$. By changing the value of α_i, we can control the protection level for HP and LP bits. More specifically, for a given average signal power, increasing the value of α_i increases the distance between quadrants, which leads to diminished BER for HP bits. On the other hand, the distance between the constellation points within the quadrant decreases, and hence BER for LP bits increases. As a result, HP data is protected more against errors than LP data.

The minimum distance between the quadrants and the minimum distance between the signal constellation points within the quadrants can be written respectively as

$$d_{1,i} = \sqrt{\frac{\alpha_i^2 P_i}{2(\alpha_i + 1)^2 + 2}}, \quad d_{2,i} = \sqrt{\frac{P_i}{2(\alpha_i + 1)^2 + 2}} \tag{2.1}$$

where P_i denotes the average transmission power.

2.2 Delay QoS Constraints and Effective Capacity

In wireless video transmissions, queue length in the buffer is subject to limitations in order to control the queueing delay in wireless transmissions is addressed in [63]. More specifically, the stationary queue length in the buffer is required to decay exponentially for large buffer threshold as follows:

$$\Pr\{Q \geq q_{\max}\} \doteq e^{-\theta q_{\max}}, \tag{2.2}$$

where Q and $q_{\max}$ are the queue length and buffer overflow threshold, respectively. θ, referred to the QoS exponent, is defined as

$$\theta = - \lim_{q_{\max} \to \infty} \frac{\ln \Pr\{Q \geq q_{\max}\}}{q_{\max}}, \tag{2.3}$$

20

and describes the decay rate of the buffer overflow probability. It is obvious that larger θ leads to more stringent QoS requirements while smaller θ represents looser QoS requirements. Effective capacity characterizes the maximum constant arrival rate which can be supported by the service process (or the wireless transmission rate) subject to the statistical buffer overflow constraint specified by the QoS exponent θ. For an ergodic and stationary service process $c[i]$, the asymptotic logarithmic moment generating function (LMGF) is defined as

$$\Lambda_c(\theta) = \lim_{q_{max} \to \infty} \frac{\log \mathbb{E}\{e^{\theta \sum_{i=1}^{n} c[i]}\}}{n}, \tag{2.4}$$

and for an arrival process $a[i]$, the asymptotic LMGF $\Lambda_a(\theta)$ defined as

$$\Lambda_a(\theta) = \lim_{q_{max} \to \infty} \frac{\log \mathbb{E}\{e^{\theta \sum_{i=1}^{n} a[i]}\}}{n}. \tag{2.5}$$

According to theory of effective capacity, for a transmitter with constant arrival rate $a[i] = R$, time-varying service rate $c[i]$, and QoS exponent θ, the maximum constant arrival rate is determined from the solution of

$$\Lambda_a(\theta) + \Lambda_c(-\theta) = 0. \tag{2.6}$$

For constant arrival process, $a[i] = R$, the LMGF can be easily verified as $\Lambda_a(\theta) = \log \mathbb{E}\{e^{\theta a[i]}\} = \theta R$. Therefore, the effective capacity for a single hop is defined as

$$C = -\lim_{n \to \infty} \frac{\log \mathbb{E}\{e^{-\theta \sum_{i=1}^{n} c[i]}\}}{n\theta}. \tag{2.7}$$

Therefore, the constant source rate can be expressed as follows:

$$R = \frac{C}{T} = -\frac{1}{\theta T} \log \mathbb{E}\{e^{-\theta r}\} \tag{2.8}$$

21

where T is the channel coherence time and r is the instantaneous transmission rate.

2.3 Video Quality-Rate Model

Lossy data compression, which focuses on the tradeoff between the distortion and bit rate, is used in video coding algorithms, where an increased distortion leads to a decreased rate and vice-versa. Rate-distortion (R-D) theory addresses the problem of determining the minimal bit rate of the data transmission over a channel so that the distortion of the reconstructed data at the receiver does not exceed a given distortion value. Thus, the R-D function can estimate the bit rate at given distortion, or estimate the distortion at a given bit rate. Moreover, operational R-D (ORD) theory is applied to lossy data compression with finite number of possible R-D pairs, and the ORD function shows that the bit rate is a convex function of distortion. In [64], the quality of video is measured in terms of the reversed difference mean opinion score (RDMOS), and a rate-quality model to predict $q_u(t)$ using the video data rate $r_u(t)$ is employed as follows:

$$q_u(t) = \alpha_u(t) \log(r_u(t)) + \beta_u(t) \tag{2.9}$$

where model parameters $\alpha_u(t)$ and $\beta_u(t)$ can be determined by minimizing the prediction error. Also several R-D models are proposed in [65], in which the quality is measured in terms of the peak signal-to-noise ratio (PSNR). The exponential model for the rate-PSNR curve is used in this thesis. Thus, PSNR-rate curve is described by a logarithmic model and can be expressed as follows:

$$Q = \alpha \ln(R) + \beta \tag{2.10}$$

22
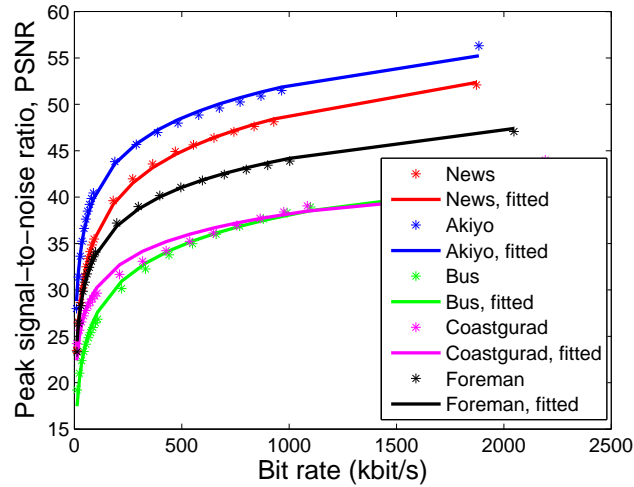
Figure 2.2: Actual PSNR values vs. rate and fitted quality rate curves.

where R and Q are the source rate and PSNR, respectively, and α and β are the parameters that can be determined by minimizing the prediction error.

Five CIF video sequences namely 'Akiyo', 'Bus', 'Coastguard', 'Foreman' and 'News' are used for the simulation results [66]. Size of each frame is 352×288 pixels. FFMPEG is used for encoding the video sequences and GOP is set as 10. Frame rate is set as 15 frames per second. Table 2.1 shows the parameters α and β that make the rate-distortion function of the five video sequences fit the quality rate model in (2.10), where the unit of R is kbit/s.

Table 2.1: Parameter values of the quality rate model for different video sequences

	Akiyo	Bus	Coastguard	Foreman	News
α	5.0545	4.7205	3.5261	4.5006	5.6218
β	17.1145	5.4764	13.8425	13.0780	10.0016

Fig. 2.2 shows the actual PSNR values as a function of the source bit rate for different video sequences, where we see that the increasing concave quality rate model fits the actual values very well.

2.4 Definitions used in Monotonic Optimization

We introduce some definitions used in monotonic optimization (MO) from [67].

Definition 2.1 (Box) *For two vectors $\mathbf{a} \in \mathcal{R}^n$, $\mathbf{b} \in \mathcal{R}^n$ with $\mathbf{a} \le \mathbf{b}$, the box $[\mathbf{a}, \mathbf{b}]$ is the set of all vectors $\mathbf{x} \in \mathcal{R}^n$ satisfying $\mathbf{a} \le \mathbf{x} \le \mathbf{b}$. In other words, a hyperrectangle $[\mathbf{a}, \mathbf{b}] = \{\mathbf{x} | a_j \le x_j \le b_j, j = 1, 2, ..., n\}$ is referred to as a box.*

Definition 2.2 (Normal set) *A set $\mathcal{G} \subset \mathcal{R}^n_+$ (the n-dimensional nonnegative real domain) is normal if for any element $\mathbf{x} \in \mathcal{G}$, all other elements $\mathbf{x}'$ such that $\mathbf{0} \le \mathbf{x}' \le \mathbf{x}$ are in the same set $\mathcal{G}$. In other words, $\mathcal{G} \subset \mathcal{R}^n_+$ is normal if for any $\mathbf{x} \in \mathcal{G}$, the set $[\mathbf{0}, \mathbf{x}] \subset \mathcal{G}$.*

Definition 2.3 (Conormal set) *A set $\mathcal{H} \subset \mathcal{R}^n_+$ is conormal if for any element $\mathbf{x} \in \mathcal{H}$, all other elements $\mathbf{x}'$ such that $\mathbf{x}' \ge \mathbf{x}$ are in the same set $\mathcal{H}$. In other words, a set $\mathcal{H}$ is conormal in $[\mathbf{0}, \mathbf{b}]$ if for any $\mathbf{x} \in \mathcal{H}$, $[\mathbf{x}, \mathbf{b}] \subset \mathcal{H}$.*

Definition 2.4 (Upper boundary) *An element $\bar{\mathbf{x}}$ of a normal closed set $\mathcal{G}$ is an upper boundary point of $\mathcal{G}$ if $\mathcal{G} \cap \{\mathbf{x} \in \mathcal{R}^n_+ | \mathbf{x} > \bar{\mathbf{x}}\} = \emptyset$. The set of all upper boundary points of the set $\mathcal{G}$ is called its upper boundary and denoted by $\partial^+ \mathcal{G}$.*

Definition 2.5 (Polyblocks) *A set $\mathcal{S} \subset \mathcal{R}^n_+$ is a polyblock if it is a union of a finite number of boxes $[\mathbf{0}, \mathbf{z}]$, where $\mathbf{z} \in \mathcal{T}$ and $|\mathcal{T}| < +\infty$. The set $\mathcal{T}$ is the vertex set of the polyblock.*

Definition 2.6 (Proper) *An element $\bar{\mathbf{x}} \in \mathcal{T}$ is said to be proper if there is no $\mathbf{x}' \in \mathcal{T}$ such that $\mathbf{x}' \ne \mathbf{x}$ and $\mathbf{x}' \ge \mathbf{x}$. If every element $\mathbf{x}' \in \mathcal{T}$ is proper, then the set $\mathcal{T}$ is a proper set.*

Chapter 3

Multimedia Transmission over Cognitive Radio Channels under Sensing Uncertainty

This chapter studies the performance of hierarchical modulation-based multimedia transmission in cognitive radio (CR) systems with imperfect channel sensing results under constraints on both transmit and interference power levels. Unequal error protection (UEP) of data transmission using hierarchical quadrature amplitude modulation (HQAM) is considered in which high priority (HP) data is protected more than low priority (LP) data. In this setting, closed-form bit error rate (BER) expressions for HP data and LP data are derived in Nakagami-m fading channels in the presence of sensing errors. Subsequently, the optimal power control that minimizes weighted sum of average BERs of HP bits and LP bits or its upper bound subject to peak/average transmit power and average interference power constraints is derived and a low-complexity power control algorithm is proposed. Power levels are determined in three different scenarios, depending on the availability of perfect channel side information (CSI) of the transmission and interference links, statistical CSI of both

links, or perfect CSI of the transmission link and imperfect CSI of the interference link. The impact of imperfect channel sensing decisions on the error rate performance of cognitive transmissions is also evaluated. In addition, tradeoffs between the number of retransmissions, the severity of fading, and peak signal-to-noise ratio (PSNR) quality are analyzed numerically. Moreover, performance comparisons of multimedia transmission with conventional quadrature amplitude modulation (QAM) and HQAM, and the proposed power control strategies are carried out in terms of the received data quality and number of retransmissions.

3.1 System Model

3.1.1 Channel Sensing

We consider a CR system in which a secondary transmitter sends multimedia data i.e., image and/or video to a secondary receiver by utilizing the spectrum licensed to the primary users as illustrated in Fig. 3.1. To peacefully coexist with the primary users, secondary users should initially learn the primary users' activity through channel sensing. Channel sensing can be formulated as a binary hypothesis testing problem in which hypotheses $\mathcal{H}_0$ and $\mathcal{H}_1$ denote that the primary users are inactive and active in the channel, respectively. Several spectrum sensing methods includ-
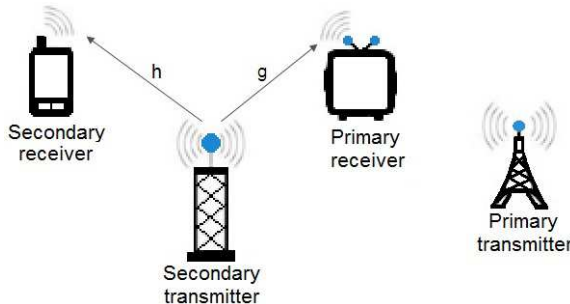
Figure 3.1: Cognitive radio channel model

ing matched filter detection, energy detection, and cyclostationary feature detection,
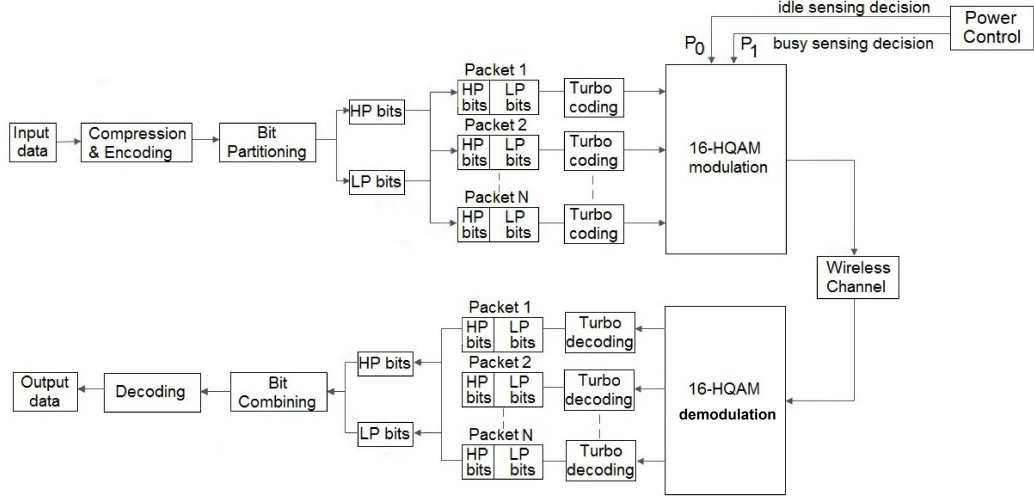
Figure 3.2: Block diagram of the multimedia transmission and reception system.

have been developed in the literature [68] and the corresponding sensing performance is characterized by two parameters, namely the probabilities of detection and false alarm, which are defined as

$$P_{\mathrm{d}} = \Pr\{\hat{\mathcal{H}}_1|\mathcal{H}_1\}, \quad P_{\mathrm{f}} = \Pr\{\hat{\mathcal{H}}_1|\mathcal{H}_0\}, \tag{3.1}$$

where $\hat{\mathcal{H}}_0$ and $\hat{\mathcal{H}}_1$ correspond to the events that the channel is detected as idle and busy, respectively. In a missed detection event, secondary users fail to detect active primary users and hence secondary users can collide with the primary users' transmission while in a false alarm event, secondary users detect the channel as busy while in fact there is no active primary user, resulting in the underutilization of the channel.

3.1.2 Cognitive Channel Model

After performing channel sensing, the secondary transmitter starts sending multimedia data to a secondary receiver over a flat-fading channel. It is assumed that the secondary users are allowed to transmit under both idle and busy sensing decisions.

27

Under this assumption, the channel input-output relation is given by

$$y = \begin{cases} hs + n & \text{in the absence of primary user activity} \\ hs + n + w & \text{in the presence of primary user activity} \end{cases}.$$ (3.2)

Above, s and y are the complex-valued transmitted and received signals, respectively and w denotes the primary users' received faded signal distributed according to a circularly symmetric complex Gaussian distribution with zero mean and variance σ_w^2. Also, n represents the circularly symmetric complex Gaussian noise with zero mean and variance σ_n^2. In addition, h is the channel fading coefficient of the transmission link between the secondary transmitter and the secondary receiver as shown in Fig. 3.1.

3.1.3   Multimedia Transmission System

The block diagram of the multimedia transmission system is depicted in Fig. 3.2. Input image or video is first compressed before transmission. JPEG2000 image coder is chosen as the compression technique for image transmission. In the case of video transmission, H.264/MPEG-4 codec is employed to compress the video content [69].

Following compression, data partitioning is applied. In particular, the compressed data is divided into two priority levels, namely HP and LP. The structure of JPEG2000 codestream is shown in Fig 3.3, which consists of a sequence of marker segments and layers with unequal importance [70]. Main header and tile-part header have a sequence of marker segments which contain important coding parameters and the layers in the packet data have different sensitivity to the corruption of the data. Therefore, for the images, the codestream header (i.e., main header and tile-part header) and lower layers are classified as HP data whereas the rest of the codestream is assigned as LP data. In the case of videos, there are three types of frames, namely
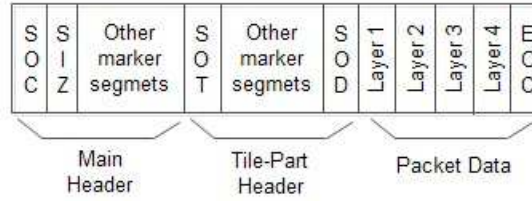
Figure 3.3: JPEG2000 codestream structure

I, P and B frames. I frame is the key frame in the coded video sequence. It can be encoded independently from other frames by using only its own information. Therefore, this frame is used as a reference frame for coding inter-coded frames such as P frames and B frames, and it is also employed for indexing and prevention of error propagation [69]. Any loss of I frames has more devastating impact on video quality than loss in other frames. Therefore, I frame is regarded as HP data while the rest of the frames are assigned as LP data.

After identifying HP data and LP data, the compressed data sequence is divided into N packets of equal size. Each packet contains both HP data and LP data in such a way that the ratio of HP bits and LP bits is the same. Subsequently, channel coding based on Turbo codes [71] is employed in order to enhance the resilience of the compressed data to wireless channel impairments, e.g., noise, interference from other users, and fading. Finally, HP bits and LP bits within packets are modulated using 16-HQAM and transmission power is determined based on the sensing decision, as further discussed in the following sections, and then each packet is transmitted over the wireless channel. At the receiver, ARQ mechanism is employed. More specifically, if the received power of the packet is less than a certain threshold, the secondary receiver requests the retransmission of the packet. On the other hand, if the received power of the packet is greater than the threshold, the output data is obtained by performing the inverse operations i.e., demodulation, turbo decoding, bit combining, and source decoding as shown in Fig. 3.2.

29

3.1.4 Bit Error Rate Analysis

Secondary users are assumed to employ 16-HQAM, which provides two priority layers, HP and LP. The 16-HQAM constellation is shown as 2.1 in Chapter 2.1. It is assumed that the sensing decisions and the perfect knowledge of the fading realizations are available at the secondary receiver. Thus, any phase shift due to fading can be removed by multiplying the received signal with the phase of the fading coefficient h. Under these assumptions, the optimal MAP decision rule for any arbitrary M-ary digital modulation under sensing decision $\hat{\mathcal{H}}_i$ is given as follows:

$$\hat{s} = \underset{0 \leq k \leq M-1}{\arg\max} \ \Pr\{s_k | y, h, \hat{\mathcal{H}}_i\} \tag{3.3}$$

$$= \underset{0 \leq k \leq M-1}{\arg\max} \ p_k f(y | s_k, h, \hat{\mathcal{H}}_i) \tag{3.4}$$

$$= \underset{0 \leq k \leq M-1}{\arg\max} \ \sum_{j=0}^{1} p_k \Pr\{\mathcal{H}_j | \hat{\mathcal{H}}_i\} f(y | s_k, h, \hat{\mathcal{H}}_i, \mathcal{H}_j), \tag{3.5}$$

where $\hat{s}$ is the MAP detector output, p_k is the prior probability of the signal constellation point s_k. Above, (3.4) is obtained by Bayes' rule, and can further be expanded by conditioning the density function $f(y | s_k, h, \hat{\mathcal{H}}_i)$ on the hypotheses $\mathcal{H}_0$ and $\mathcal{H}_1$ as in (3.5). Also, $f(y | s_k, h, \hat{\mathcal{H}}_i, \mathcal{H}_j)$ in (3.5) is the conditional distribution of the received real signal y given the transmitted signal s_k, channel fading coefficient h, channel sensing decision $\hat{\mathcal{H}}_i$, and true state of the channel $\mathcal{H}_j$, and can be expressed as

$$f(y | s_k, h, \hat{\mathcal{H}}_i, \mathcal{H}_j) = \begin{cases} \frac{1}{\pi \sigma_n^2} e^{-\frac{|y - s_k h|^2}{\sigma_n^2}}, & j = 0 \\ \frac{1}{\pi(\sigma_n^2 + \sigma_w^2)} e^{-\frac{|y - s_k h|^2}{\sigma_n^2 + \sigma_w^2}}, & j = 1 \end{cases} . \tag{3.6}$$

Note that the sensing decision $\hat{\mathcal{H}}_i$ has an impact on the density function through P_i, the power of the transmitted signal s_k. Additionally, the conditional probabilities in

(3.5) can be written as

$$\Pr\{\mathcal{H}_j|\hat{\mathcal{H}}_i\} = \frac{\Pr\{\mathcal{H}_j\}\Pr\{\hat{\mathcal{H}}_i|\mathcal{H}_j\}}{\Pr\{\mathcal{H}_0\}\Pr\{\hat{\mathcal{H}}_i|\mathcal{H}_0\}+\Pr\{\mathcal{H}_1\}\Pr\{\hat{\mathcal{H}}_i|\mathcal{H}_1\}} \quad i \in \{0,1\}.$$

Above, $\Pr\{\mathcal{H}_0\}$ and $\Pr\{\mathcal{H}_1\}$ denote the prior probabilities of primary users being inactive and active in the channel, respectively.

The average bit error probability for the MAP decision rule in (3.3) can be computed as

$$\text{BER} = 1 - \frac{1}{\log_2 M}\sum_{m=0}^{M-1}\sum_{v=1}^{\log_2 M}\sum_{i,j=0}^{1} p_m \Pr\{\mathcal{H}_j,\hat{\mathcal{H}}_i\}\Pr\{b_v|s_m,\hat{\mathcal{H}}_i,\mathcal{H}_j\}. \tag{3.7}$$

where b_v is the v-th bit for the symbol and $\Pr\{b_v|s_m,\hat{\mathcal{H}}_i,\mathcal{H}_j\}$ denotes the probability of correctly detecting the bit b_v given the symbol s_m, sensing decision $\hat{\mathcal{H}}_i$ and true channel state $\mathcal{H}_j$.

It was shown in [72] that the midpoints between the signal constellation points are optimal thresholds for rectangular QAM signaling in the presence of channel sensing errors. Since HQAM is a modification of conventional QAM primarily through the new bit assignment scheme, the optimal detector structure in HQAM is the same as in QAM signaling.

Next, we analyze the BER performance of HP and LP bits in 16-HQAM. The signals are assumed to be equally likely. Since HP data is mapped to two most significant bits in the signal constellation, the corresponding BER can be found by analyzing the change of in-phase bits. Hence, BER of HP bits for a given fading coefficient can be expressed as

$$P_{\text{HP}}(\mathbf{P},h) = \frac{1}{32}\sum_{k=0}^{15}\sum_{i,j=0}^{1}\Pr\{\mathcal{H}_j,\hat{\mathcal{H}}_i\}\left(P_e(b_1|s_k,h,\hat{\mathcal{H}}_i,\mathcal{H}_j)+P_e(b_2|s_k,h,\hat{\mathcal{H}}_i,\mathcal{H}_j)\right) \tag{3.8}$$

where $\mathbf{P} = [P_0,P_1]$ and $P_e(.)$ denotes the probability of an error in a single bit. As seen in Fig. 2.1, the most significant bit b_1 does not change in the in-phase direction, and only changes in the quadrature direction in the form of $0-0-1-1$. Similarly, the

31

second bit b_2 just changes in the in-phase direction in the same form of $0 - 0 - 1 - 1$.
Hence, BER expression can be calculated as

$$P_{\text{HP}}(\mathbf{P}, h) = \frac{1}{2} \sum_{j=0}^{1} \sum_{i=0}^{1} \sum_{l=0}^{1} \Pr\{\mathcal{H}_j, \hat{\mathcal{H}}_i\} Q\left(\sqrt{\frac{c_{l,i} P_i |h|^2}{\sigma_j^2}}\right), \qquad (3.9)$$

where $c_{0,i} = \frac{(\alpha_i+2)^2}{(\alpha_i+1)^2+1}$ and $c_{1,i} = \frac{\alpha_i^2}{(\alpha_i+1)^2+1}$. Also, $Q(x) = \int_x^\infty \frac{1}{\sqrt{2\pi}} e^{-t^2/2} dt$ is the Gaussian Q-function and σ_j^2 is defined as

$$\sigma_j^2 = \begin{cases} \sigma_n^2, & j = 0 \\ \sigma_n^2 + \sigma_w^2, & j = 1 \end{cases}. \qquad (3.10)$$

Subsequently, LP bits correspond to the two least significant bits in the signal constellation. Thus, BER of LP bits can be calculated by considering the change of quadrature bits as follows:

$$P_{\text{LP}}(\mathbf{P}, h) = \frac{1}{32} \sum_{k=0}^{15} \sum_{i,j=0}^{1} \Pr\{\mathcal{H}_j, \hat{\mathcal{H}}_i\} \left(P_e(b_3|s_k, h, \hat{\mathcal{H}}_i, \mathcal{H}_j) + P_e(b_4|s_k, h, \hat{\mathcal{H}}_i, \mathcal{H}_j) \right). \quad (3.11)$$

As observed from Fig. 2.1, the third bit, b_3, changes according to the pattern $0 - 1 - 1 - 0$ in the quadrature direction while it does not change in the in-phase direction. The last bit, b_4, has similar changes but in the other direction. As a result, BER expression is given by (3.12).

$$P_{\text{LP}}(\mathbf{P}, h) = \frac{1}{2} \sum_{j=0}^{1} \sum_{i=0}^{1} \Pr\{\mathcal{H}_j, \hat{\mathcal{H}}_i\} \left\{ 2Q\left(\sqrt{\frac{\beta_{0,i} P_i |h|^2}{\sigma_j^2}}\right) + Q\left(\sqrt{\frac{\beta_{1,i} P_i |h|^2}{\sigma_j^2}}\right) - Q\left(\sqrt{\frac{\beta_{2,i} P_i |h|^2}{\sigma_j^2}}\right) \right\}$$

$$\text{where } \beta_{0,i} = \frac{1}{(\alpha_i+1)^2+1} \quad \beta_{1,i} = \frac{(2\alpha_i+1)^2}{(\alpha_i+1)^2+1} \quad \beta_{2,i} = \frac{(2\alpha_i+3)^2}{(\alpha_i+1)^2+1}.$$

$$(3.12)$$

Note that the above BER expressions are for a given instantaneous realization of the fading coefficient, h. The averaged BER of HP bits and LP bits over Nakagami-m fading distribution are given in (3.13) and (3.14), respectively, at the top of the next page, where $_2F_1(.,.;.;.)$ denotes the Gauss hypergeometric function [73, eq. 9.10].

The derivation steps of these expressions are given in Appendix A.1.

$$P_{\text{HP}}(\mathbf{P}) = \frac{1}{4\sqrt{\pi}} \frac{\Gamma(m+\frac{1}{2})}{\Gamma(m+1)} \sum_{j=0}^{1} \sum_{i=0}^{1} \sum_{l=0}^{1} \left\{ \frac{\Pr\{\mathcal{H}_j, \hat{\mathcal{H}}_i\} \sqrt{\frac{c_{l,i} P_i \Omega}{2m\sigma_j^2}}}{\left(\frac{c_{l,i} P_i \Omega}{2m\sigma_j^2} + 1\right)^{m+\frac{1}{2}}} \, 2 \right.$$
$$\left. F_1\left(1, m+1/2; m+1; \frac{2m\sigma_j^2}{c_{l,i} P_i \Omega + 2m\sigma_j^2}\right) \right\} \tag{3.13}$$

$$P_{\text{LP}}(\mathbf{P}) = \frac{1}{4\sqrt{\pi}} \frac{\Gamma(m+\frac{1}{2})}{\Gamma(m+1)} \sum_{j=0}^{1} \sum_{i=0}^{1} \left\{ \frac{2\Pr\{\mathcal{H}_j, \hat{\mathcal{H}}_i\} \sqrt{\frac{\beta_{0,i} P_i \Omega}{2m\sigma_j^2}}}{\left(\frac{\beta_{0,i} P_i \Omega}{2m\sigma_j^2} + 1\right)^{m+\frac{1}{2}}} \, {}_2F_1\left(1, m+1/2; m+1; \frac{2m\sigma_j^2}{\beta_{0,i} P_i \Omega + 2m\sigma_j^2}\right) \right.$$
$$+ \frac{\Pr\{\mathcal{H}_j, \hat{\mathcal{H}}_i\} \sqrt{\frac{\beta_{1,i} P_i \Omega}{2m\sigma_j^2}}}{\left(\frac{\beta_{1,i} P_i \Omega}{2m\sigma_j^2} + 1\right)^{m+\frac{1}{2}}} \, {}_2F_1\left(1, m+1/2; m+1; \frac{2m\sigma_j^2}{\beta_{1,i} P_i \Omega + 2m\sigma_j^2}\right)$$
$$\left. - \frac{\Pr\{\mathcal{H}_j, \hat{\mathcal{H}}_i\} \sqrt{\frac{\beta_{2,i} P_i \Omega}{2m\sigma_j^2}}}{\left(\frac{\beta_{2,i} P_i \Omega}{2m\sigma_j^2} + 1\right)^{m+\frac{1}{2}}} \, {}_2F_1\left(1, m+1/2; m+1; \frac{2m\sigma_j^2}{\beta_{2,i} P_i \Omega + 2m\sigma_j^2}\right) \right\}. $$
$$\tag{3.14}$$

For the special case where m is an integer in the BER expression of HP bits given in (3.13), using the property for Gauss hypergeometric function with integer argument [74, Appendix A], we can simplify the corresponding BER expression as

$$P_{\text{HP}}(\mathbf{P}) = \frac{1}{2} \sum_{j=0}^{1} \sum_{i=0}^{1} \sum_{l=0}^{1} \Pr\{\mathcal{H}_j, \hat{\mathcal{H}}_i\} \left[H\left(\frac{c_{l,i} P_i \Omega}{2m\sigma_j^2}\right)\right]^m \times \sum_{r=0}^{m-1} \binom{m-1+r}{r} \left[1 - H\left(\frac{c_{l,i} P_i \Omega}{2m\sigma_j^2}\right)\right]^r \tag{3.15}$$

where

$$H(x) = \frac{1}{2}\left(1 - \sqrt{\frac{x}{1+x}}\right) \qquad x \geq 0. \tag{3.16}$$

In a similar fashion, the BER of LP bits for integer values of m is given in (3.17).

$$P_{\text{LP}}(\mathbf{P}) = \frac{1}{2} \sum_{i,j=0}^{1} \Pr\{\mathcal{H}_j, \hat{\mathcal{H}}_i\} \left\{ 2 \left[H\left(\frac{\beta_{1,i} P_i \Omega}{2m\sigma_j^2} \right) \right]^m \sum_{r=0}^{m-1} \binom{m-1+r}{r} \left[1 - H\left(\frac{\beta_{1,i} P_i \Omega}{2m\sigma_j^2} \right) \right]^r \right.$$
$$+ \left[H\left(\frac{\beta_{2,i} P_i \Omega}{2m\sigma_j^2} \right) \right]^m \sum_{r=0}^{m-1} \binom{m-1+r}{r} \left[1 - H\left(\frac{\beta_{2,i} P_i \Omega}{2m\sigma_j^2} \right) \right]^r$$
$$\left. - \left[H\left(\frac{\beta_3 P_i \Omega}{2m\sigma_j^2} \right) \right]^m \sum_{r=0}^{m-1} \binom{m-1+r}{r} \left[1 - H\left(\frac{\beta_3 P_i \Omega}{2m\sigma_j^2} \right) \right]^r \right\}$$

(3.17)

3.2 Optimal Power Control

In this section, we characterize the optimal power control policies that minimize the weighted sum of BERs of HP bits and LP bits or its upper bound subject to peak/average transmit power and average interference power constraints, assuming the availability of either the instantaneous or statistical CSI of the transmission link and interference link at the secondary transmitter.

3.2.1 Peak transmit and average interference power constraints

In this subsection, we consider peak transmit and average interference power constraints being imposed on secondary transmissions.

3.2.1.1 Perfect CSI of both transmission and interference links

Here, we assume that the instantaneous values of the fading coefficients of the transmission link, h, and interference link, g, are perfectly known by the secondary trans-

mitter. In this case, the optimal power control problem is given by

$$\min_{P_0(h,g),P_1(h,g)} \mathbb{E}\big\{\lambda P_{\mathrm{HP}}(\mathbf{P},h) + (1-\lambda)P_{\mathrm{LP}}(\mathbf{P},h)\big\} \qquad (3.18)$$

subject to

$$P_0(h,g) \leq P_{\mathrm{pk}} \qquad (3.19)$$

$$P_1(h,g) \leq P_{\mathrm{pk}} \qquad (3.20)$$

$$\mathbb{E}\{(1-P_{\mathrm{d}})\, P_0(h,g)\, |g|^2 + P_{\mathrm{d}}\, P_1(h,g)\, |g|^2\} \leq Q_{\mathrm{avg}} \qquad (3.21)$$

where $P_{\mathrm{HP}}(\mathbf{P},h)$ and $P_{\mathrm{LP}}(\mathbf{P},h)$ are instantaneous BER expressions for given fading coefficients h and g, and $\lambda \in [0,1]$. Above, when $\lambda = 1$ or 0, the optimal power levels are chosen to minimize only the BER of HP bits or LP bits, respectively. In the case of $\lambda = 1/2$, BER of HP bits and LP bits are equally weighed in the objective function to determine the optimal transmission power levels. Hence, the value of λ can be adjusted to reflect the importance of the HP and LP bits. In (3.19) and (3.20), P_{pk} denotes the peak transmit power limit of the secondary transmitter due to hardware/battery constraints and in (3.21), Q_{avg} represents average interference power limit at the primary receiver, which is imposed to satisfy the long-term QoS requirements of the primary users. In addition, since instantaneous CSI is available at the secondary transmitter, the power levels $P^{(0)}(h,g)$ and $P^{(1)}(h,g)$ are functions of both h and g.

Note that the objective function in (3.18), or in particular $P_{\mathrm{LP}}(\mathbf{P},h)$, consists of a sum of Gaussian Q functions with positive and negative weights. Therefore, the Hessian of the objective function is not necessarily positive semidefinite due to the sum of exponential functions with different positive and negative weights. On the other hand, by removing the negative-weighted Q functions in (3.12), we can obtain an upper bound on the BER expression in the objective function. Now, being composed of only positive weighted sum of Q functions that are convex for positive arguments,

this upper bound is convex. Therefore, the minimization problem becomes convex with affine constraints in (3.19), (3.20) and (3.21). In the following result, we identify the optimal power control scheme that minimizes this upper bound.

Proposition 3.1 *The optimal power control policy that minimizes the BER upper bound under the constraints in (3.19), (3.20) and (3.21) is given by*

$$P_{opt}^{(0)}(h,g) = \min\left(P_{\mathrm{pk}}, P_0^*\right) \tag{3.22}$$

$$P_{opt}^{(1)}(h,g) = \min\left(P_{\mathrm{pk}}, P_1^*\right) \tag{3.23}$$

where P_0^* is solution to

$$\sum_{j,l=0}^{1} \frac{P(\mathcal{H}_j,\hat{\mathcal{H}}_0)}{4\sqrt{2\pi}} \left\{ \lambda \frac{e^{\frac{-c_{l,0}P_0^*|h|^2}{2\sigma_j^2}}}{\sqrt{\frac{\sigma_j^2 P_0^*}{c_{l,0}|h|^2}}} + (1-\lambda)\rho_l \frac{e^{\frac{-\beta_{l,0}P_0^*|h|^2}{2\sigma_j^2}}}{\sqrt{\frac{\sigma_j^2 P_0^*}{\beta_{l,0}|h|^2}}} \right\} = \mu_1(1-P_{\mathrm{d}})|g|^2 \tag{3.24}$$

and P_1^* is solution to

$$\sum_{j,l=0}^{1} \frac{P(\mathcal{H}_j,\hat{\mathcal{H}}_1)}{4\sqrt{2\pi}} \left\{ \lambda \frac{e^{\frac{-c_{l,1}P_1^*|h|^2}{2\sigma_j^2}}}{\sqrt{\frac{\sigma_j^2 P_1^*}{c_{l,1}|h|^2}}} + (1-\lambda)\rho_l \frac{e^{\frac{-\beta_{l,1}P_1^*|h|^2}{2\sigma_j^2}}}{\sqrt{\frac{\sigma_j^2 P_1^*}{\beta_{l,1}|h|^2}}} \right\} = \mu_1 P_{\mathrm{d}}|g|^2. \tag{3.25}$$

Above, $\rho_0 = 2$, $\rho_1 = 1$, and μ_1 is the Lagrange multiplier, which can be determined by satisfying the average interference constraint in (3.21) with equality.

Proof: See Appendix A.2.

The above expressions are strictly monotonically decreasing functions of P_0^* and P_1^*, respectively. By taking the first derivate of the above expressions and analyzing the limits as P_0^* and P_1^* approach 0 and ∞, respectively, it can be easily shown that there always exists unique solutions for P_0^* and P_1^* due to the strict monotonicity. The optimal power control algorithm for this scenario is given in Algorithm 1.

In the following result, we identify closed-form approximations for the power levels in a specific scenario.

Proposition 3.2 *At high SNRs, the optimal power control policy that minimizes the BER of HP bits, (i.e., when $\lambda = 1$) under perfect sensing decision (i.e., when $P_{\mathrm{d}} = 1$ and $P_{\mathrm{f}} = 0$) subject to the constraints (3.19), (3.20) and (3.21) can be approximated in closed-form as*

$$P_{opt}^{(0)}(h, g) = P_{\mathrm{pk}} \tag{3.26}$$

$$P_{opt}^{(1)}(h, g) = \min \left(P_{\mathrm{pk}}, \frac{W_0 \left(\frac{(c_{1,1}|h|^2 P(\mathcal{H}_1))^2}{32\pi((\sigma_n^2 + \sigma_w^2)\mu_1|g|^2)^2} \right)}{\frac{c_{1,1}|h|^2}{\sigma_n^2 + \sigma_w^2}} \right) \tag{3.27}$$

where $W_0(.)$ represents the primary branch of the Lambert function [75].

Proof: See Appendix A.3.

Algorithm 1 The optimal power control algorithm under the peak transmit power and average interference power constraints

---

1: Initialize $\epsilon > 0$, $t > 0$, $\mu_1^{(0)} = \mu_{1,\mathrm{init}}$, $n = 0$

2: **repeat**

3:   Solve P_0^* and P_1^* in (3.24) and (3.25), respectively by bisection search and then determine $P_{\mathrm{opt}}^{(0)}(h, g)$ in (3.22) and $P_{\mathrm{opt}}^{(1)}(h, g)$ in (3.23).

4:   Update μ_1 using the projected subgradient method as follows

5:   $\mu_1^{(n+1)} = \left(\mu_1^{(n)} + t \left(\mathbb{E}\{(1 - P_{\mathrm{d}}) P_0(h, g) |g|^2 + P_{\mathrm{d}} P_1(h, g) |g|^2\} - Q_{\mathrm{avg}} \right) \right)^+$ where $(.)^+ = \max(., 0)$

6:   $n \leftarrow n + 1$

7: **until** $|\mu_1^{(n)}(\mathbb{E}\{(1 - P_{\mathrm{d}}) P_0(h, g) |g|^2 + P_{\mathrm{d}} P_1(h, g) |g|^2\} - Q_{\mathrm{avg}})| \leq \epsilon$

3.2.1.2 Perfect CSI of transmission link and imperfect CSI of interference link

In this case, we assume the transmitter has imperfect CSI of the interference link fading coefficient g, which is expressed as $g = \hat{g} + \tilde{g}$, where $\hat{g}$ is the estimate of the interference link and $\tilde{g}$ is the error in the estimate. It is assumed that $\hat{g}$ and $\tilde{g}$ are

37

independent, circularly symmetric complex Gaussian distributed with mean zero and variances $\sigma_g^2 - \sigma_e^2$ and σ_e^2, respectively. Thus, the average interference constraint can be written as

$$
\begin{aligned}
Q_{\text{avg}} &\geq \mathbb{E}\{[(1 - P_{\text{d}})\,P_0(h, \hat{g}) + P_{\text{d}}\,P_1(h, \hat{g})]\,|g|^2\} \\
&= \mathbb{E}\{[(1 - P_{\text{d}})\,P_0(h, \hat{g}) + P_{\text{d}}\,P_1(h, \hat{g})]\,(|\hat{g}|^2 + |\tilde{g}|^2)\} \\
&= \mathbb{E}\{[(1 - P_{\text{d}})\,P_0(h, \hat{g}) + P_{\text{d}}\,P_1(h, \hat{g})]\,(|\hat{g}|^2 + \sigma_e^2)\}.
\end{aligned}
\tag{3.28}
$$

Hence, the optimal power control problem is expressed as

$$
\min_{P_0(h,\hat{g}), P_1(h,\hat{g})} \mathbb{E}\{\lambda P_{\text{HP}}(\mathbf{P}, h, \hat{g}) + (1 - \lambda)P_{\text{LP}}^u(\mathbf{P}, h, \hat{g})\}
\tag{3.29}
$$

$$
\text{subject to } P_0(h, \hat{g}) \leq P_{\text{pk}}, \ P_1(h, \hat{g}) \leq P_{\text{pk}}
\tag{3.30}
$$

$$
\mathbb{E}\{[(1 - P_{\text{d}})\,P_0(h, \hat{g}) + P_{\text{d}}\,P_1(h, \hat{g})]\,(|\hat{g}|^2 + \sigma_e^2)\} \leq Q_{\text{avg}}
\tag{3.31}
$$

where $P_{\text{HP}}(\mathbf{P}, h, \hat{g})$ and $P_{\text{LP}}^u(\mathbf{P}, h, \hat{g})$ are the instantaneous BER expressions for given fading coefficients h and $\hat{g}$. In this setting, the optimal power control scheme is determined as follows:

Proposition 3.3 *The optimal power control scheme subject to the constraints in (3.30) and (3.31) under imperfect CSI of the interference link is given by*

$$
P_{opt}^{(0)}(h, \hat{g}) = \min(P_0^*(h, \hat{g}), P_{\text{pk}}),
\tag{3.32}
$$

$$
P_{opt}^{(1)}(h, \hat{g}) = \min(P_1^*(h, \hat{g}), P_{\text{pk}})
\tag{3.33}
$$

where P_0^* and P_1^* are solutions to the following equations, respectively:

$$
\sum_{j,l=0}^{1} \frac{P(\mathcal{H}_j, \hat{\mathcal{H}}_0)}{4\sqrt{2\pi}} \left\{ \lambda \frac{e^{\frac{-c_{l,0} P_0^* |h|^2}{2\sigma_j^2}}}{\sqrt{\frac{\sigma_j^2 P_0^*}{c_{l,0}|h|^2}}} + (1-\lambda)\rho_l \frac{e^{\frac{-\beta_{l,0} P_0^* |h|^2}{2\sigma_j^2}}}{\sqrt{\frac{\sigma_j^2 P_0^*}{\beta_{l,0}|h|^2}}} \right\} = \mu_1(1 - P_{\text{d}})(|\hat{g}|^2 + \sigma_e^2),
\tag{3.34}
$$

$$
\sum_{j,l=0}^{1} \frac{P(\mathcal{H}_j, \hat{\mathcal{H}}_1)}{4\sqrt{2\pi}} \left\{ \lambda \frac{e^{\frac{-c_{l,1} P_1^* |h|^2}{2\sigma_j^2}}}{\sqrt{\frac{\sigma_j^2 P_1^*}{c_{l,1}|h|^2}}} + (1-\lambda)\rho_l \frac{e^{\frac{-\beta_{l,1} P_1^* |h|^2}{2\sigma_j^2}}}{\sqrt{\frac{\sigma_j^2 P_1^*}{\beta_{l,1}|h|^2}}} \right\} = \mu_1 P_{\text{d}}(|\hat{g}|^2 + \sigma_e^2),
\tag{3.35}
$$

38

where μ_1 is the Lagrange multiplier associated with the average interference power constraints in (3.31).

The proof of Proposition 3.3 is similar to that of Proposition 3.1, and hence it is omitted for brevity.

3.2.1.3 Statistical CSI of both transmission and interference links

Different from the previous subsections where the knowledge (or the estimate) of the instantaneous values of the fading coefficients is available at the secondary transmitter, the secondary transmitter in this case is assumed to know only the statistics of the transmission and interference links, (i.e., only the distributions of the fading coefficients are known). Hence, the optimal power levels are no longer functions of h and g (or $\hat{g}$). Under this assumption, we can formulate the optimization problem as follows:

$$\min_{P_0, P_1} \lambda P_{\mathrm{HP}}(\mathbf{P}) + (1 - \lambda) P_{\mathrm{LP}}(\mathbf{P}) \tag{3.36}$$

subject to

$$P_0 \leq P_{\mathrm{pk}}, \; P_1 \leq P_{\mathrm{pk}} \tag{3.37}$$

$$(1 - P_{\mathrm{d}}) \, P_0 \, \mathbb{E}\{|g|^2\} + P_{\mathrm{d}} \, P_1 \, \mathbb{E}\{|g|^2\} \leq Q_{\mathrm{avg}} \tag{3.38}$$

where $P_{\mathrm{HP}}(\mathbf{P})$ and $P_{\mathrm{LP}}(\mathbf{P})$ are closed-form expressions of the average BER over Nakagami-m fading, given in (3.13) and (3.14), respectively. We solve (3.36) exactly by performing an exhaustive search, which has low complexity due to being performed over a one-dimensional bounded line which defines the boundary of the region of feasible power pairs (P_0, P_1) satisfying (3.37) and (3.38). Additionally, as we describe in the previous subsection, if a convex upper bound on error rates is obtained using a similar approach, convex optimization tools can be employed to find the optimal power levels, $P_{\mathrm{opt}}^{(0)}$ and $P_{\mathrm{opt}}^{(1)}$, that minimize this upper bound.

3.2.2 Average transmit and average interference power constraints

Now, we consider the presence of average transmit and average interference power constraints. We again address the cases of instantaneous and statistical CSI.

3.2.2.1 Perfect CSI of both transmission and interference links

In this case, the optimization problem subject to average transmit power and average interference power constraints is formulated as follows:

$$\min_{P_0(h,g), P_1(h,g)} \mathbb{E}\big\{\lambda P_{\text{HP}}(\mathbf{P}, h) + (1 - \lambda)P_{\text{LP}}(\mathbf{P}, h)\big\} \qquad (3.39)$$

subject to

$$\mathbb{E}\{P(\hat{\mathcal{H}}_0)\, P_0(h,g) + P(\hat{\mathcal{H}}_1)P_1(h,g)\} \leq P_{\text{avg}} \qquad (3.40)$$

$$\mathbb{E}\{(1 - P_{\text{d}})\, P_0(h,g)\, |g|^2 + P_{\text{d}}\, P_1(h,g)\, |g|^2\} \leq Q_{\text{avg}} \qquad (3.41)$$

where P_{avg} denotes the average transmit power limit at the secondary transmitter. Similarly as in the previous subsection, we again consider an upper bound on the BER in the objective function. Under these constraints, the optimal power control scheme is determined as follows:

Proposition 3.4 *The optimal power control policy that minimizes the BER upper bound under the constraints in (3.40) and (3.41) is obtained as*

$$P_{opt}^{(0)} = P_0^*, \; P_{opt}^{(1)} = P_1^* \qquad (3.42)$$

where P_0^* and P_1^* are solutions to the following equations, respectively:

$$\sum_{j,l=0}^{1} \frac{P(\mathcal{H}_j, \hat{\mathcal{H}}_0)}{4\sqrt{2\pi}} \left\{ \lambda \frac{e^{\frac{-c_{l,0} P_0^* |h|^2}{2\sigma_j^2}}}{\sqrt{\frac{\sigma_j^2 P_0^*}{c_{l,0} |h|^2}}} + (1-\lambda)\rho_l \frac{e^{\frac{-\beta_{l,0} P_0^* |h|^2}{2\sigma_j^2}}}{\sqrt{\frac{\sigma_j^2 P_0^*}{\beta_{l,0} |h|^2}}} \right\} = \mu_1(1-P_d)|g|^2 + \mu_2 P(\hat{\mathcal{H}}_0) \qquad (3.43)$$

$$\sum_{j,l=0}^{1} \frac{P(\mathcal{H}_j, \hat{\mathcal{H}}_1)}{4\sqrt{2\pi}} \left\{ \lambda \frac{e^{\frac{-c_{l,1} P_1^* |h|^2}{2\sigma_j^2}}}{\sqrt{\frac{\sigma_j^2 P_1^*}{c_{l,1} |h|^2}}} + (1-\lambda)\rho_l \frac{e^{\frac{-\beta_{l,1} P_1^* |h|^2}{2\sigma_j^2}}}{\sqrt{\frac{\sigma_j^2 P_1^*}{\beta_{l,1} |h|^2}}} \right\} = \mu_1 P_d |g|^2 + \mu_2 P(\hat{\mathcal{H}}_1) \qquad (3.44)$$

where μ_1 and μ_2 are the Lagrange multipliers associated with the average transmit power and average interference power constraints in (3.40) and (3.41), respectively.

Proposition 3.4 is proved similarly as Proposition 3.1, and hence we omit the proof for brevity. Below, we provide Algorithm 2 for obtaining the optimal power levels.

Algorithm 2 The optimal power control algorithm under average transmit power and average interference power constraints

---

1: Initialize $\epsilon, t_1, t_2 > 0$, $\mu_1^{(0)} = \mu_{1,\text{init}}$, $\mu_2^{(0)} = \mu_{2,\text{init}}$, $n = 0$

2: **repeat**

3:   Solve P_0^* and P_1^* in (3.43) and (3.44), respectively by bisection search.

4:   Update μ_1 and μ_2 using the projected subgradient method as follows

5:   $\mu_1^{(n+1)} = \left(\mu_1^{(n)} + t_1 \left(\mathbb{E}\{(1 - P_d) P_0(h, g) |g|^2 + P_d P_1(h, g) |g|^2\} - Q_{\text{avg}} \right) \right)^+$

6:   $\mu_2^{(n+1)} = \left(\mu_2^{(n)} + t_2 \left(\mathbb{E}\{P(\mathcal{H}_0) P_0(h, g) + P(\mathcal{H}_1)P_1(h, g)\} - P_{\text{avg}} \right) \right)^+$

7:   $n \leftarrow n + 1$

8: **until** $|\mu_1^{(n)}(\mathbb{E}\{(1 - P_d) P_0(h, g) |g|^2 + P_d P_1(h, g) |g|^2\} - Q_{\text{avg}})| \le \epsilon$ and

  $|\mu_2^{(n)}(\mathbb{E}\{P(\mathcal{H}_0) P_0(h, g) + P(\mathcal{H}_1)P_1(h, g)\} - P_{\text{avg}})| \le \epsilon$

With slight change in Algorithm 2, we can incorporate a retransmission mechanism into the power control scheme. In particular, we can assume that the transmitter is silent and therefore does not send a packet if the channel fading coefficient is less than a certain threshold, e.g., during deep fading, which lowers the energy consumption.

Hence, the power is set to zero if the channel fading coefficient is below this threshold in Algorithm 2 and the corresponding Lagrange multipliers satisfying the constraints are found. In that case, more power is allocated for favorable channel conditions since the transmitter does not consume power when the channel undergoes deep fading.

Next, we discuss a special case for which we again have closed-form approximations for the optimal power levels.

Proposition 3.5 *At high SNRs, the optimal power control policy minimizing the BER of HP bits, (i.e., when $\lambda = 1$) in the presence of perfect sensing results under the average transmit power constraint in (3.40) and average interference power constraint in (3.41) can be approximated in closed-form as*

$$P_{opt}^{(0)}(h, g) = \frac{\sigma_n^2}{c_{1,0} |h|^2} W_0 \left(\frac{(c_{1,0}|h|^2 P(\mathcal{H}_0))^2}{32\pi(\sigma_n^2 \mu_2 P(\mathcal{H}_0))^2} \right) \tag{3.45}$$

$$P_{opt}^{(1)}(h, g) = \frac{W_0 \left(\frac{(c_{1,1} |h|^2 P(\mathcal{H}_1))^2}{32\pi \left((\sigma_n^2 + \sigma_w^2)(\mu_1|g|^2 + \mu_2 P(\mathcal{H}_1)) \right)^2} \right)}{\frac{c_{1,1}|h|^2}{\sigma_n^2 + \sigma_w^2}}. \tag{3.46}$$

Since the proof of Proposition 3.5 is similar to that of Proposition 3.2, it is omitted for brevity.

3.2.2.2 Perfect CSI of transmission link and imperfect CSI of interference link

In this case, the optimal power control problem is expressed as

$$\min_{P_0(h,\hat{g}),P_1(h,\hat{g})} \mathbb{E}\big\{\lambda P_{\mathrm{HP}}(\mathbf{P}, h, \hat{g}) + (1 - \lambda)P_{\mathrm{LP}}^u(\mathbf{P}, h, \hat{g})\big\} \tag{3.47}$$

subject to

$$\mathbb{E}\{P(\hat{\mathcal{H}}_0)\, P_0(h, \hat{g}) + P(\hat{\mathcal{H}}_1)P_1(h, \hat{g})\} \leq P_{\mathrm{avg}} \tag{3.48}$$

$$\mathbb{E}\{[(1-P_{\mathrm{d}})\, P_0(h, \hat{g}) + P_{\mathrm{d}}\, P_1(h, \hat{g})]\, (|\hat{g}|^2 + \sigma_e^2)\} \leq Q_{\mathrm{avg}}. \tag{3.49}$$

Under the above constraints, the optimal power control scheme is determined in the following:

Proposition 3.6 *The optimal power control scheme subject to average transmit power constraint in (3.48) and average interference power constraint in (3.49) is given by*

$$P_{opt}^{(0)}(h, \hat{g}) = P_0^*, \ P_{opt}^{(1)}(h, \hat{g}) = P_1^* \tag{3.50}$$

where P_0^* and P_1^* are solutions to the following equations, respectively:

$$\sum_{j,l=0}^{1} \frac{P(\mathcal{H}_j, \hat{\mathcal{H}}_0)}{4\sqrt{2\pi}} \left\{ \lambda \frac{e^{\frac{-c_{l,0}P_0^*|h|^2}{2\sigma_j^2}}}{\sqrt{\frac{\sigma_j^2 P_0^*}{c_{l,0}|h|^2}}} + (1-\lambda)\rho_l \frac{e^{\frac{-\beta_{l,0}P_0^*|h|^2}{2\sigma_j^2}}}{\sqrt{\frac{\sigma_j^2 P_0^*}{\beta_{l,0}|h|^2}}} \right\} = \mu_1(1-P_d)(|\hat{g}|^2 + \sigma_e^2) + \mu_2 P(\hat{\mathcal{H}}_0),$$

$$\tag{3.51}$$

$$\sum_{j,l=0}^{1} \frac{P(\mathcal{H}_j, \hat{\mathcal{H}}_1)}{4\sqrt{2\pi}} \left\{ \lambda \frac{e^{\frac{-c_{l,1}P_1^*|h|^2}{2\sigma_j^2}}}{\sqrt{\frac{\sigma_j^2 P_1^*}{c_{l,1}|h|^2}}} + (1-\lambda)\rho_l \frac{e^{\frac{-\beta_{l,1}P_1^*|h|^2}{2\sigma_j^2}}}{\sqrt{\frac{\sigma_j^2 P_1^*}{\beta_{l,1}|h|^2}}} \right\} = \mu_1 P_d(|\hat{g}|^2 + \sigma_e^2) + \mu_2 P(\hat{\mathcal{H}}_1), \quad \tag{3.52}$$

where μ_1 and μ_2 are the Lagrange multipliers associated with the average transmit power and average interference power constraints in (3.48) and (3.49), respectively.

The proof of Proposition 3.6 is similar to that of Proposition 3.1, and therefore, we omitted the proof for brevity.

3.2.2.3 Statistical CSI of both transmission and interference links

In this case, the optimal power control problem is given by

$$\min_{P_0, P_1} \lambda P_{\text{HP}}(\mathbf{P}) + (1 - \lambda)P_{\text{LP}}(\mathbf{P}) \tag{3.53}$$

subject to

$$P(\hat{\mathcal{H}}_0) P_0 + P(\hat{\mathcal{H}}_1)P_1 \leq P_{\text{avg}} \tag{3.54}$$

$$(1 - P_d) P_0 \mathbb{E}\{|g|^2\} + P_d P_1 \mathbb{E}\{|g|^2\} \leq Q_{\text{avg}}. \tag{3.55}$$

(a) P_0 and P_1 vs. P_d (b) N_{re} vs. P_d (c) PSNR vs. P_d
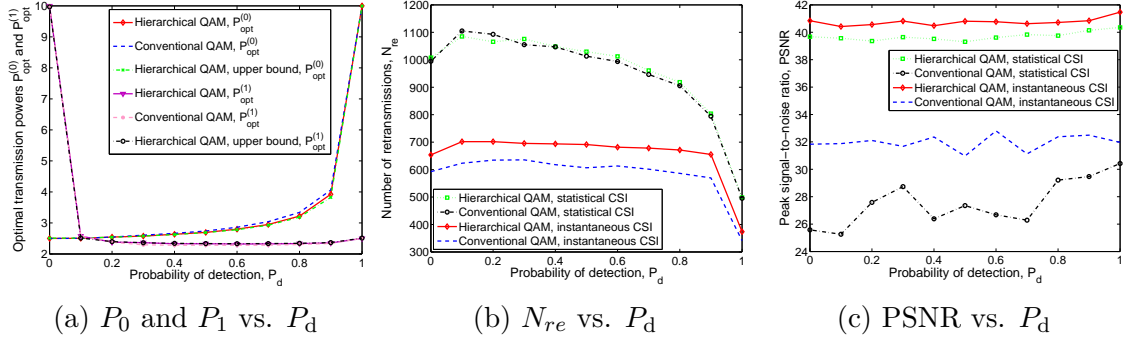
Figure 3.4: (a) Optimal transmission powers P_0 and P_1 vs. P_d; (b) number of retransmissions, N_{re} vs. P_d; (c) Peak signal-to-noise ratio, PSNR vs. P_d.

(a) P_0 and P_1 vs. P_f (b) N_{re} vs. P_f (c) PSNR vs. P_f
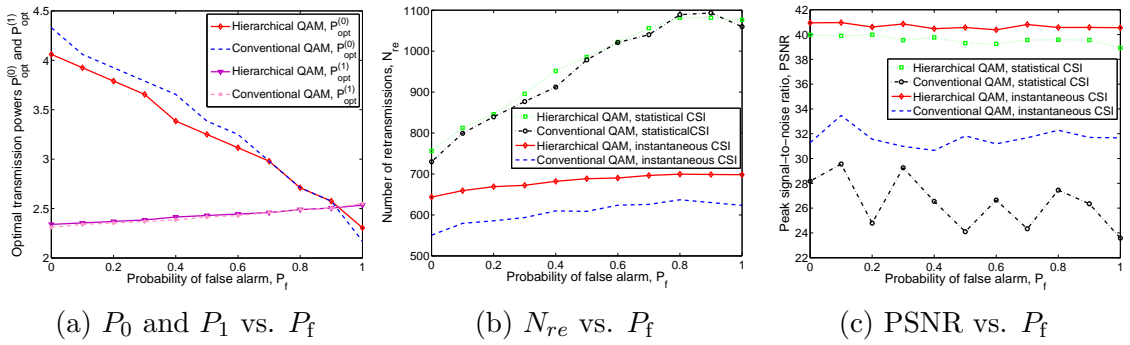
Figure 3.5: (a) Optimal transmission powers P_0 and P_1 vs. P_f; (b) number of retransmissions, N_{re} vs. P_f; (c) Peak signal-to-noise ratio, PSNR vs. P_f.

Similarly as in Section 3.2.1.3, transmission power levels, $P_\mathrm{opt}^{(0)}$ and $P_\mathrm{opt}^{(1)}$ can be obtained numerically by either exhaustive search or by employing convex optimization tools if upper bounds on error rates are considered as the objective function.

3.3   Numerical and Simulation Results

In this section, we perform comprehensive numerical computations and simulations to evaluate the performance of multimedia transmissions of cognitive users with optimal power control and only imperfect sensing results under different severity levels of fading.

3.3.1 Simulation Settings

In the case of image transmission, test image is chosen as the gray-scale "Lena" and "Boat" images with size 512×512 pixels. For video transmission, standard test video sequence "Bus" is used in the simulations. It is assumed that the noise variance is $\sigma_n^2 = 0.01$, the variance of the primary user signal is $\sigma_\omega^2 = 0.5$, the step size t is set to 0.001 and tolerance ϵ is chosen as 10^{-7}. Prior probabilities of the primary users being active and inactive in the channel are set to 0.4 and 0.6, respectively, i.e., $\Pr\{\mathcal{H}_1\} = 0.4$ and $\Pr\{\mathcal{H}_0\} = 0.6$. Unless mentioned explicitly, we also assume that the channel power gains $|h|^2$ and $|g|^2$ follow exponential distributions with unit mean, threshold for retransmission Thr is chosen as 1.8, the peak transmit power constraint is $P_{\text{pk}} = 10$ dB, the average transmit power constraint is $P_{\text{avg}} = 10$ dB, and the average interference power constraint is $Q_{\text{avg}} = 4$ dB. In order to present average simulation results in the presence of randomly-varying fading, results of 50 simulations are averaged.

PSNR is chosen as the performance metric to measure the quality of the reconstructed data. PSNR is defined for an 8-bit-pixel image of size m by n pixels as

$$\text{PSNR} = 10 \log_{10} \left(\frac{255^2}{\frac{1}{mn} \sum_{i=0}^{m-1} \sum_{j=0}^{n-1} (S_{m,n} - \hat{S}_{m,n})^2} \right) \qquad (3.56)$$

where $S_{m,n}$ and $\hat{S}_{m,n}$ denote the pixel intensity values of the original image and the reconstructed image, respectively.

Table 3.1: Peak signal-to-noise ratio, PSNR vs. λ.

λ	0.1	0.3	0.5	0.7	0.9
PSNR	40.1425	40.1425	40.1425	39.8876	39.8876
$P_{0,opt}$	2.809	2.803	2.796	2.789	2.778
$P_{1,opt}$	2.384	2.387	2.390	2.393	2.398

In Table 3.1, we have listed the PSNR values of the test image and the optimal transmission power levels, $P_{0,opt}$ and $P_{1,opt}$, for different values of the weight factor

λ, which determines the contributions of the BERs of HP bits and LP bits in the objective function. Packets are assumed to be modulated by 16-HQAM with $\alpha_0 = \alpha_1 = 1$. The results in the table are obtained based on the statistical CSI subject to the peak transmit power constraint P_{pk}, and average interference power constraint Q_{avg}. It is seen that changing the value of λ does not have significant impact on the PSNR of the reconstructed image. The reason is that giving more or less weight to the BER of HP data in the objective function does not result in much difference in the optimal transmission power levels $P_{0,opt}$ and $P_{1,opt}$ as shown in Table 3.1, which leads to only slight changes in the image quality. A similar trend is also observed when optimal power control with instantaneous CSI is applied. Therefore, for the rest of the simulations, we set $\lambda = 0.5$.

3.3.2 The impact of channel sensing performance on multimedia quality

In this subsection, we analyze the effects of the probabilities of detection and false alarm on the transmission of image and video data in CR systems. For instance, our main observations in Figs. 3.4 and 3.5, which we discuss in detail below, are that as the sensing reliability improves (i.e., detection probability increases or false probability diminishes), the number of retransmissions decreases drastically and PSNR values tend to slightly grow or stay stable. Additionally, employing HQAM instead of conventional QAM and having instantaneous CSI rather than statistical CSI all improve the multimedia quality as evidenced by higher PSNR levels.

More specifically, in Fig. 3.4, we display the optimal power levels (only for the statistical CSI case, obtained either by solving (3.36) through exhaustive search on the boundary of constraints or solving a convex optimization problem using the aforementioned upper bound on BER expressions) and number of retransmissions and PSNR values as a function of the probability of detection, P_{d}. Cognitive users employ either

16-HQAM with $\alpha_0 = \alpha_1 = 1$ or conventional QAM subject to peak transmit power constraint, P_{pk}, and average interference constraint, Q_{avg}. As P_{d} increases while keeping P_{f} fixed to 0.1, we have more reliable sensing performance. In this case, the cognitive users transmit at higher power, P_0, in an idle-sensed channel. In particular, P_0 takes its maximum value P_{pk} when $P_{\mathrm{d}} = 1$. Since more reliable sensing enables the cognitive user to transmit at higher power level, the number of retransmissions decreases with increasing P_{d} for both scenarios where power control is performed based on either the statistical CSI or instantaneous CSI. On the other hand, it is seen that PSNR performance, while showing a slight tendency to improve with increasing P_{d}, is relatively robust to variations in P_{d}, mainly due to the presence of the retransmission mechanism. In particular, we notice that approximately the same PSNR value can be attained in the presence of increased sensing uncertainty (i.e., lower P_{d}) at the cost of higher number of retransmissions under both scenarios[1]. In the figure, it is also observed that HQAM gives better PSNR performance compared to conventional QAM since HP data is protected better in HQAM signaling. Notice that this improved performance is achieved interestingly with similar number of retransmission requests and at similar power levels. It is also seen that the difference between the optimal transmission power levels obtained by solving (3.36) exactly or using an upper bound on the objective function obtained by eliminating the Q functions with negative weights is very small. Hence, we can conclude that the upper bound on BER expressions can effectively be used to determine the transmission power levels P_0 and P_1 by using standard convex optimization tools.

In Fig. 3.5, we plot the optimal power levels (only for the statistical CSI case, obtained either by solving (3.36) through exhaustive search on the boundary of constraints or solving a convex optimization problem using the aforementioned upper

---

[1]Instead, if no retransmissions are allowed or a certain upper bound on the number of retransmissions is imposed, PNSR increases as P_{d} increases. Hence, we will have better image quality as the sensing performance improves.

bound on BER expressions) and number of retransmissions and PSNR values as a function of the probability of false alarm, P_f. As P_f increases while keeping P_d fixed at 0.9, the cognitive users experience false alarm events more frequently. We notice that unless the false alarm probability P_f is close to 1, P_1 is generally smaller than P_0 in order to protect the primary users by limiting the interference in a busy-sensed channel. We also note that initially as P_f increases, cognitive secondary users more often misperceive an idle channel as busy and consequently transmit unnecessarily at the lower power level of P_1 instead of P_0. In addition, the optimal value of P_0 diminishes with increasing P_f. As a result, as seen in Fig. 3.5b, the number of retransmissions increases due to these low transmission power levels when P_f increases. When P_f is close to 1, the number of retransmissions levels off and even slightly decreases as P_1 exceeds P_0. Again, PNSR quality does not get affected much with changing P_f due to the same reasoning explained in the discussion of the impact of P_d. Also, hierarchical QAM again outperforms conventional QAM in terms of PSNR. Another important remark is that when instantaneous CSI is used to determine the optimal power levels, the secondary users obtain better image quality with smaller number of retransmissions compared to that attained by optimal power levels based only on the statistical CSI. More specifically, up to 6 dB improvement in PSNR is achieved and the number of retransmissions is reduced by nearly half. We note that similar results are observed when average transmit power and average interference power constraints are imposed. However, we have not included the corresponding simulation results for the sake of brevity.

In Fig. 3.6, we plot average BERs of HP bits and LP bits as a function of the detection probability, P_d, (left subfigure) and false alarm probability, P_f (right subfigure). We consider the cases in which either peak transmit power/average interference power constraints denoted by $(P_\mathrm{pk}, Q_\mathrm{avg})$ or average transmit power/average interference power constraints denoted by $(P_\mathrm{avg}, Q_\mathrm{avg})$ are imposed. Optimal power allocation

(a) Average BER vs. P_{d}
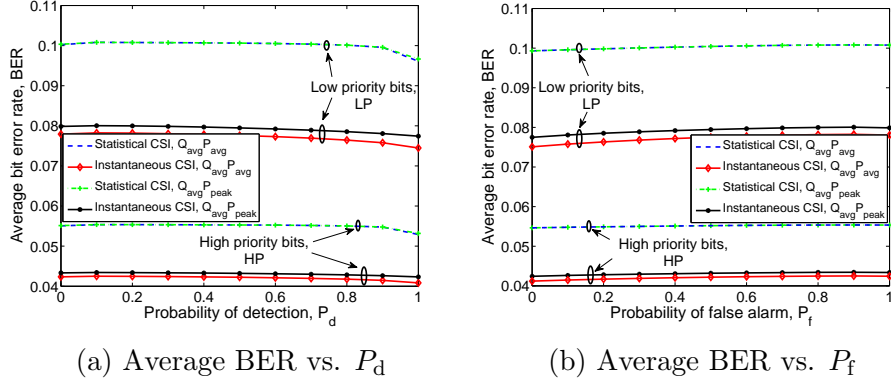
(b) Average BER vs. P_{f}

Figure 3.6: (a) Average BER vs. probability of detection, P_{d}; (b) Average BER vs. probability of false alarm, P_{f}.

is performed by assuming the availability of either instantaneous CSI or statistical CSI at the secondary transmitter. In the left subfigure, as P_{d} increases while keeping P_{f} fixed to 0.1, average BERs of HP bits and LP bits decrease. In the right subfigure, where $P_{\mathrm{d}} = 0.9$, BER performance deteriorates with increasing P_{f} because of the same reasoning explained in the discussion of Fig. 3.5. It is also seen that power control with instantaneous CSI yields better BER performance than power allocation with statistical CSI. In addition, power control with instantaneous CSI under average transmit power constraint provides smaller BERs for both HP bits and LP bits compared to that attained under peak transmit power limitations since average transmit power constraint is more flexible than the peak transmit power constraint. In contrast, if power allocation based on statistical CSI is applied, BERs of HP bits are the same for all values of P_{f} and P_{d} (except when $P_{\mathrm{d}} = 0$ or 1) under both $(P_{\mathrm{pk}}, Q_{\mathrm{avg}})$ and $(P_{\mathrm{avg}}, Q_{\mathrm{avg}})$ constraints since optimal power levels are determined by only the average interference constraints rather than the peak/average transmit power constraints. For $P_{\mathrm{d}} = 0$ or 1, the peak transmit power constraint limits the power levels and average transmit power constraint determines the optimal power levels along with the average interference constraint, which leads to different BERs for HP bits. As seen in Fig. 3.6b, the same trend is also observed for BERs for LP bits.
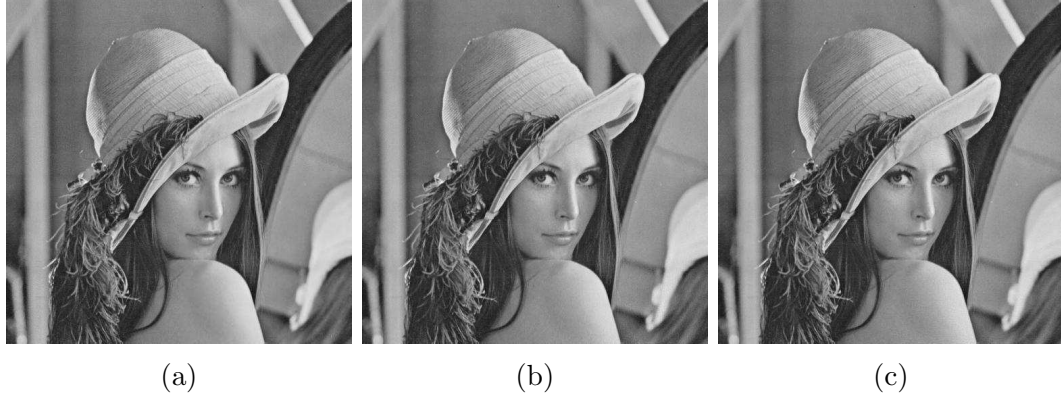
Figure 3.7: Reconstructed images with (a) $P_\mathrm{d} = 0.5$, $P_\mathrm{f} = 0$, PSNR $= 39.3902$ and $N_\mathrm{re} = 1013$; (b) $P_\mathrm{d} = 1$, $P_\mathrm{f} = 0$, PSNR $= 40.5357$ and $N_\mathrm{re} = 452$; (c) $P_\mathrm{d} = 1$, $P_\mathrm{f} = 0.2$, PSNR $= 40.2706$ and $N_\mathrm{re} = 541$.

In Fig. 3.7, the reconstructed images for different values of P_f and P_d are displayed while power allocation is performed based on the statistical CSI subject to peak transmit power and average interference constraints. It is assumed that there is no upper bound on the number of retransmissions and 16-HQAM with $\alpha_0 = \alpha_1 = 1$ is employed. It is seen that the received image quality for each scenario is nearly the same. Indeed, their PSNRs are around 40 dB. However, the number of retransmissions is different in each scenario. In perfect sensing, i.e., when $P_\mathrm{d} = 1$ and $P_\mathrm{f} = 0$, we have the least number of retransmissions with $N_\mathrm{re} = 452$. On the other hand, in the case of $P_\mathrm{d} = 0.5$ and $P_\mathrm{f} = 0$, a similar received image quality is attained with $N_\mathrm{re} = 1013$ retransmissions. Note that this significant increase in N_re implies higher delays and higher energy expenditure. Under the same setting, we have performed simulations for other cases where power control with instantaneous CSI rather than statistical CSI is applied or average transmit power/interference power constraints are imposed instead of peak transmit power/average interference power constraints. Due to the sake of brevity, the corresponding results are not displayed but we have the following important observations:

- When power control with instantaneous CSI is applied under the same power constraints, PSNR performance is improved by around 1 dB with up to 49%

50

Figure 3.8: Reconstructed images with (a) $P_{\mathrm{f}} = 0.2$, $P_{\mathrm{d}} = 0.5$, PSNR $= 22.4303$ and $N_{\mathrm{re}} = 800$; (b) $P_{\mathrm{f}} = 0.2$, $P_{\mathrm{d}} = 0.7$, PSNR $= 22.7172$ and $N_{\mathrm{re}} = 800$; (c) $P_{\mathrm{f}} = 0.2$, $P_{\mathrm{d}} = 1$, PSNR $= 40.3389$ and $N_{\mathrm{re}} = 545$; (d) $P_{\mathrm{f}} = 0.1$, $P_{\mathrm{d}} = 0.5$, PSNR $= 22.5194$ and $N_{\mathrm{re}} = 800$; (e) $P_{\mathrm{f}} = 0.1$, $P_{\mathrm{d}} = 0.7$, PSNR $= 24.6407$ and $N_{\mathrm{re}} = 800$; (f) $P_{\mathrm{f}} = 0.1$, $P_{\mathrm{d}} = 1$, PSNR $= 40.349$ and $N_{\mathrm{re}} = 498$.

reduction in the number of retransmissions, yielding lower retransmission delay compared to power allocation with statistical CSI.

- When optimal power allocation with statistical CSI is performed, imposing either peak transmit power constraint or average transmit power constraint provides nearly the same PSNR performance. However, the impact on the number of retransmissions is profound especially when instantaneous CSI is employed and sensing result is reliable, e.g., the number of retransmissions is reduced by up to 47%.

In Fig. 3.8, the reconstructed images for different values of P_{f} and P_{d} are shown. The statistical CSI is used to determine the optimal power levels. Different from the

(a) Imperfect sensing   (b) Perfect sensing

Figure 3.9: (a) Imperfect channel sensing with $P_d = 0.8$, $P_f = 0.2$, PSNR = 15.3170 dB and $N_{re} = 3059$ (b) Perfect channel sensing with $P_d = 1$, $P_f = 0$, PSNR = 15.6711 dB and $N_{re} = 889$.

previous figure, we now set an upper bound on the number of retransmissions, i.e., $N_{upper} = 800$. Cognitive transmission is again subject to peak power and average interference constraints. In contrast to the previous reconstructed images, for which PSNR is nearly the same, the received quality is now affected by the channel sensing performance. More specifically, as P_d increases and hence sensing reliability improves, PSNR increases and the received image quality becomes better. On the other hand, increasing P_f results in lower PSNR values. In Fig. 3.8, we also observe that the degradation in the image quality is generally in the lower right portion of the images. This is due to the fact that this part of the image is transmitted the last by which time the number of retransmissions has generally reached the upper bound and no more retransmissions are allowed.

In Fig. 3.9, we display a single frame from the received video with both imperfect sensing (i.e., $P_d = 0.8$, $P_f = 0.2$) and perfect sensing ($P_d = 1$, $P_f = 0$) subject to average transmit power and average interference constraints. Power control based on instantaneous CSI is applied. In the simulation of our video transmissions, cognitive users again employ 16-HQAM with $\alpha_0 = \alpha_1 = 1$ for transmission. Threshold for transmission, Thr, is set to 2.1. More retransmissions are required when sensing is imperfect. The averages of PSNR and N_{re} values are obtained by simulating the
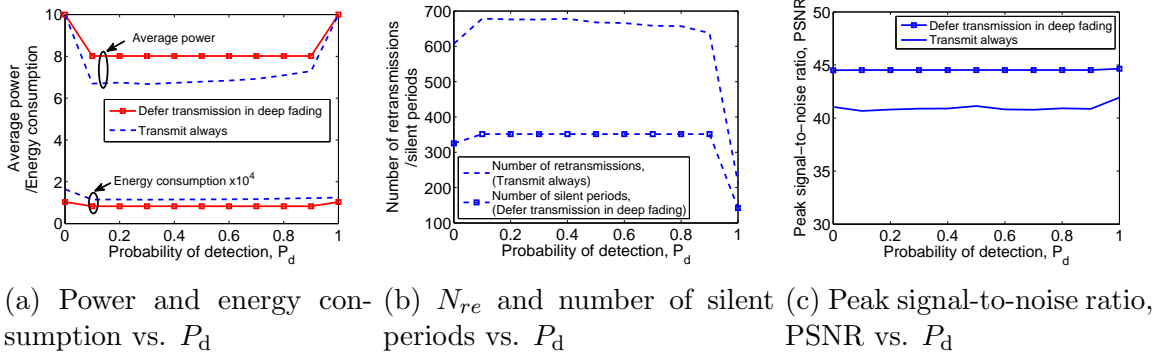
(a) Power and energy consumption vs. P_d

(b) N_{re} and number of silent periods vs. P_d

(c) Peak signal-to-noise ratio, PSNR vs. P_d

Figure 3.10: (a) Average energy and power consumption vs. probability of detection, P_d; (b) Number of retransmissions/silent periods vs. P_d; (c) Peak signal-to-noise ratio, PSNR vs. P_d.
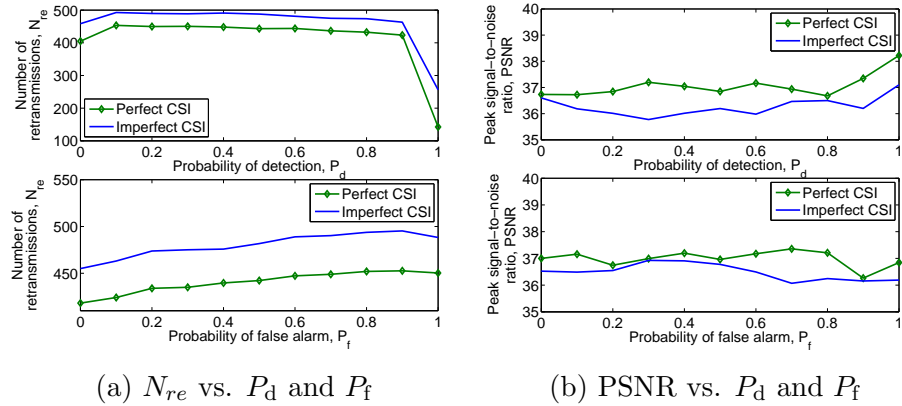
(a) N_{re} vs. P_d and P_f

(b) PSNR vs. P_d and P_f

Figure 3.11: (a) Number of retransmissions, N_{re} vs. P_d and P_f; (b) Peak signal-to-noise ratio, PSNR vs. P_d and P_f.

wireless transmission of the same video sequence 60 times. In Fig. 3.9, the 11th frame out of 60 frames in the video sequence is displayed in both cases. We observe that while image quality is similar under imperfect and perfect sensing decisions, imperfect sensing can have substantial impact on the number of retransmissions. We also analyze power allocation with statistical CSI, which gives almost the same PSNR value at the cost of higher number of retransmissions, e.g., around 49% higher under imperfect sensing and around 100% higher under perfect sensing.

In Fig. 3.10, we plot the average power and energy consumption, number of retransmissions/silent periods, and PSNR as a function of detection probability P_d. It is assumed that $P_f = 0.1$. We consider two cases: either the packets are always

transmitted or there is no packet transmission during deep fades. It is seen that we have less energy consumption, smaller number of retransmissions or silent periods, and better PSNR performance when there is no transmission in deep fading since the transmitter does not unnecessarily use power budget in case of unfavorable channel conditions and allocates more power to better channels.

3.3.3 The impact of imperfect CSI of interference link on multimedia transmission

In this section, we analyze the performance of multimedia transmission in the presence of imperfect CSI of the interference link subject to average transmit power and average interference power constraints. It is assumed that the variance of the estimation error is $\sigma_e^2 = 0.0124$. In Fig. 3.11, we plot the number of retransmissions and PSNR as a function of the probability of detection and probability of false alarm. It is seen that having perfect CSI of the interference link results in a smaller number of retransmissions and higher PSNR as compared to having only imperfect CSI of this link, as expected. It is also observed that the number of retransmissions increases with increasing P_f or decreasing P_d due to the same reasoning explained in the discussions of Fig. 3.4 and Fig. 3.5.

3.3.4 The impact of unequal error protection (HQAM) vs. equal error protection (conventional QAM) on multimedia quality

While the improvements with the use of HQAM rather than QAM have already been pointed out, we in this subsection further compare the performances of image and video transmissions with conventional QAM and HQAM. In Fig. 3.12, we display the reconstructed images for different values of the fading parameter m when conventional
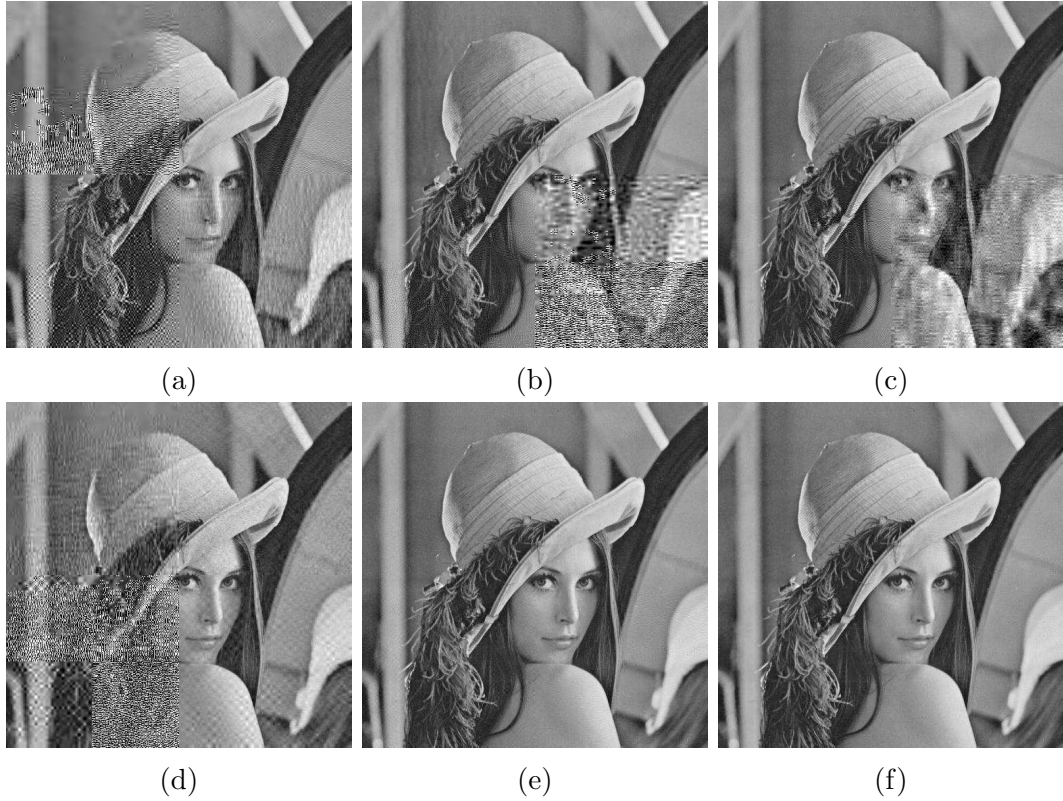
Figure 3.12: Reconstructed images with (a) QAM, $m = 1$, PSNR = 18.8928 and $N_{\text{re}} = 410$; (b) HQAM, $m = 1$, $\alpha_0 = \alpha_1 = 1$, PSNR = 21.3205 and $N_{\text{re}} = 410$; (c) HQAM, $m = 1$, $\alpha_0 = \alpha_1 = 2$, PSNR = 22.4221 and $N_{\text{re}} = 410$; (d) QAM, $m = 2$, PSNR = 19.1760 and $N_{\text{re}} = 396$; (e) HQAM, $m = 2$, $\alpha_0 = \alpha_1 = 1$, PSNR = 35.6625 and $N_{\text{re}} = 400$; (f) HQAM, $m = 2$, $\alpha_0 = \alpha_1 = 2$, PSNR = 37.8730 and $N_{\text{re}} = 366$.

| (a) | (b) | (c) | (d) |
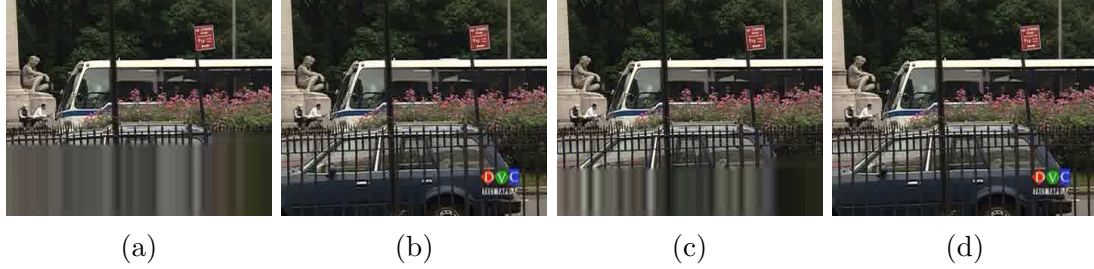
Figure 3.13: Video transmission based on power control with (a) statistical CSI and conventional QAM, PSNR = 12.4644 and N_{re} = 3694; (b) statistical CSI and hierarchical QAM, PSNR = 15.1463 and N_{re} = 3855; (c) instantaneous CSI and conventional QAM, PSNR = 14.4713 and N_{re} = 2492; (d) instantaneous CSI and hierarchical QAM, PSNR = 15.4607 and N_{re} = 2976.

QAM and HQAM with different values of α are employed, in which we consider the same modulation parameter in both sensing decisions, i.e., $\alpha_0 = \alpha_1 = \alpha$. It is assumed that power allocation with statistical CSI is applied. All image data is protected equally with conventional QAM. On the other hand, critical bits, i.e., HP bits receive higher protection with HQAM. With this, we see in the figure that HQAM generally provides better image quality when compared to conventional QAM signaling. This is further confirmed with the higher PSNR values for HQAM. We also observe that increasing α_i from 1 to 2 (i.e., increasing the protection level of HP bits) results in even higher PSNR values. Finally, we see that the received image quality expectedly improves as the fading parameter m is increased from 1 to 2 for which we have more favorable fading conditions. In our additional simulations, we have observed that as fading becomes more severe, employing power control with instantaneous CSI substantially affects the PSNR performance, e.g., we see around 9 dB of improvement over power allocation with statistical CSI. On the other hand, when fading is less severe, there is only a slight change in image quality when power control based on either instantaneous CSI or statistical CSI is performed.

In Fig. 3.13, we display a single frame from the reconstructed video sequences which are transmitted by using conventional QAM and HQAM with power control applied based on either statistical CSI or instantaneous CSI. Imperfect sensing with

$P_{\mathrm{d}} = 0.9$, and $P_{\mathrm{f}} = 0.1$ is considered. It is also assumed that $P_{\mathrm{avg}} = 10$ dB, $Q_{\mathrm{avg}} = 4$ dB, and $Thr = 2.1$. The 11th frame of the video sequence is shown. While the average numbers of retransmissions for both modulation schemes are close to each other, it is seen that HQAM can lead to significant improvements in video quality compared to conventional QAM. Also, it is observed that applying optimal power control with instantaneous CSI reduces the number of retransmissions and improves the PSNR performance. In addition, when average transmit power and average interference power constraints are imposed, nearly the same PSNR values are obtained with smaller number of retransmissions.

In Fig. 3.14, we display PSNR values as a function of α_0 when $P_{\mathrm{d}} = 0.9$ and $P_{\mathrm{f}} = 0.1$. We set $\alpha_1 = 1$ for busy sensing decision and change the values of α_0 for idle sensing decision. In the figure, we consider confidence intervals in which the confidence level is set to 95%. Average transmit power and average interference power constraints are imposed, it is assumed that $Thr = 1.8$, and instantaneous CSI is utilized in power control. It is observed that PSNR performance first improves with increasing α_0 since the distance between quadrants increases, which leads to higher protection for HP data and hence lower BERs for HP bits. By further increasing α_0, the image quality does not significantly change. This is because HP data is already protected well and BER of HP bits is much smaller than the BER of LP data bits. Hence, allocating more power to the HP data bits does not substantially affect the BER of HP data bits, which leads to almost constant PSNR values. Similar trends are also observed under peak transmit power and average interference power constraints.

In Table 3.2, we have listed BERs of HP bits and LP bits, and PSNR values when exact optimal power control and approximate power control given in Propositions 3.2 and 3.4 at high SNR levels are employed under perfect sensing subject to different peak transmit power/average interference power and average transmit power/average interference power constraints. It is seen that exact and approximate power levels
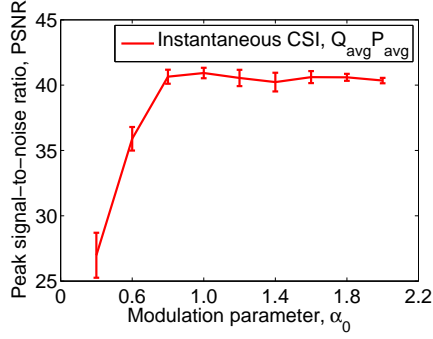
Figure 3.14: Peak signal-to-noise ratio, PSNR as a function of α_0.

Table 3.2: Performance comparison of optimal power controls (exact and approximate)

		$(P_{\text{avg}}, Q_{\text{avg}})$ dB		$(P_{\text{pk}}, Q_{\text{avg}})$ dB	
		$(10,4)$	$(15,9)$	$(10,4)$	$(15,9)$
BER	App.	0.0428	0.0182	0.044	0.0186
of HP bits	Exact	0.0404	0.0174	0.042	0.0178
BER	App.	0.0752	0.0334	0.0782	0.0344
of LP bits	Exact	0.074	0.033	0.0772	0.034
PSNR	App.	41.9002	44.7711	41.1324	44.5025
	Exact	42.8420	46.3720	42.2010	45.3714

result in very similar error rates and PSNR performances at moderate and high SNRs, which is in agreement with Propositions 3.2 and 3.4. Hence, instead of solving the exact optimal power control by bisection search, we can employ the approximate power control given in terms of the Lambert-W function, which is easier to evaluate.

Chapter 4

Multimedia Transmission over Device-to-Device Wireless Links

This chapter studies the performance of hierarchical modulation-based image transmission in device-to-device (D2D) cellular wireless networks under constraints on both transmit and interference power levels. Hierarchical quadrature amplitude modulation (HQAM) is considered in which high priority (HP) data is protected more than low priority (LP) data. In this setting, closed-form bit error rate (BER) expressions for HP data and LP data are derived over multiple Rayleigh fading subchannels in three different transmission modes. The optimal power control that minimizes weighted sum of average BERs of HP bits and LP bits or its upper bound subject to average transmit power and average interference power constraints is derived. Performance comparisons of image transmission in 3 different modes are carried out, and the proposed power control strategies are evaluated in terms of the BERs and received data quality.
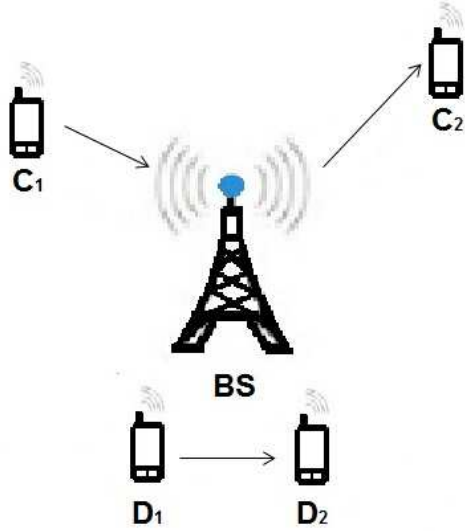
Figure 4.1: System model for D2D communication.

4.1 System Model

We consider a D2D-enabled cellular wireless system with a single base station (BS), which serves one pair of CUs denoted by $\{C_1, C_2\}$ as illustrated in Fig. 4.1. There also exists a pair of DUs denoted by $\{D_1, D_2\}$. The result of mode selection determines whether the pair of DUs communicate directly or via the BS, and whether to use dedicated channels or reuse the channels of CUs under the minimum BER analysis. There are three communication modes for DUs.

- *Cellular mode*: DUs communicate (like CUs) through the BS. Hence, in this mode, DUs communicate over two links, namely uplink from device transmitter (DT) to BS and downlink from BS to device receiver (DR). Channel resources to all users are allocated orthogonally.

- *Dedicated mode*: DUs communicate with each other directly over dedicated channels not used by the CUs. Hence, channels are again orthogonally allocated but the DUs communicate over one direct link. Hence, more spectral resources compared to *cellular mode* are available.

- *Reuse mode*: DUs communicate directly by reusing the channels that are occupied by CUs. This mode further improves the spectrum utilization, but the resulting co-channel interference should be managed properly in order to guarantee the performance of the DUs and CUs. We assume that the D2D pair reuses only the uplink channels of CUs since interference in the cellular network can be better handled in uplink than in downlink.

Considering an orthogonal frequency-division multiple-access (OFDMA) setting, we assume that there is a fixed number of subchannels to be equally allocated to uplink, downlink, and D2D direct link depending on the selected mode. More specifically, assume that there are N subchannels in total. In the cellular mode, we have two uplinks and two downlinks as both CUs and DUs communicate via the BS. Each link is allocated $K = N/4$ subchannels. In the dedicated mode, we have an uplink, downlink, and a direct link, each having $K = N/3$ subchannels. Finally, in the reuse mode, uplink and downlink each have $N/2$ subchannels and DUs communicate over the $K = N/2$ uplink subchannels. While the analysis is for an arbitrary number of subchannels, we set $N = 12$ in the numerical results.

It is assumed that the device transmitter (DT) sends the same data through all the allocated subchannels and diversity combining is considered in order to increase the overall received power. It is assumed that the MRC is employed in our channel model. Under this assumption, the channel input-output relation is given by

$$
\begin{aligned}
y &= \sum_{i=1}^{K} a_i r_i \\
&= \sum_{i=1}^{K} h_i^* (\sqrt{P_i} h_i s + n_i + w_i) \\
&= \sum_{i=1}^{K} |h_i|^2 \sqrt{P_i} s + \sum_{i=1}^{K} h_i^* (n_i + w_i).
\end{aligned}
\tag{4.1}
$$

Above, s and y are the complex-valued transmitted and received signals, respectively

and w_i denotes the received interference distributed according to a circularly symmetric complex Gaussian distribution with zero mean and variance $\sigma_{w_i}^2$. Note that this interference term exists only in the *reuse mode* and is due to transmission from the cellular transmitter (CT). Also, n_i above represents the circularly symmetric complex background Gaussian noise with zero mean and variance $\sigma_{n_i}^2$. In addition, h_i is the channel fading coefficient of the transmission link between the DT and the DR. P_i is the power allocated to each subchannel. It is relatively straightforward to prove that power proportionally allocated to each subchannel according to $\frac{P_1}{\sigma_{n_1}^2 + \sigma_{w_1}^2} = \frac{P_2}{\sigma_{n_2}^2 + \sigma_{w_2}^2} = \cdots = \frac{P_K}{\sigma_{n_K}^2 + \sigma_{w_K}^2}$ achieves the maximum SNR of the received signal under the total power constraint. It is further assumed that n_i and w_i are independent and identically distributed (i.i.d.) for $i = 1, 2, \ldots, K$ with variances σ_n^2 and σ_w^2, respectively. h_i is also i.i.d., and $z_i = |h_i|^2$ is the power gain of the i-th subchannel. Under these assumptions, equal power allocation achieves the maximum SNR.

JPEG2000 image coder, which consists of a sequence of marker segments and layers with unequal importance [70] is chosen as the compression technique for image transmission, and channel coding based on Turbo codes [71] is employed in order to enhance the resilience of the compressed data to wireless channel impairments, e.g., noise, interference from other users, and fading.

4.2 Bit Error Rate Analysis and Power Control Strategy

4.2.1 Bit error rate analysis

DU is assumed to employ 16-HQAM, which provides two priority layers, HP and LP. The 16-HQAM constellation is shown as 2.1 in Chapter 2.1. It is assumed that

the perfect knowledge of the fading realizations are available at the BS and device receiver. Under these assumptions, the optimal MAP decision rule for any arbitrary M-ary digital modulation is employed. It was shown in [72] that the midpoints between the signal constellation points are optimal thresholds for rectangular QAM signaling in the presence of channel sensing errors. Since HQAM is a modification of conventional QAM primarily through the new bit assignment scheme, the optimal detector structure in HQAM is the same as in QAM signaling. For given fading coefficients, $\sum_{i=1}^{K} h_i^*(n_i + w_i)$ is distributed with zero mean and variance $\sum_{i=1}^{K} z_i(\sigma_n^2 + \sigma_w^2)$. Under these assumptions and denoting $\gamma_{dd} = \sum_{i=1}^{K} z_{dd,i}$ (where z_{dd} is the fading power in the D2D direct link), the BERs of HP data for given subchannel power gains in dedicated mode and reuse mode can be expressed as

$$P_{\mathrm{HP}}(P_d^*, \gamma_{dd}) = \frac{1}{2} \sum_{i=0}^{1} Q\left(\sqrt{\frac{c_i P_d^* \gamma_{dd}}{(\sigma_{dd}^2 + \sigma_w^2)}} \right) \tag{4.2}$$

where $c_0 = \frac{\alpha^2}{(\alpha+1)^2+1}$ and $c_1 = \frac{(\alpha+2)^2}{(\alpha+1)^2+1}$. σ_{dd}^2 is the noise power at the device receiver (DR), $\sigma_w^2 = 0$ in dedicated mode and $\sigma_w^2 = P_c Z_{cd}$ in reuse mode, where Z_{cd} is the average channel power gain between the cellular transmitter and device receiver. Also, $Q(x) = \int_x^\infty \frac{1}{\sqrt{2\pi}} e^{-t^2/2} dt$ is the Gaussian Q-function. $P_d^* = P_d$ in dedicated mode. On the other hand, there is an interference constraint in the reuse mode. At the BS, the interference from DT cannot exceed the predefined threshold Q_{avg}, which means $Z_{db} P_d^* \leq Q_{\mathrm{avg}}$, where Z_{db} is the average channel power gain between device transmitter and BS. Thus, for the constant transmit power case, $P_d^* = \min(P_d, \frac{Q_{\mathrm{avg}}}{Z_{db}})$.

LP bits correspond to the two least significant bits in the signal constellation. Thus, BER of LP bits can be determined as in (4.3) at the top of next page.

To simplify the calculation, we assume that z_i are i.i.d. exponentially distributed with mean Z_{dd} in dedicated mode and reuse mode. Let $f(\gamma_{dd})$ denote the pdf of γ_{dd}. Then, $f(\gamma_{dd}) = \frac{e^{-\frac{\gamma_{dd}}{Z_{dd}}} \gamma_{dd}^{K-1}}{(K-1)! Z_{dd}^K}$. The averaged BERs of HP bits and LP bits can be

$$P_{\mathrm{LP}}(P_d^*, \mathbf{z}) = \frac{1}{2}\left\{ 2Q\left(\sqrt{\frac{\beta_0 P_d^* \gamma_{dd}}{(\sigma_{dd}^2 + \sigma_w^2)}}\right) + Q\left(\sqrt{\frac{\beta_1 P_d^* \gamma_{dd}}{(\sigma_{dd}^2 + \sigma_w^2)}}\right) - Q\left(\sqrt{\frac{\beta_2 P_d^* \gamma_{dd}}{(\sigma_{dd}^2 + \sigma_w^2)}}\right) \right\} \tag{4.3}$$

$$\text{where } \beta_0 = \frac{1}{(\alpha+1)^2+1} \quad \beta_1 = \frac{(2\alpha+1)^2}{(\alpha+1)^2+1} \quad \beta_2 = \frac{(2\alpha+3)^2}{(\alpha+1)^2+1}.$$

determined from the expectations

$$P_{\mathrm{HP}}(P_d) = \mathbb{E}_{\gamma_{dd}}\{P_{\mathrm{HP}}(P_d, \gamma_{dd})\}, \tag{4.4}$$

$$P_{\mathrm{LP}}(P_d) = \mathbb{E}_{\gamma_{dd}}\{P_{\mathrm{LP}}(P_d, \gamma_{dd})\}. \tag{4.5}$$

In the cellular mode, BERs in uplink and downlink separately can be obtained similarly as in the dedicated mode with no interference.

Our goal is to find the minimum weighted sum of BERs of HP bits and LP bits among all three modes. The overall BER can be expressed as

$$\mathrm{BER} = \lambda P_{\mathrm{HP}} + (1 - \lambda)P_{\mathrm{LP}} \tag{4.6}$$

where λ is the weight for HP bits.

4.2.2 Power control strategy

In this section, we characterize the optimal power control policies that minimize the weighted sum of BERs of HP bits and LP bits or its upper bound subject to average transmit power and average interference power constraints, assuming the availability the instantaneous CSI of the transmission link and interference link at the DT.

Since there is no interference in cellular and dedicated modes, the optimization

problem can be formulated as

$$\min_{P(\gamma)} \mathbb{E}\big\{\lambda P_{\mathrm{HP}}(\mathbf{P},\gamma) + (1-\lambda)P_{\mathrm{LP}}(\mathbf{P},\gamma)\big\} \tag{4.7}$$

$$\text{subject to } \mathbb{E}\big\{P(\gamma)\big\} \leq P_{\mathrm{avg}} \tag{4.8}$$

Note that the objective function in (4.7), or in particular $P_{\mathrm{LP}}(\mathbf{P},\gamma)$, consists of a sum of Gaussian Q functions with positive and negative weights. Therefore, the Hessian of the objective function is not necessarily positive semidefinite due to the sum of exponential functions with different positive and negative weights. On the other hand, by removing the negative-weighted Q functions in (4.3), we can obtain an upper bound on the BER expression in the objective function. Now, being composed of only positive weighted sum of Q functions that are convex for positive arguments, this upper bound is convex. Therefore, the minimization problem becomes convex with affine constraints in (4.8). In the following result, we identify the optimal power control scheme that minimizes this upper bound.

Proposition 4.1 *The optimal power control policy that minimizes the BER upper bound under the constraint in (4.8) is given by the solution of*

$$\sum_{l=0}^{1} \frac{1}{2\sqrt{2\pi}} \left\{ \lambda \frac{e^{\frac{-c_l P^* \gamma}{2\sigma^{*2}}}}{\sqrt{\frac{\sigma^{*2} P^*}{c_l \gamma}}} + (1-\lambda)\rho_l \frac{e^{\frac{-\beta_l P^* \gamma}{2\sigma^{*2}}}}{\sqrt{\frac{\sigma^{*2} P^*}{\beta_l \gamma}}} \right\} = \mu \tag{4.9}$$

Above, $\rho_0 = 2$, $\rho_1 = 1$, and μ is the Lagrange multiplier, which can be determined by satisfying the average power constraint in (4.8) with equality. $P^* = P_d(\gamma), \sigma^* = \sigma_{dd}$ in dedicated mode, and $P^* = P_d(\gamma), \sigma^* = \sigma_{db}$ for the uplink and $P^* = P_b(\gamma), \sigma^* = \sigma_{bd}$ for the downlink in cellular mode.

We note that there is an interference constraint in the reuse mode. Now, in this mode, under the average transmit power and average interference constraints, the

optimization problem can be expressed as

$$\min_{P_d(\gamma_{dd}, \gamma_{db})} \mathbb{E}\big\{\lambda P_{\mathrm{HP}}(\mathbf{P}, \gamma_{dd}, \gamma_{db}) + (1-\lambda)P_{\mathrm{LP}}(\mathbf{P}, \gamma_{dd}, \gamma_{db})\big\} \tag{4.10}$$

subject to

$$\mathbb{E}\big\{P_d(\gamma_{dd}, \gamma_{db})\big\} \leq P_{\mathrm{avg}} \tag{4.11}$$

$$\mathbb{E}\big\{P_d(\gamma_{dd}, \gamma_{db})\gamma_{db}\big\} \leq Q_{\mathrm{avg}} \tag{4.12}$$

Optimal power control is characterized by the following result.

Proposition 4.2 *The optimal power control policy that minimizes the BER upper bound under the constraints in (4.11) and (4.12) is given by the solution of*

$$\sum_{l=0}^{1} \frac{1}{2\sqrt{2\pi}}\left\{\lambda \frac{e^{\frac{-c_l P_d \gamma_{dd}}{2(\sigma_{dd}^2 + \sigma_w^2)}}}{\sqrt{\frac{(\sigma_{dd}^2 + \sigma_w^2)P_d}{c_l \gamma_{dd}}}} + (1-\lambda)\rho_l \frac{e^{\frac{-\beta_l P_d \gamma_{dd}}{2(\sigma_{dd}^2 + \sigma_w^2)}}}{\sqrt{\frac{(\sigma_{dd}^2 + \sigma_w^2)P_d}{\beta_l \gamma_{dd}}}}\right\} = \mu_1 + \mu_2 \gamma_{db} \tag{4.13}$$

where μ_1 and μ_2 are the Lagrange multipliers associated with the average transmit power and average interference power constraints in (4.11) and (4.12), respectively.

4.3 Numerical and Simulation Results

In this section, we perform comprehensive simulations to evaluate the performance of image transmissions of DUs in the cellular network.

4.3.1 Simulation Settings

For image transmission, test image is chosen as the gray-scale "Lena" images with size 512×512 pixels. It is assumed that the noise variances are $\sigma_{dd}^2 = \sigma_{db}^2 = \sigma_{bd}^2 = 0.01$. Let d_{dd}, d_{db}, d_{bd} and d_{cd} denote the distances between DT and DR, DT and BS, BS and DR, and cellular transmitter (CT) and DR, respectively. Unless mentioned explicitly, we also assume that the channel power gains denoted by z follow exponential distributions with mean $Z = 2\frac{1}{d}^4$, where d is the anyone of the aforementioned distances.

66

There are 12 subchannels in the system, and thus $K = 3$, $K = 4$ and $K = 6$ subchannels are allocated to the DUs in the cellular mode, dedicated mode and reuse mode, respectively. The average transmit power is $KP_{\mathrm{avg},d} = 0$ dB at DT and $KP_{\mathrm{avg},b} = 5$ dB at BS. The average interference limit is $Q_{\mathrm{avg}} = -2$ dB. λ is set to 0.5. In order to present average simulation results in the presence of randomly-varying fading, results of 50 simulations are averaged. Peak signal-to-noise ratio (PSNR) is chosen as the performance metric to measure the quality of the reconstructed data.

In the simulations, the position of DT changes while keeping the positions of cellular transmitter (CT), cellular receiver (CR), DR and BS are fixed.

4.3.2   Constant transmit power

Fig. 4.2 shows the BERs in 3 different modes with constant transmit power at different DT positions. In cellular mode, BER is smaller when DT is closer to BS since there is no interference and d_{bd} is fixed, and thus the changes of BER only depends on d_{db}. In dedicated mode, BER is smaller when DT is closer to DR since there is no interference and the changes of BER only depends on d_{dd}. In reuse mode, fixed location of DR means that the interference caused by CT at DR keeps the same. Transmission power at DT gets smaller when it is closer to BS because of the interference constraint, and that is the reason why the BER is very high when DT is near BS. The channel gain is higher when DT is closer to DR, leading to lower BER near the location of DR.

Fig. 4.3 shows the mode selection and corresponding BER and PSNR values when DT is moved. When DT is very close to DR and there is not too much interference, reuse mode is selected since this mode leads to the highest SNR. When DT is not that close to DR, dedicated mode is selected since reuse mode causes much interference which leads lower SNR. When DT is far away from DR, cellular mode is selected since the higher transmission power at BS provides the highest SNR in this case. The corresponding PSNR value is higher when DR is closer to DT.

(a) BER in cellular mode (b) BER in dedicated mode (c) BER in reuse mode
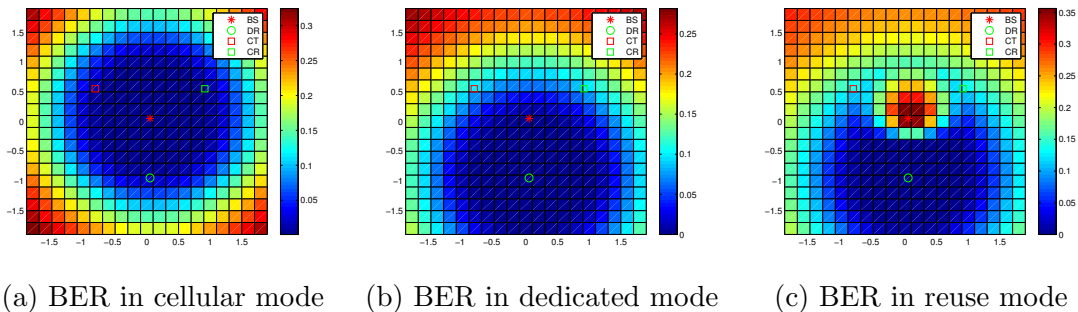
Figure 4.2: BERs at different positions of DT in (a) cellular mode; (b) dedicated mode; (c) reuse mode.

(a) Mode selection (b) Corresponding BER (c) Corresponding PSNR
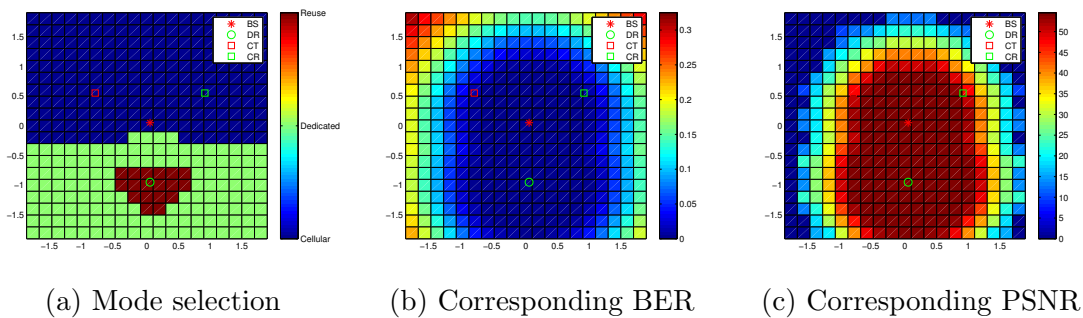
Figure 4.3: (a) Mode selection; (b) corresponding BER; (c) corresponding PSNR value at different positions of DT in constant power case.

(a) Mode selection   (b) Corresponding BER   (c) Corresponding PSNR
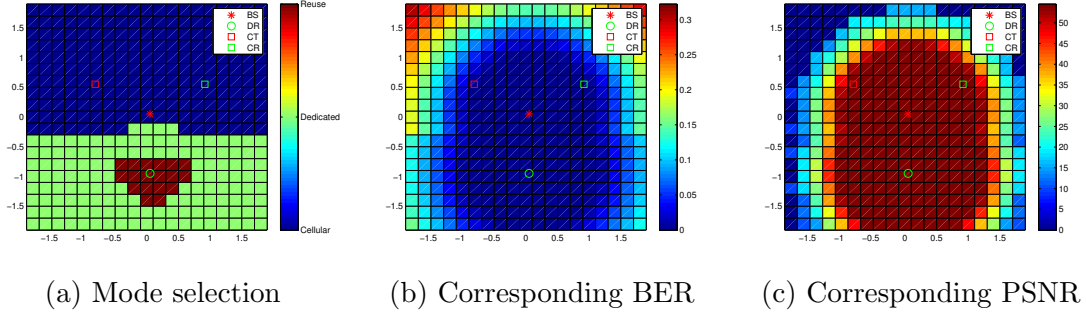
Figure 4.4: (a) Mode selection; (b) corresponding BER; (c) corresponding PSNR value at different positions of DT in power control case.

(a) BER comparison   (b) PSNR comparison
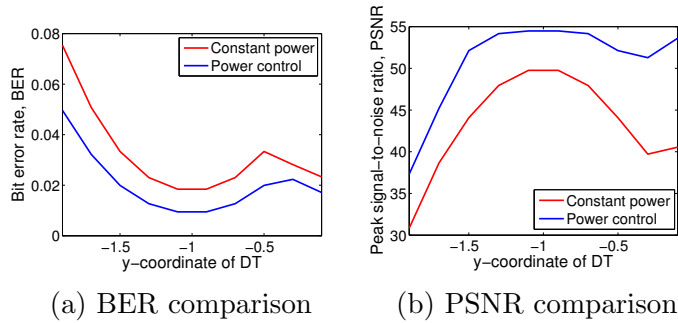
Figure 4.5: (a) BER comparison; (b) PSNR comparison between constant power case and power control case at selected positions of DT.

4.3.3 Power control strategy

Fig 4.4 shows the mode selection and the corresponding BER and PSNR values in this case of image transmission with power control. The mode selection results are similar as in constant power case. However, the red region in Fig 4.4c is larger than the red region in Fig 4.3c, demonstrating that the power control results in higher PSNR values compared to those in the constant power case at the same DT location, which also means lower BER values.

Fig 4.5 shows the differences in BERs and corresponding PSNRs between constant power case and power control case at selected locations of DT. x-axis coordinate of DT is set to -1.1 while y-axis coordinate is varied from -1.9 to -0.1. The result demonstrates that power control leads to lower BERs and higher PSNRs. The difference is also large at the selected positions.

69

Chapter 5

Video Transmission over D2D Underlaid Wireless Networks under QoS and Energy Efficiency Constraints

Device-to-device (D2D) communication underlaid with cellular networks is proposed to enhance the performance of these networks. D2D communication can achieve higher spectral efficiency, improve the energy efficiency and lower the traffic delay by allowing a pair of D2D users to communicate with each other directly without going through a base station especially when the pair of D2D users are located in close proximity. In this chapter, transmission mode selection and resource allocation with the goal of maximizing the quality of the received video at the receiver in a frequency-division duplexed (FDD) cellular network with a pair of cellular users, one base station and a pair of D2D users is studied under quality-of-service (QoS) and energy efficiency (EE) constraints.

5.1 System Model

As mentioned above, with the goal of maximizing the quality of received video at the device receiver, we study optimal strategies for mode selection and resource allocation in a cellular network with D2D pairs under QoS and EE constraints. For simplicity, we consider a D2D cellular wireless transmission network with a single base station (BS), which serves one pair of CUs denoted by $\{C_1, C_2\}$ as illustrated in Fig. 5.1. There exists also a pair of DUs denoted by $\{D_1, D_2\}$. We assume that the transmissions between D2D users and cellular users are one-way, i.e., C_1 and D_1 are transmitters while C_2 and D_2 are the receivers. The maximum transmit powers of the three transmitters, namely the BS, C_1 and D_1, are denoted by P_{bmax}, P_{cmax} and P_{dmax}, respectively. The BS, which operates as a relay, is assumed to transmit and receive data simultaneously in FDD mode. In the cellular link, C_1 sends information to the BS via the uplink channel while BS sends information to C_2 through the downlink channel. In the D2D link, D_1 transmits data to D_2 either directly or via the BS depending on the mode selection. The data packets are stored in buffers at the transmitters before they are sent to the corresponding receivers. The QoS constraints are imposed as limitations on buffer overflow probabilities. Block-fading model is considered in all links. The fading coefficients and the corresponding magnitude-squares in different links are denoted by h_i and $z_i = |h_i|^2$, respectively, as depicted in Fig. 5.1 for $i = 1, 2, \cdots, 7$. The overall bandwidth of this system is B, and the bandwidth allocated to each link is given by the components of the bandwidth allocation vector $\mathbf{B}$. The dimension of $\mathbf{B}$ varies with the selected modes. In this thesis, four different modes are considered in the system, namely the cellular mode, the dedicated mode, the uplink reuse mode and downlink reuse mode.

Cellular mode: In this mode, two DUs communicate through the BS just as conventional CUs. Since CUs, C_1 and C_2, always communicate through the BS, there are 4 communication channels in this mode. BS receives data from C_1 and D_1,
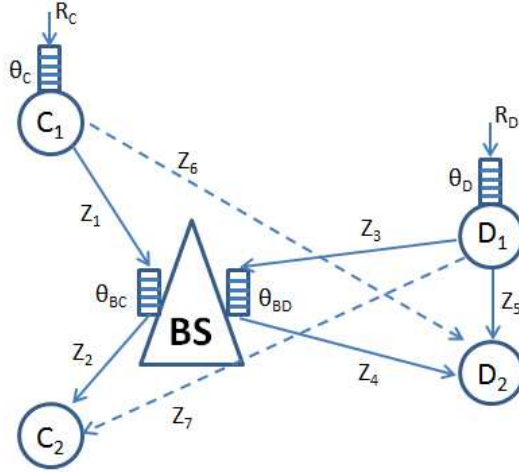
Figure 5.1: System model with queueing constraints (Dashed lines represent interference only links).

and sends data to C_2 and D_2 simultaneously. We denote the bandwidth allocated to the two cellular links and two D2D links (operating in cellular mode) as B_{c1}, B_{c2}, B_{d1} and B_{d2}. The bandwidth allocation between the two cellular links and D2D links is discussed in Section 5.3. It is assumed that there are two separate buffers at the BS. One is for storing the packets that has been received from C_1 and will be sent to C_2, the other one stores the packets delivered from D_1 and to be sent to D_2. Therefore, two different queueing constraints are imposed on these two buffers at the BS. All the links are free of interference since they each use a different frequency band for data transmission, the received signal at each receiver has the form

$$y = h_i x + n_i, \tag{5.1}$$

where x is the transmitted signal, h_i is the fading coefficient of corresponding channel, and n_i is the additive noise component. Above, in the channel input-output relationship, the noise component n_i is an independent, zero-mean, circularly symmetric, complex Gaussian random variable with noise spectral density N_0.

Dedicated mode: In this mode, DUs are dedicated their own channel to com-

municate directly with each other. Bandwidth allocated to cellular uplink, cellular downlink and D2D direct link are given by $\mathbf{B} = (B_{c1}, B_{c2}, B_d)$, respectively. Since there is again no interference, the input-output relationship has the same form as (5.1).

Reuse mode: Two DUs communicate directly by reusing the channels that are occupied by CUs. These modes could improve the channel spectrum utilization, but the resulting co-channel interference should be managed properly in order to guarantee the performance of DUs and CUs. In uplink reuse mode, the overall bandwidth B is allocated to the cellular uplink and downlink, and the D2D link shares the uplink spectrum. Since D_1 and C_1 occupy the same channel for transmission, D_2 and BS experience interference. The received signals follow the form

$$y = h_i x + h_{inter} x_{inter} + n_i, \tag{5.2}$$

where x again is the transmitted signal, h_i is the channel fading coefficient between the receiver and corresponding transmitter, x_{inter} is the interference signal, h_{inter} is the channel fading coefficient of the interfering link, and n_i is the Gaussian noise. Since there is no interference in the downlink in this mode, the received signal at C_2 has the same form as (5.1). Similarly, in the downlink reuse mode, the received signals at D_2 and C_2 follow (5.2) and received signal at the BS in the uplink follows (5.1).

In order to transmit the information efficiently and guarantee the minimum required video quality in cellular links, constraints on EE and minimum video quality Q_{cmin} are imposed on D_1 and C_2, respectively. If any one of the constraints cannot be satisfied, then the corresponding mode becomes inactive.

5.2 Throughput of Cellular Network with D2D Users

In this section, we formulate the throughput of the cellular link and D2D link in each mode under the given QoS constraints. It is assumed that C_1 and BS transmit information with power $P_c = P_{cmax}$ and $P_b = P_{bmax}$, respectively, since the cellular link has higher priority over the D2D link.

5.2.1 Throughput in the Cellular Mode

In cellular mode, bandwidths allocated to the $C_1 - BS - C_2$ and $D_1 - BS - D_2$ links are given by $B_c = B_{c1} + B_{c2}$ and $B_d = B_{d1} + B_{d2}$, respectively. Since in this mode, both the cellular link and D2D link are essentially two-hop channels and there is no interference, or more specifically, C_1 and D_1 first transmit information to the BS, and BS forwards the information to C_2 and D_2 simultaneously, the instantaneous transmission rates of the $C_1 - BS$, $BS - C_2$, $D_1 - BS$ and $BS - D_2$ links are given, respectively, as

$$r_{C,B}(B_{c1}) = B_{c1} T \log_2 \left(1 + \frac{P_c z_1}{B_{c1} N_0} \right), \tag{5.3}$$

$$r_{B,C}(B_{c2}) = B_{c2} T \log_2 \left(1 + \frac{P_b z_2}{B_{c2} N_0} \right), \tag{5.4}$$

$$r_{D,B}(B_{d1}) = B_{d1} T \log_2 \left(1 + \frac{P_d z_3}{B_{d1} N_0} \right), \tag{5.5}$$

$$r_{B,D}(B_{d2}) = B_{d2} T \log_2 \left(1 + \frac{P_b z_4}{B_{d2} N_0} \right). \tag{5.6}$$

In the two-hop case, the arrival rate at C_1 has to satisfy the QoS constraints at both C_1 and BS simultaneously. Similarly as in [76], the source rate or the maximum available transmission rate of this two-hop channel is expressed as follows:

$$R_C = -\frac{1}{\theta_C T} \log \mathbb{E}\{e^{-\theta_C r_{C,B}(\hat{B}_{c1})}\}, \tag{5.7}$$

where $\hat{B}_{c1} = \min\{\tilde{B}_{c1}, B_{c1}^*\}$, and $\tilde{B}_{c1}$ is the solution to

$$\mathbb{E}\{r_{C,B}(\tilde{B}_{c1})\} = \mathbb{E}\{r_{B,C}(B_c - \tilde{B}_{c1})\}, \tag{5.8}$$

and B_{c1}^* is the solution to

$$-\frac{1}{\theta_C T} \log \mathbb{E}\{e^{-\theta_C r_{C,B}(B_{c1}^*)}\} =$$

$$\begin{cases} -\frac{1}{\theta_{BC}T} \log \mathbb{E}\{e^{-\theta_{BC} r_{B,C}(B_c - B_{c1}^*)}\}, & \theta_C \geq \theta_{BC} \\ -\frac{1}{\theta_C T}\left(\log \mathbb{E}\{e^{-\theta_{BC} r_{B,C}(B_c - B_{c1}^*)}\} \right. \\ \left. + \log \mathbb{E}\{e^{(\theta_{BC} - \theta_C) r_{C,B}(B_{c1}^*)}\} \right), & \theta_C < \theta_{BC} \end{cases} \tag{5.9}$$

Similarly, the source rate of the $D_1 - BS - D_2$ link is

$$R_D = -\frac{1}{\theta_D T} \log \mathbb{E}\{e^{-\theta_D r_{D,B}(\hat{B}_{d1})}\}, \tag{5.10}$$

where $\hat{B}_{d1} = \min\{\tilde{B}_{d1}, B_{d1}^*\}$, and $\tilde{B}_{d1}$ is the solution to

$$\mathbb{E}\{r_{D,B}(\tilde{B}_{d1})\} = \mathbb{E}\{r_{B,D}(B_d - \tilde{B}_{d1})\}, \tag{5.11}$$

and B_{d1}^* is the solution to

$$-\frac{1}{\theta_D T} \log \mathbb{E}\{e^{-\theta_D r_{D,B}(B_{d1}^*)}\} =$$

$$\begin{cases} -\frac{1}{\theta_{BD}T} \log \mathbb{E}\{e^{-\theta_{BD} r_{B,D}(B_d - B_{d1}^*)}\}, & \theta_D \geq \theta_{BD} \\ -\frac{1}{\theta_D T}\left(\log \mathbb{E}\{e^{-\theta_{BD} r_{B,D}(B_d - B_{d1}^*)}\} \right. \\ \left. + \log \mathbb{E}\{e^{(\theta_{BD} - \theta_D) r_{D,B}(B_{d1}^*)}\} \right), & \theta_D < \theta_{BD} \end{cases} \tag{5.12}$$

5.2.2 Throughput in the Dedicated Mode

In this mode, $C_1 - BS - C_2$ link has the same source rate as in the cellular mode discussed in the previous subsection, and occupies a bandwidth of B_c. However, for the direct D2D link, since the direct link occupies a separate bandwidth of B_d, the instantaneous transmission rate is

$$r_{D_1,D_2} = B_d T \log_2\left(1 + \frac{P_d z_5}{B_d N_0}\right),\tag{5.13}$$

and the corresponding source rate is expressed as

$$R_D = -\frac{1}{\theta_D T}\log \mathbb{E}\{e^{-\theta_D r_{D_1,D_2}}\}.\tag{5.14}$$

5.2.3 Throughput in Reuse Modes

The D2D direct link shares the same spectrum occupied by the cellular uplink or cellular downlink. Therefore, the cellular link $C_1 - BS - C_2$ uses the entire available spectrum, meaning that $B_c = B_{c1} + B_{c2} = B$. In uplink reuse mode, $D_1 - D_2$ direct link shares the $C_1 - BS$ channel with bandwidth B_{c1}, which means $B_d = B_{c1}$. Then the instantaneous transmission rate for the $C_1 - BS$, $BS - C_2$ and $D_1 - D_2$ links are given by

$$r_{C,B}(B_{c1}) = B_{c1} T \log_2\left(1 + \frac{P_c z_1}{B_{c1} N_0 + P_d z_3}\right),\tag{5.15}$$

$$r_{B,C}(B_{c2}) = B_{c2} T \log_2\left(1 + \frac{P_b z_2}{B_{c2} N_0}\right),\tag{5.16}$$

$$r_{D_1,D_2}(B_{c1}) = B_{c1} T \log_2\left(1 + \frac{P_d z_5}{B_{c1} N_0 + P_c z_6}\right),\tag{5.17}$$

and the source rates of $C_1 - BS - C_2$ and $D_1 - D_2$ links can be expressed as

$$R_C = -\frac{1}{\theta_C T} \log \mathbb{E}\{e^{-\theta_C r_{C,B}(\hat{B}_{c1})}\}, \tag{5.18}$$

$$R_D = -\frac{1}{\theta_D T} \log \mathbb{E}\{e^{-\theta_D r_{D_1,D_2}(\hat{B}_{c1})}\}, \tag{5.19}$$

where $\hat{B}_{c1}$ is calculated similarly as in cellular mode. The only difference is (5.15) and (5.16) are different from (5.3) and (5.4), respectively, due to the presence of the interference terms. In downlink reuse mode, $D_1 - D_2$ direct link shares the $BS - C_2$ channel with bandwidth B_{c2}. Similar characterizations can be determined as in the uplink reuse mode, and the instantaneous transmission rates for the $C_1 - BS$, $BS - C_2$ and $D_1 - D_2$ links are given by

$$r_{C,B}(B_{c1}) = B_{c1} T \log_2 \left(1 + \frac{P_c z_1}{B_{c1} N_0}\right), \tag{5.20}$$

$$r_{B,C}(B_{c2}) = B_{c2} T \log_2 \left(1 + \frac{P_b z_2}{B_{c2} N_0 + P_d z_7}\right), \tag{5.21}$$

$$r_{D_1,D_2}(B_{c2}) = B_{c2} T \log_2 \left(1 + \frac{P_d z_5}{B_{c2} N_0 + P_b z4}\right), \tag{5.22}$$

and the source rates of $C_1 - BS - C_2$ and $D_1 - D_2$ links can be expressed as

$$R_C = -\frac{1}{\theta_C T} \log \mathbb{E}\{e^{-\theta_C r_{C,B}(\hat{B}_{c1})}\}, \tag{5.23}$$

$$R_D = -\frac{1}{\theta_D T} \log \mathbb{E}\{e^{-\theta_D r_{D_1,D_2}(\hat{B}_{c2})}\}, \tag{5.24}$$

where $\hat{B}_{c1}$ is calculated similarly as in uplink reuse mode, and $\hat{B}_{c2} = B - \hat{B}_{c1}$.

5.3   Resource Allocation

Video quality-rate model in Chapter 2.3 is employed. Based on the above throughput analysis of all four modes, in this section, we develop resource allocation strategies

that maximize the quality of the received video at D_2 under certain constraints. Both bandwidth allocation and transmit power level P_d at D_1 are optimized.

5.3.1 Cellular Mode

In cellular mode, the video quality maximization problem is formulated as

$$\max_{\mathbf{B},P_d} \quad Q_D = a_D \ln(R_D) + b_D \tag{5.25}$$

$$\text{subject to} \quad B_{c1} + B_{c2} + B_{d1} + B_{d2} \leq B \tag{5.26}$$

$$Q_C \geq Q_{cmin} \tag{5.27}$$

$$P_d \leq P_{dmax} \tag{5.28}$$

$$\frac{R_D}{P_{ci} + \frac{P_d}{\epsilon}} \geq \eta_d \tag{5.29}$$

Above, (5.29) defines the EE constraint at D_1. Energy efficiency (EE), measured by the data rate normalized by the transmission power or equivalently the number of communicated bits per unit energy, is also considered as a key factor in wireless systems. η_d is the minimum EE requirement. Since Q_C is an increasing function of $\hat{B}_{c1}$, the minimum required bandwidth $\hat{B}_{c1min}$ allocated to cellular uplink $C_1 - BS$ is the solution of (5.27) with equality. Then, there is a unique $B_{cmin} = B_{cmin1}$ that satisfies (5.8) and there is another unique $B_{cmin} = B_{cmin2}$ satisfying the equality in (5.9) depending on the value of θ. It is easy to verify that the maximum of these two values of B_{cmin} needs to be chosen as the minimum bandwidth allocated to the cellular link. Thus, $B_{cmin} = \max\{B_{cmin1}, B_{cmin2}\}$. Then, the rest of the bandwidth $B_d = B - B_{cmin}$ is allocated to the $D_1 - BS - D_2$ link since larger bandwidth allocated to the D2D link leads to higher throughput and furthermore higher PSNR value for the received video at D_2. The EE constraint (5.29) can be rewritten as

$$R_D \geq \eta_d(P_{ci} + \frac{P_d}{\epsilon}) \tag{5.30}$$

by moving the denominator to the right-hand side. It can be easily shown that the left-hand side of (5.30) is an increasing concave function, and the right-hand side of (5.30) is a linear increasing function of P_d for given $B_{d1} = B_{d1a}$ with initial points at $(0,0)$ and $(0, \eta_d P_{ci})$, respectively. By fixing B_{d1}, we consider both sides of (5.30) as functions of P_d, and the left-hand side of (5.30) will intersect the right-hand side of (5.30) at two different points, the minimum available or required power, P_{dmin1}, and the maximum again available or required power, P_{dmax1} when B_{d1} is large enough. There is no solution for the optimization problem if B_{d1} is small, since (5.30) cannot be satisfied for any value of P_d. Therefore, the transmission power at D_1 needs to be in the range $P_{dmin1} \leq P_d \leq P_{dmax1}$ in order to satisfy the EE constraint. Since the left-hand side of (5.30) is also an increasing function of B_{d1} but the right-hand side is independent of B_{d1}, larger B_{d1} leads to larger P_{dmax1} and smaller P_{dmin1}. Therefore, larger bandwidth B_{d1} allocated to the uplink of D2D link will lead to larger maximum feasible power P_{dmax1} and smaller minimum feasible power P_{dmin1} under the EE constraint. In another words, increasing B_{d1} enlarges the region of feasible transmission power levels.

Algorithm 3 Resource allocation for the cellular mode

1: Determine the minimum throughput of the cellular link, R_{cmin} by solving (5.27) with equality.

2: The minimum bandwidth, $\hat{B}_{c1min}$ allocated to cellular uplink is obtained by solving (5.7).

3: Let $\tilde{B}_{c1} = \hat{B}_{c1min}$. Then, the minimum bandwidth, $B_c = B_{cmin1}$ is the solution of (5.8). And let $B_{c1}^* = \hat{B}_{c1min}$. Then, $B_c = B_{cmin2}$ is the solution of (5.9). $B_{cmin} = \max\{B_{cmin1}, B_{cmin2}\}$ is chosen as the minimum bandwidth allocated to the cellular link. This satisfies the minimum required quality of the received video at C_2, and $B_d = B - B_{cmin}$ is allocated to the $D_1 - BS - D_2$ link.

4: As initialization, assume that $B_{d1} = B_0$ is allocated to the $D_1 - BS$ link and $B_{d2} = B_d - B_{d1}$ is allocated to the $BS - D_2$ link. P_{dmin1} and P_{dmax1} are the minimum and maximum feasible transmission power levels of D_1 limited by the two-hop link throughput constraints (5.11) and (5.12), respectively. P_{dmin2} and P_{dmax2} are the minimum and maximum feasible transmission power levels of D_1 limited by EE constraint (5.30). Let $P_{dmax1} = P_{dmax}$, $P_{dmax2} = 0$, $\epsilon_p = 0.0001$ and $\alpha = 0.001$.

5: **while** $|P_{dmax1} - P_{dmax2}| > \epsilon_p$ and $B_{d1} <= B_d$ **do**

6:     Let $\hat{B}_{d1} = B_{d1}$, and obtain P_{dmin1} and P_{dmax1} by solving (5.30) with equality, and obtain P_{dmin2} and P_{dmax2} by solving (5.11) and (5.12) as discussed above.

7:     Update $B_{d1} = B_{d1} + \alpha(P_{dmax2} - P_{dmax1})$

8: **end while**

9: **if** $B_{d1} > B_d$ **then**

10:     No solution.

11: **else**

12:     $P_d = \min\{P_{dmax2}, P_{dmax1}\}$ and $\hat{B}_{d1} = B_{d1}$. Quality of the received video at D_2, Q_D, is obtained by calculating (5.10) and (**??**).

13: **end if**

Also, for fixed B_{d1}, P_{dmax2a} is determined by (5.11) and P_{dmax2b} is determined by (5.12). It is easy to verify that the minimum one should be chosen as the transmission power at D_1, and hence we assume that $P_{dmax2} = \min\{P_{dmax2a}, P_{dmax2b}\}$. Therefore, the transmission power at D_1 should satisfy $0 \leq P_d \leq P_{dmax2}$ for the two-hop link in cellular mode. For this fixed P_{dmax2}, the left-hand sides of (5.11) and (5.12) are increasing functions of B_{d1}, and the right-hand sides are decreasing functions of B_{d1}. A bandwidth larger than B_{d1} cannot be allocated to D2D uplink under this fixed transmission power P_{dmax2}. However, left-hand sides of (5.11) and (5.12) are increasing functions of P_d, therefore, lower P_{dmax2} can satisfy the two-hop link throughput when B_{d1} increases. In another words, increasing B_{d1} shrinks the region of feasible levels of the transmission power, P_d and decreases the throughput of this two-hop link.

Therefore, we can decrease B_{d1} if $P_{dmax2} < P_{dmax1}$, or otherwise, we increase B_{d1} until we satisfy $P_{dmax1} = P_{dmax2}$ since the quality of the received video at D_2 is determined by B_{d1} and $\min\{P_{dmax1}, P_{dmax2}\}$. The detailed algorithm of resource allocation for the cellular mode is explained in Algorithm. 3.

5.3.2   Dedicated Mode

In dedicated mode, since a separate bandwidth of B_d is allocated to the D2D direct link, the minimum bandwidth, B_{cmin}, allocated to the cellular link is obtained similarly as in cellular mode. Therefore, $B_d = B - B_{cmin}$ is allocated to the D2D link and the maximum transmission power P_{dmax} can be obtained by using (5.14) and satisfying the EE constraint $\frac{R_D}{P_{ci} + \frac{P_{dmax}}{\epsilon}} \geq \eta_d$ with equality. Q_D reaches the maximum value at (B_d, P_{dmax}) since P_{dmax} is an increasing function of B_d as discussed in cellular mode and Q_D is an increasing function of B_d and P_{dmax}, separately.

5.3.3 Reuse Modes

In reuse modes, we seek to maximize the Q_D by allocating the bandwidths B_{c1}, B_{c2} and choosing the transmission power P_d at D_1 optimally in the presence of interference constraints in the system. The optimization problem is formulated as

$$\max_{\mathbf{B}, P_d} \quad Q_D = a_D \ln(R_D) + b_D \tag{5.31}$$

$$\text{subject to} \quad B_{c1} + B_{c2} \leq B \tag{5.32}$$

$$Q_C \geq Q_{cmin} \tag{5.33}$$

$$P_d \leq P_{dmax} \tag{5.34}$$

$$\frac{R_D}{P_{ci} + \frac{P_d}{\epsilon}} \geq \eta_d \tag{5.35}$$

In uplink reuse mode, Q_C depends on B_{c1} and P_d due to the interference from D_1. Let us substitute (5.15) and (5.16) into (5.8) and (5.9). Let us set B_{c1} and P_{dmin1} as the bandwidth allocated to the $C_1 - BS$ link and corresponding minimum feasible transmission power at D_1, which achieves the maximum throughput in the cellular link. When B_{c1} increases, the right-hand sides of both (5.8) and (5.9) decrease because $B_{c2} = B - B_{c1}$ decreases. In order to satisfy (5.8) and (5.9) with equality, P_{dmin1} has to be increased since left-hand sides of (5.8) and (5.9) are decreasing functions on P_d. Therefore, increasing B_{c1} leads to increased P_{dmin1} and decreased throughput in the cellular link. Letting $P_d = P_{dmax}$ and $P_d = 0$, we can obtain the corresponding maximum bandwidth B_{c1max} and the minimum bandwidth B_{c1min}, respectively. Similarly as we discussed in cellular mode, decreasing B_{c1} leads to smaller region of feasible levels of transmission power P_d, indicating an increased minimum power P_{dmin2} and decreased maximum power P_{dmax2} under the EE constraint. Since Q_D depends on B_{c1} and P_d due to presence of the interference, we cannot determine the minimum bandwidth B_{cmin} as we did in cellular mode and dedicated mode.

For a given B_{c1}, the maximum power P_{dmax3} is obtained by satisfying (5.33) with equality since Q_C is a decreasing function of P_d. Therefore, the minimum transmission power is $P_{dmint} = \max\{P_{dmin1}, P_{dmin2}\}$ and the maximum transmission power is $P_{dmaxt} = \min\{P_{dmax2}, P_{dmax3}\}$. Since $P_d = P_{dmax}$ is the only power value that can be used when $B_{c1} = B_{c1max}$, the optimal solution is $(P_d, B_{c1}) = (P_{dmax}, B_{c1max})$ if $P_{dmax2} = P_{dmax3} = P_{dmax}$ is also achieved when $B_{c1} = B_{c1max}$. Otherwise, $P_{dmaxt} < P_{dmin1}$ when $B_{c1} = B_{c1max}$. Since Q_D is an increasing function of B_{c1} and P_{dmaxt} and decreasing B_{c1} leads to reduced P_{dmin1} and P_{dmaxt}, the first point of $P_d = P_{dmin1} = P_{dmaxt}$ achieved by decreasing B_{c1} from B_{c1max} is the optimal solution. The detailed algorithm is described in Algorithm. 4.

Algorithm 4 Resource allocation for the uplink reuse mode

1: Substitute (5.15) and (5.16) into (5.8) and (5.9) and obtain the maximum feasible bandwidth B_{c1max} and minimum bandwidth B_{c1min} by setting $P_d = P_{dmax}$ and $P_d = 0$, respectively. Another minimum bandwidth value, B_{c1min2} can be found by solving (5.33) with the equality and setting $P_d = 0$.

2: Initialize that $B^*_{c1max} = B_{c1max}$, $B^*_{c1min} = \max\{B_{c1min}, B_{c1min2}\}$, $B_{c1} = B_{c1max}$, $\epsilon_p = 0.0001$, $\alpha = 0.001$, $P_{dmaxt} = 0$ and $P_{dmin1} = P_{dmax}$.

3: **while** $|P_{dmaxt} - P_{dmin1}| > \epsilon_p$ and $B_{c1} > B^*_{c1min}$ **do**

4:     Find P_{dmin1} by letting CUs satisfy two-hop link conditions (5.8) and (5.9) as discussed in cellular mode. Obtain the minimum power P_{dmin2} and maximum power P_{dmax2} by solving the EE constraint (5.35) with equality. Determining the maximum power P_{dmax3} by satisfying minimum quality requirement (5.33) with equality.

5:     Let $P_{dmaxt} = \min\{P_{dmax2}, P_{dmax3}\}$.

6:     Update $B_{c1} = B_{c1} + \alpha(P_{dmaxt} - P_{dmin1})$.

7: **end while**

8: **if** $B_{c1} < B^*_{c1min}$ **then**

9:     No solution.

10: **else**

11:     Maximum Q_D is achieved at $(B_{c1}, \min\{P_{dmaxt}, P_{dmin1}\})$

12: **end if**

In downlink reuse mode, the minimum bandwidth B_{c1min} allocated to the cellular uplink is obtained by satisfying the minimum quality requirement (5.33) with equality since there is no interference term in R_D. Thus, a bandwidth of $B_d = B - B_{c1min}$ is allocated to the cellular downlink and the D2D link. For given $\hat{B}_{c1} = B_{c1min}$, P_{dmax1} is obtained by solving (5.8) with equality. P_{dmax2} is obtained by solving (5.9) with equality after substituting (5.20) and (5.21) into (5.8). And the minimum one is chosen as

the maximum transmission power at D_1, i.e., $P_{dmaxt} = \min\{P_{dmax1}, P_{dmax2}\}$. Similarly as in uplink reuse mode, for a given B_d, P_{dmin3} and P_{dmax3} are determined by satisfying the EE constraint (5.35) with equality. Therefore, $P_d = \min\{P_{dmaxt}, P_{dmax3}\}$ is the optimal transmission power that leads to maximum Q_D.

5.4 Numerical Results

In this section, we perform comprehensive simulations to evaluate the performance of video transmissions by the DUs in the D2D underlaid cellular networks.

5.4.1 Simulation Settings

It is assumed that the noise variance of each link is $N_0 = 0.01$. Let d_{dd}, d_{db}, d_{bd}, d_{cd}, d_{cb}, d_{bc} and d_{dc} denote the distances between D_1 and D_2, D_1 and BS, BS and D_2, C_1 and D_2, C_1 and BS, BS and C_2, and D_1 and C_2, respectively. Unless mentioned explicitly, we also assume that the channel power gains, denoted by z, follows exponential distributions with mean $Z = 3\frac{1}{d^4}$, where d denotes distance. The maximum transmission powers are $P_{dmax} = 10$ dB at D_1, $P_c = 10$ dB at C_1 and $P_b = 20$ dB at the BS. Total bandwidth $B = 2$ MHz, EE coefficient η_d is set to 5×10^4, and the circuit power is $P_{ci} = 0.1$. PSNR is chosen as the performance metric to measure the quality of the received video and the minimum required quality of the received video at C_2 is 30 dB. Channel coherence time is set to 0.01.

5.4.2 Simulation Results

Fig. 5.2a - Fig. 5.2d show the PSNR values Q_D in four different modes as we vary the location of D_1 while keeping the locations of other nodes the same. In Fig. 5.2a, D_1 whose location is closer to the BS has a higher Q_D value since there is no interference in cellular mode and D_1 transmits data to D_2 via the BS while keeping the distance

between D_2 and BS the same, and the link $D_1 - BS$ has better channel quality or higher channel gain when D_1 is closer to BS. Fig. 5.2b shows that the direct D2D link has better performance when the distance between D_1 and D_2 is smaller due to the larger channel gain. In Fig. 5.2c, not all the constraints can be satisfied in the region close to BS due to the strong interference from D_1 at BS and also in the region far away from D_2 due to worsened channel quality. The region in which D_1 is closer to D_2 has higher quality of the received video. We have similar observations in Fig. 5.2d, but different from the uplink reuse mode, there is no convex region near BS since D2D link shares the cellular downlink spectrum and C_2 is far away from D_1. Fig. 5.2e is the color-coded plot of optimal model selection results among four different modes, depending on the location of D_1. We notice that uplink reuse mode is selected in the region that is closest to the BS due to C_1 and D_1 being relatively far away from D_2 and BS, respectively, and the interferences between these two links are small enough and more bandwidth being allocated results in higher video quality. Dedicated mode is selected in the yellow region, since D_1 is close enough to D_2 and this mode has better performance compared to the cellular mode. The dedicated mode is also better than uplink reuse mode since the channel gain between D_1 and D_2 is getting smaller and the impact of interference is starting to dominate the performance in uplink reuse mode. Cellular mode is selected in the light blue region since the channel gain of direct D2D link is worse than what is experienced in the two-hop link. Downlink reuse mode is not selected since the interference at D_2 caused by BS is larger than the interference at BS caused by D_1 while the distance between D_1 and D_2 is small, and any other mode is selected when D_1 is far away from D_2. And in the dark blue region, not all the constraints can be satisfied. Fig. 5.2f demonstrates the corresponding PSNR values of the received video with the optimally selected modes.

Fig. 5.3a - Fig. 5.3d show the PSNR values Q_D for four different modes as we change the location of D_2 while keeping the locations of the other nodes fixed. In

(a) Cellular mode   (b) Dedicated mode   (c) Uplink reuse mode

(d) Downlink reuse mode   (e) Mode selection   (f) Corresponding Q_D values
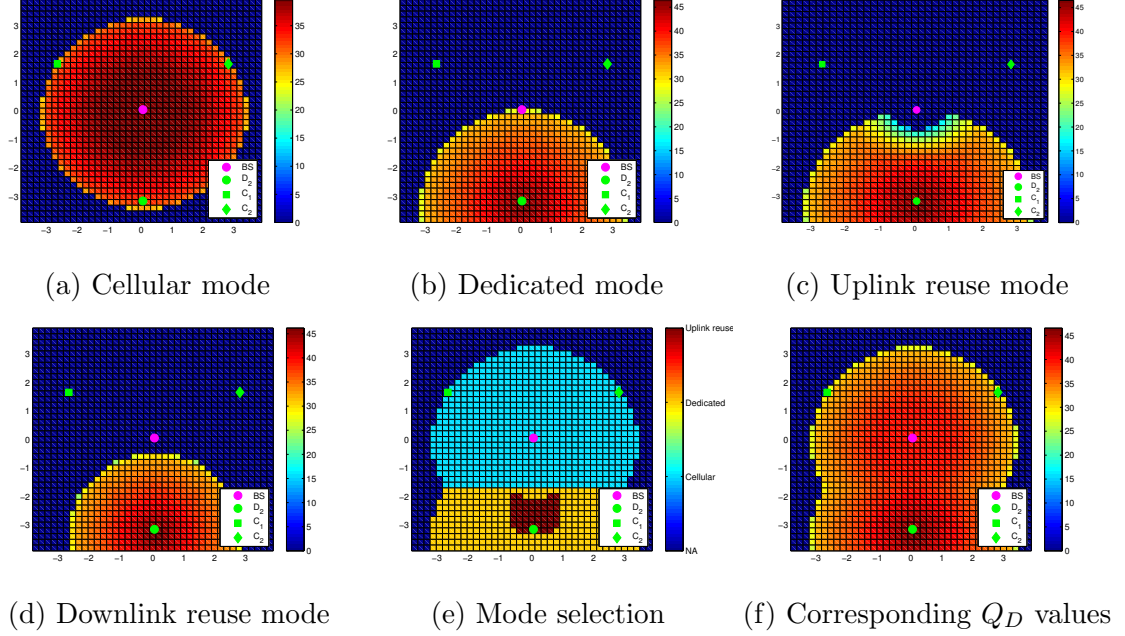
Figure 5.2: Q_D values for different locations of D_1 for (a) cellular mode; (b) dedicated mode; (c) uplink reuse mode and (d) downlink reuse mode; (e) the optimal mode selection and (f) the corresponding Q_D values

Fig. 5.3a, D_2 whose location is closer to the BS receives video with higher quality Q_D since there is no interference in cellular mode, D_1 transmits data to D_2 though the BS while the distance between D_1 and BS is being kept the same, and the link $BS - D_2$ has better channel quality or higher channel gain when D_2 is closer to BS. Since the distance between D_1 and BS is fixed and close enough, all constraints are satisfied in almost the entire region, which is not the case when the location off D_1 was varied. Fig. 5.3b shows that the direct D2D link has better performance when the distance between D_1 and D_2 is smaller due to same reason as discussed when D_1 was being moved. In Fig. 5.3c, unlike the case of D_1 being moved, there is no convex region when D_2 is closer to the BS since there is no interference between D_2 and BS. The region in which D_2 is closer to D_1 has higher quality of received video. This is similar to the observation in Fig. 5.3c. The region in which D_2 is closer to D_1 has higher received video quality in Fig. 5.3d, but different from the uplink reuse mode, the upper boundary of the lower (yellow) region is flat due to D_2 being closer to BS,

(a) Cellular mode   (b) Dedicated mode   (c) Uplink reuse mode

(d) Downlink reuse mode   (e) Mode selection   (f) Corresponding Q_D values
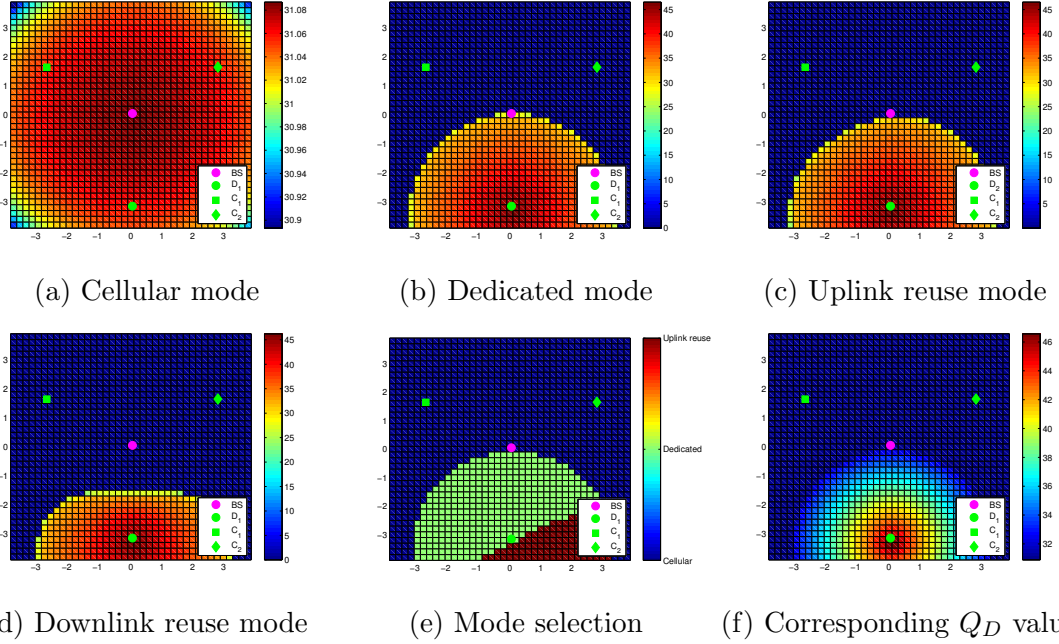
Figure 5.3: Q_D values for different locations of D_2 for (a) cellular mode; (b) dedicated mode; (c) uplink reuse mode and (d) downlink reuse mode; (e) the optimal mode selection and (f) the corresponding Q_D values

and BS inflicts larger interference to D_2 in downlink reuse mode. Fig. 5.3e plots the optimal mode selection results among the four different modes. Uplink reuse mode is selected in the right bottom region because C_1 and D_1 are relatively far away from D_2 and BS, respectively, and the interferences between these two links are small enough and more bandwidth being allocated leads to higher video quality. Dedicated mode is selected in the light green region, since D_1 is close enough to D_2 and this mode has better performance compared to the cellular mode. This mode is also better than uplink reuse mode since the channel gain between D_1 and D_2 is smaller and the impact of interference dominates the performance in uplink reuse mode. Cellular mode is selected in the dark blue region since the channel gain of the direct D2D link is worse than that in the two-hop link. Similarly as in the case in which D_1 is moved, downlink reuse mode is not selected. Fig. 5.3f demonstrates the corresponding PSNR values of the received video when optimal model selection is performed.

Chapter 6

Optimal Resource Allocation for Full-Duplex Wireless Video Transmissions under Delay Constraints

In this chapter, wireless video transmission over full-duplex channels is studied. In order to provide the desired performance levels to the end-users in real-time video transmissions, quality of service (QoS) requirements such as statistical delay constraints are also considered. Effective capacity (EC) is used as the throughput metric in the presence of such statistical delay constraints since deterministic delay bounds are difficult to guarantee due to the time-varying nature of wireless fading channels. A communication scenario with a pair of users and multiple subchannels in which users can have different delay requirements is addressed. Following characterizations from the rate-distortion (R-D) theory, a logarithmic model of the quality-rate relation is used for predicting the quality of the reconstructed video in terms of the peak signal-to-noise ratio (PSNR) at the receiver side. Since the optimization problem

Figure 6.1: System block diagram for quality-driven resource allocation in full-duplex wireless networks

is not concave or convex, the optimal power allocation policy that maximizes the weighted sum video quality subject to total transmission power constraint is derived by using monotonic optimization (MO) theory. The optimal scheme is compared with two suboptimal strategies.

6.1   System Model

Fig. 6.1 depicts the block diagram of the proposed system. We consider a pair of FD users, denoted as U_1 and U_2, sharing K subchannels in FD mode. The bandwidth of each subchannel is B_c, and the total bandwidth of the system is $B = KB_c$. It is assumed that flat fading is experienced in each subchannel. The channel coherence time is denoted by T_c, and the timescale of video rate adaptation is much larger than T_c in practice for video transmission since video source rate is adapted at the group of pictures (GOP) time scale which is measured in seconds. The case in which the channel state changes faster than the source rate is considered in our system since if the fading channel state varies at the same timescale as the source rate, statistical delay guarantees become less interesting [28].

We assume channel reciprocity and the availability of the statistical CSI of each channel at U_1 and U_2 for resource allocation. $f_k(\gamma_k)$ denotes distribution of fading power in the kth subchannel, where γ_k denotes the ergodic and stationary fading power uncorrelated among different blocks. Thus, the instantaneous transmission

rates in the kth subchannel from U_1 to U_2 and from U_2 to U_1 are $B_c \log(1 + \frac{P_{1,k}\gamma_k}{N_0 B_c + I_{2,k}})$ and $B_c \log(1 + \frac{P_{2,k}\gamma_k}{N_0 B_c + I_{1,k}})$, respectively, for the case in which constant power allocation is performed. Above, N_0 is the power spectral density of the background Gaussian noise and $I_{1,k}$ and $I_{2,k}$ denote the self-interference at U_1 and U_2, respectively.

6.2 Preliminaries

6.2.1 Notations

Throughout this thesis, vectors are denoted by boldface letters, the j-th entry of a vector $\mathbf{x}$ is denoted by x_j. $\mathcal{R}$ and $\mathcal{R}_+$ denote the set of real numbers and nonnegative real numbers, respectively. $\mathcal{R}^n$ and $\mathcal{R}_+^n$ denote the set of n-dimensional real numbers and nonnegative real numbers, respectively. For any two vectors $\mathbf{x}, \mathbf{y} \in \mathcal{R}$, $\mathbf{x} \geq \mathbf{y}$ if $x_j \geq y_j$ for all $j = 1, 2, \ldots, n$. $\cup$, $\cap$ and $\setminus$ represent set union, set intersection and set difference operators, respectively. $\mathbf{e}_j \in \mathcal{R}^n$ denotes the j-th unit vector of $\mathcal{R}^n$, i.e., the vector such that $e_j = 1$ and $e_i = 0$ for all $i \neq j$.

6.2.2 Effective capacity in the system model

Now, we analyze the system model and EC. For independent and identically distributed fading in each coherence block of duration T_c and independent fading in

each subchannel, the EC can be expressed as

$$C_i(\theta_i, \mathbf{P}_i) = -\frac{1}{\theta_i T_c} \ln(\mathbb{E}_\Gamma\{e^{-\theta_i r_i}\})$$

$$= -\frac{1}{\theta_i T_c} \ln(\mathbb{E}_\Gamma\{e^{-\theta_i \sum_{k=1}^{K} r_{i,k}}\})$$

$$= \sum_{k=1}^{K} \left\{ -\frac{1}{\theta_i T_c} \ln(\mathbb{E}_\Gamma\{e^{-\theta_i r_{i,k}}\}) \right\}$$

$$= \sum_{k=1}^{K} \left\{ -\frac{1}{\theta_i T_c} \ln(\mathbb{E}_{\gamma_k}\{e^{-\theta_i B_c T_c \log(1+\frac{P_{i,k}\gamma_k}{N_0 B_c + I_{3-i,k}})}\}) \right\} \qquad (6.1)$$

$$= \sum_{k=1}^{K} C_{i,k}(\theta_i, P_{i,k}), \qquad (6.2)$$

where $P_{i,k}$ is the constant power allocated to U_i in the kth subchannel and $r_{i,k}$ is the instantaneous transmission rate of user U_i in subchannel k. $\mathbf{P}_i$ and Γ denote the vectors including all elements $\{P_{i,1}, P_{i,2}, \ldots, P_{i,K}\}$ and $\{\gamma_1, \gamma_2, \ldots, \gamma_K\}$, respectively.

The EC should be equal to the effective bandwidth for the given QoS exponent θ [77]. For constant arrival rate R, effective bandwidth of the arrival process is $A_i(\theta_i, \mathbf{P}_i) = R_i$. Now, the maximum constant arrival rate can be expressed as:

$$R_i = A_i(\theta_i, \mathbf{P}_i) = C_i(\theta_i, \mathbf{P}_i)$$

$$= \sum_{k=1}^{K} C_{i,k}(\theta_i, P_{i,k}), i \in \mathcal{I}. \qquad (6.3)$$

6.3 Weighted Sum Quality-Maximizing Policies

In this section, optimization problems are formulated as the maximization of the weighted sum video quality subject to maximum transmission power constraints at the users. More specifically, we address the optimal power allocation under the assumption that statistical CSI is available and the allocated power remains fixed throughout the transmission. It is assumed that each user just uses a single antenna for trans-

mitting and receiving the data in the kth subchannel. Thus, the self-interference just depends on the self-transmission power over the kth subchannel, and the maximum constant arrival rate in (6.3) can be rewritten as:

$$
\begin{aligned}
R_i &= \sum_{k=1}^{K} C_{i,k}(\theta_i, P_{i,k}) \\
&= \sum_{k=1}^{K} -\frac{1}{\theta_i T_c} \ln\left(\mathbb{E}_{\gamma_k}\left\{e^{-\theta_i B_c T_c \log\left(1 + \frac{P_{i,k}\gamma_k}{N_0 B_c + \mu_{3-i,k} P_{3-i,k}}\right)}\right\}\right)
\end{aligned} \tag{6.4}
$$

where $\mu_{i,k} \in (0, 1]$ is the self-interference suppression factor in subchannel k at U_i. Video quality-rate model in Section 2.3 is employed. Thus, the weighted sum video quality is

$$
\begin{aligned}
Q &= \omega_1 Q_1 + \omega_2 Q_2 \\
&= \sum_{i=1}^{2} \omega_i \left(\alpha_i \ln(R_i) + \beta_i\right),
\end{aligned} \tag{6.5}
$$

where $\omega_i \in [0, 1]$ denotes the weight for the video quality transmitted by user U_i such that $\sum_{i=1}^{2} \omega_i = 1$.

We address the optimization problem for power allocation in the presence of statistical CSI. The optimization problem can be expressed as follows:

$$
\max_{\mathbf{P_1}, \mathbf{P_2}} \sum_{i=1}^{2} \left(\omega_i Q_i(\hat{R}_i)\right) \tag{6.6}
$$

$$
\text{s.t.} \quad \sum_{k=1}^{K} P_{i,k} \leq P_{i,\max}, \quad \forall i \in \mathcal{I}, \tag{6.7}
$$

$$
P_{i,k} \geq 0, \quad \forall k \in \mathcal{K}, \quad \forall i \in \mathcal{I}. \tag{6.8}
$$

Above, (6.7) is the maximum transmission power constraint at each user. Specifically, $P_{i,\max}$ is the maximum available transmission power of U_i. $\mathbf{P_1}$ and $\mathbf{P_2}$ are the $K \times 1$-dimensional vectors for the powers allocated to K subchannels at U_1 and U_2,

respectively. The feasible set of $\mathbf{P}_i$ is denoted by $\mathcal{P}_i = \{\mathbf{P}_i | P_{i,k} \geq 0, \sum_{k=1}^{K} P_{i,k} \leq P_{i,\max}, \forall i \in \mathcal{I}, \forall k \in \mathcal{K}\}$.

6.3.1 Problem reformulation

From the definition in Section 2.4 and [67], an optimization problem belongs to the class of MO if it can be represented in the following form:

$$\max f(\mathbf{x}) \tag{6.9}$$

$$\text{s.t.} \quad \mathbf{x} \in \mathcal{G} \cap \mathcal{H} \tag{6.10}$$

where $f(\mathbf{x}) : \mathcal{R}_+^n \to \mathcal{R}$ is an increasing function, $\mathcal{G} \subset [\mathbf{0}, \mathbf{b}] \subset \mathcal{R}_+^n$ is a compact normal, and $\mathcal{H}$ is a closed conormal set on $[\mathbf{0}, \mathbf{b}]$. The simpler case is that $\mathcal{H}$ is not present in the formulation since the conormal set $\mathcal{H}$ is box $[\mathbf{0}, \mathbf{b}]$. If $\mathcal{G} \cap \mathcal{H} \neq \emptyset$, the problem is considered feasible.

It is not possible to obtain the optimal solution based on the theory of convex optimization [78] because of the non-convexity of Problem (6.6) on $P_{i,k}$. In operations research, the monotonicity is another important property for effectively solving an optimization problem. Therefore, we can solve the non-convex Problem (6.6) by transforming it into an MO problem, and then solve the corresponding MO problem based on recent advances in monotonic optimization [79].

Let $Y_{k+(i-1)K} = C_{i,k}$, and let $\mathbf{Y}$ denote the vector $(Y_1, Y_2, \ldots, Y_{2K})$. It is easy to see that the function $\Phi(\mathbf{Y}) = \sum_{i=1}^{2} \left(\omega_i [\alpha_i \ln \left(\sum_{k=1}^{K} C_{i,k} \right) + \beta_i] \right)$ is an increasing function of $\mathbf{Y}$ on $\mathcal{R}_+^{2 \times K}$. In other words, for any two vectors $\mathbf{Y}_1$ and $\mathbf{Y}_2$, $\Phi(\mathbf{Y}_1) \geq \Phi(\mathbf{Y}_2)$ if

94

$\mathbf{Y}_1 \geq \mathbf{Y}_2$. Therefore, Problem (6.6) can be rewritten in the MO formulation as

$$\max \Phi(\mathbf{Y}) = \sum_{i=1}^{2} \left(\omega_i [\alpha_i \ln \left(\sum_{k=1}^{K} C_{i,k} \right) + \beta_i] \right) \tag{6.11}$$

$$\text{s.t.} \quad \mathbf{Y} \in \mathcal{G} \tag{6.12}$$

where, the normal set

$$\mathcal{G} = \{ \mathbf{Y} | 0 \leq Y_{k+(i-1)K} \leq V_{k+(i-1)K}(\mathbf{P}_1, \mathbf{P}_2),$$

$$\forall i \in \mathcal{I}, \forall k \in \mathcal{K}, \mathbf{P}_1 \in \mathcal{P}_1, \mathbf{P}_2 \in \mathcal{P}_2 \} \tag{6.13}$$

and

$$V_{k+(i-1)K}(\mathbf{P}_1, \mathbf{P}_2) =$$
$$- \frac{1}{\theta_i T_c} \ln(\mathbb{E}_{\gamma_k} \{ e^{-\theta_i B_c T_c \log(1 + \frac{P_{i,k} \gamma_k}{N_0 B_c + \mu_{3-i,k} P_{3-i,k}})} \}). \tag{6.14}$$

It is easy to verify that the normal set $\mathcal{G}$ is another expression of the combination of maximum transmission power constraint (6.7) and nonnegative power constraint (6.8).

Since $\Phi(\mathbf{Y})$ is an increasing function of $\mathbf{Y}$, the optimal solution of Problem (6.11), denoted by $\mathbf{Y}^*$, must be located at the upper boundary of $\mathcal{G}$, $\partial^+ \mathcal{G}$. This means that we can find power allocations $\mathbf{P}_1^*$ and $\mathbf{P}_2^*$ corresponding to the optimal solution $\mathbf{Y}^*$ such that $Y_{k+(i-1)K}^* = -\frac{1}{\theta_i T_c} \ln(\mathbb{E}_{\gamma_k} \{ e^{-\theta_i B_c T_c \log(1 + \frac{P_{i,k}^* \gamma_k}{N_0 B_c + \mu_{3-i,k} P_{3-i,k}^*})} \})$ for all i and k. Therefore, such $\mathbf{P}_1^*$ and $\mathbf{P}_2^*$ are clearly the optimal solutions to Problem (6.6). Hence Problem (6.6) and (6.11) are equivalent to each other.

6.3.2 Initialization of the enclosing polyblock

In order to better approximate the upper boundary of the feasible set, we need to initialize the polyblock that contains the feasible set properly. In other words, we need to find the smallest box $[\mathbf{0}, \mathbf{v}']$ that contains $\mathcal{G}$. The smallest $\mathbf{v}'$ such that $[\mathbf{0}, \mathbf{v}']$ contains $\mathcal{G}$ is given by the following:

$$v'_{k+(i-1)K} = \max\{Y_{k+(i-1)K} | \mathbf{Y} \in \mathcal{G}, \forall i \in \mathcal{I}, \forall k \in \mathcal{K}\}, \tag{6.15}$$

and it is easy to verify that

$$v'_{k+(i-1)K} = -\frac{1}{\theta_i T_c} \ln(\mathbb{E}_{\gamma_k}\{e^{-\theta_i B_c T_c \log(1+\frac{P_{i,\max}\gamma_k}{N_0 B_c})}\}). \tag{6.16}$$

Thus, the initial polyblock $\mathcal{S}_1$ is $[\mathbf{0}, \mathbf{v}']$.

Before we solve the optimization problem by using MO theory, we provide the following proposition from [67].

Proposition 6.1 (Projection on the upper boundary). *Let $\mathcal{G} \subset \mathcal{R}^n_+$ be a compact normal set with nonempty interior. Then, for any point $\mathbf{x} \in \mathcal{R}^n_+ \setminus \mathcal{G}$, the line connecting $\mathbf{0}$ and $\mathbf{x}$ intersects the upper boundary $\partial^+\mathcal{G}$ of $\mathcal{G}$ at a unique point $\pi_{\mathcal{G}}(\mathbf{x})$, which is defined as*

$$\pi_{\mathcal{G}}(\mathbf{x}) = \lambda \mathbf{x}, \lambda = \arg\max\{\lambda > 0 | \lambda \mathbf{x} \in \mathcal{G}\}. \tag{6.17}$$

$\pi_{\mathcal{G}}(\mathbf{x})$ *is the projection of $\mathbf{x}$ on the upper boundary $\partial^+\mathcal{G}$.*

The detailed steps for obtaining $\pi_{\mathcal{G}}(\mathbf{Y}_j)$ within our system model is given below in Algorithm 5.

Algorithm 5 Projection algorithm (for finding $\pi_{\mathcal{G}}(\mathbf{Y}_j)$)

Input: $\mathbf{Y}_j, \mathcal{G}$

Output: λ_j such that $\lambda_j = \arg\max\{\lambda_j > 0 | \lambda_j \mathbf{Y}_j \in \mathcal{G}\}$

1: Initialize $\lambda_j = 0$

2: **for** $d = 1 : 2$ **do**

3:     From (6.14), we set $V_{j,k+(i-1)K}(P_{1,k}, P_{2,k}) = \lambda_{j,d} Y_{j,k+(i-1)K}$ for $i \in \mathcal{I}$ and $k \in \mathcal{K}$,

        where $Y_{j,k+(i-1)K}$ is the $k + (i-1)K$th entry in $\mathbf{Y}_j$).

4:     There is another equation $\sum_{k=1}^{K} P_{d,k} = P_{d,\max}$.

5:     Thus, there are $2K + 1$ equations and $2K + 1$ unknown variables, $P_{i,k}$ and $\lambda_{j,d}$.

6:     Solve those equations and get values of $P_{i,k}$ and $\lambda_{j,d}$.

7:     **if** $\sum_{k=1}^{K} P_{3-d,k} > P_{3-d,\max}$ **then**

8:         $\lambda_{j,d} = 0$

9:     **end if**

10: **end for**

11: $\lambda_j = \max\{\lambda_{j,1}, \lambda_{j,2}\}$ and $\pi_{\mathcal{G}}(\mathbf{Y}_j) = \lambda_j \mathbf{Y}_j$.

The reason for why we have $\sum_{k=1}^{K} P_{d,k} = P_{d,\max}$ reach its maximum value for all $d = 1, 2$ is that $\pi_{\mathcal{G}}(\mathbf{Y}_j)$ is at the upper boundary of $\mathcal{G}$, and the upper boundary $\partial^+ \mathcal{G}$ only occurs at the setting mentioned above.

6.3.3   Monotonic optimization

After obtaining the proper initial polyblock, we need to find the optimal solution to Problem (6.11) by using MO theory. The key idea of MO theory is to iteratively derive a new enclosing polyblock $\mathcal{S}_{j+1}$ from the old polyblock $\mathcal{S}_j$ by cutting off the points that is in the infeasible set until we find the ϵ error-tolerance solution.

From Proposition 3.8 in [67], let $\mathcal{S} \subset \mathcal{R}_+^n$ be a polyblock with a proper vertex set

$\mathcal{T} \subset \mathcal{R}^n_+$ and let $\mathbf{x} \in \mathcal{S}$. Then, the new polyblock $\mathcal{S}_*$ has a vertex set

$$\mathcal{T}' = (\mathcal{T} \setminus \mathcal{T}_*) \cup \{\mathbf{v} = \mathbf{v} + (x_l - v_l)e_l | \mathbf{v} \in \mathcal{T}_*, l \in \{1, \ldots, n\}\} \qquad (6.18)$$

where $\mathcal{T}_*$ is the subset of $\mathcal{T}$. It is easy to see that $\mathcal{S}$ is the proper polyblock such that $\mathcal{G} \subset \mathcal{S}$ and $\mathbf{x} \in \partial^+ \mathcal{G}$, $\mathcal{G} \subset \mathcal{S}_* \subset \mathcal{S}$.

After obtaining the initial enclosing polyblock $\mathcal{S}_1$, we can iteratively derive a new enclosing polyblock $\mathcal{S}_{j+1}$ from the old polyblock $\mathcal{S}_j$ by using Algorithm 6 given below. Eventually, we can get the ϵ error tolerance solution after terminating the iteration under certain conditions.

Algorithm 6 The optimal resource allocation algorithm

Input: Function $\Phi(\mathbf{Y}) : \mathcal{R}_+^{2 \times K} \to \mathcal{R}$, compact normal set $\mathcal{G} \subset \mathcal{R}_+^{2 \times K}$.

Output: An ϵ error tolerance solution $\mathbf{Y}^*$ and the corresponding $\mathbf{P}_1^*$, $\mathbf{P}_2^*$.

1: Initialization: Let the initial polyblock $\mathcal{S}_1$ be the box $[\mathbf{0}, \mathbf{v}']$ that encloses $\mathcal{G}$. The vertex set $\mathcal{T}_1 = \mathbf{v}'$. $\epsilon > 0$ is a small positive number. CBV $\Omega_0 = 0$ and $j = 0$.

2: **repeat**

3:   $j = j + 1$.

4:   Select $\mathbf{Y}_j \in \arg\max\{\Phi(\mathbf{Y})|\mathbf{Y} \in \mathcal{T}_j\}$.

5:   Compute $\pi_{\mathcal{G}}(\mathbf{Y}_j)$ by projecting $\mathbf{Y}_j$ on the upper boundary of $\mathcal{G}$ (Algorithm 5).

6:   **if** $\pi_{\mathcal{G}}(\mathbf{Y}_j) = \mathbf{Y}_j$, i.e., $\mathbf{Y}_j \in \partial^+\mathcal{G}$ **then**

7:     CBS $\mathbf{Y}' = \mathbf{Y}_j$ and CBV $\Omega_j = \Phi(\mathbf{Y}_j)$.

8:   **else**

9:     **if** $\Phi(\pi_{\mathcal{G}}(\mathbf{Y}_j)) \geq \Omega_{j-1}$ **then**

10:       $\mathbf{Y}'_j = \pi_{\mathcal{G}}(\mathbf{Y}_j)$ and $\Omega_j = \Phi(\pi_{\mathcal{G}}(\mathbf{Y}_j))$.

11:     **else**

12:       $\mathbf{Y}'_j = \mathbf{Y}'_{j-1}$ and $\Omega_j = \Omega_{j-1}$.

13:     **end if**

14:     Let $\mathbf{x} = \pi_{\mathcal{G}}(\mathbf{Y}_j)$ and $\mathcal{T}_{j+1} = (\mathcal{T}_j \setminus \mathcal{T}_*) \cup \{\mathbf{v} = \mathbf{v} + (x_t - v_t)e_t | \mathbf{v} \in \mathcal{T}_*, t \in \{1, \ldots, 2 \times K\}\}$, where $\mathcal{T}_* = \{\mathbf{v} \in \mathcal{T}_j | \mathbf{v} > \mathbf{x}\}$.

15:     Remove the improper vertices from $\mathcal{T}_{j+1}$.

16:   **end if**

17: **until** $|\Phi(\mathbf{Y}_j) - \Omega_j| \leq \epsilon$.

18: $\mathbf{Y}^* = \mathbf{Y}'_j$ is the optimal solution and corresponding $\mathbf{P}_1^*$ and $\mathbf{P}_2^*$ is the optimal resource allocation.

In our analysis, in addition to the optimal power control scheme, we consider two suboptimal strategies for comparison. Overall, the considered three different

strategies of power allocation are the following:

- Optimal power allocation (OPA): This strategy is identified by solving the optimization problem in (6.6).

- Single-user occupied (SUO): Each subchannel can only be occupied by one user U_1 or U_2, and thus there is no self-interference in the subchannels. Optimal power allocation and subchannel allocation is also employed with the goal of maximizing the weighted sum video quality.

- Equal power allocation (EPA): Equal power $P_{i,k} = \frac{P_{i,\max}}{K}$ is allocated to each subchannel at U_i.

6.4   Simulation Results

Unless mentioned explicitly, we assume that the subchannel power gain for each link is exponentially distributed with expected value denoted by $\mathbb{E}\{z_k\}$. The power spectrum density of the AWGN is set to $N_0 = 10^{-6}$ W/Hz, and the channel coherence time is assumed to be 0.001 seconds. The total bandwidth is $B = 0.1$MHz and the self-interference suppression factor in each subchannel at each user is set to 0.1. The maximum transmission powers, $P_{1,\max}$ at U_1 and $P_{2,\max}$ at U_2, are both set to 5 Watts. U_1 transmits video sequence,'Bus', to U_2 while U_2 transmits video sequence, 'News', to U_1. $\alpha_1 = 4.7205$ and $\beta_1 = 5.4764$, $\alpha_2 = 5.6218$ and $\beta_2 = 10.0016$.

6.4.1   The impact of QoS exponent on multimedia quality

In this section, we consider the power allocation among all the subchannels between a pair of full-duplex users. It is assumed that $\omega_1 = \omega_2 = 0.5$, meaning that the two videos are equally weighted. Average channel gains are $\mathbb{E}\{z_1\} = 1$, $\mathbb{E}\{z_2\} = 2$ in the case of 2 subchannels and $\mathbb{E}\{z_1\} = 1$, $\mathbb{E}\{z_2\} = 2$ and $\mathbb{E}\{z_3\} = 3$ in the case of

3 subchannels. The bandwidths of each subchannel are $B_c = \frac{B}{2}$ and $B_c = \frac{B}{3}$ in the cases of 2 subchannels and 3 subchannels, respectively.

We increase the value of θ_1 from 0.01 to 0.1 with step size 0.01 while keeping $\theta_2 = 0.01$. Fig. 6.2a and Fig. 6.2c plot the PSNR values of weighted sum quality of received video sequences as θ_1 increases. PNSR value Q_1 decreases because of the fact that larger θ_1 leads to more stringent buffer constraints. This in turn leads to lower arrival rates and the lower quality of the video sequence. At the same time, Q_2 increases slightly. Fig. 6.2b and Fig. 6.2d demonstrate that P_1 decreases and P_2 is always kept at the maximum transmission power level when θ_1 increases. Since the video sequence, 'Bus', has more complex content than the video sequence 'News', the former video sequence requires more power to achieve the same PSNR value as the latter video sequence. It also has lower PSNR increase rate with respect to the arrival rate. Therefore, in order to gain higher weighted sum quality of video sequences, the former video sequence consumes less power than the latter one. Table 6.1 shows the powers allocated to each subchannel at both U_1 and U_2 in the case of 3 subchannels.

Table 6.1: Power allocations while changing θ_1 in the case of 3 subchannels

θ_1	0.01	0.03	0.05	0.07	0.09
$P_{1,1}$	0.092	4.196	4.070	3.658	3.619
$P_{1,2}$	4.107	0.241	0.285	0.323	0.333
$P_{1,3}$	0.802	0.464	0.469	0.295	0.299
$P_{2,1}$	3.236	0.108	0.091	0.162	0.159
$P_{2,2}$	0.213	3.769	3.896	2.490	2.500
$P_{2,3}$	1.530	1.123	1.014	2.348	2.341

Fig. 6.3 shows weighted sum quality of two video sequences, Q, while the value of θ_1 is being increased under 3 different strategies in both cases of 2 subchannels and 3 subchannels. All the PSNR values decrease since increasing θ_1 results in decreased arrival rate similarly as in the above discussion. OPA has the best performance, and EPA has a higher PSNR value than SUO in the case of 3 subchannels. However,
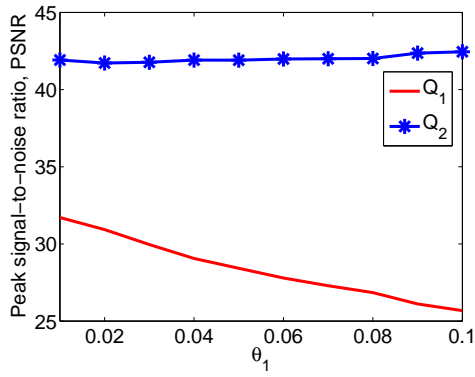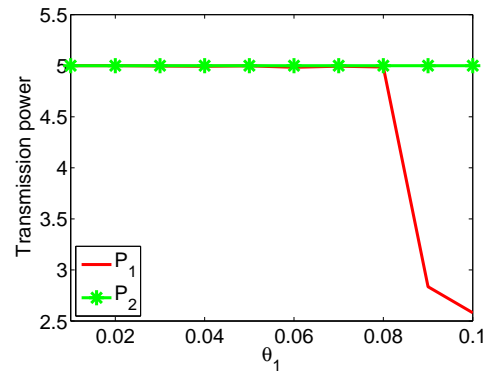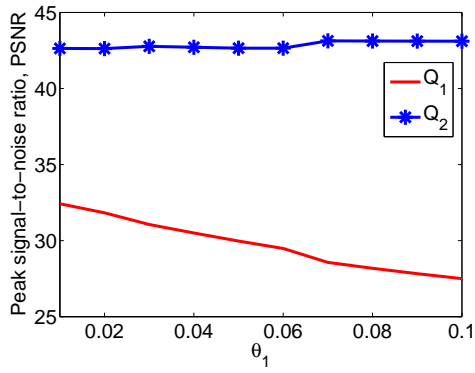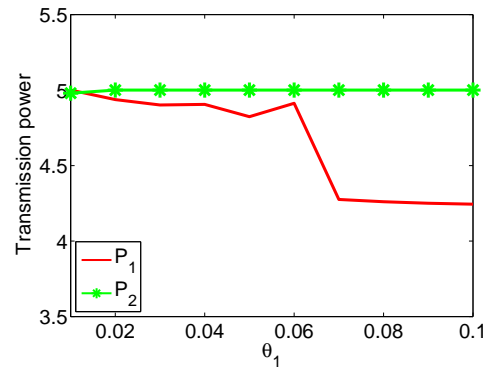
Figure 6.2: (a) PSNR values, and (b) Power allocation with 2 subchannels; and (c) PSNR values, and (d) Power allocation with 3 subchannels as θ_1 increases.
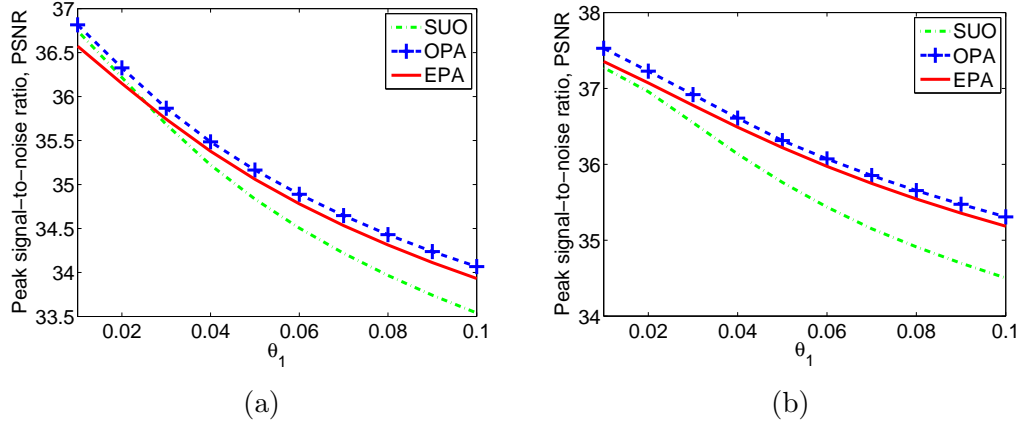
Figure 6.3: PSNR values for different strategies with (a) 2 subchannels, and (b) 3 subchannels as θ_1 increases.

when the users have only 2 subchannels, SUO initially performs better than EPA for small values for θ_1. As θ_1 increases further, EPA starts outperforming. The reason is that both U_1 and U_2 transmit the video sequences by using all subchannels while introducing interference in EPA, and U_1 and U_2 orthogonally share the subchannels without introducing any interference in SUO. Hence, there is a trade off between the number of occupied subchannels for transmission and the interference levels. The performances of EPA and SUO vary with respect to each other according to the balance in this tradeoff.

6.4.2 The impact of weights on multimedia quality

In this section, we consider power allocation among the subchannels between a pair of full-duplex users for different values of weights in the sum quality of video sequences. It is assumed that $\theta_1 = \theta_2 = 0.01$, channel gains are $\mathbb{E}\{z_1\} = 1$, $\mathbb{E}\{z_2\} = 2$ in the case of 2 subchannels and $\mathbb{E}\{z_1\} = 1$, $\mathbb{E}\{z_2\} = 2$ and $\mathbb{E}\{z_3\} = 3$ in the case of 3 subchannels. The bandwidths of each subchannel are $B_c = \frac{B}{2}$ and $B_c = \frac{B}{3}$ when there are 2 subchannels and 3 subchannels, respectively.

In the numerical analysis, ω_1 increases from 0.1 to 0.9 with step size 0.1 while

keeping $\omega_1 + \omega_2 = 1$. Fig. 6.4b and Fig. 6.4d demonstrate that P_1 increases and P_2 decreases when ω_1 increases. Hence, expectedly, higher values of weight results in more resources to be allocated to the corresponding video transmission. Fig. 6.4a and Fig. 6.4c plot the PSNR values, indicating the sum quality of the received video sequences as ω_1 grows. PNSR value Q_1 increases because larger transmission power level P_1 helps support higher arrival rates and higher quality of video sequence. At the same time, Q_2 decreases since weight ω_2 decreases. As also noted before, since the video sequence, 'Bus', has more complex content than the video sequence 'News', the former video sequence requires more power to achieve the same PSNR value as the latter video sequence. That is the reason why Q_2 is always larger than Q_1 even at $\omega_1 = 0.9$ and $\omega_2 = 0.1$. Table 6.2 shows the powers allocated to each subchannel at both U_1 and U_2 in the case of 3 subchannels.

Table 6.2: Power allocations while changing ω_1 in the case of 3 subchannels

ω_1	0.01	0.03	0.05	0.07	0.09
$P_{1,1}$	0.077	0.029	0.092	0.204	1.563
$P_{1,2}$	0.128	4.768	4.107	3.307	1.706
$P_{1,3}$	0.142	0.105	0.802	1.489	1.731
$P_{2,1}$	1.563	2.061	3.236	3.947	0.077
$P_{2,2}$	1.706	0.523	0.213	0.124	0.128
$P_{2,3}$	1.731	2.416	1.530	0.734	0.142

Fig. 6.5 plots the weighted sum quality of two video sequences, Q, as the value of ω_1 is increased. The three different power allocation strategies are considered in both cases of 2 subchannels and 3 subchannels. Even though the weight ω_1 increases, all PSNR values decrease since the content of video, 'News', is simpler and its PSNR value is higher than the video sequence, 'Bus'. OPA has the best performance, and SUO has a higher PSNR value than EPA for both 2 subchannels and 3 subchannels.
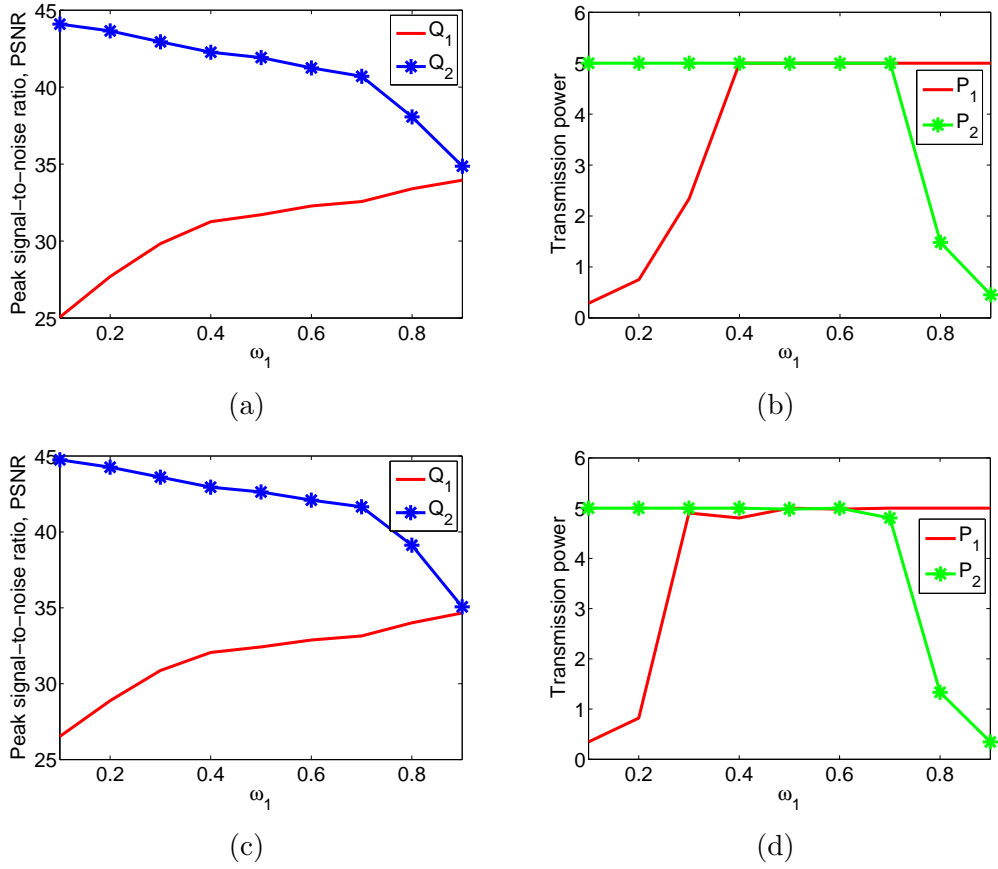
Figure 6.4: (a) PSNR values, and (b) Power allocation with 2 subchannels; and (c) PSNR values, and (d) Power allocation with 3 subchannels as ω_1 increases.
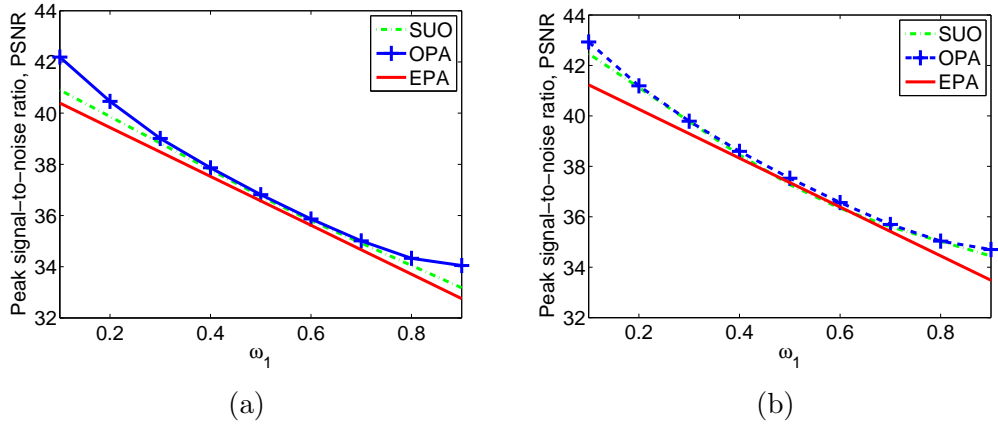
Figure 6.5: PSNR values for different strategies with (a) 2 subchannels , and (b) 3 subchannels when ω_1 increases.

Chapter 7

Quality-Driven Resource Allocation for Full-Duplex Delay-Constrained Wireless Video Transmissions

In this chapter, wireless video transmission over full-duplex channels under total bandwidth and minimum required quality constraints is studied. In order to provide the desired performance levels to the end-users in real-time video transmissions, quality of service (QoS) requirements such as statistical delay constraints are also considered. Effective capacity (EC) is used as the throughput metric in the presence of such statistical delay constraints since deterministic delay bounds are difficult to guarantee due to the time-varying nature of wireless fading channels. A communication scenario with multiple pairs of users in which different users have different delay requirements is addressed. Following characterizations from the rate-distortion (R-D) theory, a logarithmic model of the quality-rate relation is used for predicting the quality of the reconstructed video in terms of the peak signal-to-noise ratio (PSNR)

at the receiver side. Since the optimization problem is not concave or convex, the optimal bandwidth and power allocation policies that maximize the weighted sum video quality subject to total bandwidth, maximum transmission power level and minimum required quality constraints are derived by using monotonic optimization (MO) theory.

7.1 System Model

Fig. 7.1 depicts the considered system model. We consider K pairs of users, denoted as $(U_{1,1}, U_{2,1})$, $(U_{1,2}, U_{2,2})$, ..., $(U_{1,K}, U_{2,K})$[1], orthogonally sharing a total bandwidth of B Hz in full-duplex mode. Specifically, the kth full-duplex link between $U_{1,k}$ and $U_{2,k}$ is allocated a bandwidth of B_k Hz for the transmission of the video data under the constraint that the total bandwidth is $\sum_{k=1}^{K} B_k = B$. It is assumed that flat fading is experienced in each subchannel. The channel coherence time is denoted by T_c, and the timescale of video rate adaptation is much larger than T_c in practice for video transmission since video source rate is adapted at the group of pictures (GOP) time scale which is measured in seconds. The case in which the channel state changes faster than the source rate is considered in our system since if the fading channel state varies at the same timescale as the source rate, statistical delay guarantees become less interesting [28].

The practical application of this model includes, for instance, scenarios in which device-to-device (D2D) users exchange multimedia data (e.g., via social media sites) or conduct teleconferencing (i.e., engage in interactive video) in full-duplex mode. Assuming the availability of only statistical channel side information (CSI), base station acts as a coordinating agent and performs quality-driven resource allocation. Or in a different scenario, we can have one base station performing full-duplex multime-

---

[1]Throughout the thesis, the subscripts $(1, k)$ and $(2, k)$ are used for parameters and notations related to users 1 and 2 of the kth pair, respectively.
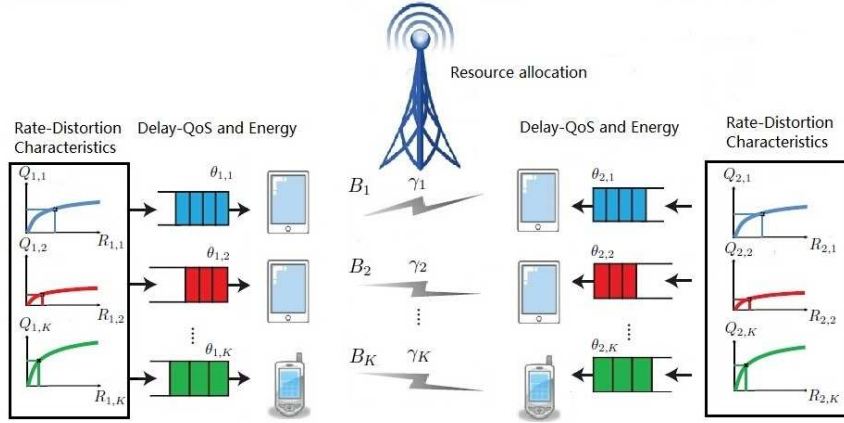
Figure 7.1: Wireless system model in which each pair of users communicates in full-duplex mode under quality and delay constraints.

dia communication with multiple users over different subchannels (e.g., via othogonal frequency division multiple access (OFDMA)). In this case, all the users on the left-hand side of Fig. 7.1 essentially represent (or collapse to) a single base station in which there are multiple buffers and multiple flows of multimedia data to be sent to different users on the right-hand side. Base station again performs quality-driven resource allocation.

7.2 Preliminaries

7.2.1 Notations

Throughout this thesis, vectors are denoted by boldface letters, the j-th entry of a vector $\mathbf{x}$ is denoted by x_j. $\mathcal{R}$ and $\mathcal{R}_+$ denote the set of real numbers and nonnegative real numbers, respectively. $\mathcal{R}^n$ and $\mathcal{R}_+^n$ denote the space of n-dimensional real-valued vectors and nonnegative real-valued vectors, respectively. For any two vectors $\mathbf{x}$, $\mathbf{y} \in \mathcal{R}^n$, $\mathbf{x} \geq \mathbf{y}$ if $x_j \geq y_j$ for all $j = 1, 2, \ldots, n$. $\cup$, $\cap$ and $\setminus$ represent set union, set intersection and set difference operators, respectively. $\mathbf{e}_j \in \mathcal{R}^n$ denotes the j-th unit vector of $\mathcal{R}^n$, i.e., the vector such that $e_j = 1$ and $e_i = 0$ for all $i \neq j$.

7.2.2   Delay QoS Constraints and Effective Capacity

Now, we express the EC formulations as in Section 2.2 for the pair of users operating in full-duplex mode. Considering independent and identically distributed fading in each coherence block of duration T_c, we can write the EC expressions for the kth pair of users as [31]

$$
\begin{aligned}
C_{1,k}(\theta_{1,k}) &= -\frac{1}{\theta_{1,k}T_c} \ln\left(\mathbb{E}_{\gamma_k}\{e^{-\theta_{1,k}r_{1,k}}\}\right) \\
&= -\frac{1}{\theta_{1,k}T_c} \ln\left(\mathbb{E}_{\gamma_k}\left\{e^{-\theta_{1,k}B_kT_c\log\left(1+\frac{P_{1,k}\gamma_k}{N_0B_k+I_{2,k}}\right)}\right\}\right) \quad (7.1)
\end{aligned}
$$

$$
\begin{aligned}
C_{2,k}(\theta_{2,k}) &= -\frac{1}{\theta_{2,k}T_c} \ln\left(\mathbb{E}_{\gamma_k}\{e^{-\theta_{2,k}r_{2,k}}\}\right) \\
&= -\frac{1}{\theta_{2,k}T_c} \ln\left(\mathbb{E}_{\gamma_k}\left\{e^{-\theta_{2,k}B_kT_c\log\left(1+\frac{P_{2,k}\gamma_k}{N_0B_k+I_{1,k}}\right)}\right\}\right) \quad (7.2)
\end{aligned}
$$

where B_k is the allocated bandwidth for the full-duplex communication of these users, $P_{i,k}$ is the power of user $U_{i,k}$, and $\theta_{i,k}$ is the QoS exponent of $U_{i,k}$. Moreover, N_0 is the power spectral density of the background Gaussian noise, and $I_{1,k}$ and $I_{2,k}$ are the self-interference terms at $U_{1,k}$ and $U_{2,k}$, respectively.

The EC should be equal to the effective bandwidth of the arrival process for the given QoS exponent θ [77] in order to support the highest arrival rates. For constant arrival rate R, the effective bandwidth of the arrival process is $A(\theta_{i,k}) = R$. Therefore, the maximum constant arrival rates at users $U_{1,k}$ and $U_{2,k}$ can be expressed,

respectively, as

$$R_{1,k} = A_{1,k}(\theta_{1,k}) = C_{1,k}(\theta_{1,k})$$

$$= -\frac{1}{\theta_{1,k}T_c} \ln \left(\mathbb{E}_{\gamma_k} \left\{ e^{-\theta_{1,k}B_kT_c \log\left(1+\frac{P_{1,k}\gamma_k}{N_0B_k+I_{2,k}}\right)} \right\} \right), \tag{7.3}$$

$$R_{2,k} = A_{2,k}(\theta_{2,k}) = C_{2,k}(\theta_{2,k})$$

$$- \frac{1}{\theta_{2,k}T_c} \ln \left(\mathbb{E}_{\gamma_k} \left\{ e^{-\theta_{2,k}B_kT_c \log\left(1+\frac{P_{2,k}\gamma_k}{N_0B_k+I_{1,k}}\right)} \right\} \right). \tag{7.4}$$

7.3 Weighted Sum Quality-Maximizing Policies

In this section, optimization problems are formulated to maximize the weighted sum video quality subject to maximum transmission power and minimum video quality constraints at each user and a total bandwidth constraint. More specifically, we address the optimal allocation of bandwidth and the determination of transmission power levels assuming the availability of statistical CSI. It is assumed that each user just has one antenna for transmitting and receiving the data. Thus, the self-interference just depends on the self-transmission power, and the maximum constant arrival rate in (7.3) and (7.4) can be rewritten as

$$R_{1,k} = C_{1,k}(\theta_{1,k})$$

$$= -\frac{1}{\theta_{1,k}T_c} \ln \left(\mathbb{E}_{\gamma_k} \left\{ e^{-\theta_{1,k}B_kT_c \log\left(1+\frac{P_{1,k}\gamma_k}{N_0B_k+\mu_{2,k}P_{2,k}}\right)} \right\} \right) \tag{7.5}$$

$$R_{2,k} = C_{2,k}(\theta_{2,k})$$

$$= -\frac{1}{\theta_{2,k}T_c} \ln \left(\mathbb{E}_{\gamma_k} \left\{ e^{-\theta_{2,k}B_kT_c \log\left(1+\frac{P_{2,k}\gamma_k}{N_0B_k+\mu_{1,k}P_{1,k}}\right)} \right\} \right) \tag{7.6}$$

where $\mu_{i,k} \in (0,1]$ is the self-interference suppression factor at $U_{i,k}$. We can now express the weighted sum video quality at users $U_{1,k}$ and $U_{2,k}$ as

$$
\begin{aligned}
Q_k &= \omega_{1,k} Q_{1,k} + \omega_{2,k} Q_{2,k} \\
&= \sum_{i=1}^{2} \omega_{i,k} \big(a_{i,k} \ln(R_{i,k}) + b_{i,k} \big),
\end{aligned}
\tag{7.7}
$$

where $\omega_{i,k} \in [0,1]$ denotes the weight for the quality of the video transmitted by user $U_{i,k}$ such that $\sum_{k=1}^{K} \sum_{i=1}^{2} \omega_{i,k} = 1$. And the quality-rate mode in Section 2.3 is employed.

Now, the problem of maximizing the overall sum video quality of all users over bandwidth and power allocation strategies can be expressed as follows:

$$
\max_{\mathbf{B}, \mathbf{P_1}, \mathbf{P_2}} \sum_{k=1}^{K} \sum_{i=1}^{2} \Big(\omega_{i,k} Q_{i,k}(R_{i,k}) \Big)
\tag{7.8a}
$$

$$
\text{s.t.} \quad \sum_{k=1}^{K} B_k \leq B; \quad B_k \geq 0, \quad \forall k \in \mathcal{K}
\tag{7.8b}
$$

$$
P_{i,k} \leq P_{i,k}^{max}; \quad P_{i,k} \geq 0, \quad \forall i \in \mathcal{I}, k \in \mathcal{K}
\tag{7.8c}
$$

$$
Q_{i,k}(R_{i,k}) \geq Q_{i,k}^{min}, \quad \forall i \in \mathcal{I}, k \in \mathcal{K}
\tag{7.8d}
$$

Above, (7.8b) is the total bandwidth constraint, (7.8c) is the maximum transmission power constraint at each user and (7.8d) is the minimum required video quality constraint. Specifically, $P_{i,k}^{max}$ and $Q_{i,k}^{min}$ are the maximum available transmission power and minimum transmitted video quality at $U_{i,k}$, respectively. $\mathbf{B}$, $\mathbf{P_1}$ and $\mathbf{P_2}$ are $K \times 1$ vectors of bandwidth allocated to each link, power allocated to $U_{1,k}$ and $U_{2,k}$, respectively. The feasible set of $\mathbf{B}$ is denoted by $\mathcal{B} = \{\mathbf{B} | \sum_{k=1}^{K} B_k \leq B\}$, and the feasible sets of $\mathbf{P_1}$ and $\mathbf{P_2}$ are denoted by $\mathcal{P}_1 = \{\mathbf{P_1} | P_{1,k} \leq P_{1,k}^{max}, \forall k \in \mathcal{K}\}$ and $\mathcal{P}_2 = \{\mathbf{P_2} | P_{2,k} \leq P_{2,k}^{max}, \forall k \in \mathcal{K}\}$, respectively.

7.3.1 Problem Reformulation as Monotonic Optimization

From the definition in Section 2.4 and [67], an optimization problem belongs to the class of MO if it can be represented in the following form:

$$\max f(\mathbf{x}) \tag{7.9}$$

$$\text{s.t.} \quad \mathbf{x} \in \mathcal{G} \cap \mathcal{H} \tag{7.10}$$

where $f(\mathbf{x}) : \mathcal{R}_+^n \to \mathcal{R}$ is an increasing function, $\mathcal{G} \subset [\mathbf{0}, \mathbf{b}] \subset \mathcal{R}_+^n$ is a compact normal set, and $\mathcal{H}$ is a closed conormal set on $[\mathbf{0}, \mathbf{b}]$. A simpler case is the one in which $\mathcal{H}$ is not present in the formulation (which occurs e.g., if the conormal set $\mathcal{H}$ is box $[\mathbf{0}, \mathbf{b}]$). In general, if $\mathcal{G} \cap \mathcal{H} \neq \emptyset$, the problem is considered feasible.

We note that it is not possible to obtain the optimal solution of (7.8a) based on the theory of convex optimization [78] because of the non-convexity of the optimization problem in (7.8a) in terms of $P_{i,k}$ and B_k jointly. This non-convexity is primarily due to the presence of the self-interference terms. In operations research, monotonicity is regarded as another important property for effectively solving an optimization problem. Therefore, we follow the approach to solve the non-convex problem (7.8a) by transforming it into an MO problem, and then solving the corresponding MO problem based on recent advances in monotonic optimization [79].

We first rewrite the objective function in (7.8a) in terms of auxiliary variables [2]. Let $\mathbf{Y}$ denote the vector $(Y_1, Y_2, \ldots, Y_{2K})$ with Y_j being the j-th component of $\mathbf{Y}$.

---

[2]Note that the objective function in (7.8a) can be expressed as

$$\sum_{k=1}^{K} \sum_{i=1}^{2} \left(\omega_{i,k} Q_{i,k}(R_{i,k}) \right) = \sum_{k=1}^{K} \sum_{i=1}^{2} \omega_{i,k} \left[a_{i,k} \ln \left(\frac{1}{\theta_{i,k} T_c} \ln \left(\mathbb{E}_{\gamma_k} \left\{ e^{-\theta_{i,k} B_k T_c \log \left(1 + \frac{P_{i,k} \gamma_k}{N_0 B_k + \mu_{3-i,k} P_{3-i,k}} \right)} \right\} \right)^{-1} \right) + b_{i,k} \right]$$

by incorporating (7.5), (7.6), and (7.7). In the ensuing discussion above, while reformulating the problem within the framework of monotonic optimization, we essentially replace $\left(\mathbb{E}_{\gamma_k} \left\{ e^{-\theta_{i,k} B_k T_c \log \left(1 + \frac{P_{i,k} \gamma_k}{N_0 B_k + \mu_{3-i,k} P_{3-i,k}} \right)} \right\} \right)^{-1}$ with auxiliary variables $Y_{(i-1)K+k}$ for $k = 1, \ldots, K$ and $i = 1, 2$.

We define the function

$$\Phi(\mathbf{Y}) = \sum_{k=1}^{K} \sum_{i=1}^{2} \omega_{i,k} \left[a_{i,k} \ln \left(\frac{1}{\theta_{i,k} T_c} \ln(Y_{(i-1)K+k}) \right) + b_{i,k} \right].$$

It is easy to see that $\Phi(\mathbf{Y})$ is an increasing function of $\mathbf{Y}$ on $\mathcal{R}_+^{2 \times K}$. In other words, for any two vectors $\mathbf{Y}_1$ and $\mathbf{Y}_2$, $\Phi(\mathbf{Y}_1) \geq \Phi(\mathbf{Y}_2)$ if $\mathbf{Y}_1 \geq \mathbf{Y}_2$. Now, problem (7.8a) can be rewritten in the MO formulation as

$$\max \Phi(\mathbf{Y}) = \sum_{k=1}^{K} \sum_{i=1}^{2} \omega_{i,k} \left[a_{i,k} \ln \left(\frac{\ln(Y_{(i-1)K+k})}{\theta_{i,k} T_c} \right) + b_{i,k} \right] \qquad (7.11a)$$

$$\text{s.t.} \quad \mathbf{Y} \in \mathcal{G} \cap \mathcal{H}. \qquad (7.11b)$$

Above, the normal set is

$$\mathcal{G} = \big\{ \mathbf{Y} | 0 \leq Y_{(i-1)K+k} \leq V_{(i-1)K+k}(P_{1,k}, P_{2,k}, B_k), \forall i \in \mathcal{I},$$

$$\forall k \in \mathcal{K}, \mathbf{P}_1 \in \mathcal{P}_1, \mathbf{P}_2 \in \mathcal{P}_2, \mathbf{B} \in \mathcal{B} \big\} \qquad (7.12)$$

where

$$V_{(i-1)K+k}(P_{1,k}, P_{2,k}, B_k)$$
$$= \left(\mathbb{E}_{\gamma_k} \left\{ e^{-\theta_{i,k} B_k T_c \log \left(1 + \frac{P_{i,k} \gamma_k}{N_0 B_k + \mu_{3-i,k} P_{3-i,k}} \right)} \right\} \right)^{-1}. \qquad (7.13)$$

Note that when $Y_{(i-1)K+k}$ in the objective function in (7.11) is replaced with the upper bound $V_{(i-1)K+k}(P_{1,k}, P_{2,k}, B_k)$, the objective function becomes the same as that in (7.8a). In (7.11b), the conormal set is

$$\mathcal{H} = \{ \mathbf{Y} | Y_{(i-1)K+k} \geq V_{(i-1)K+k}^{min}, \forall i \in \mathcal{I}, \forall k \in \mathcal{K} \} \qquad (7.14)$$

where

$$V^{min}_{(i-1)K+k} = e^{\theta_{i,k}T_c e^{\frac{Q^{min}_{i,k}-b_{i,k}}{a_{i,k}}}}.$$

Note that the normal set $\mathcal{G}$ describes the combination of total bandwidth constraint (7.8b) and maximum transmission power constraint (7.8c), and the cornormal set $\mathcal{H}$ corresponds to the minimum quality constraint (7.8d).

Since $\Phi(\mathbf{Y})$ is an increasing function of $\mathbf{Y}$, the optimal solution of Problem (7.11), denoted by $\mathbf{Y}^*$, must be located at the upper boundary of $\mathcal{G}$, denoted by $\partial^+\mathcal{G}$. This means that we can find a bandwidth allocation $\mathbf{B}^*$ and power allocations $\mathbf{P}^*_1$ and $\mathbf{P}^*_2$ corresponding to the optimal solution $\mathbf{Y}^*$ such that

$$Y^*_{(i-1)K+k} = \left(\mathbb{E}_{\gamma_{lk}} \left\{ e^{-\theta_{i,k}B^*_k T_c \log\left(1+\frac{P^*_{i,k}\gamma_k}{N_0 B^*_k+\mu_{3-i,k}P^*_{3-i,k}}\right)} \right\} \right)^{-1} \tag{7.15}$$

for all $i \in \mathcal{I}$ and $k \in \mathcal{K}$. Therefore, such $\mathbf{B}^*$, $\mathbf{P}^*_1$ and $\mathbf{P}^*_2$ are clearly the optimal solutions to Problem (7.8a). Hence Problem (7.8a) and (7.11) are equivalent. We must also note that $Y_{(i-1)K+k}$ is lower bounded by 1, i.e., $Y_{(i-1)K+k} \geq 1$ for all i and k. Consequently, the optimal solution $\mathbf{Y}^*$ to Problem (7.11), which is located only at the upper boundary of set $\mathcal{G}$, is also lower bounded by $\mathbf{1}$. That means that the optimal solution $\mathbf{Y}^* \in \mathcal{G} \cap \mathcal{H} \cap \mathcal{L}$, where

$$\mathcal{L} = \{\mathbf{Y}|Y_{(i-1)K+k} \geq 1, \forall i \in \mathcal{I}, \forall k \in \mathcal{K}\}.$$

7.3.2 Initialization of the Enclosing Polyblock

In order to better approximate the upper boundary of the feasible set, we need to initialize the polyblock that contains the feasible set properly. In other words, we need to find the smallest box $[\mathbf{0}, \mathbf{v}']$ that contains $\mathcal{G} \cap \mathcal{H} \cap \mathcal{L}$. Since both sets $\mathcal{H}$ and

$\mathcal{L}$ are cornormal, the set

$$\mathcal{J} = \mathcal{H} \cap \mathcal{L} = \{\mathbf{Y} | Y_{(i-1)K+k} \geq \max\{V_{(i-1)K+k}^{min}, 1\}, \forall i \in \mathcal{I}, \forall k \in \mathcal{K}\}$$

is also cornormal. The smallest $\mathbf{v}'$ such that $[\mathbf{0}, \mathbf{v}']$ contains $\mathcal{G} \cap \mathcal{J}$ is given by the following:

$$v_j' = \max\{Y_j | \mathbf{Y} \in \mathcal{G} \cap \mathcal{J}\} \quad \forall j = 1, \ldots, 2K. \tag{7.16}$$

Before describing the enclosing polyblock initialization algorithm, we provide the following characterization for the functional properties of $V_{(i-1)K+k}(P_{1,k}, P_{2,k}, B_k)$.

Theorem 7.1 *Consider the functions*

$$V_1(P_1, P_2, B) = \left(\mathbb{E}_\gamma \left\{ e^{-\theta B T_c \log \left(1 + \frac{P_1 \gamma}{N_0 B + \mu P_2}\right)} \right\} \right)^{-1} \quad and \tag{7.17}$$

$$V_2(P_1, P_2, B) = \left(\mathbb{E}_\gamma \left\{ e^{-\theta B T_c \log \left(1 + \frac{P_2 \gamma}{N_0 B + \mu P_1}\right)} \right\} \right)^{-1} \tag{7.18}$$

and assume that $P_1 \leq P^{\max}$ and $P_2 \leq P^{\max}$. Then, we have the following properties:

1. *For given bandwidth B, V_1 is maximized when either $P_1 = P^{\max}$ or $P_2 = P^{\max}$. Hence, at least one power value should be at its maximum level.*

2. *For given P_1 and P_2, V_1 is an increasing function of B.*

3. *The above properties hold for V_2 as well due to the similarity in their definitions (with only roles of P_1 and P_2 switched).*

4. *The bandwidth required to achieve two target values $V_1(P_1, P_2, B) = V_1^*$ and $V_2(P_1, P_2, B) = V_2^*$ is minimized if either $P_1 = P^{\max}$ or $P_2 = P^{\max}$.*

Proof: See Appendix A.4.

The detailed algorithm for initializing the enclosing polyblock is provided below in Algorithm 7. We note that Step 3 of Algorithm 7 makes use of Theorem 7.1, i.e., the fact that the minimum bandwidth always occurs at $P_{1,k} = P_{1,k}^{max}$ or $P_{2,k} = P_{2,k}^{max}$. In particular, in this step, we identify the minimum bandwidth needed by the users while power and minimum quality constraints are satisfied. Subsequently, starting with Step 8, we allocate the remaining bandwidth to user k (after providing the minimum required bandwidth to all users) and determine $V_{(i-1)K+k}^{max}$, which is essentially the solution of the maximization problem in (7.16) for $j = (i-1)K + k$ within the feasible set $\mathcal{G} \cap \mathcal{J}$.

Algorithm 7 The enclosing polyblock initialization algorithm

Input: $\mathcal{G}$, $\mathcal{H}$ and $\mathcal{L}$

Output: Polyblock $\mathcal{S}_1$

1: Initialize $s = 1$.

2: **for** $k = 1 : K$ **do**

3:     Set $V_{(i-1)K+k}(P_{1,k}, P_{2,k}, B_k) = \max\{V^{min}_{(i-1)K+k}, 1\}$ for $i = 1, 2$. Let $P_{1,k} = P^{max}_{1,k}$, find the bandwidth $B_k = B_{k1}$ and power $P_{2,k}$ by solving (7.13). Similarly, let $P_{2,k} = P^{max}_{2,k}$, find the bandwidth $B_k = B_{k2}$ and $P_{1,k}$ by solving (7.13). $B^{min}_k = \min\{B_{k1}, B_{k2}\}$ if both $P_{1,k} \in \mathcal{P}_1$ and $P_{2,k} \in \mathcal{P}_2$, and $B^{min}_k = B_{ki}$ if just one $P_{i,k} \in \mathcal{P}_i$ for $i = 1$ or $i = 2$. Otherwise, Problem (7.11) does not have solution and set $s = 0$.

4: **end for**

5: If $s = 1$, and $\sum_{l=1}^K B^{min}_l > B$, the Problem (7.11) does not have solution and set $s = 0$.

6: **if** $s = 1$ **then**

7:     **for** $k = 1 : K$ **do**

8:         $B_k = B - \sum_{l \neq k} B^{min}_l$.

9:         **for** i = 1:2 **do**

10:             Let $V_{(2-i)K+k} = \max\{V^{min}_{(2-i)K+k}, 1\}$ and $P_{3-i,k} = P^{max}_{3-i,k}$, and find the power $P_{i,k}$ from (7.13).

11:             Calculate $V^{max}_{(i-1)K+k}$ from (7.13) by substituting $P_{j,k}$ and $P_{i,k}$ obtained above.

12:         **end for**

13:     **end for**

14: **end if**

15: Therefore, the vector $\mathbf{v}' = (V^{max}_1, \ldots, V^{max}_{2K})$ is the vertex of the initial polyblock $\mathcal{S}_1$.
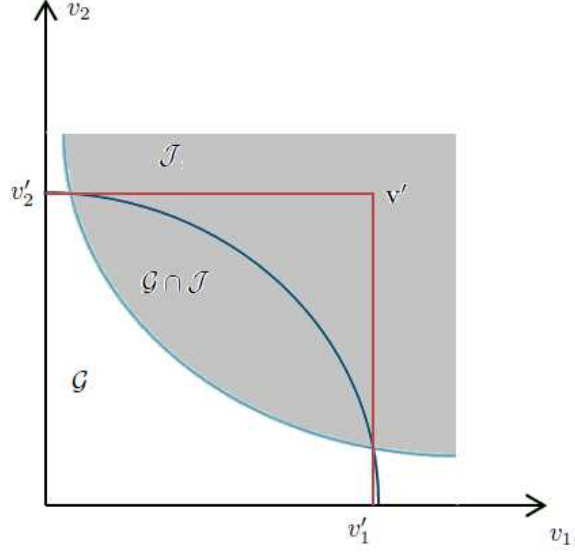
Figure 7.2: Example of initialized enclosing polyblock

We now provide an illustration for the enclosing polyblock initialization. For instance, assume that $\mathcal{G}$ and $\mathcal{J}$ are two-dimensional sets by assuming $K = 1$. As shown in Fig. 7.2, the box $[\mathbf{0}, \mathbf{v}']$ constrained by the red lines is the smallest box that contains $\mathcal{G} \cap \mathcal{J}$, where $\mathbf{v}' = (v_1', v_2')$. And $\mathbf{v}'$ can be obtained by the algorithm provided above.

Before we solve the optimization problem by using MO theory, we provide the following proposition from [67].

Proposition 7.1 (Projection on the upper boundary) *Let $\mathcal{G} \subset \mathcal{R}_+^n$ be a compact normal set with nonempty interior. Then, for any point $\mathbf{x} \in \mathcal{R}_+^n \setminus \mathcal{G}$, the line connecting $\mathbf{0}$ and $\mathbf{x}$ intersects the upper boundary $\partial^+\mathcal{G}$ of $\mathcal{G}$ at a unique point $\pi_{\mathcal{G}}(\mathbf{x})$, which is defined as*

$$\pi_{\mathcal{G}}(\mathbf{x}) = \lambda\mathbf{x}, \quad where \ \lambda = \arg\max\{\alpha > 0 \mid \alpha\mathbf{x} \in \mathcal{G}\}. \tag{7.19}$$

$\pi_{\mathcal{G}}(\mathbf{x})$ *is the projection of $\mathbf{x}$ on the upper boundary $\partial^+\mathcal{G}$.*

Due to the presence of $\mathcal{J}$, $\pi_{\mathcal{G}(\mathbf{x})}$ may be located outside the feasible set $\mathcal{G} \cap \mathcal{J}$ if one end point of the line is $\mathbf{0}$. In order to avoid this situation, we modify the projection by

118

changing the line connecting $\mathbf{0}$ and $\mathbf{x}$ to the line connecting $\mathbf{u}$ and $\mathbf{x}$, and we denote by $\pi_{\mathcal{G}}^{\mathbf{u}}(\mathbf{x})$ the projection of $\mathbf{x}$ on the upper boundary $\partial^+ \mathcal{G}$ with $\mathbf{u}$ acting as the origin. Therefore,

$$\pi_{\mathcal{G}}^{\mathbf{u}}(\mathbf{x}) = \lambda(\mathbf{x} - \mathbf{u}) + \mathbf{u}, \tag{7.20}$$

where $\lambda = \arg\max\{\alpha > 0 \mid \alpha\mathbf{x} \in \mathcal{G}\}$ and $\mathbf{u} = (\max\{V_1^{min}, 1\}, \dots, \max\{V_{2K}^{min}, 1\})$.

7.3.3 Algorithms and Optimal Solution via Monotonic Optimization

After obtaining the proper initial polyblock, we next develop algorithms and determine the optimal solution to Problem (7.11) via MO approach. The key idea of MO is to iteratively derive a new enclosing polyblock $\mathcal{S}_{j+1}$ from the previous polyblock $\mathcal{S}_j$ by cutting off the points that is in the infeasible set until reaching the ϵ-error-tolerance solution. Following Proposition 3.8 in [67], we let $\mathcal{S} \subset \mathcal{R}_+^n$ be a polyblock with a proper vertex set $\mathcal{T} \subset \mathcal{R}_+^n$ and let $\mathbf{x} \in \mathcal{S}$. Then, the new polyblock $\mathcal{S}_*$ has a vertex set

$$\mathcal{T}' = (\mathcal{T} \setminus \mathcal{T}_*) \cup \{\mathbf{v} = \mathbf{v} + (x_j - v_j)e_j | \mathbf{v} \in \mathcal{T}_*, j \in \{1, \dots, n\}\} \tag{7.21}$$

where $\mathcal{T}_*$ is the subset of $\mathcal{T}$, consisting of the vertices at which $\Phi(\mathbf{Y})$ is maximized. It is easy to see that if $\mathcal{S}$ is the proper polyblock such that $\mathcal{G} \cap \mathcal{J} \subset \mathcal{S}$ and $\mathbf{x} \in \partial^+\mathcal{G}$, then we have $\mathcal{G} \cap \mathcal{J} \subset \mathcal{S}_* \subset \mathcal{S}$.

We first construct a proper polyblock $\mathcal{S}_1$ that contains the feasible set, $\mathcal{G} \cap \mathcal{J}$ of Problem (7.11) by using Algorithm 7, and let $\mathcal{T}_1$ denote the initial proper vertex set of $\mathcal{S}_1$. There is just one vertex, $\mathbf{v}'$, in $\mathcal{T}_1$. Since the objective function of Problem (7.11), $\Phi(\mathbf{Y})$ is monotonically increasing over set $\mathcal{S}_1$, the maximum of $\Phi(\mathbf{Y})$ occurs
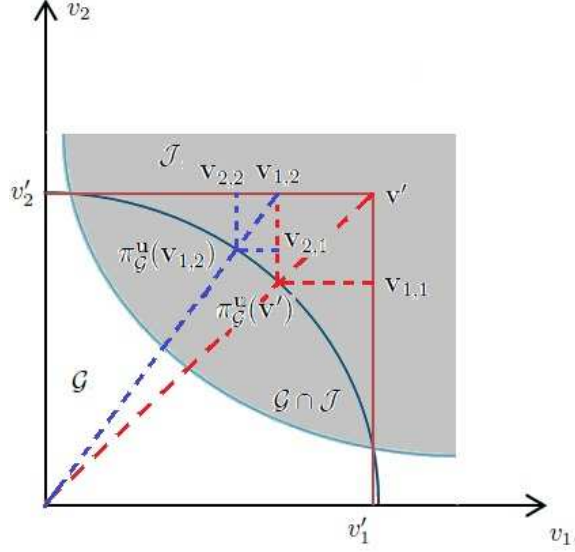
Figure 7.3: Iterative procedure of projection onto the boundary and formation of new set of vertices.

at some proper vertex $\mathbf{Y}_1$ of $\mathcal{S}_1$, i.e., $\mathbf{Y}_1 \in \mathcal{T}_1$. If $\mathbf{Y}_1$ is also in the feasible set $\mathcal{G} \cap \mathcal{J}$, then the optimization problem is solved and $\mathbf{Y}^* = \mathbf{Y}_1$. Otherwise, a smaller polyblock $\mathcal{S}_2 \subset \mathcal{S}_1$ is constructed such that $\mathcal{G} \cap \mathcal{J} \subset \mathcal{S}_2$ but excludes $\mathbf{Y}_1$ by using Proposition 3.8 in [67]. Therefore, a new vertex set $\mathcal{T}_2$ is constructed by replacing $\mathbf{Y}_1$ in $\mathcal{T}_1$ with $2 \times K$ new vertices and removing the improper vertices. This procedure is repeated until an ϵ-error-tolerance solution is found. If $\mathbf{Y}_j$ denotes the optimal vertex that maximizes $\Phi(\mathbf{Y})$ over set $\mathcal{S}_j$ at the j-th iteration, we have $\mathcal{S}_1 \supset \mathcal{S}_2 \supset \cdots \supset \mathcal{G}$ and $\Phi(\mathbf{Y}_1) \geq \Phi(\mathbf{Y}_2) \geq \cdots \geq \Phi(\mathbf{Y}^*)$. $\mathbf{Y}'_j = \arg\max\{\Phi(\mathbf{Y})|\mathbf{Y} \in \{\pi^{\mathbf{u}}_{\mathcal{G}}(\mathbf{Y}_j), \mathbf{Y}'_{j-1}\}\}$ denotes the current best solution (CBS), and the current best value (CBV) is $\Phi(\mathbf{Y}'_j)$ in the j-th iteration. Consequently, we have $\Phi(\mathbf{Y}'_1) \leq \Phi(\mathbf{Y}'_2) \leq \cdots \leq \Phi(\mathbf{Y}^*)$. The algorithm terminates at the j-th iteration if $\mathbf{Y}_j \in \mathcal{S}_j$, and $(1 + \epsilon)\Phi(\mathbf{Y}'_j) \geq \Phi(\mathbf{Y}_j)$ or $|\Phi(\mathbf{Y}'_j) - \Phi(\mathbf{Y}_j)| \leq \epsilon$ based on the chosen strategy, where $\epsilon > 0$ is a small positive number representing the error tolerance. $\mathbf{Y}'_j$ is the optimal ϵ-error-tolerance solution.

In order to illustrate the iterative process described above, we again consider the simple setting of Fig. 7.2 with $K = 1$ and plot Fig. 7.3 above. As seen in the figure, in the first iteration, the vertex $\mathbf{v}'$ is projected onto the boundary at point $\pi^{\mathbf{u}}_{\mathcal{G}}(\mathbf{v}')$

by using the projection algorithm. Following this, we generate the polyblock with vertices $\mathbf{v}_{1,1}$ and $\mathbf{v}_{1,2}$ and form the set of vertices $\mathcal{T}$. Any point inside this polyblock is possible to be the optimal one. Let us assume that $\mathbf{v}_{1,2}$ leads to a higher value of the objective function than $\mathbf{v}_{1,1}$. Then, in the second iteration, we project $\mathbf{v}_{1,1}$ onto the boundary and get the projection point $\pi_{\mathcal{G}}^{\mathbf{u}}(\mathbf{v}_{1,2})$. Following this, two new vertices $\mathbf{v}_{2,1}$ and $\mathbf{v}_{2,2}$ are added to $\mathcal{T}$ while the previous vertex point $\mathbf{v}_{1,2}$ is removed from $\mathcal{T}$. Therefore, the updated set of vertices now contains $\mathbf{v}_{1,1}$, $\mathbf{v}_{2,1}$ and $\mathbf{v}_{2,2}$, and these three vertices form the new polyblock. And, we continue this procedure iteratively until an $\epsilon-$error-tolerance solution is obtained.

Algorithm 8 Projection algorithm (for finding $\pi_{\mathcal{G}}(\mathbf{Y}_j)$)

Input: $\mathbf{Y}_j, \mathcal{G}$

Output: λ_j such that $\lambda_j = \arg\max\{\lambda_j > 0 | \lambda_j \mathbf{Y}_j \in \mathcal{G}\}$

1: Initialize $\lambda_j = 0$

2: **for** $d = 0 : 2^K - 1$ **do**

3:     Let c be a K-digit binary integer corresponding to d, and c_l denote the l-th

   binary digit of c.

4:     **for** $k = 1 : K$ **do**

5:         **if** $c_k = 0$ **then**

6:             $P_{1,k} = P_{1,k}^{max}$

7:         **else**

8:             $P_{2,k} = P_{2,k}^{max}$

9:         **end if**

10:        From (7.13), we set $V_{(i-1)K+k}(P_{1,k}, P_{2,k}, B_k) = \lambda_{j,d+1}(Y_{(i-1)K+k}^j - u_{(i-1)K+k}) +$

    $u_{(i-1)K+k}$.

11:    **end for**

12:    Set $\sum_{k=1}^{K} B_k = B$.

13:    Therefore, we get $2K+1$ equations, K unknown power variables $P_{1,k}$ or $P_{2,k}$, K

    unknown bandwidth variables B_k for all $k = 1, \ldots, K$, and unknown variable

    $\lambda_{j,d+1}$. We can get the value of $\lambda_{j,d+1}$ by solving this $2K + 1$ equations. If

    $P_{i,k} \leq P_{i,k}^{max}$ for all $i = 1, 2$ and $k = 1, \ldots, K$, $\lambda_j = \max\{\lambda_j, \lambda\}$.

14: **end for**

15: $\pi_{\mathcal{G}}^{\mathbf{u}}(\mathbf{Y}_j) = \lambda_j(\mathbf{Y}_j - \mathbf{u}) + \mathbf{u}$.

As discussed in the previous subsection with Proposition 7.1, iterations in finding $\{\mathbf{Y}_j\}$ involve projection on the upper boundary. We provide our projection algorithm for finding $\pi_{\mathcal{G}}^{\mathbf{u}}(\mathbf{Y}_j)$ as Algorithm 8 above. In steps 6 and 8 of this algorithm, the reason for considering $P_{1,k}$ or $P_{2,k}$ to be at the maximum level for all $k = 1, \ldots, K$

and $\sum_{k=1}^{K} B_k = B$ is that $\pi_{\mathcal{G}}^{\mathbf{u}}(\mathbf{Y}_j)$ is attained at the upper boundary of $\mathcal{G}$, and the upper boundary $\partial^{+}\mathcal{G}$ is reached only if one of the users transmits at the peak power level. The proof for this characterization is provided in Appendix A.5, which primarily follows from the results of Theorem 7.1.

After having obtained the initial enclosing polyblock $\mathcal{S}_1$ and identified the algorithm for projection on the boundary, we can now iteratively derive a new enclosing polyblock $\mathcal{S}_{j+1}$ from the previous polyblock $\mathcal{S}_j$ by using Algorithm 9 below. Eventually, we obtain the ϵ-error-tolerance solution after terminating the iteration under a certain condition.

Algorithm 9 The optimal resource allocation algorithm

Input: Function $\Phi(\mathbf{Y}) : \mathcal{R}_+^{2 \times K} \to \mathcal{R}$, compact normal set $\mathcal{G} \subset \mathcal{R}_+^{2 \times K}$, and a closed conormal set $\mathcal{J} \subset \mathcal{R}_+^{2 \times K}$ such that $\mathcal{G} \cap \mathcal{J} \neq \emptyset$

Output: An ϵ error tolerance solution $\mathbf{Y}^*$ and the corresponding $\mathbf{P}_1^*$, $\mathbf{P}_2^*$ and $\mathbf{B}^*$.

1: Initialization: Let the initial polyblock $\mathcal{S}_1$ be the box $[\mathbf{0}, \mathbf{b}]$ that encloses $\mathcal{G} \cap \mathcal{J}$ (This can be obtained by using Algorithm 7). The vertex set $\mathcal{T}_1 = \mathbf{b}$. $\epsilon > 0$ is a small positive number. CBV $\Omega_0 = 0$ and $j = 0$.

2: **repeat**

3:      $j = j + 1$.

4:      Select $\mathbf{Y}_j \in \arg\max\{\Phi(\mathbf{Y}) | \mathbf{Y} \in \mathcal{T}_j\}$.

5:      Compute $\pi_{\mathcal{G}}^{\mathbf{u}}(\mathbf{Y}_j)$ by projecting $\mathbf{Y}_j$ on the upper boundary of $\mathcal{G}$ (Algorithm 8).

6:      **if** $\pi_{\mathcal{G}}^{\mathbf{u}}(\mathbf{Y}_j) = \mathbf{Y}_j$, i.e., $\mathbf{Y}_j \in \partial^+\mathcal{G}$ **then**

7:         CBS $\mathbf{Y}' = \mathbf{Y}_j$ and CBV $\Omega_j = \Phi(\mathbf{Y}_j)$.

8:      **else**

9:         **if** $\Phi(\pi_{\mathcal{G}}^{\mathbf{u}}(\mathbf{Y}_j)) \geq \Omega_{j-1}$ **then**

10:            $\mathbf{Y}_j' = \pi_{\mathcal{G}}^{\mathbf{u}}(\mathbf{Y}_j)$ and $\Omega_j = \Phi(\pi_{\mathcal{G}}^{\mathbf{u}}(\mathbf{Y}_j))$.

11:         **else**

12:            $\mathbf{Y}_j' = \mathbf{Y}_{j-1}'$ and $\Omega_j = \Omega_{j-1}$.

13:         **end if**

14:         Let $\mathbf{x} = \pi_{\mathcal{G}}^{\mathbf{u}}(\mathbf{Y}_j)$ and $\mathcal{T}_{j+1} = (\mathcal{T}_j \setminus \mathcal{T}_*) \cup \{\mathbf{v} = \mathbf{v} + (x_t - v_t)e_t | \mathbf{v} \in \mathcal{T}_*, t \in \{1, \ldots, 2K\}\}$, where $\mathcal{T}_* = \{\mathbf{v} \in \mathcal{T}_j | \mathbf{v} > \mathbf{x}\}$.

15:         Remove the improper vertices from $\mathcal{T}_{j+1}$.

16:      **end if**

17: **until** $|\Phi(\mathbf{Y}_j) - \Omega_j| \leq \epsilon$.

18: $\mathbf{Y}^* = \mathbf{Y}_j'$ is the optimal solution and corresponding $\mathbf{P}_1^*$, $\mathbf{P}_2^*$ and $\mathbf{B}^*$ is the optimal resource allocation.

Via Algorithms 7–9, we determine the optimal bandwidth allocation and power allocation (BAPA) maximizing weighted sum quality of the videos of the users under total bandwidth, individual power, and individual video quality constraints (i.e., we solve the optimization problem in (7.8a)).

In the numerical results presented in the next section, we demonstrate the optimal performance and identify the key tradeoffs. Additionally, we analyze the equal-bandwidth (EB) scenario in which bandwidth is equally allocated to the users, i.e., $B_k = \frac{B}{K}$, and power allocation is performed separately for each pair of full-duplex users, and provide comparisons.

7.4 Numerical and Simulation Results

Five CIF video sequences namely *Akiyo, Bus, Coastguard, Foreman* and *News* are used for the simulation results [66]. Size of each frame is 352×288 pixels. FFMPEG is used for encoding the video sequences and GOP is set as 10. Frame rate is set as 15 frames per second. Table 7.1 as the same as in Chapter 2 shows the parameters a_k and b_k that make the rate-distortion function of the five video sequences fit the quality rate model in (2.10), where the unit of R_k is kbit/s. Unless mentioned explicitly, we assume that the subchannel power gain for each link is exponentially distributed with mean $Z_k = \mathbb{E}\{\gamma_k\}$. The power spectrum density of the AWGN is set to $N_0 = 10^{-6}$ W/Hz, and the channel coherence time is assumed to be 0.001 seconds. The self-interference factor at each user is set to 0.1.

Table 7.1: Parameter values of the quality rate model for different video sequences

	Akiyo	Bus	Coastguard	Foreman	News
a_k	5.0545	4.7205	3.5261	4.5006	5.6218
b_k	17.1145	5.4764	13.8425	13.0780	10.0016

Fig. 7.4 as the same in Chapter 2 shows the actual PSNR values as a function
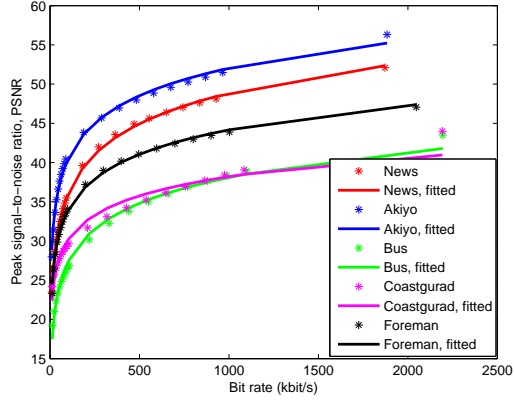
Figure 7.4: Actual PSNR values vs. rate and fitted quality rate curves.

of the source bit rate for different video sequences, where we see that the increasing concave quality rate model fits the actual values very well. Throughout the numerical results, we assume the minimum required video quality is $Q_{i,k}^{min} = 20$dB and maximum transmission power is $P_{i,k}^{max} = 5$ for all users.

7.4.1 One Pair of Full-Duplex Users

In this section, we consider the power allocation between a single pair of full-duplex users. The bandwidth B is set to 0.1 MHz, average channel power gain is $Z_1 = 1$. $U_{1,1}$ transmits video sequence *Bus* to $U_{2,1}$, while $U_{2,1}$ transmits video sequence *Coastguard* to $U_{1,1}$, with the corresponding parameters ($a_{1,1} = 4.7205$, $b_{1,1} = 5.4764$), and ($a_{2,1} = 3.5261$, $b_{2,1} = 13.8425$) from Table I.

7.4.1.1 The Impact of the QoS Exponent on Multimedia Quality

In Fig. 7.5, we set $\omega_{1,1} = \omega_{2,1} = 0.5$ (meaning that two videos are equally weighted), and increase the value of $\theta_{1,1}$ (the QoS exponent of user $U_{1,1}$) from 0.01 to 0.1 while keeping $\theta_{2,1} = 0.01$. Note that increased $\theta_{1,1}$ implies that more stringent delay constraints are imposed on the video transmission of $U_{1,1}$. Fig. 7.5a plots the power allocated to the users as $\theta_{1,1}$ increases. Since quality parameter $a_{1,1}$ of *Bus* video is

Figure 7.5: (a) Optimal power allocation and (b) the corresponding quality Q (or equivalently PSNR) of video sequences as a function of $\theta_{1,1}$.

greater than $a_{2,1}$ of *Coastguard* video, quality $Q_{1,1}$ of the *Bus* video increases faster than $Q_{2,1}$ of the *Coastguard* video as the transmission power and correspondingly the arrival rate R grow, according to the logarithmic model in (2.10). Therefore, initially when $\theta_{1,1} = \theta_{2,1} = 0.01$ and $U_{1,1}$ and $U_{2,1}$ are subject to the same delay constraint, $U_{1,1}$ transmits at the peak power level in a greedy fashion to maximize the sum video quality, while $U_{2,1}$ uses less power.

As $\theta_{1,1}$ increases, more stringent delay constraints are imposed on user $U_{1,1}$ and the arrival rate $R_{1,1}$ of the *Bus* video is reduced to avoid delay violations. Consequently, the video quality $Q_{1,1}$ (or equivalently the PSNR of the video) starts diminishing as seen in Fig. 7.5b. Eventually, when $\theta_{1,1}$ exceeds 0.06, the lower arrival rates can be supported by smaller transmission power and $P_{1,1}$ is reduced as observed in Fig. 7.5a. In the meantime, we notice that quality $Q_{2,1}$ of *Costguard* video slightly increases due to increased transmission power $P_{2,1}$ at $U_{2,1}$ and smaller self-interference at $U_{1,1}$ (because of smaller transmission power $P_{1,1}$). However, since the drop in $Q_{1,1}$ is more significant, the weighted sum quality Q_ω is seen to decrease in Fig. 7.5b. Finally, it is interesting to note that, as predicted by Theorem 7.1 and discussed subsequently, at least power value is at the maximum level of 5, i.e., $P_{1,1} = 5$ or $P_{2,1} = 5$, for any given value of $\theta_{1,1}$ in Fig. 7.5a.
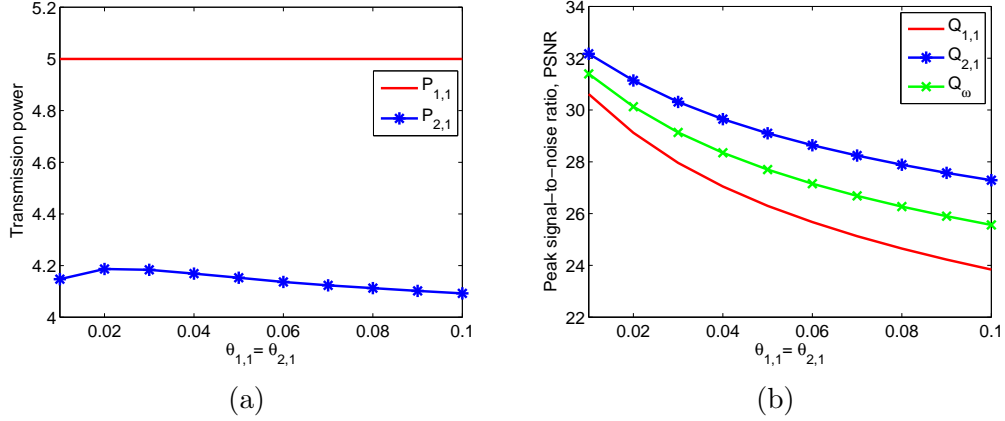
Figure 7.6: (a) Optimal power allocation and (b) the corresponding quality Q (or equivalently PSNR) of video sequences as a function of $\theta_{1,1} = \theta_{2,1}$.

In Fig. 7.6, both $\theta_{1,1}$ and $\theta_{2,1}$ increase from 0.01 to 0.1 together. Since $U_{1,1}$ and $U_{2,1}$ now all the time operate under the same QoS constraints while transmitting different video sequences, Fig. 7.6a demonstrates that $P_{1,1}$ is always greater than $P_{2,1}$ due to, as discussed above, the impact of video quality parameters, or more specifically due to having $a_{1,1} > a_{2,1}$. Fig. 7.6b shows that both $Q_{1,1}$ and $Q_{2,1}$ decrease as both $\theta_{1,1}$ and $\theta_{2,1}$ increase. That is because larger $\theta_{1,1}$ and $\theta_{2,1}$ lead to smaller source rates $R_{1,1}$ and $R_{2,1}$, which in turn reduce the video quality.

7.4.1.2 The Impact of Weights on Multimedia Quality

Now, we set $\theta_{1,1} = \theta_{2,1} = 0.01$, and increase the weight $\omega_{1,1}$ from 0 to 1 while keeping $\omega_{1,1} + \omega_{2,1} = 1$. Hence, the weight of user $U_{1,1}$ gradually increases in the weighted sum quality maximization in (7.8a). Fig. 7.7a shows that, as expected, $P_{1,1}$ grows and reaches the peak value as $\omega_{1,1}$ increases due to higher emphasis on the quality $Q_{1,1}$. At the same time, $P_{2,1}$ starts diminishing when $\omega_{1,1}$ increases beyond 0.4 and hence $\omega_{2,1}$ drops below 0.6. Fig. 7.7b plots the corresponding qualities of the video sequences. Following similar trends as in the power curves, $Q_{1,1}$ improves whereas $Q_{2,1}$ is reduced. Finally, we note that we have $Q_{1,1} = 20\text{dB}$ when $\omega_{1,1} = 0$, and $Q_{2,1} = 20\text{dB}$ when $\omega_{1,1} = 1$ due to the fact that a minimum quality of 20dB is imposed on both video
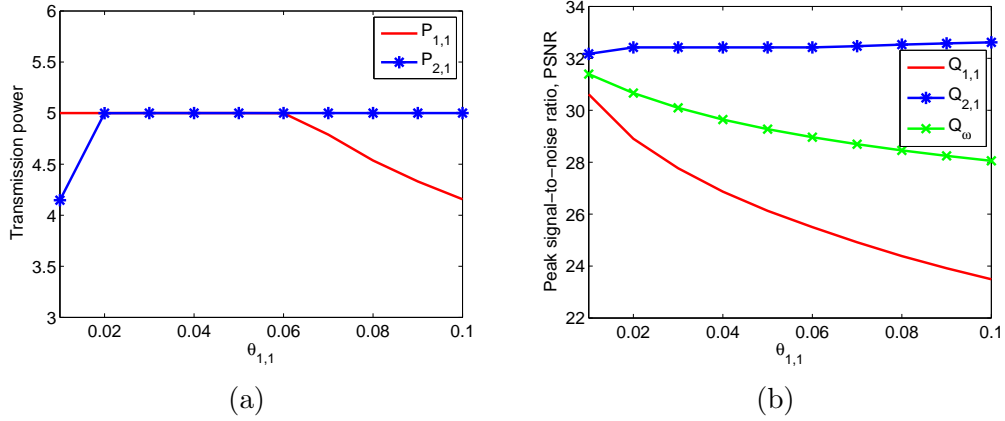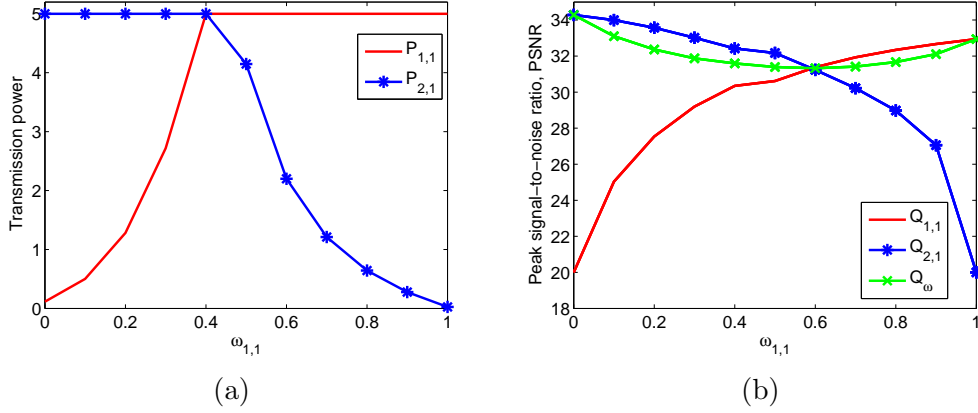
Figure 7.7: (a) Optimal power allocation and (b) the corresponding quality Q (or equivalently PSNR) of video sequences as a function of $\omega_{1,1}$.

transmissions.

7.4.2 Two Pairs of Full-Duplex Users

In this section, we consider bandwidth and power allocation for two pairs of full-duplex users. The total bandwidth B is set to 0.2 MHz, and the average channel power gains are $Z_1 = 1$ between first pair of users and $Z_2 = 3$ between the second pair of users. $U_{1,1}$ and $U_{1,2}$ transmit the same video sequence *Bus* to $U_{2,1}$ and $U_{2,2}$, respectively. And video sequence *Coastguard* is transmitted to $U_{1,1}$ and $U_{1,2}$ by $U_{2,1}$ and $U_{2,2}$ respectively. For these video sequences, we have $a_{1,1} = a_{1,2} = 4.7205$ and $b_{1,1} = b_{1,2} = 5.4764$, $a_{2,1} = a_{2,2} = 3.5261$ and $b_{2,1} = b_{2,2} = 13.8425$.

7.4.2.1 The Impact of the QoS Exponent on Multimedia Quality

In this subsection, we initially set $\omega_{1,1} = \omega_{2,1} = \omega_{1,2} = \omega_{2,2} = 0.25$, and increase the values of the QoS exponents of the first pair of users $\theta_{1,1}$ and $\theta_{2,1}$ from 0.01 to 0.1 together (i.e., $\theta_{1,1} = \theta_{2,1}$) while keeping the QoS exponents of the second pair of users at $\theta_{1,2} = \theta_{2,2} = 0.01$. Fig. 7.8a and Fig. 7.8b show the results of the optimal power and bandwidth allocation as a function of $\theta_{1,1} = \theta_{2,1}$. Note that as QoS exponents $\theta_{1,1} = \theta_{2,1}$ increase (hence more stringent QoS constraints are imposed), lower arrival

129
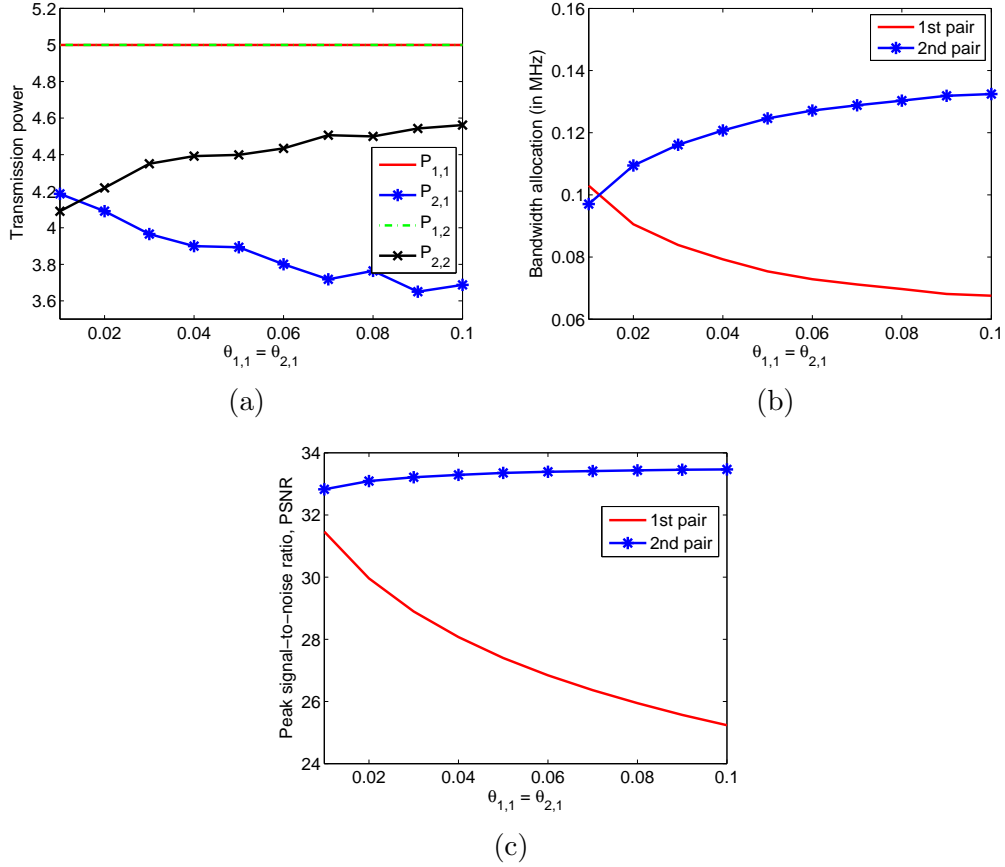
Figure 7.8: (a) Optimal power allocation, (b) optimal bandwidth allocation, and (c) the corresponding quality of video sequences as $\theta_{1,1} = \theta_{2,1}$ increase.

rates are supported and the quality of the video sequences of the first pair of users degrades. With this, bandwidth allocated to the first pair of users is reduced as noticed in Fig. 7.8b. Due to similar reasons (regarding the video quality parameters) as discussed in the case of one pair of full-duplex users (i.e., $a_{1,k} > a_{2,k}$ for $k = 1, 2$), $P_{1,1}$ and $P_{1,2}$ are always at their maximum levels. We also observe that as $\theta_{1,1} = \theta_{2,1}$ increase, $P_{2,1}$ diminishes whereas $P_{2,2}$ grows. These are due to the facts that the bandwidth allocated to the link between $U_{1,1}$ and $U_{2,1}$ decreases while the bandwidth allocated to the link between $U_{1,2}$ and $U_{2,2}$ increases. Hence, an opportunistic strategy is employed and more power is allocated to the link with more bandwidth. Fig. 7.8c demonstrates that the average PSNR value of first pair of video sequences degrades due to increasing QoS exponents and smaller bandwidth.

Fig. 7.9 plots the weighted sum quality of video sequences assuming optimal and also equal bandwidth allocation. In both cases, power is optimally allocated. We note that the equal bandwidth optimal power (EBOP) allocation scheme provides a performance close to that of the optimal bandwidth and power allocation scheme, but the gap widens as $\theta_{1,1} = \theta_{2,1}$ increase.

Hence, the performance improvements are highly dependent on the parameter values. For instance, in Fig. 7.10, we consider smaller values of the QoS exponent, which imply looser QoS requirements. Specifically, we vary $\theta_{1,1}$ and $\theta_{2,1}$ from 0.001 to 0.01 together while keeping the QoS exponents of the second pair of users at $\theta_{1,2} = \theta_{2,2} = 0.001$. We also set $\omega_{1,1} = \omega_{2,1} = 0.45$ and $\omega_{1,2} = \omega_{2,2} = 0.05$. In Fig. 7.10a, we plot the PSNR for both optimal bandwidth and power allocation, EBOP allocation, and equal bandwidth and maximum power (EBMP) allocation. We observe the performance gains of optimal allocation while EBOP and EBMP curves are almost overlapping. More interestingly, as seen in Fig. 7.10b where average power consumption is plotted, the performance improvements with optimal allocation is attained while consuming less average power. Hence optimal allocation improves power efficiency as well. Expectedly, EBMP is the worst strategy, consuming the highest levels of power without any improvements in PSNR.

Next, we address in more detail the impact of having different weights in the weighted sum video quality maximization.

7.4.2.2 The Impact of Weights on Multimedia Quality

Fig. 7.11 shows the optimal bandwidth and power allocation and the corresponding quality of video sequences as the weights $\omega_{1,1} = \omega_{2,1}$ vary from 0.05 to 0.45. We also assume that $\omega_{1,2} = \omega_{2,2}$ while keeping the sum of all weights equal to 1. Fig. 7.11b indicates that bandwidth B_1 allocated to the first pair of users increases with increasing $\omega_{1,1} = \omega_{2,1}$ since growing emphasis is given to the quality of the video sequences trans-
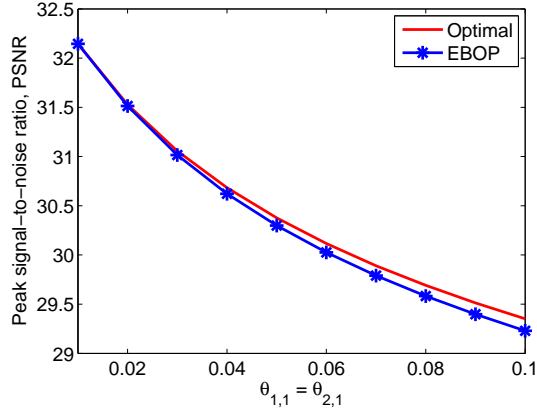
Figure 7.9: Quality of video sequences as a function of $\theta_{1,1} = \theta_{2,1}$. Both optimal and equal bandwidth allocation are considered.

(a) (b)
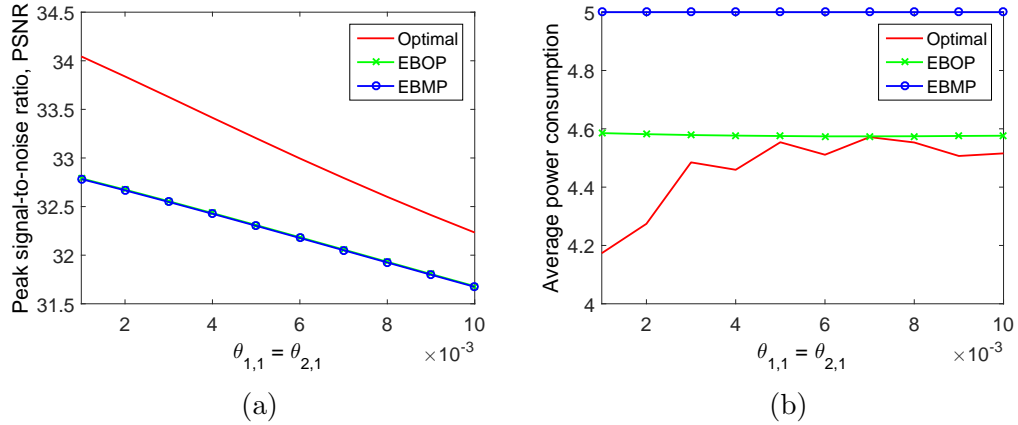
Figure 7.10: (a) Quality of video sequences as a function of $\theta_{1,1} = \theta_{2,1}$ and (b) average power consumption as a function of $\theta_{1,1} = \theta_{2,1}$.
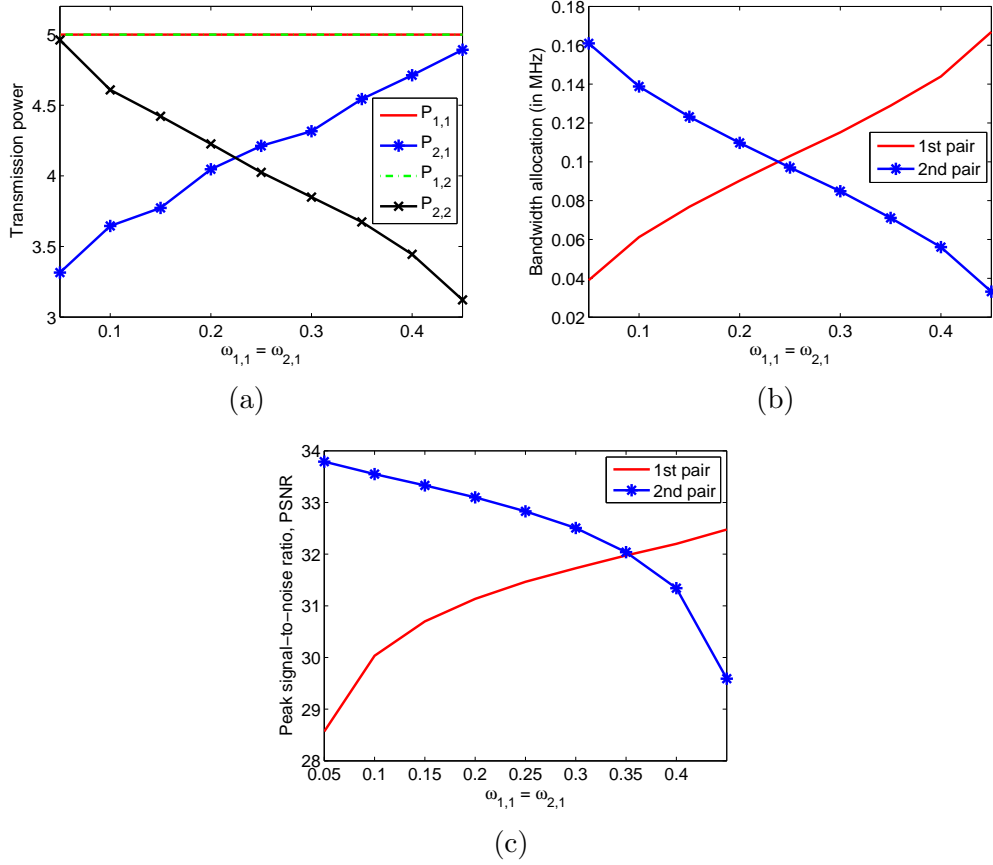
Figure 7.11: (a) Optimal power allocation, (b) Optimal bandwidth allocation, and (c) the corresponding quality of video sequences as a function of $\omega_{1,1} = \omega_{2,1}$.

mitted between first pair of users. Consequently, the bandwidth allocated to the link between second pair of users $U_{1,2}$ and $U_{2,2}$ decreases. Since $\omega_{1,1} = \omega_{2,1}$ and $a_{1,1} > a_{2,1}$, $U_{1,1}$ always transmits the video sequence at the maximum transmission power level. Due to the same reason, $P_{1,2}$ always attains the maximum level. Again, due to the optimality of the opportunistic approach, $P_{2,1}$ increases as B_1 gets larger, whereas $P_{2,2}$ diminishes as B_2 becomes smaller. Correspondingly, Fig. 7.11c demonstrates that the average PSNR values $Q_{1,1}$ and $Q_{2,1}$ improve as higher weights $\omega_{1,1} = \omega_{2,1}$ are given to the video communication between the first pair of users, while the average PSNR values $Q_{1,2}$ and $Q_{2,2}$ are lowered.

Fig. 7.12 shows the weighted sum quality of video sequences again considering optimal and equal bandwidth allocation schemes. As expected, the optimal band-
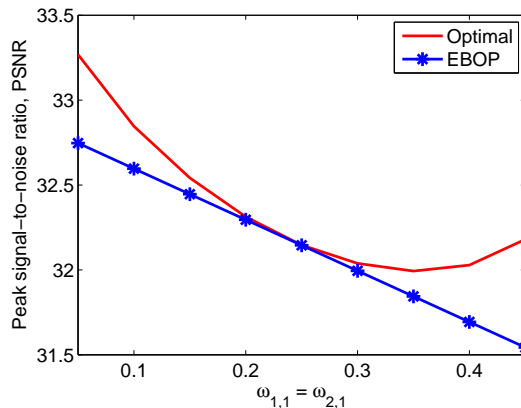
Figure 7.12: Quality of video sequences as a function of $\omega_{1,1} = \omega_{2,1}$. Both optimal and equal bandwidth allocation are considered.

width and power allocation scheme outperforms the case in which bandwidth is equally allocated among the pairs of users and power is allocated optimally (i.e., EBOP scheme). The performance gap is smallest when the weights are all equal (i.e., $\omega_{1,1} = \omega_{2,1} = \omega_{1,2} = \omega_{2,2} = 0.25$), and the gap grows as the difference in the weights increases.

7.4.2.3 Performance Comparison of Full-Duplex and Half-Duplex Operations

In Fig. 7.13, we compare the performances of half-duplex and full-duplex operations. In particular, we plot the PSNR (or equivalently the quality) of the video sequences as a function of the QoS exponents $\theta_{1,1} = \theta_{2,1}$ for four different cases (i.e., three full-duplex scenarios and one half-duplex). Since full-duplex performance is interference dependent, self interference suppression factor, μ, plays an important role in these cases. In the figure, for the three curves corresponding to full-duplex operation, we set $\mu = 0.1$, $\mu = 0.05$, and $\mu = 0.01$ respectively. $\mu = 0.01$ reflects the highest level of self-interference cancelation. We note that in the half-duplex case, the communicating pair of users employ time-division multiplexing, i.e., each user in the pair transmits half of the time and receives in the remaining half with no interference. We further
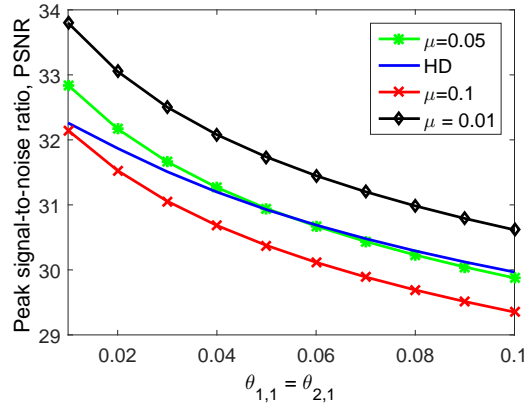
Figure 7.13: PSNR vs. QoS exponents $\theta_{1,1} = \theta_{2,1}$ for both full-duplex and half-duplex (HD) operations. Self-interference suppression factors are $\mu = 0.1$, $\mu = 0.05$, and $\mu = 0.01$ in the three full-duplex curves, respectively.

note that while the users always transmit at the peak power level in the half-duplex case, bandwidth is still optimally allocated among different pairs of users by solving a convex optimization problem.

In the figure, we notice that half-duplex operation outperforms full-duplex case when $\mu = 0.1$. On the other hand, when self-interference is suppressed further i.e., when we have $\mu = 0.05$, full-duplex operation performs better as long as θ values are less than approximately 0.05. As the QoS exponent grows further, half-duplex starts leading to slightly higher PSNR levels. Hence, we interestingly observe that under stringent buffer/delay constraints, we need more self-interference suppression in order to surpass the performance levels achieved with half-duplex communication. Indeed, when we have $\mu = 0.01$, full-duplex operation outperforms half-duplex scheme over all values of the QoS exponents shown in the figure.

7.4.3 More than Two Pairs of Full-Duplex Users

In this subsection, we apply our optimal resource allocation algorithms to cases in which there are more than two pairs of full-duplex users Table 7.2 provides results on the optimal bandwidth and power allocation and the resulting video qualities

when there 3 pairs of users. In these results, it is assumed that $\omega_{1,1} = \omega_{2,1} = 0.05$, $\omega_{1,2} = \omega_{2,2} = 0.3$ and $\omega_{1,3} = \omega_{2,3} = 0.15$. Moreover, we set $\theta_{1,1} = \theta_{2,1} = 0.1$, $\theta_{1,2} = \theta_{2,2} = 0.07$ and $\theta_{1,3} = \theta_{2,3} = 0.04$. Overall, optimal bandwidth and power allocation leads to a weighted sum quality of 33.9269dB. We notice that since the weights $\omega_{1,2}$ and $\omega_{2,2}$ of the second pair of users are the largest, most bandwidth (out of a total bandwidth of $B = 0.3$MHz $= 300$kHz) is allocated to these users. Also, it is interesting to note that due to the need to control the self-interference, several power levels are less than the maximum allowed peak power level of 5 (while at least one power value is at the peak level), as also noted in the previous cases.

Table 7.2: Performance with 3 pairs of full-duplex users

k	$P_{1,k}$	$P_{2,k}$	B_k	$Q_{1,k}$	$Q_{2,k}$
1	5	3.8971	51.626	23.2390	26.7099
2	5	4.0473	150.691	34.5854	38.8709
3	5	4.3400	97.683	28.1572	34.4601

Table 7.3 shows the performances of video transmissions between 4 pairs of full-duplex users again considering optimal bandwidth and power allocation with $\omega_{1,1} = \omega_{2,1} = 0.05$, $\omega_{1,2} = \omega_{2,2} = 0.2$, $\omega_{1,3} = \omega_{2,3} = 0.05$ and $\omega_{1,4} = \omega_{2,4} = 0.2$. The total bandwidth is $B = 0.4$MHz $= 400$kHz. It is further assumed that $\theta_{1,1} = \theta_{2,1} = 0.1$, $\theta_{1,2} = \theta_{2,2} = 0.07$, $\theta_{1,3} = \theta_{2,3} = 0.04$ and $\theta_{1,4} = \theta_{2,4} = 0.01$. The weighted sum quality of video sequences achieved with optimal allocations is 36.8243dB.

Table 7.3: Performance with 4 pairs of full-duplex users

k	$P_{1,k}$	$P_{2,k}$	B_k	$Q_{1,k}$	$Q_{2,k}$
1	5	3.7464	26.720	22.4085	25.9285
2	5	4.9929	146.759	34.4014	39.0498
3	5	4.3079	36.258	26.7723	33.0397
4	5	4.9990	190.263	43.6321	40.0009

Chapter 8

Quality-Driven Resource Allocation for Wireless Video Transmissions under Energy Efficiency and Delay Constraints

In this chapter, wireless video transmissions are studied under total bandwidth and energy efficiency (EE) constraints. In order to provide the desired performance levels to the end-users in real-time video transmissions, quality of service (QoS) requirements such as statistical delay constraints are also considered. Effective capacity (EC) is used as the throughput metric in the presence of such statistical delay constraints since deterministic delay bounds are difficult to guarantee due to the time-varying nature of wireless fading channels. A multiuser setup where different users have different delay guarantees is addressed. Following characterizations from the rate-distortion (R-D) theory, a logarithmic model of the quality-rate relation is used for predicting the quality of the reconstructed video in terms of the peak signal-to-noise ratio (PSNR) at the receiver side. The optimal bandwidth allocation and the

optimal power allocation/power control policies that maximize the sum video quality subject to total bandwidth and minimum EE constraints are derived. Five different resource allocation strategies are investigated, and simulation results show that the joint optimization of the bandwidth allocation and power control provides the best performance. Tradeoff between EE and video quality is also demonstrated since higher EE results in lower quality of received video sequence.

8.1   System Model

Fig. 8.1 depicts the block diagram of the proposed system. A downlink from a base station (or an access point) where K users orthogonally share a bandwidth of B Hz is considered in this thesis. Specifically, a bandwidth of B_k Hz is allocated to transmission to user k under the constraint that the total bandwidth is B, i.e., $\sum_{k=1}^{K} B_k = B$. The base station has K different data traffic flows, each intended for a particular user. Different flows of traffic are stored in different buffers at the base station as shown in Fig. 8.1 [1]. Each traffic flow has its distinct delay QoS requirement and energy efficiency constraint. The base station takes into account these requirements and constraints as well as multimedia quality models (derived via rate-distortion characteristics) and CSI, and allocates the bandwidth and power resources efficiently.

The timescale of video rate adaptation is much larger than the coherence time of the channel, denoted by T_c, in practice for video transmission since video source rate is adapted at the group of pictures (GOP) time scale which is measured in seconds. Hence, the case in which the channel state changes faster than the source rate is considered in our system since if the fading channel state varies at the same timescale

---

[1]These buffers can be physical or virtual buffers. In the case of virtual buffers (when, for instance, the base station has a single physical buffer), the base station needs to keep track of where each data intended for different users is located, and extract out the required data from its location in the buffer when transmission to a given user is initiated. Hence, while the virtual buffers are operating in first-in first-out mode, the physical buffer does not necessarily operate in such a mode.
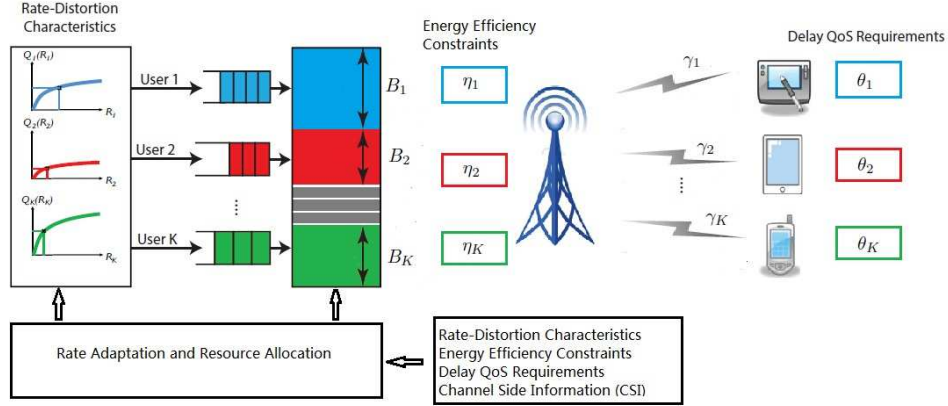
Figure 8.1: Proposed system block diagram for quality-driven resource allocation and rate adaptation of delay and energy efficiency constrained video streams

as the source rate, statistical delay guarantees become less interesting [28].

The fading power in the link between the base station and user k is denoted by γ_k. We address the cases of perfect CSI and statistical CSI. When only statistical CSI is available at the base station (i.e., base station only knows the statistics of channel fading), we consider bandwidth and power allocation to maximize the sum video quality. If, on the other hand, the base station perfectly knows the realizations of the fading coefficients, we study bandwidth allocation and power control in which case power is varied as a function of the channel fading (or equivalently channel conditions).

8.2   Sum-Quality Maximizing Policies

In this section, optimization problems are formulated in order to maximize the sum video quality subject to energy efficiency constraints per user and a total bandwidth constraint. More specifically, we consider two types of optimizations. In the first one, we address the optimal allocation of bandwidth and power. Here, it is assumed that only statistical CSI is available at the transmitter and the allocated power remains fixed throughout the transmission. In the second optimization problem, it is assumed

that the transmitter has instantaneous CSI and performs both bandwidth allocation and power control. Hence, power varies over time depending on the fading. Effective capacity and Quality-Rate model in Section 2.2 and Section 2.3 are employed.

8.2.1   Bandwidth and Power Allocation with Statistical CSI

In the case of bandwidth and power allocation, the optimization problem can be expressed as follows:

$$\max_{\mathbf{B},\mathbf{P}} \sum_{k=1}^{K} Q_k(R_k) \tag{8.1a}$$

$$\text{s.t.} \sum_{k=1}^{K} B_k = B; \quad B_k \geq 0 \quad \forall k \tag{8.1b}$$

$$\frac{-\frac{1}{\theta_k T_c} \ln \left(\mathbb{E}_{\gamma_k} \left\{ e^{-\theta_k B_k T_c \log(1+\frac{P_k \gamma_k}{N_0 B_k})} \right\} \right)}{P_c + \frac{1}{\epsilon} P_k} \geq \eta_k \quad \forall k. \tag{8.1c}$$

Above, $\mathbf{B}$ and $\mathbf{P}$ are the vectors of bandwidth allocation and power allocation, respectively. Additionally, the constraint in (8.1c) is the energy efficiency (EE) constraint. Note that this constraint imposes a lower bound η_k on the EE metric which is defined as the effective capacity (or equivalently throughput) normalized by the total power consumption. Hence EE is measured by the throughput per unit power. In the power consumption formula, P_c denotes the circuit power and ϵ is the power amplifier efficiency factor. Note that the constraint in (8.1c) can be rewritten as

$$-\frac{1}{\theta_k T_c} \ln \left(\mathbb{E}_{\gamma_k} \left\{ e^{-\theta_k B_k T_c \log(1+\frac{P_k \gamma_k}{N_0 B_k})} \right\} \right) \geq \eta_k (P_c + \frac{1}{\epsilon} P_k) \quad \forall k. \tag{8.2}$$

Notice that the left-hand side of (8.2) is the effective capacity and hence is equal to R_k, and the right-hand side is evidently a linear increasing function of P_k. We first have the following characterization.

Theorem 8.1 *Effective capacity, which is formulated as*

$$R_k = -\frac{1}{\theta_k T_c} \ln \left(\mathbb{E}_{\gamma_k} \left\{ e^{-\theta_k B_k T_c \log(1+\frac{P_k \gamma_k}{N_0 B_k})} \right\} \right), \tag{8.3}$$

is an increasing concave function of the power level P_k for a given B_k.

Proof: See Appendix A.6.

As illustrated in Fig. 8.2, for given B_k and η_k, the linearly increasing function $\eta_k(P_c + \frac{1}{\epsilon}P)$ intersects the concave curve $R_k(B_k, P)$ at two points or only one tangent point (not depicted in the figure) if there exist P_k values that satisfy the inequality in (8.2), and the two endpoints or the only one tangent point satisfy (8.2) with equality. In the case of a single tangent point, the corresponding power level at the tangent point is the only feasible and hence the optimal value which can be obtained by solving $R_k = \eta_k(P_c + \frac{1}{\epsilon}P_k)$. In the case of two endpoints satisfying (8.2) with equality, the larger P_k value, denoted as $\hat{P}_k$ in the figure, needs to be chosen since the quality/PSNR function Q_k is an increasing function of P_k (since Q_k is an increasing function of R_k, which in turn increases with increasing P_k). For any power level greater than $\hat{P}_k$, we have $R_k < \eta_k(P_c + \frac{1}{\epsilon}P_k)$, and hence the EE constraint is not satisfied. Therefore, again the optimal power value can be obtained by solving

$$R_k = \eta_k \left(P_c + \frac{1}{\epsilon}P_k \right) \quad \forall k \tag{8.4}$$

for P_k and choosing the larger of the two solutions (or equivalently the larger of the two power values). Hence, for sum-quality maximizing policies, EE constraint should be satisfied with equality.

In Fig. 8.2, two bandwidth values $B_{k,2} > B_{k,1}$ are considered. It is clearly seen that the optimal power level $\hat{P}_k$ varies with the bandwidth B_k. Next, we provide the following result.
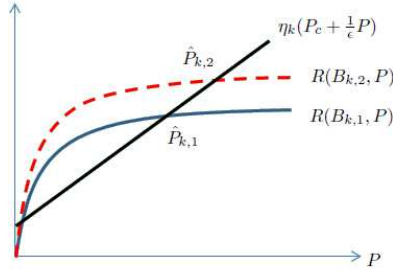
Figure 8.2: Both sides of the EE constraint in (8.2) as a function of the power, P

Theorem 8.2 *Effective capacity R_k is an increasing and concave function of bandwidth B_k for a given P_k.*

Proof: See Appendix A.7.

As also seen in Fig. 8.2, since R_k is an increasing concave function of B_k for a given P_k, we readily conclude that $\hat{P}_k$ is an increasing function of B_k. In another words, if $B_{k,2} > B_{k,1}$, we have $\hat{P}_{k,2} > \hat{P}_{k,1}$.

Thus, the optimization problem can be now be simplified as

$$\max_{\mathbf{B}} \sum_{k=1}^{K} Q_k(R_k(B_k, \hat{P}_k(B_k))) \tag{8.5a}$$

$$\text{s.t.} \sum_{k=1}^{K} B_k = B; \quad B_k \geq 0 \quad \forall k \tag{8.5b}$$

where $\hat{P}_k(B_k)$ is the solution of (8.4). Hence, using the properties of the effective capacity R_k with respect to bandwidth and power as established in Theorems 8.1 and 8.2, we have incorporated the EE constraint in (8.1c) into the objective function via $\hat{P}_k(B_k)$.

The next results shows the concave nature of $\hat{P}_k(B_k)$ with respect to B_k.

Theorem 8.3 *Assume that $\hat{P}_k(B_k)$ is the solution of (8.4) for given B_k. Then, $\hat{P}_k(B_k)$ is an increasing concave function of B_k.*

Proof: See Appendix A.8.

142

Hence, $R_k(B_k, \hat{P}_k(B_k))$ is also an increasing concave function of B_k. Furthermore, since Q_k is an increasing concave function of R_k, $Q_k(R_k(B_k, \hat{P}_k(B_k)))$ is an increasing concave function of B_k. Thus, the simplified optimization problem in (8.5) is a concave maximization problem subject to an affine constraint, and the optimal bandwidth allocation can be determined by using the Lagrangian optimization approach. In particular, the Lagrangian can be expressed as

$$L(\mathbf{B}, \mu) = \sum_{k=1}^{K} Q_k(R_k(B_k, \hat{P}_k(B_k))) + \mu \left(B - \sum_{k=1}^{K} B_k \right) \tag{8.6}$$

According to the Karush-Kuhn-Tucker (KKT) conditions, the optimal bandwidth allocation must satisfy the following:

$$\mu = \frac{\partial Q_k(R_k(B_k, \hat{P}_k(B_k)))}{\partial B_k}, \quad k = 1, 2, ...K \tag{8.7}$$

$$\mu \left(B - \sum_{k=1}^{K} B_k \right) = 0. \tag{8.8}$$

Following these characterizations, this problem can be easily solved using convex optimization methods.

8.2.2 Bandwidth Allocation and Power Control with Perfect CSI

We now assume that the transmitter has perfect CSI and knows the channel gains $\{\gamma_k\}$. In this case, the transmit power levels, which we denote as $\{P_k(\gamma_k)\}$, are adapted to channel gains. Now the sum-quality-maximizing optimal bandwidth allo-

cation and power control problem can be expressed as

$$\max_{\mathbf{B},\{P_k(\gamma_k)\}_{k=1}^K} \sum_{k=1}^K Q_k(R_k) \tag{8.9a}$$

$$\text{s.t.} \sum_{k=1}^K B_k = B; \quad B_k \geq 0 \quad \forall k \tag{8.9b}$$

$$\frac{-\frac{1}{\theta_k T_c} \ln\left(\mathbb{E}_{\gamma_k}\left\{e^{-\theta_k B_k T_c \log(1+\frac{P_k(\gamma_k)\gamma_k}{N_0 B_k})}\right\}\right)}{P_c + \frac{1}{\epsilon}\mathbb{E}_{\gamma_k}\{P_k(\gamma_k)\}} \geq \eta_k \quad \forall k \tag{8.9c}$$

Note that bandwidth allocation does not depend on the instantaneous CSI, which means that bandwidth allocated to each user does not vary with the channel gains, which is a practical assumption as varying the bandwidth with the instantaneous channel conditions can be complicated. Note further that the transmission power level $P_k(\gamma_k)$ appears via the individual energy efficiency constraint in (8.9c).

Similarly as in the previous subsection, (8.9c) needs to be satisfied with equality since R_k is an increasing concave function of $\mathbb{E}_{\gamma_k}\{P_k(\gamma_k)\}$ under the optimal power control policy. And, for a given B_k, the largest possible $\tilde{P}_k = \mathbb{E}_{\gamma_k}\{P_k(\gamma_k)\}$ with which (8.9c) is satisfied with equality should be chosen.

For given average power value $\bar{P}_k$, the optimal power control strategy for transmission to user k is the one that maximizes effective capacity R_k (since individual power control for each user is limited by the individual energy efficiency constraint in (8.9c) for given k and hence power control schemes for different users are essentially decoupled). Therefore, we first solve the following maximization problem in order to identify the optimal power control policy $P_k(\gamma_k)$:

$$\max_{P_k(\gamma_k)} -\frac{1}{\theta_k T_c} \ln\left(\mathbb{E}_{\gamma_k}\left\{e^{-\theta_k B_k T_c \log(1+\frac{P_k(\gamma_k)\gamma_k}{N_0 B_k})}\right\}\right) \tag{8.10a}$$

$$\text{s.t.} \quad \mathbb{E}_{\gamma_k}\{P_k(\gamma_k)\} = \bar{P}_k \quad \forall k \tag{8.10b}$$

Note that the above problem is a convex optimization problem and is already ad-

144

dressed in the literature (see e.g., [80]). The optimal power control can be immediately obtained as

$$P_k(\gamma_k) = \frac{N_0 B_k}{\gamma_k} \left[\left(\frac{\theta_k T_c \gamma_k}{\lambda_k N_0 \ln 2} \right)^{\frac{1}{\frac{\theta_k B_k T_c}{\ln 2} + 1}} - 1 \right]^+ \tag{8.11}$$

where λ_k is the Lagrangian multiplier whose value can be obtained by solving $\mathbb{E}_{\gamma_k}\{P_k(\gamma_k)\} = \bar{P}_k$. Substituting $P_k(\gamma_k) = \frac{N_0 B_k}{\gamma_k} \left[\left(\frac{\theta_k T_c \gamma_k}{\lambda_k N_0 \ln 2} \right)^{\frac{1}{\frac{\theta_k B_k T_c}{\ln 2} + 1}} - 1 \right]^+$ into (8.9c), there are at most two values for the Lagrange multiplier, e.g., $\lambda_{k1} < \lambda_{k2}$, satisfying (8.9c) with equality (similarly as in Fig. 8.2 where the linear curve intersects the curve R_k at most at two different points with two different values for the slope of the R_k curve). The smaller Lagrange multiplier λ_{k1} (corresponding to the smaller slope of effective capacity R_k) is the one that leads to the largest average power, i.e., $\mathbb{E}_{\gamma_k}\{P_k(\gamma_k)\} = \tilde{P}_k$.

Similarly as in the power allocation case, $Q_k(R_k(B_k, \tilde{P}_k(B_k)))$ is an increasing concave function of B_k since $\tilde{P}_k(B_k)$ is an increasing concave function of B_k, and the optimization problem can rewritten as

$$\max_{\mathbf{B}} \sum_{k=1}^{K} Q_k(R_k(B_k, \tilde{P}_k(B_k))) \tag{8.12a}$$

$$\text{s.t.} \sum_{k=1}^{K} B_k = B; \quad B_k \geq 0 \quad \forall k. \tag{8.12b}$$

Again, the above optimization problem is a concave maximization problem and can be solved via convex optimization tools.

8.2.3 Optimal Allocation Algorithm and Different Policies

We have thus far considered two optimization problems:

- *Joint optimal bandwidth allocation and power allocation (JBAPA)* with statistical CSI, determined by solving the optimization problem in (8.1).

- *Joint optimal bandwidth allocation and power control (JBAPC)* with perfect CSI, determined by solving the optimization problem in (8.9).

An algorithm for determining both optimal JBAPA and JBAPC via solving (8.5) and (8.12), respectively, is shown in Algorithm 10 below.

Algorithm 10 The optimal bandwidth allocation algorithm under the total bandwidth and EE constraints

1: Initialize $\epsilon_1 > 0$, $\mu = \mu_{initial}$, $\delta > 0$,

2: **repeat**

3:    **for** k = 1:K **do**

4:        Find out B_k by solving $\mu = \frac{\partial Q_k(R_k(B_k,\hat{P}_k(B_k)))}{\partial B_k}$ for JBAPA case or $\mu = \frac{\partial Q_k(R_k(B_k,\tilde{P}_k(B_k)))}{\partial B_k}$ for JBAPC case

5:        **if** $|B - \sum_{k=1}^{K} B_k| > \epsilon_1$ **then**

6:          $\mu = \mu - \delta * (B - \sum_{k=1}^{K} B_k)$

7:        **end if**

8:    **end for**

9: **until** $|B - \sum_{k=1}^{K} B_k| \leq \epsilon_1$

For comparison, we also consider the following three simpler but suboptimal strategies:

- *Equal bandwidth (EB)* $B_k = \frac{B}{K}$ is allocated to each user, and the power $\hat{P}_k$ is obtained by solving (8.4) for given bandwidth.

- *Separate bandwidth allocation and power control-1 (SBAPC-1)* is the method that uses the same bandwidth allocation and constant average power given by JBAPA, but introduces power control. For the given B_k and $\hat{P}_k$, the power control policy is determined by solving (8.10) and maximizing the effective capacity of user k.

146

- *Separate bandwidth allocation and power control-2 (SBAPC-2)* is a scheme that uses the same bandwidth allocation obtained by JBAPA. For this given B_k, the power control policy is determined by again solving (8.10). Different from the previous case of SBAPC-1, there is no predetermined average power level. The optimal average power level is dictated by the EE constraint and hence is obtained by solving (8.4).

Note that in SBAPC-1 and SBAPC-2 schemes, the bandwidth allocation and power control are being obtained separately in two steps instead of being determined jointly as in JBAPC.

8.3   Numerical Results

Five CIF video sequences namely Akiyo, Bus, Coastguard, Foreman and News are used for the numerical results [66]. Size of each frame is 352×288 pixels. FFMPEG is used for encoding the video sequences and GOP is set as 10. Frame rate is set as 15 frames per second. Table 8.1 shows the parameters a_k and b_k that make the rate-distortion function of the five video sequences fit the quality rate model in (??), where the unit of R_k is kbit/s. Unless mentioned explicitly, we assume that the circuit power is $P_c = -10$ dB, and the subchannel power gain for each user is exponentially distributed with mean 1. The power spectrum density of the AWGN is set to $N_0 = 10^{-6}$ W/Hz, and the channel coherence time is assumed to be 0.01 seconds. The quality increasing rate (QIR) on bandwidth is defined as the derivative of PSNR with respect to bandwidth.

Table 8.1: Parameter values of the quality rate model for different video sequences

	Akiyo	Bus	Coastguard	Foreman	News
a_k	5.0545	4.7205	3.5261	4.5006	5.6218
b_k	17.1145	5.4764	13.8425	13.0780	10.0016
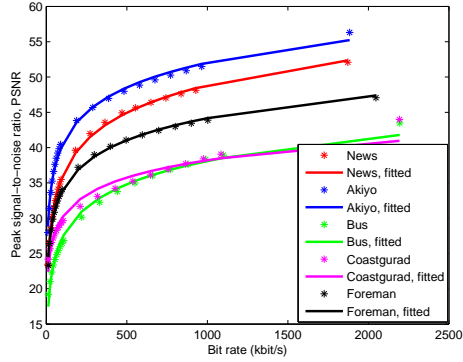
Figure 8.3: Actual PSNR values vs. rate and fitted quality rate curves

Fig. 8.3 shows the actual PSNR values as a function of the source bit rate for different video sequences, where we see that the increasing concave quality rate model fits the actual values very well.

In the numerical results, we consider a scenario in which the base station serves two users. Fig. 8.4a displays the relationship between the allocated bandwidth and the delay QoS exponent, θ_2, for the second user. We assume that the same video sequence, Bus, is transmitted to 2 users, with delay QoS exponents $\theta_1 = 10^{-4}$ and varying θ_2, while keeping the other parameters the same. Total bandwidth B for 2 users is 2 MHz, and the EE thresholds are $\eta_1 = \eta_2 = 10^5$. In the range of bandwidth shown in Fig. 8.5, QIR is a decreasing convex function of the bandwidth, and the smaller θ value leads to higher QIR for both cases of JBAPA and JBAPC when the bandwidth is large. This lets us conclude that in order to obtain the same QIR, more bandwidth is required for smaller θ values since quality is an increasing concave function of the bandwidth. That is the reason why Fig. 8.4a shows that the bandwidth B_2 is less than B_1 for both cases of JBAPA and JBAPC when θ_2 is greater than θ_1. Fig. 8.4a shows that the bandwidth B_2 is decreasing and B_1 is increasing when θ_2 is increasing for both cases of JBAPA and JBAPC since the larger the difference is between θ_2 and θ_1, the larger the difference between B_1 and B_2 under fixed total bandwidth constraint. Fig. 8.4b shows the average transmit power levels for cases of JBAPA, SBAPC-2 and

JBAPC, and SBAPC-1 and JBAPA use the same transmit power level. It shows that user 1 consumes more power than user 2 and the power level for user 1 increases when θ_2 decreases. That is because that $\theta_2 \leq \theta_1$ causes user 2 using less bandwidth, further more, user 2 consumes less power under the energy efficiency constraint (satisfy with equality). And decreasing θ_2 leads to decreasing B_2 and increasing B_1 which causes decreasing power level used by user 2 and increasing power level used by user 1. Fig. 8.4b also shows that SBAPC-2 uses more power than JBAPA since these two cases have the same bandwidth allocation shown in Fig. 8.4a shows and SBAPC-2 employs power control strategy that leads to higher effective capacity and higher power level under EE constraints. It also shows that SBAPC-2 has higher transmit power for user 1 and less transmit power for user 2 than in JBAPC case since in SBAPC-2 case, user 1 occupies more bandwidth and user 2 occupies less bandwidth than in JBAPC case, and both of them employs power control strategy. Fig. 8.4c demonstrates that increasing θ_2 leads to decreased average PSNR of the two video sequences. Since larger θ means more stringent of delay-QoS constraints, we have smaller effective capacity or equivalently smaller rates, which result in lower PSNR values for the received video sequences. The EB has the lowest average PSNR value since the bandwidth is allocated equally and there is no optimization. JBAPA has better performance since the bandwidth and constant power are optimally allocated under total bandwidth and EE constraints. SBAPC-1 is better than JBAPA since it utilizes the instantaneous CSI for improving the effective capacity under total power constraint for each user. And SBAPC-2 performs better than SBAPC-1 because not all users have total power constraint as in SBAPC-2. The JBAPC has the highest average PSNR value as it takes advantage of the availability of the instantaneous CSI and performs joint optimization.

In Fig. 8.6a, we display the allocated bandwidth while the EE coefficient of user 2, η_2 is varied while $\eta_1 = 10^4$. We again assume that the same video, Bus, is transmitted
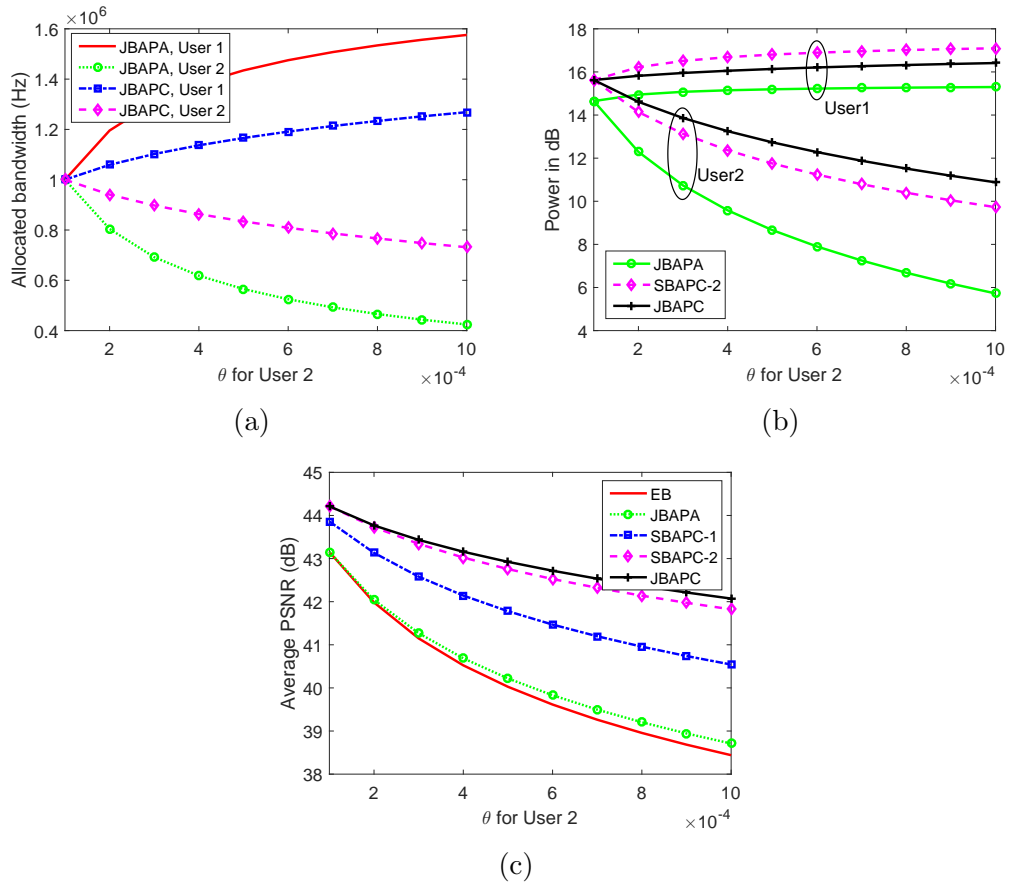
Figure 8.4: (a) Bandwidth allocation, (b) Power levels and (c) Average quality of video sequences when θ_2 is increasing
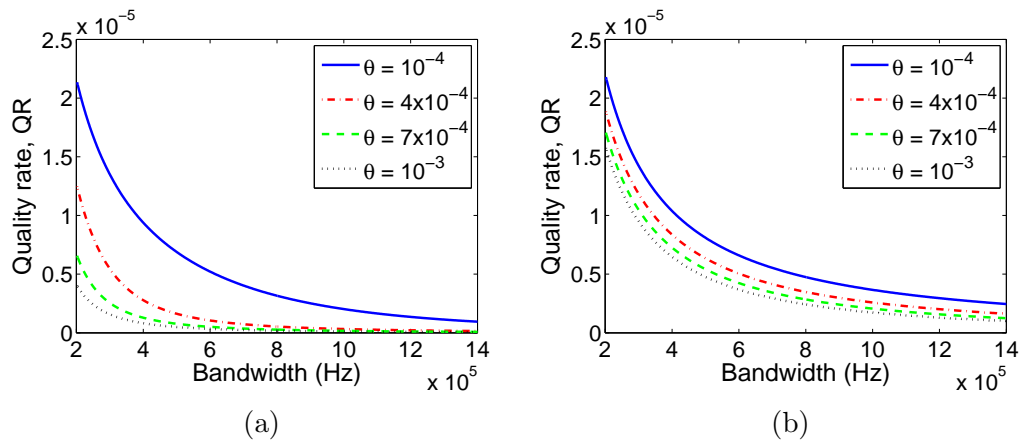
Figure 8.5: QIR vs. bandwidth with different θ in (a) BAPA, and (b) BAPC cases.

to 2 users, but with different η values while keeping the other parameters the same. B is set to 2 MHz, and delay-QoS exponents are $\theta_1 = \theta_2 = 5 \times 10^{-4}$. Fig. 8.7a shows that QIR is a decreasing convex function of bandwidth, and the higher η value leads to higher QIR in the case of JBAPA if bandwidth is large enough. However, for the JBAPC case, Fig. 8.7b shows that the higher η value results in lower QIR in the large bandwidth range. Thus, in order to achieve the same QIR, the higher η value leads to lower bandwidth in the JBAPC case, and requires larger bandwith in JBAPA. Therefore, Fig. 8.6a shows that the bandwidth allocated to user 2, B_2 is smaller than B_1 when η_2 is greater than η_1. And, for JBAPA, Fig. 8.6a shows that B_2 is larger than B_1 when η_2 is greater than η_1. The reason that the bandwidth allocated to user 2 decreases as η_2 increases is that the larger the difference is between η_2 and η_1, the larger the difference between B_1 and B_2 under the fixed total bandwidth constraint in JBAPC. And, for JBAPA, Fig. 8.6a shows that the bandwidth allocated to user 2 is increasing and the difference of allocated bandwidths is increasing as η_2 increases in JBAPA because of the similar reason. Fig. 8.6b shows that user 1 consumes more power than user 2 since increasing η_2 shrinks the feasible power region for user 2. And SBAPC-2 has more power levels for both user 1 and user 2 than in JBAPA due to the same reason that SBAPC-2 has the same bandwidth allocation as in JBAPA and SBAPC-2 employs power control strategy. It also shows that SBAPC-2 has higher transmit power for user 1 and less transmit power for user 2 than in JBAPC case since in SBAPC-2 case, user 1 occupies more bandwidth and user 2 occupies less bandwidth than in JBAPC case, and both of them employs power control strategy. Fig. 8.6c shows that the average PSNR decreases when η_2 is increasing since the higher EE leads to lower power consumption, which in turn leads to lower effective capacity and lower quality of the received video.

Table. 8.2 lists the performances of five different strategies of bandwidth allocation and power allocation /power control with total bandwidth $B = 5$ MHz. Five different

151
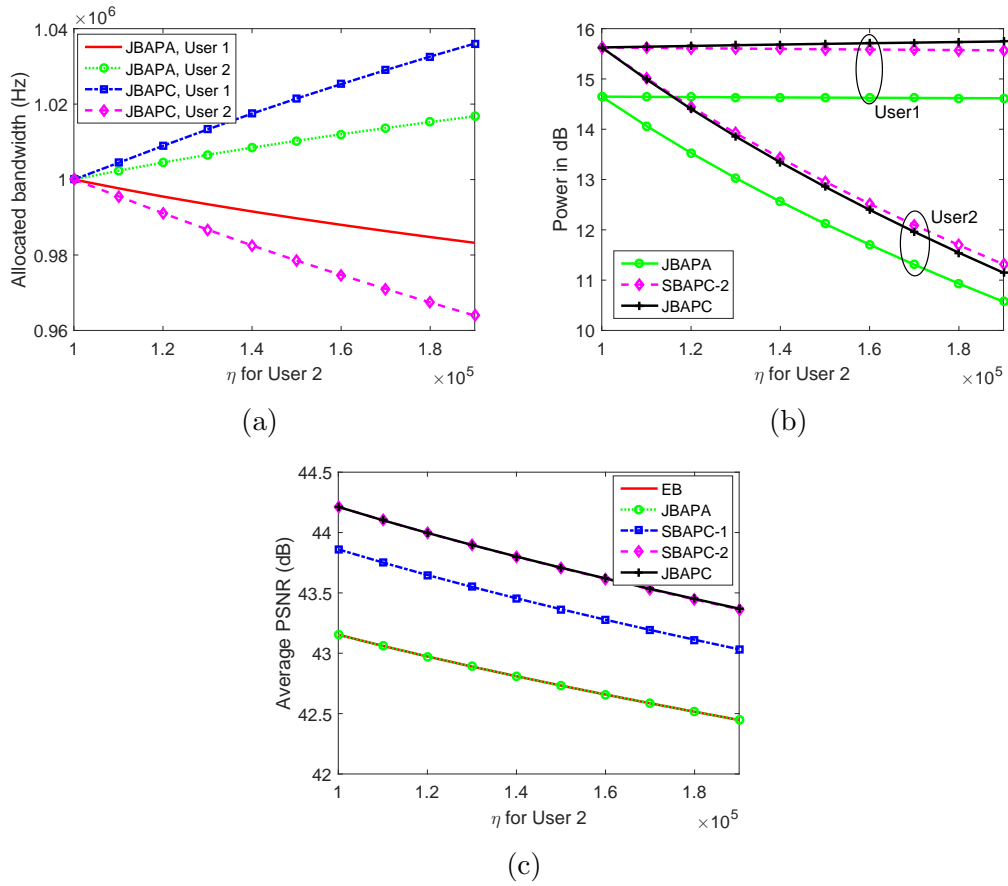
Figure 8.6: (a) Bandwidth allocation, (b) Power levels and (c) Average quality of video sequences when η_2 is increasing
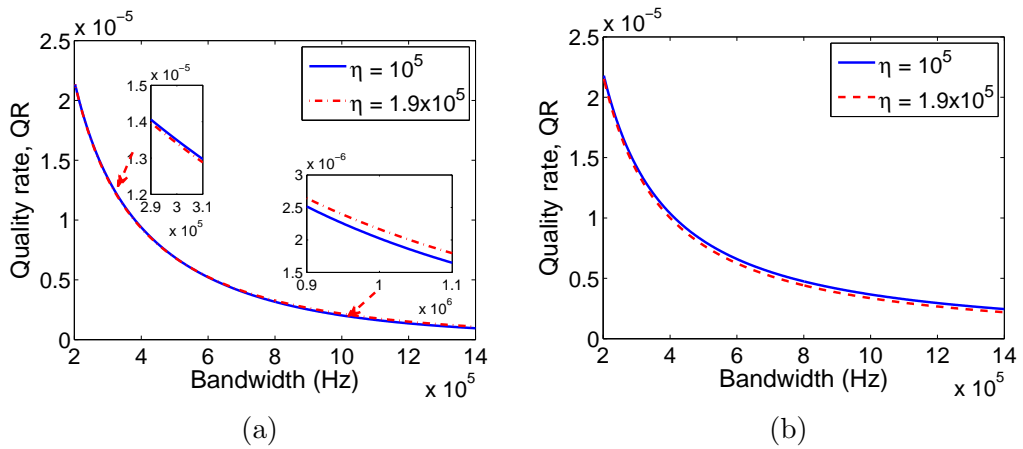
Figure 8.7: QIR vs. bandwidth with different η in (a) BAPA, and (b) BAPC cases.

video sequences are considered. The performance is increasing in the order of EP, JBAPA, SBAPC-1, SBAPC-2, JBAPC.

Table 8.2: Performance for received video sequences and different resource allocation schemes

	η	θ	PSNR				
			EB	JBAPA	SBAPC-1	SBAPC-2	JBAPC
Akiyo	10^5	10^{-3}	47.3621	47.3454	50.5284	53.4757	53.7547
Bus	1.1×10^5	9×10^{-4}	34.0583	34.0461	36.8294	39.4472	39.5806
Coastguard	1.2×10^5	8×10^{-4}	35.4883	35.4697	37.3692	39.1354	39.0702
Foreman	1.3×10^5	7×10^{-4}	41.1555	41.1646	43.5118	45.7804	45.6720
News	1.4×10^5	6×10^{-4}	45.7478	45.8077	48.6358	51.4529	51.2739
Average			40.7624	40.7667	43.3749	45.8583	45.8703

Chapter 9

Power Control and Mode Selection for VBR Video Streaming in D2D Networks

In this chapter, we investigate the problem of power control for streaming variable-bit-rate (VBR) videos in a device-to-device (D2D) wireless network. A VBR video traffic model that considers video frame sizes and playout buffers at the mobile users is adopted. A setup with one pair of D2D users (DUs) and one cellular user (CU) is considered and three modes, namely cellular mode, dedicated mode and reuse mode, are employed. Mode selection for the data delivery is determined and the transmit powers of the base station (BS) and device transmitter are optimized with the goal of maximizing the overall transmission rate while VBR video data can be delivered to the CU and DU without causing playout buffer underflows or overflows. A low-complexity algorithm is proposed. Through simulations with VBR video traces over fading channels, we demonstrate that video delivery with mode selection and power control achieves a better performance than just using a single mode throughout the transmission.

9.1   System Model

As mentioned above, with the goal of maximizing the overall transmission rate at the device user (DU) and cellular user (CU), we study optimal strategies for mode selection and resource allocation in a cellular network with D2D pairs operating under peak transmission power and buffer underflow and overflow constraints. For simplicity, we consider a D2D cellular wireless transmission network with a single base station (BS), which serves one CU denoted by $\{C_1\}$ as illustrated in Fig. 9.1. There also exists a pair of DUs denoted by $\{D_1, D_2\}$. We assume that the transmissions between D2D users and also between cellular user and BS are one-way, i.e., BS and D_1 are transmitters while C_1 and D_2 are the receivers. The maximum transmit powers of the two transmitters, namely the BS and D_1, are denoted by P_{bmax} and P_{dmax}, respectively. In the cellular link, BS sends information to C_1 via the downlink channel. In the D2D link, D_1 transmits data to D_2 either directly or via the BS depending on the mode selection. The data packets are stored in buffers at the receivers before playout. Underflow and overflow constraints are imposed on these receiving buffers. The total bandwidth is denoted as B, and three modes, namely cellular mode, dedicated mode and reuse mode are employed in the system. The bandwidth is equally allocated, i.e., the bandwidth allocated to each link is denoted as $B_c = \frac{B}{3}$, $B_d = \frac{B}{2}$ and $B_r = B$ in cellular mode, dedicated mode and reuse mode, respectively.

Let $z_{1,1}(t)$, $z_{1,2}(t)$, $z_{2,1}(t)$, $z_{2,2}(t)$ and $z_{2,3}(t)$ denote the instantaneous channel power gains of the links BS-C_1, BS-D_2, D_1-C_1, D_1-D_2 and D_1-BS at time t, respectively. And also let $U_1(t)$ and $U_2(t)$ be the cumulative data consumption curves at the receiving users C_1 and D_2, representing the cumulative amount of data consumed by the decoders at time t, respectively. The cumulative data consumption curve is determined by the video characteristics such as frame sizes and rates, and the playout schedule. It is assumed that the playout buffers of C_1 and D_2 have sizes of b_1 and b_2 bits, and their videos have L_1 and L_2 frames, respectively. The cumulative overflow
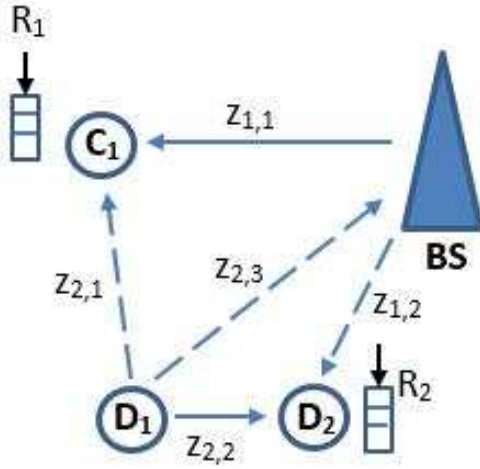
Figure 9.1: Proposed system block diagram for VBR video streaming in D2D networks

curve is formulated as [51]

$$O_m(t) = \min\{U_m(t-1) + b_m, U_m(L_m)\}, 0 \le t \le L_m, \tag{9.1}$$

where $O_m(t)$ is the maximum amount of accumulated received bits at time t without an overflow in the playout buffer. The cumulative transmission curves $A_1(t)$ and $A_2(t)$ are defined as the cumulative amount of bits received at C_1 and D_2 at time slot t, respectively. For simplicity, it is assumed that the videos have identical frame rates and the frame intervals are synchronized, which means that a time slot t is the same as the t-th frame interval, for $0 \le t \le \max_m\{L_m\}$. Since $O_m(t)$, $U_m(t)$ and $A_m(t)$ are cumulative curves, they are all nondecreasing functions over time. Fig. 9.2 shows that the feasible transmission schedule needs to generate a cumulative transmission curve $A_m(t)$ that lies within $O_m(t)$ and $U_m(t)$ in order to play the video without stall events or overflows leading to missing frames.
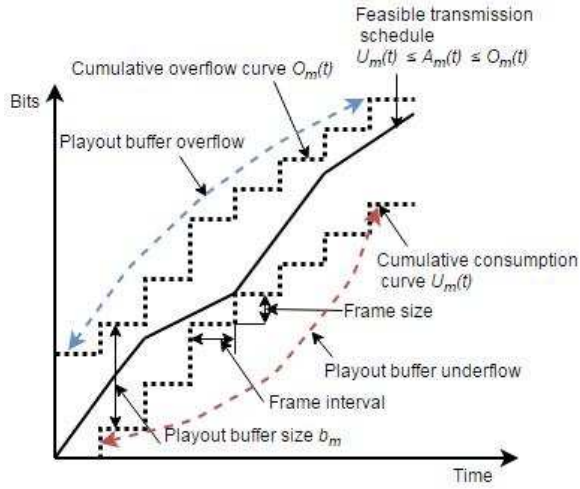
Figure 9.2: Cumulative overflow and cumulative consumption curves and a feasible transmission schedule for video

9.2 Problem Formation

We consider a block fading channel with channel gains not changing within each time slot, but varying over different time slots following a certain distribution. Without loss of generality, we employ the Shannon capacity as the transmission rate in the D2D wireless network. Three different transmission modes are considered next.

9.2.1 Cellular Mode

In the cellular mode, D_1 sends the video data to D_2 via BS, which is acting as a relay node. Note that BS also sends data to C_1 directly without any interference. Since we need to guarantee that all the data transmitted from D_1 is received at D_2, BS needs to deliver all the received bits from D_1 to D_2. Therefore, the transmission rate $R_1(t)$ from BS to C_1 and the rate $R_2(t)$ from D_1 to D_2 via BS over a two-hop

link are derived as follows:

$$R_{1,1}(t, \mathbf{P}) = B_c \log \left(1 + \frac{P_{b1}(t) z_{1,1}(t)}{N_0 B_c} \right) \tag{9.2}$$

$$R_{2,1}(t, \mathbf{P}) = \min\{R_{3,1}(t), R_{4,1}(t)\} \tag{9.3}$$

where

$$R_{3,1}(t, \mathbf{P}) = B_c \log \left(1 + \frac{P_d(t) z_{2,3}(t)}{N_0 B_c} \right) \tag{9.4}$$

$$R_{4,1}(t, \mathbf{P}) = B_c \log \left(1 + \frac{P_{b2}(t) z_{1,2}(t)}{N_0 B_c} \right) \tag{9.5}$$

are the transmission rates from D_1 to BS and from BS to D_2, respectively. $\mathbf{P}$ is the transmit power vector $[P_{b1}(t), P_{b2}(t), P_d(t)]$.

9.2.2 Dedicated Mode

In dedicated mode, D_1 transmits data to D_2 directly over a separate channel without any interference. The transmission rates of BS-C_1 and D_1-D_2 links are given, respectively, by

$$R_{1,2}(t, \mathbf{P}) = B_d \log \left(1 + \frac{P_{b1}(t) z_{1,1}(t)}{N_0 B_d} \right) \tag{9.6}$$

$$R_{2,2}(t, \mathbf{P}) = B_d \log \left(1 + \frac{P_d(t) z_{2,2}(t)}{N_0 B_d} \right). \tag{9.7}$$

9.2.3 Reuse Mode

In reuse mode, D_1 transmits data to D_2 directly but this time interference is experienced since BS-C_1 and D_1-D_2 links use the same channel. The transmission rates of

BS-C_1 and D_1-D_2 links are

$$R_{1,3}(t, \mathbf{P}) = B_r \log \left(1 + \frac{P_{b1}(t) z_{1,1}(t)}{P_d(t) z_{2,1}(t) + N_0 B_r} \right) \tag{9.8}$$

$$R_{2,3}(t, \mathbf{P}) = B_r \log \left(1 + \frac{P_d(t) z_{2,2}(t)}{P_{b1}(t) z_{1,2}(t) + N_0 B_r} \right). \tag{9.9}$$

Once the arrival rate is determined, $R_{m,n}(t, \mathbf{P})\tau$ video bits will be transmitted to the corresponding receiver in that time slot, where the subscript $n \in \mathcal{N} = 1, 2, 3$ indicates the cellular mode, dedicated mode and reuse mode, respectively. The cumulative transmission curve $A_m(t)$ can be written as

$$A_m(0) = 0, A_m(t) = A_m(t-1) + R_{m,n}(t, \mathbf{P})\tau. \tag{9.10}$$

It is assumed that the peak power is P_{dmax} at D_1, and P_{bmax} at BS for the cellular link BS-C_1 and downlink BS-D_2. The problem is to determine the transmit power vector $\mathbf{P}$ and to select the transmission mode for $0 < t \leq \max_m \{L_m\}$, such that the resulting cumulative transmission curves satisfy

$$U_m(t) \leq A_m(t) \leq O_m(t), \forall m, t, \tag{9.11}$$

i.e., no playout buffer underflow or overflow occurs at C_1 and D_2. From (9.10) and (9.11), the feasible transmission rate range is

$$\max\{0, \alpha_m(t)\} \leq R_{m,n}(t, \mathbf{P}) \leq \beta_m(t), \tag{9.12}$$

where $\alpha_m(t) = \frac{U_m(t) - A_m(t-1)}{\tau}$ and $\beta_m(t) = \frac{O_m(t) - A_m(t-1)}{\tau}$.

Let $R_{tot,n}(t, \mathbf{P}) = R_{1,n}(t, \mathbf{P}) + R_{2,n}(t, \mathbf{P})$ be the total transmission rate in 3 different modes. The optimal power control and mode selection problem for VBR video

streaming is formulated as follows:

$$\max_{n \in \mathcal{N}, \mathbf{P}} R_{tot}(t, \mathbf{P}) = \sum_{m=1}^{2} R_{m,n}(t, \mathbf{P}) \tag{9.13}$$

$$s.t. \quad P_{b1}(t) < P_{bmax} \tag{9.14}$$

$$P_{b2}(t) < P_{bmax} \tag{9.15}$$

$$P_d(t) < P_{dmax} \tag{9.16}$$

$$R_{m,n}(t, \mathbf{P}) \geq \max\{0, \alpha_m(t)\}, \forall m, \tag{9.17}$$

$$R_{m,n}(t, \mathbf{P}) \leq \beta_m(t), \forall m. \tag{9.18}$$

9.3 Optimal Power Control and Mode Selection Strategies

In this section, the optimal power control strategies in 3 different modes are identified and the best one among these 3 strategies is chosen as the final decision.

9.3.1 Cellular Mode

In cellular mode, there is no interference among the cellular link BS-C_1, uplink D_1-BS and downlink BS-D_2 since these 3 links are operating in different channels. Hence, the maximum sum rate of $R_{tot,1}(t)$ is the sum of maximum rates $R_{1,1}(t)$ and $R_{2,1}(t)$. From (9.2) and (9.18), and the maximum power constraint (9.14), the maximum transmission rate through link BS-C_1 is determined as

$$R_{c1}^*(t, \mathbf{P}) = \min \left\{ B_c \log \left(1 + \frac{P_{bmax} z_{1,1}(t)}{N_0 B_c} \right), \beta_1(t) \right\}. \tag{9.19}$$

Then, the optimal transmission power at BS for the cellular link is found as

$$P_{b1,1}^* = \left(2^{\frac{R_{c1}^*(t,\mathbf{P})}{B_c}} - 1 \right) \frac{N_0 B_c}{z_{1,1}(t)}. \tag{9.20}$$

Considering (9.3) and (9.18), and the maximum power constraints (9.15) and (9.16), we determine the maximum transmission rate through the two-hop link D_1-BS-D_2 as

$$R_{c2}^*(t,\mathbf{P}) = \min \left\{ B_c \log \left(1 + \frac{P_{dmax} z_{2,3}(t)}{N_0 B_c} \right), \right.$$
$$\left. B_c \log \left(1 + \frac{P_{bmax} z_{1,2}(t)}{N_0 B_c} \right), \beta_2(t) \right\}. \tag{9.21}$$

Hence, the optimal transmission powers in the uplink and downlink are derived as follows:

$$P_{b2,1}^* = \left(2^{\frac{R_{c2}^*(t,\mathbf{P})}{B_c}} - 1 \right) \frac{N_0 B_c}{z_{1,2}(t)} \tag{9.22}$$

$$P_{d,1}^* = \frac{z_{1,2}(t)}{z_{2,3}(t)} P_{b2,1}^*. \tag{9.23}$$

Thus, the optimal transmit power vector is $\mathbf{P}_1 = [P_{b1,1}^*, P_{b2,1}^*, P_{d,1}^*]$.

There are three scenarios based on the values of $R_{c1}^*(t,\mathbf{P})$ and $R_{c2}^*(t,\mathbf{P})$.

1. First, let us assume that $R_{c1}^*(t,\mathbf{P}) \geq \alpha_1(t)$ and $R_{c2}^*(t,\mathbf{P}) \geq \alpha_2(t)$, which means that the underflow and overflow playout buffer constraints at both C_1 and D_2 are satisfied. This has the highest priority, and let $pri(1) = 1$;

2. Second case is that either $R_{c1}^*(t,\mathbf{P}) \geq \alpha_1(t)$ or $R_{c2}^*(t,\mathbf{P}) \geq \alpha_2(t)$, which means that the underflow and overflow playout buffer constraints at either C_1 or D_2 are satisfied only. The priority of this scenario is lower, and let $pri(1) = 2$;

3. The last scenario is that neither conditions ($R_{c1}^*(t,\mathbf{P}) \geq \alpha_1(t)$ and $R_{c2}^*(t,\mathbf{P}) \geq \alpha_2(t)$) are satisfied, which means that the underflow and overflow playout buffer

161

constraints at both C_1 and D_2 are not satisfied. This case has the lowest priority, and let $pri(1) = 3$;

9.3.2 Dedicated Mode

Similarly as in cellular mode, from (9.6), (9.18) and the constraint in (9.14), the maximum transmission rate in link BS-C_1 is

$$R_{d1}^*(t, \mathbf{P}) = \min \left\{ B_d \log \left(1 + \frac{P_{bmax} z_{1,1}(t)}{N_0 B_d} \right), \beta_1(t) \right\}, \tag{9.24}$$

and the optimal transmission power at BS in cellular link is

$$P_{b1,2}^* = \left(2^{\frac{R_{d1}^*(t)}{B_d}} - 1 \right) \frac{N_0 B_d}{z_{1,1}(t)}. \tag{9.25}$$

Since D_1 transmits data to D_2 directly in the dedicated mode, the maximum transmission rate in direct link D_1-D_2 is

$$R_{d2}^*(t, \mathbf{P}) = \min \left\{ B_d \log \left(1 + \frac{P_{dmax} z_{2,2}(t)}{N_0 B_d} \right), \beta_2(t) \right\}, \tag{9.26}$$

and the optimal transmission power at BS in cellular link is

$$P_{d,2}^* = \left(2^{\frac{R_{d2}^*(t)}{B_d}} - 1 \right) \frac{N_0 B_d}{z_{2,2}(t)}. \tag{9.27}$$

Thus, the optimal transmit power vector is $\mathbf{P}_2 = [P_{b1,2}^*, P_{b2,2}^*, P_{d,2}^*]$, where $P_{b2,2}^* = 0$.

Similar as in cellular mode, there are 3 scenarios based on the values of $R_{d1}^*(t, \mathbf{P})$ and $R_{d2}^*(t, \mathbf{P})$:

1. If $R_{d1}^*(t, \mathbf{P}) \geq \alpha_1(t)$ and $R_{d2}^*(t, \mathbf{P}) \geq \alpha_2(t)$, let $pri(2) = 1$;

2. If $R_{d1}^*(t, \mathbf{P}) \geq \alpha_1(t)$ or $R_{d2}^*(t, \mathbf{P}) \geq \alpha_2(t)$, let $pri(2) = 2$;

3. If $R_{d1}^*(t, \mathbf{P}) < \alpha_1(t)$ and $R_{d2}^*(t, \mathbf{P}) < \alpha_2(t)$, let $pri(2) = 3$.

9.3.3 Reuse Mode

Reuse mode is the most complicated case due to the impact of interference. From (9.8), (9.9) and (9.18), the powers $P_{b1}(t) = P_1(t)$ and $P_d(t) = P_2(t)$ can be determined by having $R_{1,3}(t, \mathbf{P})$ and $R_{2,3}(t, \mathbf{P})$ attain their upper bounds $\beta_1(t)$ and $\beta_2(t)$ as follows:

$$B_r \log \left(1 + \frac{P_1(t)z_{1,1}(t)}{P_2(t)z_{2,1}(t) + N_0 B_r} \right) = \beta_1(t) \tag{9.28}$$

$$B_r \log \left(1 + \frac{P_2(t)z_{2,2}(t)}{P_1(t)z_{1,2}(t) + N_0 B_r} \right) = \beta_2(t). \tag{9.29}$$

After simple algebraic steps, (9.28) and (9.29) can be rewritten as

$$P_1(t)z_{1,1}(t) - \left(2^{\frac{\beta_1(t)}{B_r}} - 1 \right)\left(P_2(t)z_{2,1}(t) + N_0 B_r \right) = 0 \tag{9.30}$$

$$P_2(t)z_{2,2}(t) - \left(2^{\frac{\beta_2(t)}{B_r}} - 1 \right)\left(P_1(t)z_{1,2}(t) + N_0 B_r \right) = 0. \tag{9.31}$$

Since (9.30) and (9.31) constitute a system of linear equations with two unknowns, $P_1(t)$ and $P_2(t)$ can be derived in closed-form as follows:

$$P_1(t) = \frac{(2^{\frac{\beta_1(t)}{B_r}} - 1)\left(z_{2,2}(t) + (2^{\frac{\beta_2(t)}{B_r}} - 1)z_{2,1}(t) \right) N_0 B_r}{z_{1,1}(t)z_{2,2}(t) - (2^{\frac{\beta_1(t)}{B_r}} - 1)(2^{\frac{\beta_2(t)}{B_r}} - 1)z_{1,2}(t)z_{2,1}(t)} \tag{9.32}$$

$$P_2(t) = \frac{(2^{\frac{\beta_2(t)}{B_r}} - 1)\left(z_{1,1}(t) + (2^{\frac{\beta_1(t)}{B_r}} - 1)z_{1,2}(t) \right) N_0 B_r}{z_{1,1}(t)z_{2,2}(t) - (2^{\frac{\beta_1(t)}{B_r}} - 1)(2^{\frac{\beta_2(t)}{B_r}} - 1)z_{1,2}(t)z_{2,1}(t)}. \tag{9.33}$$

If $0 \le P_1(t) \le P_{bmax}$ and $0 \le P_2(t) \le P_{dmax}$, $\mathcal{P}^* = [P_1(t), 0, P_2(t)]$ is the optimal solution in reuse mode. Otherwise, under the constraints (9.14), (9.15), (9.16) and (9.18), the optimal solution (P_{b1}^*, P_d^*) always satisfies either $P_{b1}^* = P_{bmax}$ or $P_d^* = P_{dmax}$. We can show that this leads to either $R_{1,3}(t, \mathbf{P}) < \beta_1(t)$ and $R_{2,3}(t, \mathbf{P}) < \beta_2(t)$

or $R_{1,3}(t, \mathbf{P}) = \beta_1(t)$ or $R_{2,3}(t, \mathbf{P}) = \beta_2(t)$. Hence, we need to consider both cases of $P_{b1}^* = P_{bmax}$ and $P_d^* = P_{dmax}$.

9.3.3.1 Case 1: $P_{b1}^* = P_{bmax}$

In this section, we analyze the strategy to find the optimal solution subject to $P_{b1}^* = P_{bmax}$. After setting $P_{b1}^* = P_{bmax}$, we can find the feasible region of P_d by solving (9.18) and (9.17) as follows:

$$P_{dl1} \leq P_d \leq P_{dh1} \tag{9.34}$$

$$P_{dl2} \leq P_d \leq P_{dh2} \tag{9.35}$$

where

$$P_{dl1} = \frac{P_{bmax} z_{1,1}(t)}{2^{\frac{\beta_1(t)}{B_r}} z_{2,1}(t)} - \frac{N_0 B_r}{z_{2,1}(t)} \tag{9.36}$$

$$P_{dh1} = \frac{P_{bmax} z_{1,1}(t)}{2^{\frac{\max\{0,\alpha_1(t)\}}{B_r}} z_{2,1}(t)} - \frac{N_0 B_r}{z_{2,1}(t)} \tag{9.37}$$

$$P_{dl2} = \frac{(2^{\frac{\max\{0,\alpha_2(t)\}}{B_r}} - 1)(N_0 B_r + P_{bmax} z_{1,2}(t))}{z_{2,2}(t)} \tag{9.38}$$

$$P_{dh2} = \frac{(2^{\frac{\beta_2(t)}{B_r}} - 1)(N_0 B_r + P_{bmax} z_{1,2}(t))}{z_{2,2}(t)}. \tag{9.39}$$

Let

$$P_{dmin1} = \max\{0, P_{dl1}\} \tag{9.40}$$

$$P_{dmax1} = \min\{P_{dmax}, P_{dh1}\} \tag{9.41}$$

$$P_{dmin2} = \max\{0, P_{dl2}\} \tag{9.42}$$

$$P_{dmax2} = \max\{P_{dmax}, P_{dh2}\} \tag{9.43}$$

$$P_{dl} = \max\{P_{dmin1}, P_{dmin2}\} \tag{9.44}$$

$$P_{dh} = \min\{P_{dmax1}, P_{dmax2}\}. \tag{9.45}$$

We again have 3 cases to consider:

1. If $P_{dl} \le P_{dh}$, then the underflow and overflow playout buffer constraints are satisfied at both C_1 and D_2. This case has the highest priority, and let $pri_3(1) = 1$. We can show that the optimal solution always occurs at the endpoints. Therefore, the optimal transmit power vector is $\mathbf{P}_{3,1} = [P_{bmax}, 0, P_{dl}]$ if $R_{tot}(t, [P_{bmax}, 0, P_{dl}]) > R_{tot}(t, [P_{bmax}, 0, P_{dh}])$; otherwise, $\mathbf{P}_{3,1} = [P_{bmax}, 0, P_{dh}]$.

2. If $P_{dmin1} \le P_{dmax1}$ or $P_{dmin2} \le P_{dmax2}$, then the underflow and overflow playout buffer constraints are satisfied at either only C_1 or D_2. For this case, we let $pri_3(1) = 2$. Similarly, there are four endpoint vectors $[P_{bmax}, 0, P_{d,j}]$ where $P_{d,1} = P_{dmin1}$, $P_{d,2} = P_{dmax1}$, $P_{d,3} = P_{dmin2}$ and $P_{d,4} = P_{dmax2}$. The optimal transmit power vector is $\mathbf{P}_{3,1} = [P_{bmax}, 0, P_{d,k}]$ if $R_{tot}(t, [P_{bmax}, 0, P_{d,k}])$ is the highest value among $R_{tot}(t, [P_{bmax}, 0, P_{d,j}])$ for all $j \in 1, 2, 3, 4$.

3. If $P_{dmin1} > P_{dmax1}$ and $P_{dmin2} > P_{dmax2}$, then the underflow and overflow playout buffer constraints are not satisfied at C_1 and D_2. This case has the lowest priority, and we let $pri_3(1) = 3$. Similarly, there are two endpoint vectors, and the optimal transmit power vector is $\mathbf{P}_{3,1} = [P_{bmax}, 0, 0]$ if $R_{tot}(t, [P_{bmax}, 0, 0]) > R_{tot}(t, [P_{bmax}, 0, P_{dmax}])$; otherwise, $\mathbf{P}_{3,1} = [P_{bmax}, 0, P_{dmax}]$.

9.3.3.2 Case 2: $P_d^* = P_{dmax}$

Similarly as in the case of $P_b^* = P_{bmax}$, after fixing $P_d^* = P_{dmax}$, we can find the feasible region of P_{b1} by solving (9.18) and (9.17):

$$P_{bl1} \leq P_{b1} \leq P_{bh1} \tag{9.46}$$

$$P_{bl2} \leq P_{b1} \leq P_{bh2} \tag{9.47}$$

where

$$P_{bl1} = \frac{(2^{\frac{\max\{0,\alpha_1(t)\}}{B_r}} - 1)(N_0 B_r + P_{dmax} z_{2,1}(t))}{z_{1,1}(t)} \tag{9.48}$$

$$P_{bh1} = \frac{(2^{\frac{\beta_1(t)}{B_r}} - 1)(N_0 B_r + P_{dmax} z_{2,1}(t))}{z_{1,1}(t)} \tag{9.49}$$

$$P_{bl2} = \frac{P_{dmax} z_{2,2}(t)}{2^{\frac{\beta_2(t)}{B_r}} z_{1,2}(t)} - \frac{N_0 B_r}{z_{1,2}(t)} \tag{9.50}$$

$$P_{bh2} = \frac{P_{dmax} z_{2,2}(t)}{2^{\frac{\max\{0,\alpha_2(t)\}}{B_r}} z_{1,2}(t)} - \frac{N_0 B_r}{z_{1,2}(t)}. \tag{9.51}$$

Let

$$P_{bmin1} = \max\{0, P_{bl1}\} \tag{9.52}$$

$$P_{bmax1} = \min\{P_{bmax}, P_{bh1}\} \tag{9.53}$$

$$P_{bmin2} = \max\{0, P_{bl2}\} \tag{9.54}$$

$$P_{bmax2} = \max\{P_{bmax}, P_{bh2}\} \tag{9.55}$$

$$P_{bl} = \max\{P_{bmin1}, P_{bmin2}\} \tag{9.56}$$

$$P_{bh} = \min\{P_{bmax1}, P_{bmax2}\}. \tag{9.57}$$

There are also 3 cases:

1. If $P_{bl} \leq P_{bh}$, then the underflow and overflow playout buffer constraints are sat-

166

isfied at both C_1 and D_2. This case has the highest priority, and let $pri_3(2) = 1$. We can show that the optimal solution always occurs at the endpoints. Therefore, the optimal transmit power vector is $\mathbf{P}_{3,2} = [P_{bl}, 0, P_{dmax}]$ if $R_{tot}(t, [P_{bl}, 0, P_{dmax}]) > R_{tot}(t, [P_{bh}, 0, P_{dmax}])$; otherwise, $\mathbf{P}_{3,1} = [P_{bh}, 0, P_{dmax}]$.

2. If $P_{bmin1} \leq P_{bmax1}$ or $P_{bmin2} \leq P_{bmax2}$, then the underflow and overflow playout buffer constraints are satisfied at either only C_1 or D_2. For this case, we let $pri_3(2) = 2$. Similarly, there are four endpoint vectors $[P_{b1,j}, 0, P_{dmax}]$ where $P_{b1,1} = P_{bmin1}$, $P_{b1,2} = P_{bmax1}$, $P_{b1,3} = P_{bmin2}$ and $P_{b1,4} = P_{bmax2}$. The optimal transmit power vector is $\mathbf{P}_{3,2} = [P_{b1,k}, 0, P_{dmax}]$ if $R_{tot}(t, [P_{b1,k}, 0, P_{dmax}])$ is the highest value among $R_{tot}(t, [P_{b1,j}, 0, P_{dmax}])$ for all $j \in 1, 2, 3, 4$.

3. If $P_{bmin1} > P_{bmax1}$ and $P_{bmin2} > P_{bmax2}$, then the underflow and overflow playout buffer constraints are not satisfied at C_1 and D_2. This case has the lowest priority, and we let $pri_3(2) = 3$. Similarly, there are two endpoint vectors, and the optimal transmit power vector is $\mathbf{P}_{3,2} = [0, 0, P_{dmax}]$ if $R_{tot}(t, [0, 0, P_{dmax}]) > R_{tot}(t, [P_{bmax}, 0, P_{dmax}])$; otherwise, $\mathbf{P}_{3,2} = [P_{bmax}, 0, P_{dmax}]$.

The overall optimal transmit power is selected from the above two cases in reuse mode. If $pri_3(i_1) < pri_3(i_2)$, the optimal transmit power vector is $\mathbf{P}_3 = \mathbf{P}_{3,i_1}$, where $i_1, i_2 \in 1, 2$ and $i_1 \neq i_2$. Otherwise, $\mathbf{P}_3 = \mathbf{P}_{3,i_1}$ if $R_{tot}(t, \mathbf{P}_{3,i_1}) \geq R_{tot}(t, \mathbf{P}_{3,i_2})$. Let $pri(3) = pri_3(i_1)$ and the optimal transmit power vector is $\mathbf{P}_3 = \mathbf{P}_{3,i_1}$.

After determining the optimal transmit power vectors in three different transmission modes, we need to decide which mode to select as the best strategy for data transmission. Since we want to choose the one with the highest priority, if $pri(l) = \min\{pri(1), pri(2), pri(3)\}$ for only one value of $l \in 1, 2, 3$, then the optimal transmit power vector is $\mathbf{P} = \mathbf{P}_l$ and the mode selection is l. And if $pri(1) = pri(2) = pri(3)$, then the one with the highest $R_{tot}(t, \mathbf{P}_l)$ is chosen. Otherwise, if $pri(l_1) = pri(l_2) < pri(l_2)$, then $\mathbf{P} = \mathbf{P}_{l_1}$ if $R_{tot}(t, \mathbf{P}_{l_1}) \geq R_{tot}(t, \mathbf{P}_{l_2})$.

167

9.4   Numerical and Simulation Results

In this section, we evaluate the performance of the proposed transmission strategies. Rayleigh fading is considered in the channels in all simulations, where the normalized path gain is exponentially distributed as $f(z_{i,j}(t)) = \frac{1}{G_{i,j}} \exp\left\{\frac{-z_{i,j}(t)}{G_{i,j}}\right\}$ with path gain averages $G_{i,j}$, where $i \in \{1,2\}$ and $j \in \{1,2,3\}$. The peak power constraints are $P_{dmax} = 0$ dB and $P_{bmax} = 2$ dB at D_1 and BS, respectively. The movie *Tokyo Olympics* is transmitted through cellular link and *NBC News* is transmitted from D_1 to D_2 through different links according to the mode selection. The used VBR video traces in all the simulations are from the Video Trace Library hosted at Arizona State University [66]. The playout buffer size is set to be 1.5 times the largest frame size in all the videos.

Fig. 9.3 shows the consumption curves of the buffer at D_2 from frame-time slot 1 to 10000. In Fig. 9.4, we plot the cumulative overflow, transmission, and consumption curves when transmitting *NBC News* between the D2D users from frame-time slot 6360 to 6380 in different transmission modes. In this time period, the cumulative transmission curves are lower than the cumulative consumption curves all the time in the cellular mode and dedicated mode. The reason is that all the curves are cumulative, and the cumulative transmission curves are much lower than the cumulative consumption curves before frame-time slot 6360 and the transmit powers are not large enough for supporting the demanded data transmission. Additionally, the frame sizes around frame-time slot 6360 are large. There are just several overflow events happening among these frame-time slots in the reuse mode since the cumulative transmission curve satisfies the buffer constraints before frame-time slot 6360. The mode selection has the best performance since it always chooses the best transmission mode in each frame-time slot and this leads to the best cumulative transmission curve. The extra transmitted video data will be in the playout buffer to provide a cushion to variations in the network dynamics when future large frames need to be transmitted. From Fig.
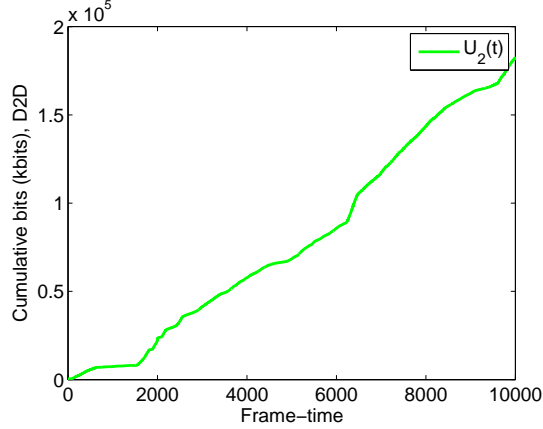
Figure 9.3: Consumption curve in D_2

9.4e, $A_2(t)$ at time slot 6360 after mode selection is much higher than in cellular, dedicated and reuse modes. This advantage is due to the cumulative benefits. Fig. 9.4d shows the mode selection after solving the optimization problem. 1, 2 and 3 denote cellular mode, dedicated mode and reuse mode, respectively.

Fig. 9.5 shows the buffer utilization from frame-time slot 1790 to 1810. We find that the buffer utilization of mode selection strategy has the highest value since this results as the solution of the optimization problem, and the values are higher than 70%. The higher buffer utilization leads to lower buffer underflow event probability. Table 9.1 shows the probability of underflow events in different modes, and mode selection strategy has the lowest probability of underflow events both at C_1 and D_2.

Table 9.1: Probability of underflow events

	cellular	dedicated	reuse	mode selection
C_1	0.0388	0.0124	3.6×10^{-4}	3.6×10^{-4}
D_2	0.0391	0.0168	0.0024	1.6×10^{-4}
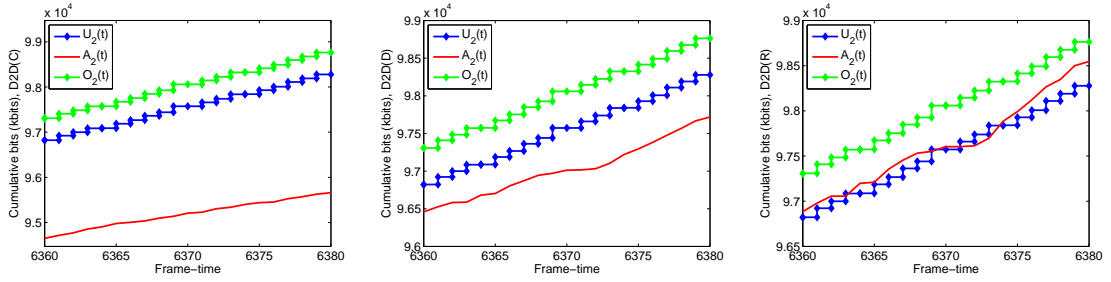
(a) Curves in cellular mode (b) Curves in dedicated mode (c) Curves in reuse mode
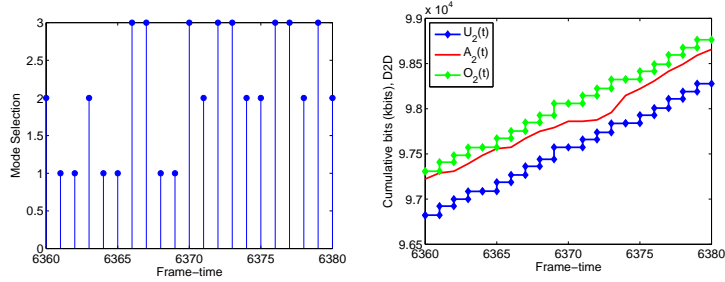
(d) Mode selection

(e) Curves after mode selection

Figure 9.4: The cumulative overflow, transmission, and consumption curves when transmitting *NBC News* at D2D link in (a) cellular mode; (b) dedicated mode; (c) reuse mode and; (d) the optimal mode selection and (e) the corresponding curves with optimal mode selection.
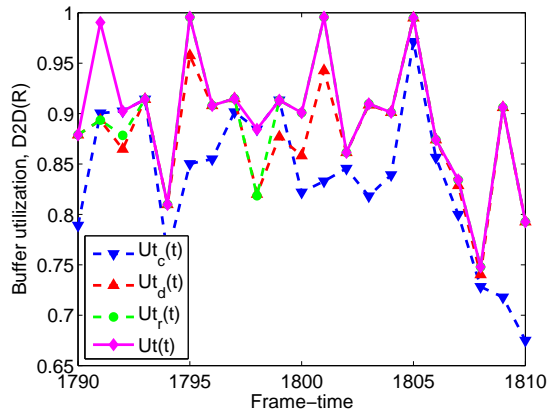
Figure 9.5: Buffer utilization in D_2

Chapter 10

Power Control for Wireless VBR Video Streaming : From Dynamic Programming to Reinforcement Learning

In this chapter, we investigate the problem of power control for streaming variable bit rate (VBR) videos over wireless links. A system model involving a transmitter (e.g., a base station (BS)) that sends VBR video data to a mobile user equipped with a playout buffer is adopted. In this setting, we analyze power control policies considering the following two objectives: 1) the minimization of the transmit power consumption, and 2) the minimization of the transmission completion time of the communication session. In order to play the video without interruptions, the power control policy should also satisfy the requirement that the VBR video data is delivered to the mobile user without causing playout buffer underflow or overflows. A directional water-filling algorithm, which provides a simple and concise interpretation of the necessary optimality conditions, is studied as the optimal offline policy.

Following this, two online policies are proposed for power control based on channel side information (CSI) prediction in each short time period. Dynamic programming is employed to determine the optimal offline and the initial online power control policies that minimize the transmit power consumption in the communication session. Subsequently, reinforcement learning (RL) based approach is employed for the second online power control policy.

10.1 System Model

We consider video streaming over a wireless fading link with multiple subchannels as shown in Fig. 10.1. It is assumed that all the data packets are stored in buffers at the transmitter (Tx) before they are sent to the receiver (Rx). There are M orthogonal subchannels between the Tx and Rx with bandwidth B_c for each subchannel, and the total bandwidth is $B = MB_c$. We assume that each channel experiences block-flat fading during each time slot t. Thus, the capacity of the ith subchannel in time slot t is

$$C_i(t) = B_c \log\left(1 + \frac{P_i(t)\gamma_i(t)}{N_0 B_c}\right), \tag{10.1}$$

where $P_i(t)$ and $\gamma_i(t)$ are the transmission power and ergodic and stationary fading power in the ith subchannel in time slot t, respectively. N_0 is the power spectral density of the background Gaussian noise. Therefore, the total throughput over all the subchannels in time slot t is $C(t) = \sum_{i=1}^{M} C_i(t)$.

Let $F(t)$ be the video consumption/frame size at the Rx, representing the amount of data played by the video player in time slot t. We assume that the video has T frames, and due to the limited storage, the playout buffer at the Rx is $F_{\max}$. Let $U(t)$ represent the cumulative consumption curve at time t, representing the cumulative amount of bits consumed by the Rx. The remaining data in the buffer at time t, which is denoted by $D(t)$, should not exceed the buffer storage capacity. In the meantime,

172
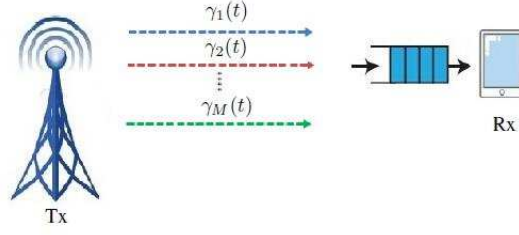
Figure 10.1: System model for VBR video streaming over a wireless link with multiple subchannels.

in order to play the video without any interruption at the Rx, $D(t)$ should not be less than the frame size required at time t, $F(t)$. Therefore, the constraints for the remaining data in the buffer at time t are formulated as follows:

$$D(t) \leq F_{\max}, \qquad 0 \leq t \leq T, \tag{10.2}$$

$$D(t) \geq F(t), \qquad 0 \leq t \leq T, \tag{10.3}$$

where we assume $F(0) = 0$. The remaining data $D(t)$ depends on the arrival data at time t and consumed data at time $t-1$, and thus the relation among remaining data and arrival data and consumed data is expressed as follows:

$$D(t) = D(t-1) - F(t-1) + C(t)\tau, 1 \leq t \leq T, \tag{10.4}$$

where τ is the duration of one time slot and we assume $D(0) = 0$. After some straightforward manipulations, (10.4) can be rewritten as

$$D(t) = \sum_{i=1}^{t} C(i)\tau - \sum_{i=1}^{t-1} F(i)$$
$$= X(t) - U(t-1), \quad 1 \leq t \leq T, \tag{10.5}$$

where $X(t) = \sum_{i=1}^{t} C(i)\tau$ denotes the amount of cumulative arrival data at time t. Let $O(t)$ denote the cumulative overflow curve, representing the maximum cumulative

173

amount of bits that does not violate the buffer length constraint. Hence, $O(t)$ and $U(t)$ can be expressed as

$$O(t) = \sum_{i=0}^{t-1} F(i) + F_{\max}, \quad 1 \le t \le T, \tag{10.6}$$

$$U(t) = \sum_{i=1}^{t} F(i), \qquad 1 \le t \le T. \tag{10.7}$$

Therefore, constraints in (10.2) and (10.3) can now be rewritten as

$$X(t) \le O(t), \qquad 1 \le t \le T, \tag{10.8}$$

$$X(t) \ge U(t), \qquad 1 \le t \le T, \tag{10.9}$$

10.2   Optimal Offline Policies

In this section, we analyze optimal offline policies. We initially characterize the optimal policy that minimizes the power consumption in wireless video streaming. Subsequently, we will address the minimization of time duration of video streaming. In both cases, overflow and underflow constraints will be imposed.

10.2.1   Minimizing power consumption

In this section, the goal is to determine the optimal offline policy that minimizes the overall power consumption under the requirement that Rx plays the received video without any interruptions and missing frames. Therefore, the optimization problem can be expressed as follows:

$$\min_{\mathbf{P}} \sum_{j=1}^{T} \sum_{i=1}^{M} P_i(j) \tag{P1}$$

$$\text{s.t. } \sum_{j=1}^{t} \sum_{i=1}^{M} C_i(j)\tau \geq \sum_{j=1}^{t} F(j), \forall t = 1, \ldots, T-1, \tag{10.10}$$

$$\sum_{j=1}^{T} \sum_{i=1}^{M} C_i(j)\tau = \sum_{j=1}^{T} F(j), \tag{10.11}$$

$$\sum_{j=1}^{t} \sum_{i=1}^{M} C_i(j)\tau \leq \sum_{j=1}^{t-1} F(j) + F_{\max}, \forall t = 1, \ldots, T, \tag{10.12}$$

where $\mathbf{P}$ is an $M \times L$ power matrix with the component in the ith row and j^{th} column $P_i(j)$ denoting the power allocated to the ith channel at time j. (10.10) and (10.12) are the minimum cumulative data requirement and buffer overflow violation constraints, respectively, described in Section 10.1. (10.11) is the constraint that the overall received data should be equal to the size of the transmitted video.

The objective function in Problem (**P1**) is a linear function of $\mathbf{P}$. However, since the constraint (10.12) is a concave function with respect to $\mathbf{P}$, the optimization problem (**P1**) is not a convex optimization problem.

On the other hand, (10.1) can be rewritten as

$$P_i(t) = \left(2^{\frac{C_i(t)}{B_c}} - 1\right) \frac{N_0 B_c}{\gamma_i(t)}, \tag{10.13}$$

and therefore, the optimization problem (**P1**) can also be reformulated in terms of C_i as

$$\min_{\mathbf{C}} \sum_{j=1}^{T} \sum_{i=1}^{M} \left(2^{\frac{C_i(j)}{B_c}} - 1\right) \frac{N_0 B_c}{\gamma_i(j)} \tag{P2}$$

$$\text{s.t.} \qquad (10.10), (10.11), (10.12)$$

175

Above, the objective function of (**P2**) is an increasing convex function of **C**, and constraints (10.10), (10.11) and (10.12) are linear functions of **C**. Therefore, the optimization problem (**P2**) is convex with respect to **C** and we can employ the Lagrangian optimization framework. In particular, we can identify the Karush-Kuhn-Tucker (KKT) conditions and characterize the optimal policy. For this problem, we have the following Lagrangian function using Lagrange multipliers $\mu_k \geq 0$ and $\lambda_k \geq 0$:

$$
\begin{aligned}
L(\mu, \lambda) = &\sum_{j=1}^{T}\sum_{i=1}^{M}\left(2^{\frac{C_i(j)}{B_c}} - 1\right)\frac{N_0 B_c}{\gamma_i(j)} \\
&- \sum_{t=1}^{T-1}\left\{\mu_t\left(\sum_{j=1}^{t}\sum_{i=1}^{M}C_i(j)\tau - \sum_{j=1}^{t}F(j)\right)\right\} \\
&- \mu_T\left(\sum_{j=1}^{T}\sum_{i=1}^{M}C_i(j)\tau - \sum_{j=1}^{T}F(j)\right) \\
&+ \sum_{t=1}^{T}\left\{\lambda_t\left(\sum_{j=1}^{t}\sum_{i=1}^{M}C_i(j)\tau - \sum_{j=1}^{t-1}F(j) - F_{\max}\right)\right\},
\end{aligned} \tag{10.14}
$$

Lagrange multipliers $\mu_t, t = 1, 2, \ldots, T-1$ and μ_T are associated with the constraints in (10.10) and (10.11), respectively. $\lambda_t, t = 1, 2, \ldots, T$ are associated with the constraint (10.12). The additional complimentary slackness conditions are as follows:

$$
\mu_t\left(\sum_{j=1}^{t}\sum_{i=1}^{M}C_i(j)\tau - \sum_{j=1}^{t}F(j)\right) = 0, \quad 1 \leq t \leq T-1, \tag{10.15}
$$

$$
\mu_T\left(\sum_{j=1}^{T}\sum_{i=1}^{M}C_i(j)\tau - \sum_{j=1}^{T}F(j)\right) = 0, \tag{10.16}
$$

$$
\lambda_t\left(\sum_{j=1}^{t}\sum_{i=1}^{M}C_i(j)\tau - \sum_{j=1}^{t-1}F(j) - F_{\max}\right) = 0, \quad 1 \leq t \leq T. \tag{10.17}
$$

Taking the first derivative of (10.14) with respect to $C_i(j)$, we obtain

$$\frac{\partial L(\mu, \lambda)}{C_i(j)} = 2^{\frac{C_i(j)}{B_c}} \frac{\ln 2}{B_c} \frac{N_0 B_c}{\gamma_i(j)} + \left(\tau \sum_{t=j}^{T} (\lambda_t - \mu_t) \right). \tag{10.18}$$

From the KKT optimality conditions, the optimal arrival rates $C_i^*(j)$ to the receiver buffer can be obtained after solving

$$2^{\frac{C_i^*(j)}{B_c}} \frac{\ln 2}{B_c} \frac{N_0 B_c}{\gamma_i(j)} + \left(\tau \sum_{t=j}^{T} (\lambda_t - \mu_t) \right) = 0. \tag{10.19}$$

Now, the optimal power levels $P_i^*(j)$ in terms of the Lagrange multipliers are expressed as

$$\begin{aligned} P_i^*(j) &= \left(2^{\frac{C_i^*(j)}{B_c}} - 1 \right) \frac{N_0 B_c}{\gamma_i(j)} \\ &= \frac{\tau B_c}{\ln 2} \sum_{t=j}^{T} (\mu_t - \lambda_t) - \frac{N_0 B_c}{\gamma_i(j)} \\ &= \left[W(j) - \frac{N_0 B_c}{\gamma_i(j)} \right]^+, \end{aligned} \tag{10.20}$$

where $[x]^+ = \max\{0, x\}$, and the water level in time slot j, $W(j)$, is given by

$$W(j) = \frac{\tau B_c}{\ln 2} \sum_{t=j}^{T} (\mu_t - \lambda_t). \tag{10.21}$$

We have the following observation regarding the water levels.

Theorem 10.1 *When $F_{max} = \infty$, the optimal water levels $W(j)$ generally form a monotonically decreasing sequence i.e., $W(j) \geq W(j + 1)$. Moreover, if for some j, Tx transmits a part of the future frames, then $W(j) = W(j+1)$. And $W(j) < W(j+1)$ occurs only if the Tx sends a part of the future frames that makes the buffer at the Rx to be full in time slot j.*

Proof 1 *Since $F_{max} = \infty$, constraints in (10.12) are satisfied with strict inequality and $\lambda_t = 0$ for all t by slackness conditions in (10.17). And from (10.21), since $\mu_j \geq 0$, we have $W(j) \geq W(j+1)$. If in time slot j, Tx sends a part of the future frames, then the jth constraint in (10.10) is satisfied with strict inequality. This means that for those values of j, we have $\lambda_j = 0$ by slackness conditions in (10.15). Hence, by (10.21), $W(j) = W(j+1)$. Since F_{max} is greater than any frame size in the video sequence, i.e., $F_{max} > F(t)$ for all t, the constraints in (10.10) and (10.12) for $t = j$ cannot be satisfied with equality at the same time. In other words, we cannot have $\lambda_j > 0$ and $\mu_j > 0$ simultaneously in the same time slot j. From (10.21), $W(j) < W(j+1)$ implies that $\mu_j - \lambda_j < 0$. Therefore, $W(j) < W(j+1)$ only if $\mu_j = 0$ and $\lambda_j > 0$. $\lambda_j > 0$ means that the constraint in (10.12) at $t = j$ is satisfied with equality. Thus, $W(j) < W(j+1)$ only if Rx has received a part of the future frames that makes the buffer to be full in time slot j.* ∎

In general, it is not an easy task to determine all the water levels $W(j)$ for $1 \leq j \leq T$ by solving (10.15), (10.16), (10.17) and (10.20). We will employ a dynamic programming based approach to determine the water levels. Assume that Tx sends only the first $t - 1$ frames by time $t - 1$ and we have the optimal water levels $W(j)$ up to that time, i.e., for $0 \leq j \leq t - 1$. Let $W(0) = \infty$ and let $\mathcal{Q}_t = \{q_0, q_1, \ldots, q_{s(t)}\}$ denote the indices of the frames immediately after which the water level becomes different from the previous water level (i.e., a transition occurs in terms of the water levels in the frame $q_k + 1$). Equivalently, this also means that the water level $W(q_k + 1)$ stays the same for frames $q_k + 1$ through q_{k+1} (and the water level changes in the next frame with index $q_{k+1} + 1$). Let us set $q_0 = 0$. Also let $H(j) = \sum_{i=1}^{M} C_i(j)\tau$ denote the data Rx receives in time slot j for $0 \leq j \leq t$ and $H(0) = 0$.

When a new frame $F(t)$ is added to the video, Tx sends $F(t)$ in time slot t and

the corresponding water level is $W(t) = W_{\text{cur}}$ obtained by solving

$$F(t) = \sum_{i=1}^{M} \tau B_c \log \left(1 + \frac{\left[W_{\text{cur}} - \frac{N_0 B_c}{\gamma_i(t)} \right]^+ \gamma_i(t)}{N_0 B_c} \right). \tag{10.22}$$

Now, we compare W_{cur} with the previous water level $W_{\text{pre}} = W(q_{s(t-1)} + 1)$, and consider two cases:

1. $W_{\text{cur}} \leq W_{\text{pre}}$: From Theorem (10.1), which shows the optimal water levels as monotonically non-increasing, if the current water level is less than or equal to the previous water level, no further operation or processing is needed and the current water level is the optimal one. Thus we update $\mathcal{Q}_{t-1}$ to $\mathcal{Q}_t$ by adding t as $q_{s(t)}$.

2. $W_{\text{cur}} > W_{\text{pre}}$: We initialize $k = 0$ and update the new water levels $W(j) = W_{\text{cur}}$ for $q_{s(t-1)-k} + 1 \leq j \leq t$ until $W_{\text{cur}} \leq W(q_{s(t-1)-k-1} + 1)$ or the buffer is full in time slot $q_{s(t-1)-k}$ by replacing k with $k+1$ and updating W_{cur} from the following equation:

$$F(t) + \sum_{j=q_{s(t-1)-k}}^{t} H(j)$$
$$= \sum_{j=q_{s(t-1)-k}}^{t} \sum_{i=1}^{M} \tau B_c \log \left(1 + \frac{\left[W_{\text{cur}} - \frac{N_0 B_c}{\gamma_i(j)} \right]^+ \gamma_i(j)}{N_0 B_c} \right). \tag{10.23}$$

Then, the updated power levels $P_i(j)$ and transmitted data $H(j)$ in the corresponding time slots are expressed as follows:

$$P_i(j) = \left[W_{\text{cur}} - \frac{N_0 B_c}{\gamma_i(j)} \right]^+, \tag{10.24}$$

$$H(j) = \sum_{i=1}^{M} \tau B_c \log \left(1 + \frac{P_i(j) \gamma_i(j)}{N_0 B_c} \right), \tag{10.25}$$

for $q_{s(t-1)-k} + 1 \leq j \leq t$. We also update $\mathcal{Q}_t = \mathcal{Q}_{t-1}$ after removing all q_n with $s(t-1) - k + 1 \leq n \leq s(t-1)$ from $\mathcal{Q}_{t-1}$, and $s(t) = s(t-1) - k$.

Since if the buffer is not full and the current water level is higher than previous one, Tx can send the part of current frame $F(t)$ in the previous time slots. And from Theorem 10.1, the optimal water levels $W(j)$ should be the same for $q_{s(t)} + 1 \leq j \leq t$. Since constraints in (10.10) are satisfied at time t and the Rx receives part of current frame $F(t)$ in previous time slots $q_{s(t-1)-k} + 1 \leq j \leq t - 1$, constraints in (10.12) are also satisfied at time t. However, the buffer might be full at time slot $q_{s(t-1)-k} + 1 \leq n \leq t - 1$. Therefore, we need to check the overflows from time slots (or equivalently frames) $q_{s(t)} + 1$ to $t - 1$. Initializing $n = q_{s(t)} + 1$, we iteratively check if the inequality

$$\sum_{j=1}^{n_1} H(j) - \sum_{j=1}^{n_1-1} F(j) + F_{\max} \leq 0 \tag{10.26}$$

is satisfied or not for any $n \leq n_1 \leq t$ until (10.12) is satisfied at time t. If it is satisfied for all $n \leq n_1 \leq t - 1$, we get the optimal water levels $W(j)$ and power levels $P_i(j)$ at time t. If not, we find the smallest n_1, set $f(n_1) = 1$ (n_1 is marked as the time that the buffer is full), and update the water levels $W(j) = W_{\text{cur1}}$ for $n \leq j \leq n_1$ and $W(j) = W_{\text{cur2}}$ for $n_1 < j \leq t$ by solving the

following equations:

$$\sum_{j=1}^{n_1-1} F(j) + F_{\max} - \sum_{j=1}^{n-1} H(j)$$

$$= \sum_{j=n}^{n_1} \sum_{i=1}^{M} \tau B_c \log \left(1 + \frac{\left[W_{\mathrm{cur}1} - \frac{N_0 B_c}{\gamma_i(j)} \right]^+ \gamma_i(j)}{N_0 B_c} \right), \tag{10.27}$$

$$- \sum_{j=1}^{n_1-1} F(j) - F_{\max} + \sum_{j=1}^{t} H(j)$$

$$= \sum_{j=n_1+1}^{t} \sum_{i=1}^{M} \tau B_c \log \left(1 + \frac{\left[W_{\mathrm{cur}2} - \frac{N_0 B_c}{\gamma_i(j)} \right]^+ \gamma_i(j)}{N_0 B_c} \right), \tag{10.28}$$

since the total bits received at Rx from times n to t is $\sum_{j=n}^{t} H(j)$. Then, the updated power levels and transmitted data in the corresponding time slots are expressed as follows:

$$P_i(j) = \left[W_{\mathrm{cur}} - \frac{N_0 B_c}{\gamma_i(j)} \right]^+, \tag{10.29}$$

$$H(j) = \sum_{i=1}^{M} \tau B_c \log \left(1 + \frac{P_i(j)\gamma_i(j)}{N_0 B_c} \right), \tag{10.30}$$

for $n \leq j \leq t$. We also update $\mathcal{Q}_t$ by adding n_1 into it, we also update $s(t) = s(t) + 1$ and $n = n_1 + 1$. Let $f(n_1) = 1$ denote that the buffer storage is full at time n_1.

Based on the above detailed descriptions and analysis, the optimal power control algorithm is given below in Algorithm 11.

Algorithm 11 Dynamic programming based power control algorithm that minimizes the average power consumption

Input: The knowledge of video frame sizes $F(t)$ and CSI $\gamma_i(t)$ for all $t = 1, 2, \ldots, T$.

　　Buffer size $F_{\max}$ at Rx.

Output: The optimal power allocation $\mathbf{P}^*$.

1: Initialization: Set $\mathcal{Q}_1 = \{q_{s(0)}\}$, $s(0) = 0$, $q_0 = 0$ and $W(0) = \infty$. $f(j) = 0$ for all $1 \le j \le T$.

2: **for** $t = 1 : T$ **do**

3: 　　Find the current water level $W(t) = W_{\text{cur}}$ by solving (10.22). Initializing the previous water level $W_{\text{pre}} = W(q_{s(t-1)} + 1)$. Set $k = 0$.

4: 　　**while** $W_{\text{cur}} > W_{\text{pre}}$ and $f(q_{s(t-1)-k}) \neq 1$ **do**

5: 　　　　Update the water levels $W(j) = W_{\text{cur}}$ for $q_{s(t-1)-k} + 1 \le j \le t$ by solving (10.23).

6: 　　　　Update corresponding power levels $P_i(j)$ and received amounts of data $H(j)$ for $q_{s(t-1)-k} + 1 \le j \le t$ by (10.24) and (10.25)

7: 　　　　Update $k = k + 1$ and $W_{\text{pre}} = W(q_{s(t-1)-k} + 1)$.

8: 　　**end while**

9: 　　Remove $q_{s(t-1)-j+1}$ from $\mathcal{Q}_{t-1}$ for all $1 \le j \le k$, and set $\mathcal{Q}_t = \mathcal{Q}_{t-1}$. Therefore, $s(t) = s(t-1) - k$.

10: 　　Initialize $n = q_{s(t)} + 1$, $n_1 = n$.

11: 　　**while** $n_1 \le t - 1$ **do**

12: 　　　　**if** $\sum_{j=1}^{n_1} H(j) - \sum_{j=1}^{n_1-1} F(j) + F_{\max} > 0$ **then**

13: 　　　　　　Update the water levels $W(j) = W_{\text{cur1}}$ for $n \le j \le n_1$ by solving (10.27) and $W(j) = W_{\text{cur2}}$ for $n_1 + 1 \le j \le t$ by solving (10.28).

14: 　　　　　　Update corresponding power levels $P_i(j)$ and received amount of data $H(j)$ for $n \le j \le t$ by (10.29) and (10.30).

15: 　　　　　　$f(n_1) = 1$, update $\mathcal{Q}_t$ by adding n_1 to it. Therefore, $s(t) = s(t) + 1$ and $q_{s(t)} = n_1$.

16: 　　　　　　Set $n = n_1 + 1$　　　　　　　182

17: 　　　　**end if**

18: 　　　　$n_1 = n_1 + 1$.

10.2.2 Minimizing the time duration of video streaming

In the second scenario, the goal is to minimize the duration of time used for transmitting the entire video sequence again under the constraints that Rx plays the received video without any interruption and missing frames, i.e., without any receiver buffer underflows and overflows. Therefore, the optimization problem can be expressed as following:

$$\min_{\mathbf{P}} T_1 \tag{P3}$$

$$\text{s.t.} \quad (10.10), (10.12)$$

$$\sum_{j=1}^{T_1} \sum_{i=1}^{M} C_i(j)\tau = \sum_{j=1}^{T} F(j), \tag{10.31}$$

where constraint (10.31) describes that Tx has sent all video data at time T_1, and the goal of Problem (**P3**) is to find the minimum T_1, which satisfies the constraints (10.10), (10.12) and (10.31). Intuitively, minimizing the time consumption implies that Tx transmits as much video content as possible in each time slot, and hence this minimization problem is equal to maximizing the throughput in each time slot t for $1 \leq t \leq T_1$ until Tx completes the video transmission assignment at time T_1. Also, since the video transmission can potentially be finished very quickly in the absence of any limitations on the transmission power, we impose a maximum power constraint $P_{\max}$ for transmission over M subchannels in each time slot in the optimization problem. The available buffer capacity in time slot t before sending data from the Tx is expressed as

$$A(t) = F_{\max} + \sum_{j=1}^{t-1} F(j) - \sum_{j=1}^{t-1} H(j), \quad t \geq 2,$$

$$A(1) = F_{\max}, \tag{10.32}$$

183

Thus, the optimization problem (**P3**) is modified as follows:

$$\max_{\mathbf{P}} \sum_{i=1}^{M} C_i(j) \tag{P4}$$

$$\text{s.t.} \ \sum_{i=1}^{M} P_i(j) \leq P_{\max}, \quad \forall j \geq 1, \tag{10.33}$$

$$\sum_{i=1}^{M} C_i(j)\tau \leq R(j) \tag{10.34}$$

where

$$R(j) = \min \left\{ A(j), \ \sum_{k=0}^{T} F(k) - \sum_{k=0}^{j-1} H(k) \right\} \tag{10.35}$$

is the minimum value between the available buffer capacity and the remaining video data to be sent in time slot j. Thus, (10.34) is the combination of overflow and total video data constraints. In other words, Tx cannot send an amount of data that is greater than the available buffer capacity or the remaining video bits. We can solve Problem (**P4**) in two steps:

- First, we ignore the constraint in (10.34). The objective function of Problem (**P4**) is an increasing convex function with respect to $\mathbf{P}$ and the constraint (10.33) is linear. Therefore, the optimization problem is a convex optimization problem and it has a unique maximizer. The Lagrangian function for this problem can be expressed as:

$$G(\phi) = \sum_{i=1}^{M} B_c \log \left(1 + \frac{P_i(j)\gamma_i(j)}{N_0 B_c} \right)$$
$$- \phi \left(\sum_{i=1}^{M} P_i(j) - P_{\max} \right) \tag{10.36}$$

Above, the Lagrange multiplier ϕ is associated with the constraint in (10.33).

184

The additional complimentary slackness condition is given as follows:

$$\phi\left(\sum_{i=1}^{M} P_i(j) - P_{\max}\right) = 0, \tag{10.37}$$

Take the first derivative of (10.36) with respect to $P_i(j)$, it can be expressed as:

$$\frac{\partial L(\phi)}{P_i(j)} = \frac{B_c}{\ln 2} \frac{\gamma_i(j)}{N_0 B_c + P_i(j)\gamma_i(j)}. \tag{10.38}$$

By applying the KKT optimality conditions to the Lagrangian function and letting $\frac{\partial L(\phi)}{P_i(j)} = 0$, the optimal power levels $P_i^*(j)$ can be expressed in terms of the Lagrange multiplier as follows:

$$P_i^*(j) = \left[\frac{B_c}{\phi \ln 2} - \frac{N_0 B_c}{\gamma_i(j)}\right]^+, \tag{10.39}$$

and ϕ is the constant obtained by solving the following equation:

$$\sum_{i=1}^{M} \left[\frac{B_c}{\phi \ln 2} - \frac{N_0 B_c}{\gamma_i(j)}\right]^+ = P_{\max}. \tag{10.40}$$

- Secondly, we calculate $C_i(j)$ by using the obtained $P_i^*(j)$ in (10.39). If the obtained power levels $P_i^*(j)$ satisfy the constraint (10.34), $P_i^*(j)$ is the optimal solution. Otherwise, the obtained power levels $P_i^*(j)$ result in buffer overflows. Therefore, the constant power is obtained by solving the following equation:

$$\sum_{i=1}^{M} B_c \log\left(1 + \frac{\left[\frac{B_c}{\phi \ln 2} - \frac{N_0 B_c}{\gamma_i(j)}\right]^+ \gamma_i(j)}{N_0 B_c}\right)\tau = R(j). \tag{10.41}$$

After obtaining the lagrange multiplier ϕ, the optimal power levels are calculated

185

as in (10.39). The actual throughput is

$$H(j) = \sum_{i=1}^{M} B_c \log \left(1 + \frac{P_i^*(j)\gamma_i(j)}{N_0 B_c} \right) \tau. \tag{10.42}$$

The detailed algorithm is shown below in Algorithm 12.

Algorithm 12 Power control algorithm for time minimization in video transmission

---

Input: The knowledge of video frame sizes $F(j)$ and CSI $\gamma_i(j)$ for all $j = 1, 2, \ldots, T$.

Buffer size $F_{\max}$ at Rx.

Output: The optimal power allocation $\mathbf{P}^*$ and transmission time T.

1: Initialization: Set $H(0) = 0$, $t = 0$.

2: **while** $\sum_{j=0}^{t} H(j) < \sum_{j=1}^{T} F(j)$ **do**

3:    Update $t = t + 1$.

4:    Obtain lagrange multiplier ϕ by solving (10.40). After that, optimal power levels $P_i^*(t)$ and throughput $\sum_{i=1}^{M} C_i(j)\tau$ are found.

5:    **if** $\sum_{i=1}^{M} C_i(t)\tau > R(t)$ **then**

6:       Obtain lagrange multiplier ϕ by solving (10.41). After that, optimal power levels $P_i^*(t)$ are found.

7:    **end if**

8:    The actual throughput is calculated using (10.42).

9: **end while**

10: The transmission time $T = t$.

10.3   Online Power Control Policies

In the optimal offline policy introduced in the previous subsection, Tx is assumed to have perfect noncausal CSI for the entire duration of video transmission, and the dynamic programming is employed for solving the optimization problem. In this section, we address online power control policies under the assumption that only

the current CSI is available at the Tx side and future values of channel fading are predicted.

10.3.1 The Gauss-Markov Channel and prediction

The channel is assumed to experience first order Gauss-Markov fading whose dynamics in the ith subchannel is described by [81]

$$h_i(j+1) = \alpha h_i(j) + n_i(j+1), \tag{10.43}$$

where $h_i(j)$ is the circularly symmetric complex Gaussian channel fading coefficient at time j with zero mean and variance σ_h^2. The channel power gain is again denoted as $\gamma_i(j) = |h_i(j)|$. $n_i(j)$ is the driving noise and $n_i(j) \sim \mathcal{CN}(0, (1-\alpha^2)\sigma_h^2)$ where $0 < \alpha < 1$ describes the channel correlation. We assume that even the channel correlation may not be perfectly known and the estimated channel correlation coefficient is denoted by $\hat{\alpha}$, and the predicted channel fading coefficient at time $j+1$ is $\hat{h}_i(j+1) = \hat{\alpha}h(j)$ for $0 < j < T$ by using minimum mean square error estimation. In another words, $\hat{h}_i(j+1) = \hat{\alpha}^j h(1)$ for $0 < j < T$. In a video sequence, the number of frames is very large, and $\hat{\alpha}^j$ becomes very small for a large value of j. Due to this, the transmitted video sequence is divided into several groups each with a small number of frames. It is assumed that the group of picture (GoP) size of the video is N_g frames and L GoPs are formed as a group for channel fading coefficient estimation.

10.3.2 Online power allocation strategy 1 - Grouped water filling (GWF)

Each group has $N_g L$ frames, and we assume that Tx knows only the current fading coefficient. For the current time j in group I, Tx predicts the future channel fading

187

$$\sum_{k=j}^{l} \sum_{i=1}^{M} C_i(j + (I-1)N_gL)\tau$$

$$\geq \max\left\{\sum_{k=1}^{l} F(k + (I-1)N_gL) - \sum_{k=1}^{j-1} H(k + (I-1)N_gL), 0\right\}, \forall l = j, \ldots, N_gL - 1,$$

$$(10.45)$$

$$\sum_{k=j}^{N_gL} \sum_{i=1}^{M} C_i(j + (I-1)N_gL)\tau$$

$$= \max\left\{\sum_{k=1}^{N_gL} F(k + (I-1)N_gL) - \sum_{k=1}^{j-1} H(k + (I-1)N_gL), 0\right\}, \quad (10.46)$$

$$\sum_{k=j}^{l} \sum_{i=1}^{M} C_i(j + (I-1)N_gL)\tau$$

$$\leq \max\left\{\sum_{k=1}^{l-1} F(k + (I-1)N_gL) - \sum_{k=1}^{j-1} H(k + (I-1)N_gL), 0\right\} + F_{\max}, \forall l = j, \ldots, N_gL,$$

$$(10.47)$$

coefficients as

$$\hat{h}_i(k + j + (I-1)N_gL)$$

$$= \hat{\alpha}^k h(j + (I-1)N_gL), 0 < k \leq N_gL - j. \quad (10.44)$$

The power levels $P_i^*(j + (I-1)N_gL)$ and corresponding received amount of data $H(j + (I-1)N_gL)$ at current time j are obtained by using Algorithm 11 based on the above estimated channel fading coefficients. Following this, we move to the next frame time $j + 1$ and the Tx obtains the perfect knowledge of the current channel fading coefficient and predicts the future channel fading coefficients accordingly. Similarly as in the previous frame time j, power levels at time $j + 1$ are obtained and the procedure moves to the next frame time until the power levels are obtained for the entire group. In this online algorithm, the constraints (10.45) – (10.47) given on the next page are updated over time.

The detailed algorithm is described in Algorithm 13 below:

Algorithm 13 Power minimization for video transmission in online fading channel

---

Input: The knowledge of video frame sizes $F(j)$ and estimated channel correlation coefficient $\hat{\alpha}$. Buffer size $F_{\max}$ at Rx. GoP size N_g and number of GoPs, L in each group. It is assumed that $\frac{T}{N_g L}$ is an integer.

Output: The optimal power allocation $\mathbf{P}^*$.

1: **for** $I = 1 : \frac{T}{N_g L}$ **do**

2: **for** $j = 1 : N_g L$ **do**

3:    Predict channel fading coefficients $\hat{h}_i(k + (I-1)N_g L)$ by using (10.44) for $j < k \leq N_g L$ after perfectly learning the channel fading coefficient $h_i(j + (I-1)N_g L)$ at Tx.

4:    Obtain the optimal power level $P_i^*(j + (I-1)N_g L)$ by employing Algorithm 11 based on above predicted channel fading coefficients and calculate received amount of data $H(j + (I-1)N_g L)$.

5:    Update the constraints (10.45), (10.46) and (10.47) for calculation in the next time slot.

6: **end for**

7: **end for**

10.3.3 Online power allocation strategy 2 - Reinforcement Learning

In this section, the VBR video streaming over a point-to-point link under overflow and underflow constraints is modeled as a Markov decision process (MDP), which provides a suitable mathematical framework for sequential decision making. Following the MDP formulation, we propose an reinforcement learning (RL) algorithm similar as in [82].

As mentioned above, in time slot t, Tx has only causal knowledge about its state.

Consequently, since the duration of one time slot, τ is fixed and known, the selection of $P(t)$ depends solely on the values of the current state, frame size, and current channel fading coefficient at time t. Since the selection of $P(t)$ depends only on the current state of the system, the system can be modeled as an MDP. An MDP consists of a set of states $\mathcal{S}$, a set of actions $\mathcal{A}$, a transition model $\mathcal{P}$ and a set of rewards $\mathcal{R}$. At time t, the corresponding state $S_t \in \mathcal{S}$ is a function of stored data $D(t-1)$ and current channel fading coefficient $h_i(t)$. In our model, the set $\mathcal{S}$, contains infinite number of possible states (amount of stored data in the buffer) since the channel coefficients can take any value in a continuous range. The set of actions $\mathcal{A}$ corresponds to the values of transmit power that can be selected. $\mathcal{A}$ is finite and it is given by $\mathcal{A} = \{P(t), P(t) \in 0 : \delta : P_{\max}\}$ in our model, where δ is the step size. The action dependent transition model defines the transition probabilities denoted as $\mathbb{P}[S_{t+1} \in \mathcal{U}|S_t, P(t)]$, where $\mathcal{U}$ is a measurable subset of $\mathcal{S}$. Finally, the rewards indicate how beneficial the selected $P(t)$ is for the corresponding S_t. For each S_t and $P(t)$, we define the reward $R(t) \in \mathcal{R}$ as follows:

$$R(t) = 1 - \frac{P(t)}{P_{\max}}. \tag{10.48}$$

$R(t)$ can be calculated at the Tx with the knowledge of $h_i(t)$ and the selected total power $P(t)$. Since Tx only has information of its state at time t, it is preferred to achieve a higher reward at the current t over future ones and the goal is to achieve the highest reward during the entire process. Taking into account this preference, $0 \le \gamma \le 1$ is defined as the discount factor of future rewards. The goal is to select $P(t), \forall t$, in order to maximize the expected reward given by

$$R = \lim_{T \to \infty} \mathbb{E}\left[\sum_{t=1}^{T} \gamma^t R(t)\right]. \tag{10.49}$$

A policy π is defined as a mapping from a given state S_t to the $P(t)$. i.e., $P(t) =$

190

$\pi(S_t)$. The value functions are defined to measure how good a policy π is from S_t onward. These functions can depend solely on the states, called state-value functions or on the state-action pairs, called action-value functions based on different model or application[82]. The state-value function V^π is the expected reward given that Tx follows the policy π from state S_t onwards and the action-value function Q^π is the expected reward starting from the state S_t, selecting the action $P(t)$ and following policy π thereafter [83]. Following the formulation in [82], the action-value function is written as

$$Q^\pi(S_t, P(t)) = \mathbb{E}\left\{\sum_{k=0}^{\infty} \gamma^k R(t+k+1) \middle| S_t, P(t)\right\}. \qquad (10.50)$$

The optimal policy π^* is the policy whose state-value function is greater than or equal to any other policy for every state. The corresponding action-value function for the optimal policy π^* is denoted by Q^*. Since the value functions can be written in a recursive manner in what is known as the Bellman equations [82], this recursive representation facilitates the design of RL algorithms [83]. The general form of this Bellman optimality equation for the action-value function is given in [82] as

$$Q^*(S_t, P(t)) =$$
$$\sum_{S_{t+1} \in \mathcal{S}} f_{S_t,S_{t+1}}^{P(t)} \left[R(t) + \gamma \max_{P(t+1) \in \mathcal{A}} Q^*\left(S_{t+1}, P(t+1)\right)\right], \qquad (10.51)$$

where $f_{S_t,S_{t+1}}^{P(t)}$ is the transition probability from S_t to S_{t+1} with the corresponding action $P(t)$.

An on-policy temporal difference RL algorithm, termed State-Action-Reward-State-Action (SARSA), is employed in this thesis. Since the number of states is infinite, we use a set of binary functions and linear function approximation to approximate $Q^\pi(S_t, P(t))$. The following steps are considered for the implementation of the SARSA RL algorithm. First, the estimation and update of $Q^\pi(S_t, P(t))$ is presented. Secondly, the policy for the selection of $P(t)$ according to the estimated

$Q^\pi(S_t, P(t))$ is defined. Thirdly, the linear function approximation for the computation of $Q^\pi(S_t, P(t))$ is applied. Then, the set of binary functions which are used in linear function approximation are linearly combined, and finally, the resulting SARSA algorithm is presented.

10.3.3.1 ϵ-greedy policy

When the number of states is finite, acting greedily with respect to $Q^\pi(S_t, P(t))$ leads to the optimal policy [82]. This is because of that $Q^\pi(S_t, P(t))$ is the expected reward given the state-action pair $(S_t, P(t))$ and the action $P(t)$ that maximizes $Q^\pi(S_t, P(t))$ leads to the highest expected reward. However, it has no opportunity to explore transmit power values that can potentially lead to higher rewards if Tx always acts greedily. In order to solve this problem, the ϵ-greedy policy is considered instead:

$$\Pr\left[P(t) = \max_{p \in \mathcal{A}} Q^\pi(S_t, p)\right] = 1 - \epsilon, 0 < \epsilon < 1. \tag{10.52}$$

In another words, with probability ϵ, Tx selects a transmit power value from the action set $\mathcal{A}$ randomly. Since the chosen action $P(t)$ may lead to buffer overflow or underflow, we can precalculate $P_{\min}(t)$ and $P_{\max}(t)$, which denote the minimum and maximum transmission power levels that satisfy buffer overflow and underflow constraints by letting $P_{\min}(t) \leq P(t) \leq \min\{P_{\max}(t), P_{\max}\}$. If $P_{\min}(t) > P_{\max}$, the underflow occurs and cannot be avoided and we let $P(t) = P_{\max}$. However, we can always choose a lower power level to avoid the occurrence of an overflow.

10.3.3.2 Linear function approximation

We employ the on-policy SARSA algorithm in this thesis due to its favorable convergence properties when linear function approximation is used [82]. In SARSA, the next state-action pair $(S_{t+1}, P(t+1))$ is obtained from the current state-action pair

$(S_t, P(t))$ with a given policy π, and $Q^\pi(S_t, P(t))$ is estimated from this transition process. When the system is in state S_t, Tx selects $P(t)$ following policy π. After that, it obtains a reward $R(t)$ and moves to state S_{t+1}. According to the current values of $Q^\pi(S_t, P(t))$ and the policy π, the next action $P(t+1)$ is selected. After that, action value $Q^\pi(S_t, P(t))$ is updated using the previous experience and the current value. The updating rule in the SARSA algorithm is given as follows:

$$Q^\pi(S_t, P(t)) \leftarrow$$
$$Q^\pi(S_t, P(t))(1 - \beta_t) + \beta_t[R(t) + \gamma Q^\pi(S_{t+1}, P(t+1))], \qquad (10.53)$$

where β_t is a small positive fraction which influences the learning rate.

In order to handle the infinite number of states, the concept of linear function approximation is considered [83]. With linear function approximation, $Q^\pi(S_t, P(t))$ is represented by a linear combination of K feature functions $f_k(S_t, P(t))$, $k = 1, 2, \ldots, K$. Each $f_k(S_t, P(t))$ maps the state-action pair $(S_t, P(t))$ into a feature value. Let $\mathbf{f} \in \mathbb{R}^K$ be a vector containing the feature values for a given state-action pair and let $\mathbf{w} \in \mathbb{R}^K$ be the vector containing the corresponding weights indicating the contribution of each feature to the value. Therefore, the action-value function approximation is given as [82]

$$\hat{Q}^\pi(S_t, P(t), \mathbf{w}) = \mathbf{f}^\mathrm{T}\mathbf{w}. \qquad (10.54)$$

In approximate SARSA, the action-value updates are performed on the weights instead of in (10.53). At time t, the vector $\mathbf{w}$ is updated in the direction that reduces the error between $Q^\pi(S_t, P(t))$ and $\hat{Q}^\pi(S_t, P(t), \mathbf{w})$ following the gradient descent

approach. The update rule is expressed as

$$\mathbf{w} = \mathbf{w} + \alpha_t \left[R(t) + \gamma \hat{Q}^\pi \left(S_{t+1}, P(t+1), \mathbf{w} \right) \right.$$

$$\left. - \hat{Q}^\pi \left(S_t, P(t), \mathbf{w} \right) \right] \nabla_\mathbf{w} \hat{Q}^\pi (S_t, P(t), \mathbf{w}), \qquad (10.55)$$

where $\nabla_\mathbf{w} \hat{Q}^\pi (S_t, P(t), \mathbf{w})$ is the gradient of $\hat{Q}^\pi (S_t, P(t), \mathbf{w})$ with respect to $\mathbf{w}$, and

$$\nabla_\mathbf{w} \hat{Q}^\pi (S_t, P(t), \mathbf{w}) = \mathbf{f}. \qquad (10.56)$$

10.3.3.3   Feature functions

The definition of the feature functions is an important step in the implementation of the approximate SARSA algorithm. The features should provide a good model of the effect of possible transmit power values on the state. In our scenario, the most important characteristics are the capacity of the playout buffer and the minimum required video data to be played at Rx. $K = 3$ binary functions are used by taking into consideration playout buffer size and the power allocation problem.

Since overflows are undesirable, the first feature function $f_1(S_t, P(t))$ indicates if a given $P(t)$ avoids the overflow of the data in the playout buffer at Rx. Additionally, it evaluates if the given action $P(t)$ fulfills the constraints in (10.2). The function is assigned value "1" if no overflow is caused, and is "0" otherwise. Now, the corresponding feature function is written as

$$f_1(S_t, P(t)) = \begin{cases} 1, & D(t) \leq F_{\max} \\ 0, & \text{otherwise} \end{cases} \qquad (10.57)$$

The second feature considers the underflow event. Since Rx needs to play the tth frame at time t, the amount of stored date in the ployout buffer at time t should be

194

no less than the tth frame size in order to avoid an underflow. The second feature function is assigned value "1" if no underflow occurs and the corresponding feature function is formulated as

$$f_2(S_t, P(t)) = \begin{cases} 1, & D(t) \geq F(t) \\ 0, & \text{otherwise.} \end{cases} \tag{10.58}$$

The third feature function $f_3(S_t, P(t))$ addresses the power allocation problem. We have determined in the offline case that a directional water-filling algorithm can be used to optimally allocate the power. However, the knowledge of future channel coefficients is unavailable in the online scenario. Therefore, we propose to use past channel realizations to estimate the mean value of the distribution of the channel gain and to perform water-filling considering the estimated mean value of the channel gain and the current channel realization. For the estimation, the sample mean estimator is used and the estimated mean value $|\hat{h}_i(t)|^2$ is calculated as

$$|\hat{h}_i(t)|^2 = \frac{1}{t} \sum_{j=1}^{t} |h_i(t)|^2. \tag{10.59}$$

The reason for applying water-filling between $|\hat{h}_i(t)|^2$ and $|h_i(t)|^2$ is that we are assuming that $|\hat{h}_i(t)|^2$ approximates the state of the channel in the subsequent time slot and consequently, the amount of data required has to be considered. And the value of this amount is

$$D_n(t) = \max\{0, F(t) + F(t+1) - D(t)\}. \tag{10.60}$$

195

The water level $v(t)$ is the solution for

$$\sum_{i=1}^{M} \left[\log_2 \left\{ 1 + [v(t) - \frac{N_0 Bc}{|h_i(t)|^2}]^+ \frac{|h_i(t)|^2}{N_0 B_c} \right\} \right.$$
$$\left. + \log_2 \left\{ 1 + [v(t) - \frac{N_0 Bc}{|\hat{h}_i(t)|^2}]^+ \frac{|\hat{h}_i(t)|^2}{N_0 B_c} \right\} \right] = \frac{D_n(t)}{\tau B_c}, \tag{10.61}$$

where $[x]^+$ is the maximum value between x and 0.

The power allocated to i^{th} subchannel and the and total power values are given by

$$p_{i,\text{WF}}(t) = \max \left\{ 0, v(t) - \frac{N_0 Bc}{|h_i(t)|^2} \right\}, \tag{10.62}$$

$$p_{\text{WF}}(t) = \sum_{i=1}^{M} p_{i,\text{WF}}(t), \tag{10.63}$$

respectively. Since power levels are assumed to have discrete values, the calculated $p_{\text{WF}}(t)$ has to be rounded such that $p_{\text{WF}}(t) \in \mathcal{A}$ holds. $f_3(S_t, P(t))$ is now expressed as

$$f_3(S_t, P(t)) = \begin{cases} 1, & \delta \lfloor \frac{p_{\text{WF}}(t)}{\delta} \rfloor = P(t) \\ 0, & \text{otherwise} \end{cases} \tag{10.64}$$

where δ is the step size and $\lfloor x \rfloor$ is the rounding operation to the nearest integer less than or equal to x.

10.3.3.4 Approximate SARSA

The detailed approximate SARSA algorithm for power control in VBR video wireless transmission system is shown in Algorithm 14. It has been shown in [84] that if β_t satisfies $\sum_t \beta_t = \infty$ and $\sum_t \beta_t^2 < \infty$ and the policy is not changed during the learning process, the approximate SARSA algorithm converges to a bounded region with probability one. $\beta_t = \frac{1}{t}$ is assumed in our scenario.

Algorithm 14 Approximate SARSA for power control

Input: The knowledge of video frame sizes $F(t)$ and current CSI $h_i(t)$. Buffer size

    $F_{\max}$ at Rx.

Output: The optimal power allocation $\mathbf{P}^*$.

  1: Initialization: Initialize γ, β_1, ϵ and $\mathbf{w}$.

  2: Observe S_t

  3: Select $P(t)$ using ϵ-greedy

  4: **for** $t = 1 : T$ **do**

  5:    Transmit using the selected power $P(t)$.

  6:    Calculate corresponding reward $R(t)$ by using (10.48).

  7:    Observe next state S_{t+1}

  8:    Select next transmit power $P(t+1)$ using ϵ-greedy

  9:    Update $\mathbf{w}$ by using (10.55).

10: **end for**

10.4   Experiment Results

To evaluate the performance of the proposed power control and video transmission strategies in the simulations, we have used VBR video traces *Tokyo Olympics*, *NBC News* and *Terminator* in all the simulations from the Video Trace Library hosted at Arizona State University [66]. The video rate in frames per second (FPS) is 30 f/s. The playout buffer size is set to be 1.5 times the largest frame size among the frames to be transmitted. $P_{\max}$ in time minimization (TM) scheme is set to the maximum power level allocated among all frame time slots in the power minimization (PM) scheme.

We further assume that the bandwidth of each subchannel is $B_c = 10$ kHz and the number of subchannels is set to $M = 100$. Therefore the total bandwidth for the

system is 1 MHz.

10.4.1   Offline power control

In the offline power strategy, we assume Rayleigh fading channels in the simulations, for which the normalized path gain is exponentially distributed with probability density function $f(\gamma_i) = \exp\{\frac{-\gamma_i}{G_i}\}/G_i$ where path gain averages are $G_i = 2$ for subchannels, where $i \in \{1, 2, \ldots, M\}$.

Fig. 10.2 shows the consumption curves of the buffer at Rx from frame-time slot 1 to 20000. The cumulative overflow, transmission, and consumption curves for TM and PM schemes are plotted when transmitting *Tokyo Olympics*. The higher slope of the underflow curve means that frame sizes during that time period are larger. PM scheme completes video transmission mission at the end of frame time slot 20000 while TM scheme finishes it at frame time slot 19988. This saving in time depends on the buffer size and the maximum transmission power. When the transmission power is large enough, larger buffer size leads to more saving in time. In Fig. 10.3, we observe that both cumulative consumption curves obtained by considering PM and TM schemes are in between the underflow curve and the overflow curve, implying that Rx plays the video smoothly without any interruptions or missing frames. The consumption curve of TM scheme is always above that of PM due to the fact that TM scheme attempts to send as much data as possible in each frame time slot during the entire video transmission session, and consumption curve of TM reaches the overflow curve in most of frame time slots. In Fig. 10.3a, consumption curve of PM reaches the overflow curve at frame time 280 and then decreases to the underflow curve at frame time 430. The reason is that, the frame sizes after frame time 430 are small enough, which leads the buffer to store enough frames for playing. Parts of further future frames are not needed to be stored in order to save power. However, In Fig. 10.3b, consumption curve of PM reaches the underflow curve at frame time 11610
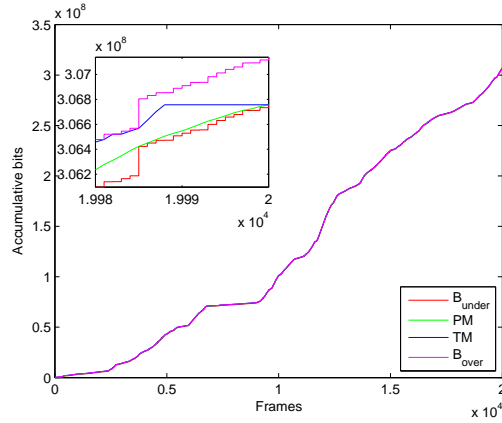
Figure 10.2: Cumulative transmitted data in 2 different schemes
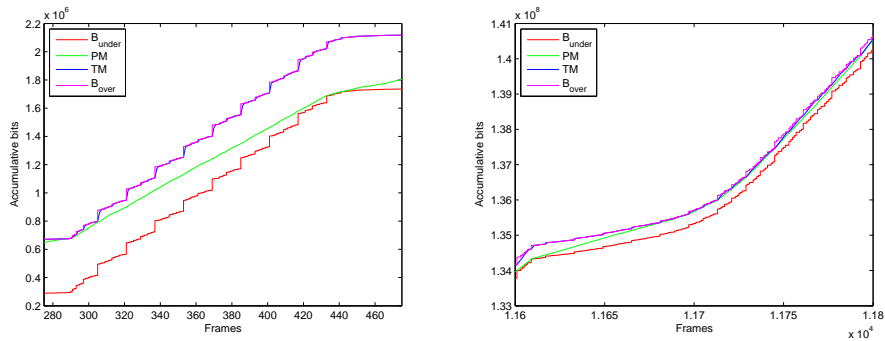
(a) Curves between frame time slot 275 and 475

(b) Curves between frame time slot 11600 and 11800

Figure 10.3: The cumulative overflow, transmission, and consumption curves when transmitting *Tokyo* in two different time periods (a) frame time slot 275-475; (b) frame time slot 11600-11800.

and then increases to the overflow curve at frame time 11680 because the frame sizes after frame time 11680 are very large and the buffer has to store enough frames for playing the video without any interruption and lowering the power consumed after frame time 11680.

Fig. 10.4 displays the consumed power in each frame time slot during the entire video transmission in PM and TM schemes. Fig. 10.4a demonstrates that power levels around time slot 12000 are the highest since the slope around that time is the largest as seen in Fig. 10.2, meaning that the frame sizes around that time slot are the largest and Tx needs much more energy for completing the transmission of such
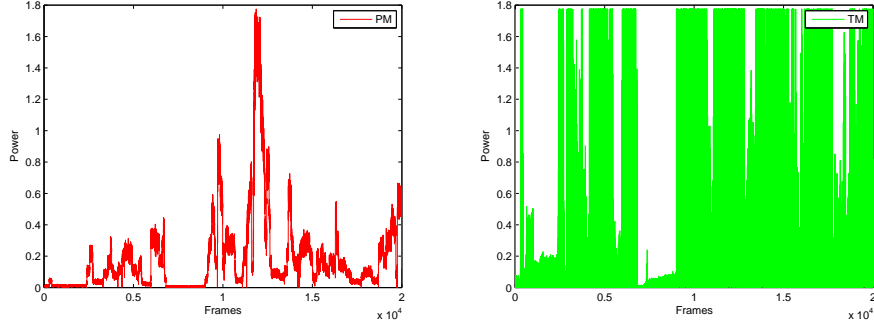
(a) Power consumption in the PM (b) Power consumption in the TM
scheme   scheme

Figure 10.4: The power consumption when transmitting *Tokyo* in two different schemes (a) power minimization (PM); (b) time minimization (TM).

large-sized frames. There also exists several peaks, which are located at time slots with larger frame sizes compared to other time slots. Fig. 10.4b shows that the peak transmission power level in the TM scheme around 1.8 Watts and Tx transmits frames by using P_{max} most of the time because the buffer at Rx tries to store as much data as possible in each time slot without violating the buffer overflow and maximum transmission power constraints. And the buffer is full after receiving data from Tx if the transmission power level is less than P_{max} in this time slot, otherwise, the buffer can store more data by using higher power level. The average power levels are 0.1827 and 0.2635 Watts in PM scheme and TM scheme, respectively.

Table 10.1 shows the power consumptions for transmitting different video sequences. The number of frames is 20000 for all video sequences. The power is in the units of Watts. We notice that PM scheme saves much power while TM scheme saves a small number of time slots in video transmission. If the buffer size is larger, the saving in time can be more.

Changing buffer size F_{max} also affects the power consumption at Tx. Fig. 10.5 shows the relation between buffer size at Rx and average power level at Tx. The average power level at Tx decreases as the buffer size at Rx increases since Rx can store more data before it is played, and the instantaneous powers can be adjusted

200

Table 10.1: Power consumption for different video sequences

	$P_{\max}$	PM	TM	Time saving (slots)
Tokyo Olympics	1.7745	0.1827	0.2635	12
NBC News	4.4814	0.6382	1.0240	10
Terminator	4.3549	0.2939	0.5670	13
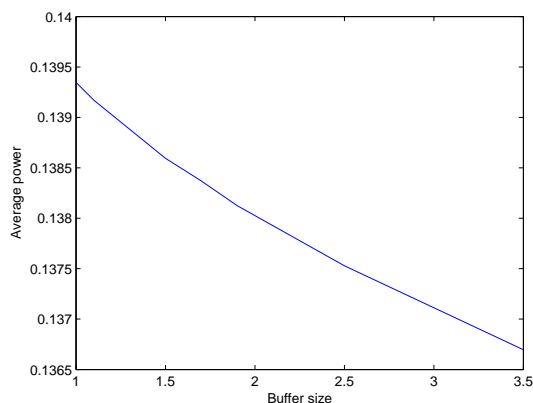
Figure 10.5: The relation between buffer size at Rx and average power level at Tx

more efficiently. If the buffer size increases from 1.5 to 2.5 times the largest frame size, the average power level drops from 0.1386 W to 0.1375 W. Note that even small power saving can translate into substantial savings in energy especially if the video sequence is long since average energy will be average power times the duration of the video.

10.4.2 Online power control

In online transmission strategy, we assume Gauss-Markov Rayleigh fading channels in the simulations, where $h_i(j) \sim \mathcal{CN}(0, 5.093)$. Thus, the path gain with average $G_i = 2$ for subchannels, where $i \in \{1, 2, \ldots, M\}$. VBR video trace *Tokyo Olympics* is used in simulations. GoP is $N_g = 16$ frames and channel correlation coefficient is $\alpha = 0.99$.

Fig. 10.6 demonstrates the relation between average power level and estimated channel correlation coefficient $\hat{\alpha}$ value with group size, $L = 4$. We observe that Tx
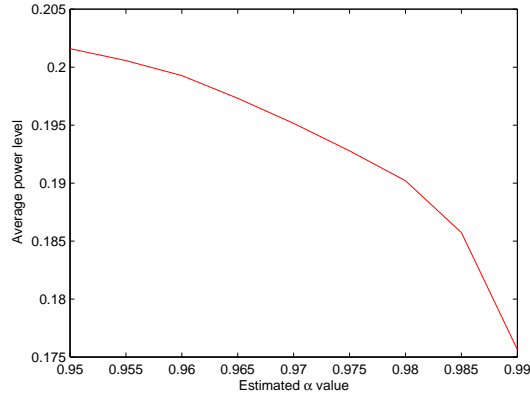
Figure 10.6: Average power level with different $\hat{\alpha}$ values

sends video sequence with lower average power level if $\hat{\alpha}$ has higher value. (10.44) indicates that smaller $\hat{\alpha}$ leads to larger channel fading coefficient difference between two time slots and $\hat{h}_i(j)$ is lower than the case with high $\hat{\alpha}$ value. Thus, the first several time slots in a group need to send more data by using higher power level in the case of small $\hat{\alpha}$ value compared to the case of large $\hat{\alpha}$ value. In another words, the frames in one group are sent just within first few number of slots when the value of $\hat{\alpha}$ is small, and are sent using all the available frame time slots when $\hat{\alpha}$ has a larger value. Note also that, the estimation quality improves when $\hat{\alpha}$ increases from 0.95 to 0.99 with step size 0.05. Therefore, Tx sends video sequences with higher average power level if $\hat{\alpha}$ has a smaller value.

Fig. 10.7 demonstrates the relation between average power level and group size L (L GoPs) considering offline and online power control strategies. Fig. 10.7a demonstrates that the average transmission power gets smaller when group size L increases in the case of offline power control, because the system minimizes power consumption in each individual group. In another words, the number of groups is larger if the group size L is smaller. Thus, the power minimization strategy is implemented as a unit to more number of frames if the group size is larger. This further leads to lower power level. However, in online power control, average transmission power initially decreases and then starts getting larger as the group size L grows further as shown

202

(a) Average power level with offline power control

(b) Average power level with online power control
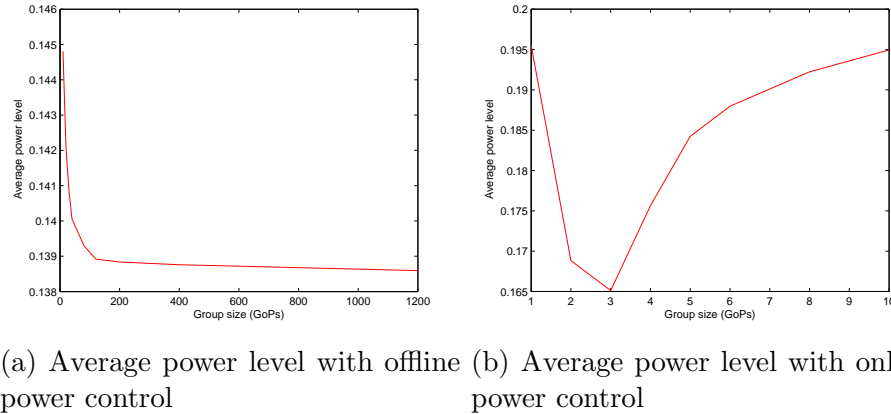
Figure 10.7: The average power level when transmitting *Tokyo* in (a) offline; (b) online strategies with different group sizes.

in Fig. 10.7b. At first, the communication system consumes more power if the group size is small since the online strategy is implemented in each individual group with small number of frames. Theoretically, if the strategy is implemented in a group with larger number of frames, the average power is lower. However, as discussed in the case of varying $\hat{\alpha}$ values, the larger group size leads to smaller channel coefficients among the latter frame time slots in each group. Thus, the entire group of frames need to be sent in the first few frame time slots and the system consumes more power. Therefore, the average power level eventually starts increasing when the group size L grows beyond a threshold.

Next, we address the performance achieved with the SARSA algorithm. VBR video trace *Terminator* is used in simulations. GoP is $N_g = 16$ frames, $L = 4$ and channel correlation coefficient α varies. For each α value, we generate the channel side information 10 times, and for each set of channel side information, we run the algorithm 10 times. Therefore, for each α value, we run the code 100 times.

Fig. 10.8 shows the maximum transmit power levels used in the GWF algorithm in order to avoid underflow and overflows. Note that since channel correlation varies, the maximum transmit power levels changes depending on α values.

Fig. 10.9 plots the average transmit power levels for different α values attained

203
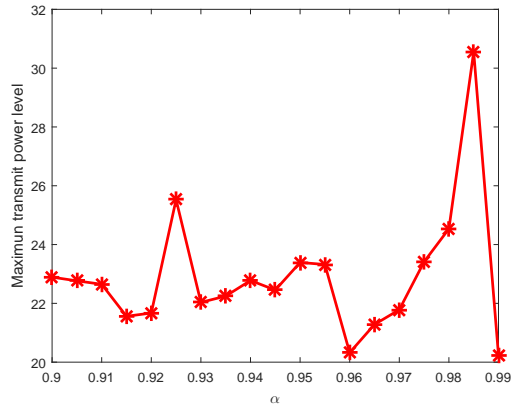
Figure 10.8: Maximum transmit power levels in GWF method
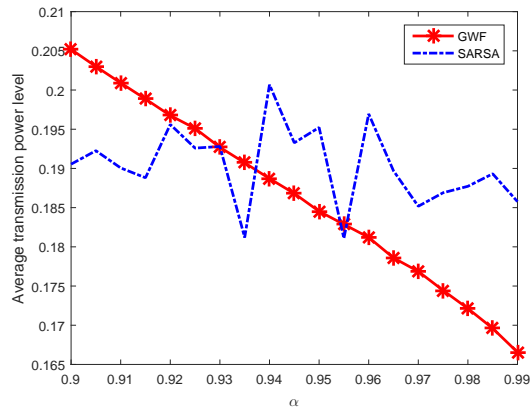
Figure 10.9: Transmit power levels for different α values

204
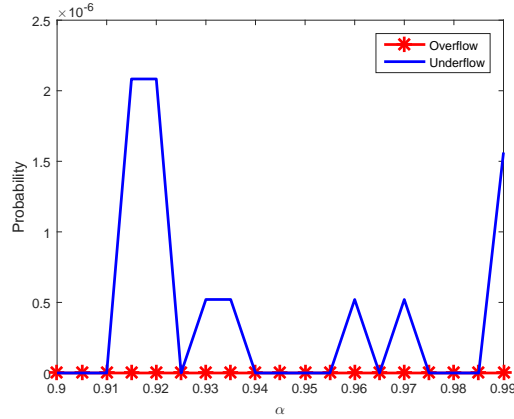
Figure 10.10: Underflow probability and overflow probability for different α values

with both GWF and reinforcement learning SARSA strategies. We see that if the channels are more correlated, meaning that the value of α is larger and the future channel side information can be estimated more accurately, the average transmit power level is lower. We also observe that, with SARSA strategy, the average power levels fluctuate but within a certain small range. Note that SARSA scheme estimates the channel side information just in the next time slot. Fig. 10.9 also shows that the transmit power attained with the GWF strategy is higher than that achieved with the SARSA strategy when α is smaller than a certain value, because small α value leads to a large channel estimated error that propagates over the entire group of frames used in the GWF strategy. SARSA strategy just estimates the channel in the next time slot, thus the error is smaller than in the GWF strategy. However, if channel is highly correlated (implying a high α value), the GWF strategy is close to the optimal solution in each group of frames. Therefore, GWF strategy consumes less power than SARSA strategy.

Fig. 10.10 presents the underflow probability and overflow probability for different α values in SARSA strategy. Since the GWF is the approach to find the optimal power with predicted channel information while avoiding underflows and overflows, the underflow and overflow probabilities are 0. In SARSA strategy, the overflow

probability is 0 as we noted in the discussion of the ϵ-greedy policy. On the other hand, if the channel is too bad, and the maximum transmit power $P_{\max}$ cannot support the minimum amount of video data to be sent to the Rx, underflow event happens. However, the underflow probability is very small as shown in Fig. 10.10.

Chapter 11

Conclusion

11.1 Summary

In this thesis, we have studied multimedia wireless transmission in different wireless networks by taking into consideration of BER, QoS constrained EC, EE or buffer size limitation at receiver. The contributions of this thesis are summarized below.

In Chapter 3, we have studied the performance of multimedia transmissions with HQAM in CR systems in the presence of imperfect sensing results and constraints on both the transmit and interference power levels. By exploiting the unequal importance of the compressed data bits, we have provided more protection to high priority bits of JPEG2000 coded image and H.264/MPEG-4 coded video by employing 16-HQAM. We have obtained closed-form expressions for the error probabilities of HP and LP bits in HQAM over Nakagami-m fading channels under sensing uncertainty. We have determined the optimal power levels that minimize the total average error probability or its upper bound under peak power and average interference constraints by assuming the availability of instantaneous CSI or statistical CSI. Via simulations, we have analyzed the impact of channel sensing performance, modulation parameter α_i, and severity of the fading on the received data quality. Simulation results

demonstrate that HQAM performs better than conventional QAM in terms of average PSNR. In addition, power control with instantaneous CSI outperforms power allocation with statistical CSI. We have shown that received data quality is robust to imperfect channel sensing results if there is no upper bound on the number of retransmissions. In these cases, the number of retransmissions increases with decreasing P_{d} or increasing P_{f}, resulting in larger delays and energy consumption. If there is a constraint on the number of retransmissions, PSNR performance of multimedia transmission is affected by sensing errors. We have observed that improved sensing performance leads to better quality at reception. Less severe fading (i.e., larger m) is also shown to improve the received multimedia data quality.

In Chapter 4, we have derived optimal power policies which minimize the weighted sum of upper bound on BER of HP bits and LP bits under the constraints on both the transmit and interference power levels among 3 different modes in D2D cellular wireless networks. MRC is employed since different number of subchannels are used in different modes and MRC achieves the highest SNR, leading to lowest BER. Through simulations, we have analyzed the BERs of all 3 modes and performed mode selection to achieve the lowest PSNR at each DT location. Comparisons of the performances with power control and constant power have been carried out in terms of PSNR and BER. Simulation results show that power control strategy results in lower BERs and higher PSNRs.

In Chapter 5, we have studied the mode selection and resource allocation in an D2D underlaid cellular network with a pair of cellular users and a pair of D2D users operating under QoS and EE constraints. Initially, the throughput is formulated by using effective capacity formulation, and the logarithmic PSNR-rate model is selected for quantifying the received video quality for different transmission rates. Efficient algorithms for maximizing the quality of the received video at D_2 under minimum quality requirement Q_c at the cellular user and EE constraint on the D2D link are

proposed. Optimal mode selection among four possible modes, namely the cellular mode, the dedicated mode, the uplink reuse mode and the downlink reuse mode is executed with the proposed algorithms. The influence of the positions of D_1 and D_2 are analyzed via numerical results.

In Chapter 6, we have addressed the maximization of the weighted sum quality of received video sequences under maximum transmission power constraints at both users U_1 and U_2 in a full-duplex multiple-subchannel wireless communication scenario. LTPRS model is employed as the full-duplex model in this thesis and the self-interference is measured by multiplying a self-interference suppression factor with the transmission power. Due to the nonconvexity of the optimization problem, MO is employed to determine the optimal power allocation. Results show that larger value of the QoS exponent θ leads to lower PSNR levels, because the more stringent the delay constraints, the smaller the supported video arrival rate becomes. The user with larger ω value will consume more and more resources since it has higher importance, which futher leads to higher and higher PSNR values for the reconstructed video. Three different strategies of transmission are proposed and OPA has the best performance compared to EPA and SUO, and the difference is small if two transmitted video sequences are equally weighted. However, the performance difference is large when the differences among the weights of the transmitted videos are large.

In Chapter 7, we have addressed the maximization of the weighted sum quality of received video sequences under total bandwidth, minimum video quality, maximum transmission power, and delay QoS constraints in a full-duplex wireless model. LT-PRS model is employed as the full-duplex model and the self-interference is measured by multiplying a self-interference factor with the transmission power. We have reformulated the original nonconvex optimization problem as a monotonic optimization problem, and developed algorithms to determine the optimal bandwidth and power allocation levels in an efficient manner using this framework.

We have gleaned several practical insights from our analysis. We have shown analytically that at least one of the transmission powers of the full-duplex user pair should be at its peak level in order to maximize the performance and minimize the bandwidth requirements. We have also noted that larger values of the QoS exponent θ lead to lower PSNR levels since more stringent delay constraints result in smaller video rates, lowering the quality. We have demonstrated that the user with a larger θ is allocated smaller transmission power and bandwidth. We have seen that video quality parameters have influence on optimal resource allocation policies, e.g., if the video quality increases faster with increased source rate (i.e., $a_{i,k}$ is larger for a video sequence), transmission power is higher. We have also shown that optimal bandwidth and power allocation has better performance than the equal bandwidth and optimal power (EBOP) allocation scheme, and the performance gap widens as the weight differences among the transmitted videos grow.

In Chapter 8, we have addressed the maximization of the sum quality of received video sequences under total bandwidth and EE constraints and delay QoS requirements in a downlink wireless model. In particular, we have studied sum-quality maximizing bandwidth allocation and power allocation/power control policies. Optimal strategies for determining the transmission power levels for each user are identified based on the allocated bandwidth and the given EE constraint. The quality of the received video is shown to be an increasing concave function of the bandwidth. With these characterizations, we have simplified the optimization problem as a bandwidth allocation problem and have shown it to be a convex optimization problem. The simulation results reveal that increasing the QoS exponent θ leads to a decrease in quality. Additionally, increasing the EE threshold η decreases the performance. Overall, we have considered five different strategies of bandwidth allocation and power allocation/power control, and we have demonstrated that the JBAPC has the best performance since it maximizes the PSNR by allocating bandwidth and performing

210

power control jointly while taking advantage of the instantaneous CSI of each channel.

In Chapter 9, we have studied power control and mode selection for VBR video streaming in D2D networks. The problem formulation takes into account power control at the base station and device transmitter, the two-hop link model (as seen in cellular mode), interference (as experienced in reuse mode), VBR video characteristics and playout buffer requirements. We have proposed a low complexity strategy that can determine the optimal solution by comparing limited numbers of values out of which the best is chosen. The results demonstrate that the power control and mode selection strategy significantly improves the performance over just using a single mode. Specifically, power control and mode selection lead to better utilization of buffer and a smaller number of buffer overflows and underflows and video stall events, and hence provide improved quality of experience (QoE) to the users.

In Chapter 10, we have studied both offline and online power control for wireless VBR video streaming over multiple subchannels. The problem formulation considers power control at the Tx subject to VBR video characteristics and playout buffer requirements. A directional water filling algorithm that achieves the optimal solution is employed to solve the problem in the offline case. Following the analysis of the optimal offline policy, the algorithm is modified to solve the extended optimization problem in the online setting. The result shows that the PM strategy saves more than 20% of consumed energy in the TM strategy. And the group size should be carefully chosen in the online scenario. The RL SARSA algorithm is proposed to find an efficient power allocation in this online scenario and the results have shown that the RL SARSA performs better than GWF strategy if the channel is not highly correlated.

11.2   Future Research Directions

11.2.1   Bounded Interference in Wireless Video Transmission

In Chapter 8, we consider the downlink wireless video transmission system, with multiple users sharing the spectrum orthogonally. We also consider the case in which all users share the same spectrum, leading to significant interference than can degrade the quality of the received video at the receivers. Due to the existence of interference, the power control problem is not convex. However, if bounding techniques are applied to interference, the problem can be converted into a convex one and suboptimal solutions can be obtained. These solutions can be compared with those obtained via monotonic optimization.

11.2.2   Deep Learning for Wireless Video Transmission over Full-Duplex Channels

In Chapter 6 and Chapter 7, we have employed monotonic optimization to solve the optimization problem in the presence of interference, which makes the problem is non-convex. One disadvantage of monotonic optimization is its relatively slow convergence rate especially if a large number of users are present in the system.

In order to reduce the complexity of the problem and the runtime, we can employ a deep learning approach. First, we obtain the training data set by employing monotonic optimization. Then, deep neuron network is trained with this data, and we can obtain the optimal power level as the output of the trained neural network, when new channel conditions are experienced.

11.2.3 Improvement of RL on VBR Video Streaming

In Chapter 10, we have assumed that we just estimate the channel side information of the next time slot in SARSA approach and we optimally minimize the power consumption in these two consecutive time slots. However, this does not lead to the optimal solution for the entire video transmission. One approach that can improve the performance is to estimate/predict the channel conditions in more future time slots. This will significantly enhance the performance especially if the channel coherence is high.

Appendix A

Appendix

A.1 Derivation of Equations (3.13) and (3.14)

In order to find the averaged BER of HP bits and LP bits over Nakagami-m fading distribution, we evaluate the expectations below with respect to channel power gain $z = |h|^2$:

$$P_{\text{HP}}(\mathbf{P}) = \frac{m^m}{\Omega^m \Gamma(m)} \int_0^\infty P_{\text{HP}}(\mathbf{P}, z) z^{m-1} e^{-\frac{m}{\Omega} z} dz$$
$$P_{\text{LP}}(\mathbf{P}) = \frac{m^m}{\Omega^m \Gamma(m)} \int_0^\infty P_{\text{LP}}(\mathbf{P}, z) z^{m-1} e^{-\frac{m}{\Omega} z} dz \qquad \text{(A.1)}$$

where $\Gamma(.)$ is the gamma function [85, eq. 6.1.1], m is the fading parameter that controls the severity of the amplitude fading, $m \geq 0.5$, and $P_{\text{HP}}(\mathbf{P}, h)$ and $P_{\text{LP}}(\mathbf{P}, h)$ are given in (3.9) and (3.12), respectively. In order to evaluate the above integrals, the following alternative representation of the Gaussian Q function is employed:

$$Q(x) = \frac{1}{2\sqrt{\pi}} \Gamma\left(\frac{1}{2}, \frac{x^2}{2}\right). \qquad \text{(A.2)}$$

Inserting the above Q function expression into (3.9) and (3.12), and using the identity [73, eq. 6.455.1], we obtain the closed-form BER expressions for HP and LP bits,

respectively in (3.13) and (3.14).

A.2 Proof of Proposition 3.1

By removing the Q functions with negative weight in (3.12), the objective function becomes convex subject to affine inequality constraints given in (3.19), (3.20) and (3.21). Hence, the optimal power can be obtained by using the Lagrangian optimization approach as follows:

$$
\begin{aligned}
L(P_0(h,g), P_1(h,g), \mu_1) = {} & \mathbb{E}\{\lambda P_{\mathrm{HP}}(\mathbf{P}, h) + (1-\lambda)P_{\mathrm{LP}}^u(\mathbf{P}, h)\} \\
& + \mu_1(\mathbb{E}\{(1-P_{\mathrm{d}})\, P_0(h,g)\, |g|^2 + P_{\mathrm{d}}\, P_1(h,g)\, |g|^2\} - Q_{\mathrm{avg}}).
\end{aligned}
\tag{A.3}
$$

Above, the superscript u in $P_{\mathrm{LP}}^u(\mathbf{P}, h)$ indicates that this is the upper bound on $P_{\mathrm{LP}}(\mathbf{P}, h)$ and μ_1 is the nonnegative Lagrange multiplier. The Lagrange dual problem is defined as

$$
\max_{\substack{\mu_1 \geq 0}} \min_{\substack{0 \leq P_0(h,g) \leq P_{\mathrm{pk}} \\ 0 \leq P_1(h,g) \leq P_{\mathrm{pk}}}} L(P_0(h,g), P_1(h,g), \mu_1), \mu_1).
\tag{A.4}
$$

For fixed μ_1 and fading coefficients, the subproblem is formulated, by applying the Lagrange dual decomposition method, as follows:

$$
\min_{\substack{0 \leq P_0(h,g) \leq P_{\mathrm{pk}} \\ 0 \leq P_1(h,g) \leq P_{\mathrm{pk}}}} \lambda P_{\mathrm{HP}}(\mathbf{P}, h) + (1-\lambda)P_{\mathrm{LP}}^u(\mathbf{P}, h) + \mu_1\big((1-P_{\mathrm{d}})\, P_0(h,g)\, |g|^2 + P_{\mathrm{d}}\, P_1(h,g)\, |g|^2\big).
$$

$$
\tag{A.5}
$$

According to the Karush-Kuhn-Tucker (KKT) conditions, the optimal power levels $P_{\text{opt}}^{(0)}(h, g)$ and $P_{\text{opt}}^{(1)}(h, g)$ must satisfy the following:

$$\sum_{j,l=0}^{1} \frac{P(\mathcal{H}_j, \hat{\mathcal{H}}_0)}{4\sqrt{2\pi}} \left\{ \lambda \frac{e^{\frac{-c_{l,0} P_0(h,g)|h|^2}{2\sigma_j^2}}}{\sqrt{\frac{\sigma_j^2 P_0(h,g)}{c_{l,0}|h|^2}}} + (1-\lambda)\rho_l \frac{e^{\frac{-\beta_{l,0} P_0(h,g)|h|^2}{2\sigma_j^2}}}{\sqrt{\frac{\sigma_j^2 P_0(h,g)}{\beta_{l,0}|h|^2}}} \right\} - \mu_1(1-P_{\text{d}})|g|^2 = 0, \quad \text{(A.6)}$$

$$\sum_{j,l=0}^{1} \frac{P(\mathcal{H}_j, \hat{\mathcal{H}}_1)}{4\sqrt{2\pi}} \left\{ \lambda \frac{e^{\frac{-c_{l,1} P_1(h,g)|h|^2}{2\sigma_j^2}}}{\sqrt{\frac{\sigma_j^2 P_1(h,g)}{c_{l,1}|h|^2}}} + (1-\lambda)\rho_l \frac{e^{\frac{-\beta_{l,1} P_1(h,g)|h|^2}{2\sigma_j^2}}}{\sqrt{\frac{\sigma_j^2 P_1(h,g)}{\beta_{l,1}|h|^2}}} \right\} - \mu_1 P_{\text{d}}|g|^2 = 0, \quad \text{(A.7)}$$

$$\mu_1 \left(\mathbb{E}\{(1 - P_{\text{d}}) \, P_0(h, g) \, |g|^2 + P_{\text{d}} \, P_1(h, g) \, |g|^2\} - Q_{\text{avg}} \right) = 0, \tag{A.8}$$

$$\mu_1 \geq 0, \tag{A.9}$$

$$\mathbb{E}\{(1 - P_{\text{d}}) \, P_0(h, g) \, |g|^2 + P_{\text{d}} \, P_1(h, g) \, |g|^2\} - Q_{\text{avg}} \leq 0. \tag{A.10}$$

Solving the above equations (A.6) and (A.7), and combining the solutions denoted by P_0^* and P_1^* with peak power constraints (3.19) and (3.20), respectively, yield the desired result in (3.22) and (3.23).

A.3 Proof of Proposition 3.2

When the sensing is perfect (i.e., $P_{\text{d}} = 1$ and $P_{\text{f}} = 0$), the optimal power levels that minimize the BER of HP bits can be found by solving the following optimization problem:

$$\min_{P_0(h,g), P_1(h,g)} \mathbb{E}\{P_{\text{HP}}(\mathbf{P}, h)\} \tag{A.11}$$

subject to

$$P_0(h, g) \leq P_{\text{pk}}, \; P_1(h, g) \leq P_{\text{pk}} \tag{A.12}$$

$$\mathbb{E}\{P_{\text{d}} \, P_1(h, g) \, |g|^2\} \leq Q_{\text{avg}} \tag{A.13}$$

Since Q function decreases rapidly in its argument, BER in (A.11) is dominated by the Q function with the smaller argument at high SNRs. Therefore, the objective function becomes

$$\frac{1}{2}\Pr\{\mathcal{H}_0\}\mathbb{E}\left\{Q\left(\sqrt{\frac{c_{1,0}P_0(h,g)|h|^2}{\sigma_n^2}}\right)\right\} + \frac{1}{2}\Pr\{\mathcal{H}_1\}\mathbb{E}\left\{Q\left(\sqrt{\frac{c_{1,1}P_1(h,g)|h|^2}{\sigma_n^2+\sigma_w^2}}\right)\right\}. \quad \text{(A.14)}$$

It is seen that the only constraint related to P_0 is the peak transmit power constraint in (A.12), and hence the minimum BER is achieved when the secondary user transmits at the maximum available instantaneous power. Therefore, $P^{(0)}(h,g) = P_{\text{pk}}$. In order to find the optimal P_1, we first express the Lagrangian function and take its derivative with respect to P_1 and set it to zero, which results in

$$P_1 e^{\frac{c_{1,1}|h|^2 P_1}{\sigma_n^2+\sigma_w^2}} = \frac{c_{1,1}|h|^2 P(\mathcal{H}_1)^2}{32\pi(\mu_1|g|^2)^2(\sigma_n^2+\sigma_w^2)}. \quad \text{(A.15)}$$

Solving for P_1 in the above equation and combining the result with peak transmit power constraint in (A.12) provide the optimal power policy in (3.27).

A.4   Proof of Theorem 7.1

Let us assumer $P_1 \leq P^{\text{max}}$ and $P_2 \leq P^{\text{max}}$, and consider the function

$$V_1(P_1, P_2, B) = \left(\mathbb{E}_\gamma\left\{e^{-\theta B T_c \log\left(1+\frac{P_1\gamma}{N_0 B+\mu P_2}\right)}\right\}\right)^{-1}. \quad \text{(A.16)}$$

We first show that V_1 is maximized if $P_1 = P^{\text{max}}$ or $P_2 = P^{\text{max}}$. Hence, at least one power value should be at the maximum level. Consider two power values strictly less than the maximum level, i.e., $P_1 < P^{\text{max}}$ and $P_2 < P^{\text{max}}$. Then, there exists some $\tau > 1$ such that $\tau P_1 \leq P^{\text{max}}$ and $\tau P_2 \leq P^{\text{max}}$. Then, considering the fraction in the

exponent in (A.16), we can easily see for $\tau > 1$ that

$$\frac{\tau P_1 \gamma}{N_0 B + \mu \tau P_2} = \frac{P_1 \gamma}{\frac{N_0 B}{\tau} + \mu P_2} > \frac{P_1 \gamma}{N_0 B + \mu P_2}, \tag{A.17}$$

which leads to the result that

$$V_1(\tau P_1, \tau P_2, B) > V_1(P_1, P_2, B). \tag{A.18}$$

Hence, for given $P_1 < P^{\mathrm{max}}$ and $P_2 < P^{\mathrm{max}}$, we can increase the value of V_1 by increasing the power values to τP_1 and τP_2 for some $\tau > 1$ (with which the maximum power constraint P^{max} is still satisfied). Therefore, with this characterization, we conclude that in order to achieve the maximum value of V_1, we should have P_1 or P_2 attain its maximum value.

Next, we prove that V_1 is an increasing function of bandwidth B. Let us define $\chi = e^{-\theta T_c B \log\left(1 + \frac{P_1 \gamma}{N_0 B + \mu P_2}\right)}$. Taking the first derivative of $V_1(P_1, P_2, B)$ with respect to B, we obtain

$$\frac{\partial V_1}{\partial B} = \frac{\theta T_c \mathbb{E}_\gamma \left\{ \chi \left(\ln\left(1 + \frac{P_1 \gamma}{N_0 B + \mu P_2}\right) - \frac{P_1 \gamma_k N_0 B}{(N_0 B + \mu P_2 + P_1 \gamma)(N_0 B + \mu P_2)} \right) \right\}}{(\mathbb{E}_\gamma \{\chi\})^2 \ln 2}. \tag{A.19}$$

Let us also define

$$g(x) = \ln\left(1 + \frac{1}{x}\right) - \frac{1}{1+x}. \tag{A.20}$$

The first derivative of $g(x)$ with respect to x is

$$\frac{dg(x)}{dx} = -\frac{1}{x(1+x)^2} < 0, \tag{A.21}$$

and hence $g(\cdot)$ is a decreasing function of $x \geq 0$. Moreover, $\lim_{x \to 0} g(x) = \infty$ and

218

$\lim_{x \to \infty} g(x) = 0$. Thus, $g(x) \geq 0$ for all $x \geq 0$, which also implies that

$$\ln\left(1 + \frac{1}{x}\right) \geq \frac{1}{1+x} \quad \text{for } x \geq 0. \tag{A.22}$$

Now, assume $x = \frac{N_0 B + \mu P_2}{P_1 \gamma}$. Then, we have

$$\ln\left(1 + \frac{P_1 \gamma}{N_0 B + \mu P_2}\right) \geq \frac{P_1 \gamma}{N_0 B + \mu P_2 + P_1 \gamma} \tag{A.23}$$

$$> \frac{P_1 \gamma}{N_0 B + \mu P_2 + P_1 \gamma} \frac{N_0 B}{N_0 B + \mu P_2}, \tag{A.24}$$

where (A.23) follows from (A.22), and (A.24) is due to the fact that $\frac{N_0 B}{N_0 B + \mu P_2} \leq 1$. The lower bound in (A.24) shows that the derivative in (A.19) is greater than zero because the numerator is greater than zero. Therefore, we conclude that V_1 is an increasing function of B.

Note that these derivations immediately apply to

$$V_2(P_1, P_2, B) = \left(\mathbb{E}_\gamma \left\{e^{-\theta B T_c \log\left(1 + \frac{P_2 \gamma}{N_0 B + \mu P_1}\right)}\right\}\right)^{-1} \tag{A.25}$$

due to the symmetry and similarity in the formulations.

Finally, we consider two target values V_1^* and V_2^* for the functions V_1 and V_2, respectively, i.e., $V_1(P_1, P_2, B) = V_1^*$ and $V_2(P_1, P_2, B) = V_2^*$, and show that the minimum bandwidth B required to achieve these target values is attained if $P_1 = P^{\max}$ or $P_2 = P^{\max}$. Assume that both power values are strictly less than the maximum level, i.e., $P_1 < P^{\max}$ and $P_2 < P^{\max}$, and B_a is the bandwidth value with which we satisfy $V_1(P_1, P_2, B_a) = V_1^*$ and $V_2(P_1, P_2, B_a) = V_2^*$. Then, as also discussed above, there exists $\tau > 1$ such that $P_{1a} = \tau P_1 \leq P^{\max}$ and $P_{2a} = \tau P_2 \leq P^{\max}$. With these increased power levels, we now have $V1(P_{1a}, P_{2a}, B_a) > V1^*$ and $V2(P_{1a}, P_{2a}, B_a) > V2^*$ as shown in (A.17) and (A.18). Since V_1 and V_2 are increasing functions of B, there exists $B_b < B_a$, such that $V_1(P_{1a}, P_{2a}, B_b) = V_1^*$ and $V_2(P_{1a}, P_{2a}, B_b) = V_2^*$.

Therefore, if both $P_1 < P^{\max}$ and $P_2 < P^{\max}$, we can always increase the power values and lower the bandwidth requirement while attaining the target levels V_1^* and V_2^*. Hence, the minimum required bandwidth is achieved if $P_1 = P^{\max}$ or $P_2 = P^{\max}$.

A.5 Proof of the Required Conditions for Obtaining the Upper Bound $\partial^+ \mathcal{G}$

Assume that there exists an upper boundary point $\mathbf{V}^u$ such that $\sum_{k=1}^{K} B_k < B$, i.e., $V_{(i-1)K+k}(P_{1,k}, P_{2,k}, B_k) = V_{(i-1)K+k}^u$ for all $i \in \mathcal{I}$ and $k \in \mathcal{K}$. From Theorem 7.1 and its proof in Appendix **??**, we know that $V_{(i-1)K+k}$ is an increasing function of B_k. Then, there exists a small positive δ such that $\sum_{k=1}^{K}(B_k + \delta) < B$ and $V_{(i-1)K+k}(P_{1,k}, P_{2,k}, B_k + \delta) > V_{(i-1)K+k}^u$, which implies that $\mathbf{V}^u$ is not a upper boundary point. Similarly, assume that there exists a upper boundary point $\mathbf{V}^u$ such that $P_{1,k} < P_{1,k}^{max}$ and $P_{2,k} < P_{2,k}^{max}$ for some $k \in \mathcal{K}$. Again, from the proof in Appendix **??**, we know that we can find a $\tau > 1$ such that $\tau P_{1,k} < P_{1,k}^{max}$ and $\tau P_{2,k} < P_{2,k}^{max}$, and with these increased power values, we have $V_{(i-1)K+k}(\tau P_{1,k}, \tau P_{2,k}, B_k) > V_{(i-1)K+k}^u$. This also means that $\mathbf{V}^u$ is not a upper boundary point. Therefore, the upper boundary point $\mathbf{V}^u$ only occurs when $\sum_{k=1}^{K} B_k = B$ and at least one power value is at its maximum level, i.e., $P_{1,k} = P_{1,k}^{max}$ or $P_{2,k} = P_{2,k}^{max}$, for all $k \in \mathcal{K}$.

A.6 Proof of Theorem 8.1 (Concavity of R_k with respect to P_k)

Let $r_k = B_k \log(1 + \frac{P_k \gamma_k}{N_0 B_k})$. Then, taking the first derivative of R_k with respect to P_k, we have

$$\frac{\partial R_k}{\partial P_k} = \frac{\mathbb{E}_{\gamma_k}\left\{e^{-\theta_k T_c r_k}\left(\frac{B_k}{\ln 2}\frac{\gamma_k}{N_0 B_k + P_k \gamma_k}\right)\right\}}{\mathbb{E}_{\gamma_k}\left\{e^{-\theta_k T_c r_k}\right\}}, \tag{A.26}$$

and the second derivative of R_k with respect to P_k is

$$\frac{\partial^2 R_k}{\partial P_k^2} = -\frac{\theta_k T_c}{(\mathbb{E}_{\gamma_k}\{e^{-\theta_k T_c r_k}\})^2} \times$$

$$\left(\mathbb{E}_{\gamma_k}\{e^{-\theta_k T_c r_k}\}\mathbb{E}_{\gamma_k}\left\{e^{-\theta_k T_c r_k}\left(\frac{B_k}{\ln 2}\frac{\gamma_k}{N_0 B_k + P_k \gamma_k}\right)^2\right\}\right.$$

$$\left. - \left(\mathbb{E}_{\gamma_k}\left\{e^{-\theta_k T_c r_k}\left(\frac{B_k}{\ln 2}\frac{\gamma_k}{N_0 B_k + P_k \gamma_k}\right)\right\}\right)^2\right)$$

$$- \frac{\mathbb{E}_{\gamma_k}\left\{e^{-\theta_k T_c r_k}\frac{B_k}{\ln 2}\frac{\gamma_k^2}{(N_0 B_k + P_k \gamma_k)^2}\right\}}{\mathbb{E}_{\gamma_k}\{e^{-\theta_k T_c r_k}\}}. \tag{A.27}$$

By applying the Cauchy-Schwarz inequality, we have

$$\mathbb{E}_{\gamma_k}\{e^{-\theta_k T_c r_k}\}\mathbb{E}_{\gamma_k}\left\{e^{-\theta_k T_c r_k}\left(\frac{B_k}{\ln 2}\frac{\gamma_k}{N_0 B_k + P_k \gamma_k}\right)^2\right\}$$

$$- (\mathbb{E}_{\gamma_k}\left\{e^{-\theta_k T_c r_k}\left(\frac{B_k}{\ln 2}\frac{\gamma_k}{N_0 B_k + P_k \gamma_k}\right)\right\})^2 \geq 0. \tag{A.28}$$

Hence, (A.27) is less than 0. We can also immediately see that (A.26) is greater than 0. Therefore, R_k is a increasing concave function of P_k.

A.7   Proof of Theorem 8.2 (Concavity of R_k with respect to B_k)

Taking the first derivative of R_k with respect to B_k, we obtain

$$\frac{\partial R_k}{\partial B_k} = \frac{1}{\ln 2} \frac{\mathbb{E}_{\gamma_k}\{e^{-\theta_k T_c r_k}(\ln{(1 + \frac{P_k \gamma_k}{N_0 B_k})} - \frac{P_k \gamma_k}{N_0 B_k + P_k \gamma_k})\}}{\mathbb{E}_{\gamma_k}\{e^{-\theta_k T_c r_k}\}}, \tag{A.29}$$

and the second derivative of R_k with respect to B_k is

$$\frac{\partial^2 R_k}{\partial B_k^2} = -\frac{\theta_k T_c}{(\ln 2 \mathbb{E}_{\gamma_k}\{e^{-\theta_k T_c r_k}\})^2} \Bigg(\mathbb{E}_{\gamma_k}\{e^{-\theta_k T_c r_k}\} \times$$

$$\mathbb{E}_{\gamma_k}\{e^{-\theta_k T_c r_k}(\ln{(1 + \frac{P_k \gamma_k}{N_0 B_k})} - \frac{P_k \gamma_k}{N_0 B_k + P_k \gamma_k})^2\}$$

$$- \Big(\mathbb{E}_{\gamma_k}\{e^{-\theta_k T_c r_k}(\ln{(1 + \frac{P_k \gamma_k}{N_0 B_k})} - \frac{P_k \gamma_k}{N_0 B_k + P_k \gamma_k})\} \Big)^2 \Bigg)$$

$$- \frac{1}{\ln 2} \frac{\mathbb{E}_{\gamma_k}\{e^{-\theta_k T_c r_k} \frac{(P_k \gamma_k)^2}{(N_0 B_k + P_k \gamma_k)^2 B_k}\}}{\mathbb{E}_{\gamma_k}\{e^{-\theta_k T_c r_k}\}}. \tag{A.30}$$

By applying the Cauchy-Schwarz inequality, we can establish

$$\mathbb{E}_{\gamma_k}\{e^{-\theta_k T_c r_k}\}\mathbb{E}_{\gamma_k}\{e^{-\theta_k T_c r_k}(\ln{(1 + \frac{P_k \gamma_k}{N_0 B_k})} - \frac{P_k \gamma_k}{N_0 B_k + P_k \gamma_k})^2\}$$

$$- \Big(\mathbb{E}_{\gamma_k}\{e^{-\theta_k T_c r_k}(\ln{(1 + \frac{P_k \gamma_k}{N_0 B_k})} - \frac{P_k \gamma_k}{N_0 B_k + P_k \gamma_k})\} \Big)^2 \geq 0. \tag{A.31}$$

Hence, (A.30) is less than 0. Since $\ln{(1 + \frac{P_k \gamma_k}{N_0 B_k})} - \frac{P_k \gamma_k}{N_0 B_k + P_k \gamma_k} > 0$, (A.29) is greater than 0. Therefore, R_k is a increasing concave function of B_k.

A.8 Proof of Theorem 8.3 (Concavity of $\hat{P}_k$ with respect to B_k)

In order to prove that $\hat{P}(B_k)$ is an increasing concave function of B_k, we need to show that $\frac{\partial^2 \hat{P}_k}{\partial B_k^2}$ is nonpositive. It is mentioned before that $\hat{P}(B_k)$ is an increasing function of B_k. (8.4) can be rewritten as

$$R_k = -\frac{1}{\theta_k T_c} \ln(\mathbb{E}_{\gamma_k}\{e^{-\theta_k B_k T_c \log(1+\frac{\hat{P}_k \gamma_k}{N_0 B_k})}\}) = \eta_k(P_c + \frac{1}{\epsilon}\hat{P}_k). \tag{A.32}$$

By differentiating both sides of (A.32) with respect to B_k, we have

$$\frac{\eta_k}{\epsilon}\frac{d\hat{P}_k}{dB_k} = \frac{dR_k}{dB_k} = \frac{\partial R_k}{\partial B_k} + \frac{\partial R_k}{\partial \hat{P}_k}\frac{d\hat{P}_k}{dB_k}. \tag{A.33}$$

Then, by taking the second derivative of both sides of (A.32) with respect to B_k, we obtain (A.34) given on the next page.

Let $q = \frac{d\hat{P}_k}{dB_k}$, $m(\gamma_k) = e^{-\theta_k B_k T_c \log(1+\frac{\hat{P}_k \gamma_k}{N_0 B_k})}$, $n(\gamma_k) = (\theta_k T_c \log(1+\frac{\hat{P}_k \gamma_k}{N_0 B_k}) - \frac{\theta_k T_c \hat{P}_k \gamma_k}{\ln 2(N_0 B_k + \hat{P}_k \gamma_k)})$ and $u(\gamma_k) = \frac{\theta_k T_c B_k \gamma_k}{\ln 2(N_0 B_k + \hat{P}_k \gamma_k)}$.

Then, (A.34) can be rewritten as in (A.35) below by moving the last term to the left-hand side:

$$(\frac{\eta_k}{\epsilon} - \frac{\partial R_k}{\partial \hat{P}_k})\frac{d^2 \hat{P}_k}{dB_k^2} = -\frac{1}{\theta_k T_c(\mathbb{E}_{\gamma_k}\{e^{-\theta_k B_k T_c \log(1+\frac{\hat{P}_k \gamma_k}{N_0 B_k})}\})^2}$$

$$\left(\{\mathbb{E}_{\gamma_k}\{m(\gamma_k)\}\mathbb{E}_{\gamma_k}\{m(\gamma_k)[n(\gamma_k) + qu(\gamma_k)]^2\} \right.$$

$$- [\mathbb{E}_{\gamma_k}\{m(\gamma_k)(n(\gamma_k) + qu(\gamma_k))\}]^2\}$$

$$+ \mathbb{E}_{\gamma_k}\{e^{-\theta_k B_k T_c \log(1+\frac{\hat{P}_k \gamma_k}{N_0 B_k})}$$

$$\left. [\sqrt{\frac{\theta_k T_c(\hat{P}_k \gamma_k)^2}{\ln 2(N_0 B_k + \hat{P}_k \gamma_k)^2 B_k}} - q\sqrt{\frac{\theta_k T_c B_k \gamma_k^2}{\ln 2(N_0 B_k + \hat{P}_k \gamma_k)^2}}]^2\} \right). \tag{A.35}$$

223

$$\frac{\eta_k}{\epsilon}\frac{d^2\hat{P}_k}{dB_k^2} = \frac{d^2R_k}{dB_k^2}$$

$$=\frac{\partial^2 R_k}{\partial B_k^2} + 2\frac{\partial^2 R_k}{\partial B_k \partial \hat{P}_k}\frac{d\hat{P}_k}{dB_k} + \frac{\partial^2 R_k}{\partial \hat{P}_k^2}(\frac{d\hat{P}_k}{dB_k})^2 + \frac{\partial R_k}{\partial \hat{P}_k}\frac{d^2\hat{P}_k}{dB_k^2}$$

$$=-\frac{1}{\theta_k T_c(\mathbb{E}_{\gamma_k}\{e^{-\theta_k B_k T_c \log(1+\frac{\hat{P}_k\gamma_k}{N_0 B_k})}\})^2}\bigg(\{\mathbb{E}_{\gamma_k}\{e^{-\theta_k B_k T_c \log(1+\frac{\hat{P}_k\gamma_k}{N_0 B_k})}\}$$

$$\big[\mathbb{E}_{\gamma_k}\{e^{-\theta_k B_k T_c \log(1+\frac{\hat{P}_k\gamma_k}{N_0 B_k})}[(\theta_k T_c \log(1+\frac{\hat{P}_k\gamma_k}{N_0 B_k}) - \frac{\theta_k T_c \hat{P}_k\gamma_k}{\ln 2(N_0 B_k + \hat{P}_k\gamma_k)})^2]\}$$

$$+ \mathbb{E}_{\gamma_k}\{2\frac{d\hat{P}_k}{dB_k}e^{-\theta_k B_k T_c \log(1+\frac{\hat{P}_k\gamma_k}{N_0 B_k})}[(\theta_k T_c \log(1+\frac{\hat{P}_k\gamma_k}{N_0 B_k}) - \frac{\theta_k T_c \hat{P}_k\gamma_k}{\ln 2(N_0 B_k + \hat{P}_k\gamma_k)})(\frac{\theta_k T_c B_k\gamma_k}{\ln 2(N_0 B_k + \hat{P}_k\gamma_k)})]\}$$

$$+ \mathbb{E}_{\gamma_k}\{(\frac{d\hat{P}_k}{dB_k})^2 e^{-\theta_k B_k T_c \log(1+\frac{\hat{P}_k\gamma_k}{N_0 B_k})}(\frac{\theta_k T_c B_k\gamma_k}{\ln 2(N_0 B_k + \hat{P}_k\gamma_k)})^2\}\big]$$

$$-\big[\mathbb{E}_{\gamma_k}\{e^{-\theta_k B_k T_c \log(1+\frac{\hat{P}_k\gamma_k}{N_0 B_k})}(\theta_k T_c \log(1+\frac{\hat{P}_k\gamma_k}{N_0 B_k}) - \frac{\theta_k T_c \hat{P}_k\gamma_k}{\ln 2(N_0 B_k + \hat{P}_k\gamma_k)})\}$$

$$+ \mathbb{E}_{\gamma_k}\{\frac{d\hat{P}_k}{dB_k}e^{-\theta_k B_k T_c \log(1+\frac{\hat{P}_k\gamma_k}{N_0 B_k})}(\frac{\theta_k T_c B_k\gamma_k}{\ln 2(N_0 B_k + \hat{P}_k\gamma_k)})\}\big]^2\}$$

$$+ \mathbb{E}_{\gamma_k}\{e^{-\theta_k B_k T_c \log(1+\frac{\hat{P}_k\gamma_k}{N_0 B_k})}\}$$

$$\mathbb{E}_{\gamma_k}\{e^{-\theta_k B_k T_c \log(1+\frac{\hat{P}_k\gamma_k}{N_0 B_k})}[\frac{\theta_k T_c(\hat{P}_k\gamma_k)^2}{\ln 2(N_0 B_k + \hat{P}_k\gamma_k)^2 B_k} + (\frac{d\hat{P}_k}{dB_k})^2\frac{\theta_k T_c B_k\gamma_k^2}{\ln 2(N_0 B_k + \hat{P}_k\gamma_k)^2} - 2\frac{d\hat{P}_k}{dB_k}\frac{\theta_k T_c \hat{P}}{\ln 2(N_0 B_k}$$

$$+ \frac{\partial R_k}{\partial \hat{P}_k}\frac{d^2\hat{P}_k}{dB_k^2}. \tag{A.34}$$

By applying the Cauchy-Schwarz inequality, we can establish

$$\mathbb{E}_{\gamma_k}\{m(\gamma_k)\}\mathbb{E}_{\gamma_k}\{m(\gamma_k)[n(\gamma_k) + qu(\gamma_k)]^2\}$$

$$- [\mathbb{E}_{\gamma_k}\{m(\gamma_k)\big(n(\gamma_k) + qu(\gamma_k)\big)\}]^2 \geq 0. \tag{A.36}$$

Hence, (A.35) is no greater than 0. With the fact that $\frac{\eta_k}{\epsilon} - \frac{\partial R_k}{\partial \hat{P}_k} > 0$, we obtain $\frac{d^2 \hat{P}_k}{dB_k^2} \leq 0$ and $\hat{P}_k$ is an increasing concave function of B_k.

Bibliography

[1] Cisco, "Cisco visual networking index: Global mobile data traffic forecast update, 2016-2021 white paper," Feb. 2017. [Online]. Available: http://www.cisco.com/c/en/us/solutions/collateral/service-provider/visual-networking-index-vni/mobile-white-paper-c11-520862.html

[2] FCC Spectrum Policy Task Force, "Report of the spectrum efficiency working group," http://transition.fcc.gov/sptf/reports.html, 2002.

[3] J. M. Iii, "An integrated agent architecture for software defined radio," 2000.

[4] S. Haykin, "Cognitive radio: brain-empowered wireless communications," *IEEE Journal on Selected Areas in Communications*, vol. 23, no. 2, pp. 201–220, Feb 2005.

[5] Q. Zhao and B. M. Sadler, "A survey of dynamic spectrum access," *IEEE Signal Processing Magazine*, vol. 24, no. 3, pp. 79–89, May 2007.

[6] D. Niyato and E. Hossain, "Spectrum trading in cognitive radio networks: A market-equilibrium-based approach," *IEEE Wireless Communications*, vol. 15, no. 6, pp. 71–80, December 2008.

[7] K. B. L. J. W. Mwangoka and Z. Cao, "Full length article: Joint power control and spectrum allocation for cognitive radio networks via pricing,"

Phys. Commun., vol. 2, no. 1-2, pp. 103–115, Mar. 2009. [Online]. Available: http://dx.doi.org/10.1016/j.phycom.2009.02.010

[8] B. Wang and K. J. R. Liu, "Advances in cognitive radio networks: A survey," *IEEE Journal of Selected Topics in Signal Processing*, vol. 5, no. 1, pp. 5–23, Feb 2011.

[9] V. Mishra, L. C. Tong, S. Chan, and J. Mathew, "Mac protocol for two level QoS support in cognitive radio network," in *IEEE, International Symposium on Electronic System Design (ISED), 2011*. IEEE, December 2011, pp. 296–301.

[10] D. Hu, S. Mao, Y. T. Hou, and J. H. Reed, "Scalable video multicast in cognitive radio networks," *IEEE Journal on Selected Areas in Communications*, vol. 28, no. 3, pp. 334–344, April 2010.

[11] D. Hu and S. Mao, "Streaming scalable videos over multi-hop cognitive radio networks," *IEEE Transactions on Wireless Communications*, vol. 9, no. 11, pp. 3501–3511, November 2010.

[12] X. L. Huang, G. Wang, F. Hu, and S. Kumar, "The impact of spectrum sensing frequency and packet-loading scheme on multimedia transmission over cognitive radio networks," *IEEE Transactions on Multimedia*, vol. 13, no. 4, pp. 748–761, Aug 2011.

[13] H. Luo, S. Ci, and D. Wu, "A cross-layer design for the performance improvement of real-time video transmission of secondary users over cognitive radio networks," *IEEE Transactions on Circuits and Systems for Video Technology*, vol. 21, no. 8, pp. 1040–1048, Aug 2011.

[14] M. Z. Bocus, J. P. Coon, C. N. Canagarajah, S. M. D. Armour, A. Doufexi, and J. P. McGeehan, "Per-subcarrier antenna selection for H.264 MGS/CGS video

transmission over cognitive radio networks," *IEEE Transactions on Vehicular Technology*, vol. 61, no. 3, pp. 1060–1073, March 2012.

[15] T. Jiang, H. Wang, and A. V. Vasilakos, "QoE-driven channel allocation schemes for multimedia transmission of priority-based secondary users over cognitive radio networks," *IEEE Journal on Selected Areas in Communications*, vol. 30, no. 7, pp. 1215–1224, August 2012.

[16] X. L. Huang, G. Wang, F. Hu, S. Kumar, and J. Wu, "Multimedia over cognitive radio networks: Towards a cross-layer scheduling under bayesian traffic learning," *Computer Communications*, vol. 51, pp. 48 – 59, 2014. [Online]. Available: http://www.sciencedirect.com/science/article/pii/S0140366414002254

[17] Z. He, S. Mao, and S. Kompella, "QoE driven video streaming in cognitive radio networks: The case of single channel access," in *2014 IEEE Global Communications Conference*, Dec 2014, pp. 1388–1393.

[18] R. Yao, Y. Liu, J. Liu, P. Zhao, and S. Ci, "Utility-based H.264/SVC video streaming over multi-channel cognitive radio networks," *IEEE Transactions on Multimedia*, vol. 17, no. 3, pp. 434–449, March 2015.

[19] Q. Jiang, V. C. M. Leung, M. T. Pourazad, H. Tang, and H. S. Xi, "Energy-efficient adaptive transmission of scalable video streaming in cognitive radio communications," *IEEE Systems Journal*, vol. 10, no. 2, pp. 761–772, June 2016.

[20] K. Doppler, M. Rinne, C. Wijting, C. Ribeiro, and K. Hugl, "Device-to-device communication as an underlay to LTE-advanced networks," *Communications Magazine, IEEE*, vol. 47, no. 12, pp. 42–49, Dec 2009.

[21] K. Doppler, M. Rinne, P. Janis, C. Ribeiro, and K. Hugl, "Device-to-device communications; functional prospects for LTE-advanced networks," in *Communica-*

tions Workshops, 2009. ICC Workshops 2009. IEEE International Conference on, June 2009, pp. 1–6.

[22] N. Golrezaei, A. Molisch, and A. Dimakis, "Base-station assisted device-to-device communications for high-throughput wireless video networks," in *Communications (ICC), 2012 IEEE International Conference on*, June 2012, pp. 7077–7081.

[23] H. Meshgi, D. Zhao, and R. Zheng, "Joint channel and power allocation in underlay multicast device-to-device communications," in *Communications (ICC), 2015 IEEE International Conference on*, June 2015, pp. 2937–2942.

[24] G. Yu, L. Xu, D. Feng, R. Yin, G. Li, and Y. Jiang, "Joint mode selection and resource allocation for device-to-device communications," *IEEE Transactions on Communications*, vol. 62, no. 11, pp. 3814–3824, Nov. 2014.

[25] D. Wu, J. Wang, R. Q. Hu, Y. Cai, and L. Zhou, "Energy-efficient resource sharing for mobile device-to-device multimedia communications," *IEEE Transactions on Vehicular Technology*, vol. 63, no. 5, pp. 2093–2103, Jun. 2014.

[26] Y. Wu, J. Wang, L. Qian, and R. Schober, "Optimal power control for energy efficient D2D communication and its distributed implementation," *IEEE Communications Letters*, vol. 19, no. 5, pp. 815–818, May 2015.

[27] W. Cheng, X. Zhang, and H. Zhang, "Optimal power allocation with statistical QoS provisioning for D2D and cellular communications over underlaying wireless networks," *IEEE Journal on Selected Areas in Communications*, vol. 34, no. 1, pp. 151–162, Jan. 2016.

[28] A. Khalek, C. Caramanis, and R. Heath, "Delay-constrained video transmission: Quality-driven resource allocation and scheduling," *IEEE Journ. on Selected Topics in Signal Processing*, vol. 9, no. 1, pp. 60–75, Feb 2015.

[29] Y. Xu, R. Hu, L. Wei, and G. Wu, "QoE-aware mobile association and resource allocation over wireless heterogeneous networks," in *2014 IEEE Global Communications Conference (GLOBECOM)*, Dec 2014, pp. 4695–4701.

[30] Y. Ma, H. Zhang, D. Yuan, and D. Jiang, "Power-efficient resource allocation with QoS guarantees for TDMA fading channels," *Wirel. Commun. Mob. Comput.*, vol. 12, no. 11, pp. 1023–1036, Aug. 2012. [Online]. Available: http://dx.doi.org/10.1002/wcm.1036

[31] J. Jia and Q. Zhang, "Competitions and dynamics of duopoly wireless service providers in dynamic spectrum market," in *Proceedings of the 9th ACM International Symposium on Mobile Ad Hoc Networking and Computing*, ser. MobiHoc '08. New York, NY, USA: ACM, 2008, pp. 313–322. [Online]. Available: http://doi.acm.org/10.1145/1374618.1374660

[32] Y. Wang, P. Ren, and Q. Du, "Statistical QoS driven power allocation for cognitive networks under primary user's outage probability constraint," in *2012 IEEE 23rd International Symposium on Personal, Indoor and Mobile Radio Communications - (PIMRC)*, Sept 2012, pp. 167–172.

[33] A. Sadeghi, M. Luvisotto, F. Lahouti, S. Vitturi, and M. Zorzi, "Statistical QoS analysis of full duplex and half duplex heterogeneous cellular networks," in *2016 IEEE International Conference on Communications (ICC)*, May 2016, pp. 1–6.

[34] W. Cheng, X. Zhang, and H. Zhang, "QoS driven power allocation over full-duplex wireless links," in *2012 IEEE International Conference on Communications (ICC)*, June 2012, pp. 5286–5290.

[35] Y. Wang and S. Mao, "Distributed power control in full duplex wireless networks," in *2015 IEEE Wireless Communications and Networking Conference (WCNC)*, March 2015, pp. 1165–1170.

[36] S. Buzzi, G. Colavolpe, D. Saturnino, and A. Zappone, "Potential games for energy-efficient power control and subcarrier allocation in uplink multicell OFDMA systems," *Selected Topics in Signal Processing, IEEE Journal of*, vol. 6, no. 2, pp. 89–103, April 2012.

[37] J. Deng, R. Zhang, L. Song, Z. Han, G. Yang, and B. Jiao, "Joint power control and subchannel allocation for OFDMA femtocell networks using distributed auction game," in *Wireless Communications Signal Processing (WCSP), 2012 International Conference on*, Oct 2012, pp. 1–6.

[38] T. Thanabalasingham, S. Hanly, L. Andrew, and J. Papandriopoulos, "Joint allocation of subcarriers and transmit powers in a multiuser OFDM cellular network," in *Communications, 2006. ICC '06. IEEE International Conference on*, vol. 1, June 2006, pp. 269–274.

[39] D. Wang, Z. Li, and X. Wang, "Joint optimal subcarrier and power allocation for wireless cooperative networks over OFDM fading channels," *Vehicular Technology, IEEE Transactions on*, vol. 61, no. 1, pp. 249–257, Jan 2012.

[40] H. Zhang, Y. Ma, D. Yuan, and H. H. Chen, "Quality-of-service driven power and sub-carrier allocation policy for vehicular communication networks," *IEEE Journal on Selected Areas in Communications*, vol. 29, no. 1, pp. 197–206, January 2011.

[41] F. Raphel and S. M. Sameer, "SSIM based resource optimization for multiuser downlink OFDM video transmission systems," in *2016 IEEE Region 10 Conference (TENCON)*, Nov 2016, pp. 1583–1586.

[42] J. Wu, B. Cheng, M. Wang, and J. Chen, "Delivering high-frame-rate video to mobile devices in heterogeneous wireless networks," *IEEE Transactions on Communications*, vol. 64, no. 11, pp. 4800–4816, Nov 2016.

[43] M. S. Talebi, A. Khonsari, and M. H. Hajiesmaili, "Optimization bandwidth sharing for multimedia transmission supporting scalable video coding," in *2009 IEEE 34th Conference on Local Computer Networks*, Oct 2009, pp. 185–192.

[44] Y. Wu, F. Hu, S. Kumar, Y. Zhu, A. Talari, N. Rahnavard, and J. D. Matyjas, "A learning-based QoE-driven spectrum handoff scheme for multimedia transmissions over cognitive radio networks," *IEEE Journal on Selected Areas in Communications*, vol. 32, no. 11, pp. 2134–2148, November 2014.

[45] N. Eshraghi, V. Shah-Mansouri, and B. Maham, "QoE-aware power allocation for device-to-device video transmissions," in *2016 IEEE 27th Annual International Symposium on Personal, Indoor, and Mobile Radio Communications (PIMRC)*, Sept 2016, pp. 1–5.

[46] J. Wu, C. Yuen, B. Cheng, M. Wang, and J. Chen, "Energy-minimized multipath video transport to mobile devices in heterogeneous wireless networks," *IEEE Journal on Selected Areas in Communications*, vol. 34, no. 5, pp. 1160–1178, May 2016.

[47] J. Wu, B. Cheng, M. Wang, and J. Chen, "Energy-efficient bandwidth aggregation for delay-constrained video over heterogeneous wireless networks," *IEEE Journal on Selected Areas in Communications*, vol. 35, no. 1, pp. 30–49, Jan 2017.

[48] L. Musavian and Q. Ni, "Delay-QoS-driven spectrum and energy efficiency trade-off," in *2014 IEEE International Conference on Communications (ICC)*, June 2014, pp. 4981–4986.

[49] A. Seetharam, P. Dutta, V. Arya, J. Kurose, M. Chetlur, and S. Kalyanaraman, "On managing quality of experience of multiple video streams in wireless net-

works," *IEEE Transactions on Mobile Computing*, vol. 14, no. 3, pp. 619–631, March 2015.

[50] Y. Xu, S. E. Elayoubi, E. Altman, R. El-Azouzi, and Y. Yu, "Flow-level QoE of video streaming in wireless networks," *IEEE Transactions on Mobile Computing*, vol. 15, no. 11, pp. 2762–2780, Nov 2016.

[51] Y. Huang and S. Mao, "Downlink power control for multi-user VBR video streaming in cellular networks," *IEEE Transactions on Multimedia*, vol. 15, no. 8, pp. 2137–2148, Dec 2013.

[52] S. Chatziperis, P. Koutsakis, and M. Paterakis, "A new call admission control mechanism for multimedia traffic over next-generation wireless cellular networks," *IEEE Transactions on Mobile Computing*, vol. 7, no. 1, pp. 95–112, Jan 2008.

[53] F. D. Rango, M. Tropea, P. Fazio, and S. Marano, "Call admission control for aggregate MPEG-2 traffic over multimedia geo-satellite networks," *IEEE Transactions on Broadcasting*, vol. 54, no. 3, pp. 612–622, Sept 2008.

[54] H. Abou-zeid, H. S. Hassanein, and S. Valentin, "Energy-efficient adaptive video transmission: Exploiting rate predictions in wireless networks," *IEEE Transactions on Vehicular Technology*, vol. 63, no. 5, pp. 2013–2026, Jun 2014.

[55] J. Yang and S. Ulukus, "Optimal packet scheduling in an energy harvesting communication system," *IEEE Transactions on Communications*, vol. 60, no. 1, pp. 220–230, January 2012.

[56] A. Deshmukh and R. Vaze, "Online energy-efficient packet scheduling for a common deadline with and without energy harvesting," *IEEE Journal on Selected Areas in Communications*, vol. 34, no. 12, pp. 3661–3674, Dec 2016.

[57] D. Shaviv and A. Özgür, "Universally near optimal online power control for energy harvesting nodes," *IEEE Journal on Selected Areas in Communications*, vol. 34, no. 12, pp. 3620–3631, Dec 2016.

[58] B. Barmada, M. M. Ghandi, E. V. Jones, and M. Ghanbari, "Prioritized transmission of data partitioned H.264 video with hierarchical QAM," *IEEE Signal Processing Letters*, vol. 12, no. 8, pp. 577–580, Aug 2005.

[59] M. Morimoto, M. Okada, and S. Komaki, "Robust mobile image transmission using hierarchical QAM," *Signal Processing: Image Communication*, vol. 12, no. 2, pp. 127 – 134, 1998. [Online]. Available: http://www.sciencedirect.com/science/article/pii/S092359659700060X

[60] M. R. Mili and K. A. Hamdi, "Minimum BER analysis in interference channels," *IEEE Transactions on Wireless Communications*, vol. 12, no. 7, pp. 3191–3201, July 2013.

[61] S. Sen, D. Towsley, Z.-L. Zhang, and J. K. Dey, "Optimal multicast smoothing of streaming video over the internet," *IEEE Journal on Selected Areas in Communications*, vol. 20, no. 7, pp. 1345–1359, Sep 2002.

[62] G. Liang and B. Liang, "Balancing interruption frequency and buffering penalties in VBR video streaming," in *IEEE INFOCOM 2007 - 26th IEEE International Conference on Computer Communications*, May 2007, pp. 1406–1414.

[63] C.-S. Chang, "Stability, queue length, and delay of deterministic and stochastic queueing networks," *IEEE Transactions on Automatic Control*, vol. 39, no. 5, pp. 913–931, May 1994.

[64] G. d. V. A. C. B. Chao Chen, Xiaoqing Zhu and R. W. H. Jr., "Rate adaptation and admission control for video transmission with subjective quality constraints,"

IEEE *Journ. on Selected Topics in Signal Processing*, vol. 9, no. 1, pp. 22–36, Jul 2014.

[65] L. Teixeira, "Rate-distortion analysis for H.264/AVC video statistics," in *Recent Advances on Video Coding*, J. D. S. Lorente, Ed. Oxford: InTech, 2011.

[66] M. Reisslein, "Video trace library." [Online]. Available: http://trace.eas.asu.edu/

[67] Y. Zhang, D. Niyato, P. Wang, and E. Hossain, "Auction-based resource allocation in cognitive radio systems," *IEEE Communications Magazine*, vol. 50, no. 11, pp. 108–120, November 2012.

[68] E. Axell, G. Leus, E. G. Larsson, and H. V. Poor, "Spectrum sensing for cognitive radio : State-of-the-art and recent advances," *IEEE Signal Processing Magazine*, vol. 29, no. 3, pp. 101–116, May 2012.

[69] A. Puri, X. Chen, and A. Luthra, "Video coding using the H.264/MPEG-4 AVC compression standard," *Signal Processing: Image Communication*, vol. 19, no. 9, pp. 793 – 849, 2004, technologies enabling Movies on Internet, HD DVD, and DCinema. [Online]. Available: http://www.sciencedirect.com/science/article/pii/S0923596504000566

[70] A. Natu and D. Taubman, "Unequal protection of JPEG2000 code-streams in wireless channels," in *Global Telecommunications Conference, 2002. GLOBE-COM '02. IEEE*, vol. 1, Nov 2002, pp. 534–538 vol.1.

[71] M. C. Valenti and J. Sun, "Turbo codes," in *Handbook of RF and Wireless Technologies*, F. Dowla, Ed. Burlington: Newnes, 2004, pp. 375 – 399. [Online]. Available: http://www.sciencedirect.com/science/article/pii/B9780750676953500148

[72] G. Ozcan, M. C. Gursoy, and S. Gezici, "Error rate analysis of cognitive radio transmissions with imperfect channel sensing," *IEEE Transactions on Wireless Communications*, vol. 13, no. 3, pp. 1642–1655, March 2014.

[73] I. S. Gradshteyn and I. M. Ryzhik, *Table of integrals, series, and products*, 7th ed. Elsevier/Academic Press, Amsterdam, 2007, translated from the Russian, Translation edited and with a preface by Alan Jeffrey and Daniel Zwillinger, With one CD-ROM (Windows, Macintosh and UNIX).

[74] T. Eng and L. B. Milstein, "Coherent DS-CDMA performance in Nakagami multipath fading," *IEEE Transactions on Communications*, vol. 43, no. 2/3/4, pp. 1134–1143, Feb 1995.

[75] R. M. Corless, G. H. Gonnet, D. E. G. Hare, D. J. Jeffrey, and D. E. Knuth, "On the lambert w function," in *ADVANCES IN COMPUTATIONAL MATHEMATICS*, 1996, pp. 329–359.

[76] D. Qiao, M. C. Gursoy, and S. Velipasalar, "Effective capacity of two-hop wireless communication systems," *IEEE Transactions on Information Theory*, vol. 59, no. 2, pp. 873–885, Feb 2013.

[77] Q. Du and X. Zhang, "Statistical QoS provisionings for wireless unicast/multicast of multi-layer video streams," *IEEE Journ. on Selected Areas in Communications*, vol. 28, no. 3, pp. 420–433, April 2010.

[78] S. Boyd and L. Vandenberghe, *Convex Optimization.* New York, NY, USA: Cambridge University Press, 2004.

[79] H. Tuy, "Monotonic optimization: Problems and solution approaches," *SIAM Journal on Optimization*, vol. 11, no. 2, pp. 464–494, 2000. [Online]. Available: http://dx.doi.org/10.1137/S1052623499359828

[80] J. Tang and X. Zhang, "Quality-of-service driven power and rate adaptation over wireless links," *IEEE Trans. Wireless Commun.*, vol. 6, no. 8, p. 3058–3068, Aug. 2007.

[81] S. Misra, A. Swami, and L. Tong, "Optimal training over the gauss-markov fading channel: a cutoff rate analysis," in *2004 IEEE International Conference on Acoustics, Speech, and Signal Processing*, vol. 3, May 2004, pp. iii–809–12 vol.3.

[82] R. S. Sutton and A. G. Barto, *Reinforcement Learning: An Introduction.* Cambridge, MA, USA: MIT Press, 1998. [Online]. Available: http://www.cs.ualberta.ca/%7Esutton/book/ebook/the-book.html

[83] A. Ortiz, H. Al-Shatri, X. Li, T. Weber, and A. Klein, "Reinforcement learning for energy harvesting point-to-point communications," in *2016 IEEE International Conference on Communications (ICC)*, May 2016, pp. 1–6.

[84] G. J. Gordon, "Reinforcement learning with function approximation converges to a region," in *Advances in Neural Information Processing Systems 13*, T. K. Leen, T. G. Dietterich, and V. Tresp, Eds. MIT Press, 2001, pp. 1040–1046. [Online]. Available: http://papers.nips.cc/paper/1911-reinforcement-learning-with-function-approximation-converges-to-a-region.pdf

[85] M. Abramowitz and I. A. Stegun, *Handbook of Mathematical Functions with Formulas, Graphs, and Mathematical Tables*, ninth dover printing, tenth gpo printing ed. New York: Dover, 1964.

Vita
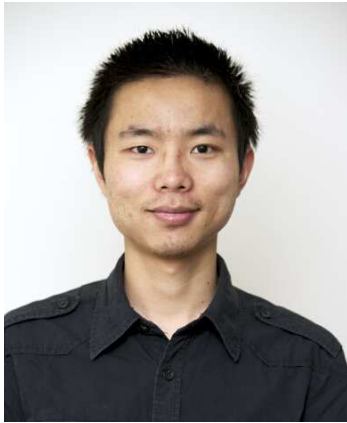
Chuang Ye received his B.S. degree in Information Engineering in 2009 and M.S. degree in Circuit and System in 2012 from Zhejiang University, Hangzhou, China. He has completed the Ph.D. degree in the Department of Electrical Engineering and Computer Science, Syracuse University, in 2018. During his Ph.D. study, he has authored two journal publications and seven conference publications. His research interests are in the fields of wireless communications, device-to-device cellular networks, and multimedia wireless transmission.